Experimental and Numerical Studies on Oil Spilling from Damaged Oil Tankers

Hao Yang

Supervisors

Dr. Shiqiang Yan and Prof. Qingwei Ma

A thesis submitted for the degree of Doctor of Philosophy

School of Mathematics, Computer Science and Engineering

City, University of London

June, 2017

Contents

Acknowledgement

Declaration

"I hereby certify that the work embodied in this Thesis is the result of original research and has not been submitted for a higher degree to any other University or Institute"

_____

Hao Yang

List of Figures

13

List of Tables

Notation

Roman Letters:

A	amplitude (L)
A_h	the hole area [L^2]
A_{he}	the external hole area [L^2]
A_{heo}	the area the external hole occupied by the oil flow [L^2]
A_{hew}	the area the external hole occupied by the water flow [L^2]
A_{hi}	the internal hole area [L^2]
A_o	the vertical overlapping area between the internal and external holes [L^2]
$\tilde{A}$	the cross-sectional area occupied by the fluid [L^2]
B	tank breadth [L]
C_d	discharge coefficient
C_o	Courant number
C_v	specific heat capacity [L^{2}T$^{-2}\Theta^{-1}$]
c	the speed of sound [LT^{-1}]
c_γ	adjustable coefficient
d	water draft [L]
D	the hole diameter [L]
D_m	the hole diameter in model [L]
D_p	the hole diameter in prototype [L]
Fr	Froude number
$\boldsymbol{F_s}$	the surface tension force [ML^{-2}T^{-2}]
$\boldsymbol{g}$	the acceleration due to gravity [LT^{-2}]
h	the oil level [L]
h_e	the vertical distance between the external hole centre and the DHT bottom [L]
h_{uo}	the oil height inside the ballast tank [L]
h_{uw}	the water height inside the ballast tank [L]
H	tank height [L]
H_b	the height of the bottom ballast space [L]
$H_{mixture}$	the level of water/oil mixture in the ballast tank [L]
H_{oil}	the height of the oil in the cargo tank [L]
H_s	the width of the side ballast space [L]
K	the effective thermal conductivity for mixture [MLT$^{-3}\Theta^{-1}$]
K_i	the thermal conductivity of phase i [MLT$^{-3}\theta^{-1}$]
K_t	turbulent thermal conductivity [MLT$^{-3}\Theta^{-1}$]
k	turbulent kinetic energy [L^{2}T^{-2}]
L_a	the average length between the two free surfaces of the U-tube in the flow oscillation direction [L]
$\dot{m}$	the unit molar weight [MN^{-1}]
p	pressure [ML^{-1}T^{-2}]
p_0	the normal pressure [ML^{-1}T^{-2}]
Q	discharge [L^{3}T^{-1}]
Q_e	discharge through the external hole [L^{3}T^{-1}]
Q_{eo}	oil discharge through the external hole [L^{3}T^{-1}]
Q_{ew}	water discharge through the external hole [L^{3}T^{-1}]

Q_i	discharge through the internal hole [L^3T^{-1}]
Q_o	discharge of oil outflow [L^3T^{-1}]
Q_w	discharge of water inflow [L^3T^{-1}]
R	ideal gas constant [$ML^2T^{-2}\Theta^{-1}N^{-1}$]
Re	Reynolds number
R^2	the square of the correlation coefficient
S_{bb}	the cross-section area of the ballast bottom space [L^2]
S_{bs}	the cross-section area of the ballast side space [L^2]
S_c	the cross-section area of the cargo tank [L^2]
T	temperature [Θ]
t	time [T]
t_g	the thickness of the tank wall [L]
t_w	the initial thicknesses of water layer inside the ballast tank [L]
u	the outflow velocity [LT^{-1}]
u_e	the average flow velocity through the external hole [LT^{-1}]
u_{eo}	the average oil flow velocity through the external hole [LT^{-1}]
u_{ew}	the average water flow velocity through the external hole [LT^{-1}]
u_i	the average flow velocity through the internal hole [LT^{-1}]
u_{i0}	the therotical average flow velocity through the internal hole [LT^{-1}]
u_m	the outflow velocity in model [LT^{-1}]
u_p	the outflow velocity in prototype [LT^{-1}]
U	the fluid velocity [LT^{-1}]
$\tilde{U}$	the areal averaged flow velocity [LT^{-1}]
U_c	the artificial compression velocity [LT^{-1}]
V_b	volume of the ballast tank [L^3]
V_f	volume of water flowing into the tank [L^3]
V_m	volume of the oil/water mixture in the cargo tank [L^3]
$V_{mixture}$	volume of the oil/water mixture in the ballast tank [L^3]
V_{oil}	oil volume inside the cargo tank [L^3]
V_s	oil volume spilled out of the tank [L^3]
W_d	water depth [L]

Greek Letters:

α	the volume fraction
α_{ds}	the ratio of the minimum cell size to the maximum cell size
α_i	the volume fraction of phase i
ζ	the non-dimensional final thickness of water layer inside the double-hull space
λ	the geometric scaling factor
λ_A	the ratio of the vertical overlapping area between the internal and external holes to the external hole area (A_o/A_{he})
ω	frequency [T^{-1}]
ω_0	first-mode natural frequency [T^{-1}]
κ	curvature of interface [L^{-1}]
σ	the surface tension coefficient [MT^{-2}]
ψ	compressibility [$L^{-2}T^2$]
ψ_i	compressibility of phase i [$L^{-2}T^2$]
ρ	the density of fluid [ML^{-3}]

ρ_0	the liquid density under the normal condition [ML^{-3}]
ρ_i	the density of phase i [ML^{-3}]
ρ_m	the density of mixture [ML^{-3}]
ρ_n	the nominal density [ML^{-3}]
ρ_o	the density of oil [ML^{-3}]
ρ_w	the density of water [ML^{-3}]
μ	the molecular dynamic viscosity [ML^{-1}T^{-1}]
μ_{eff}	the effective dynamic viscosity [ML^{-1}T^{-1}]
μ_i	the molecular dynamic viscosity of phase i [ML^{-1}T^{-1}]
μ_t	the turbulent dynamic viscosity [ML^{-1}T^{-1}]
v	the kinematic viscosity [L^{2}T^{-1}]
v_m	the kinematic viscosity in model [L^{2}T^{-1}]
v_o	the kinematic viscosity of oil [L^{2}T^{-1}]
v_p	the kinematic viscosity in prototype [L^{2}T^{-1}]
v_w	the kinematic viscosity of water [L^{2}T^{-1}]
Δ	axial offsets between the internal and external holes [L]
ΔH	the hydraulic head difference between the oil surface in the SHT tank and the broken hole [L]
ΔH_i	the hydraulic head difference between the oil surface in the cargo tank and the internal hole [L]
ΔH_e	the hydraulic head difference between the oil surface in the cargo tank and the external hole [L]
ΔH_{pi}	the potential head difference between the oil surface in the cargo tank and the internal hole [L]
ΔH_{pe}	the potential head difference between the external water surface and the external hole [L]

Abbreviation:

APG	aromatic pyrolysis gasoline
CSF	continuum surface force
DBT	double-bottom tank
DHT	double-hull tank
DNS	direct numerical simulation
DST	double-side tank
FVM	finite volume method
IMO	International Maritime Organization
LES	large eddy simulation
LNG	liquefied natural gas
MDT	mid-deck tank
MPS	moving particle semi-implicit
MTS	Maritime Transportation System
OPA-90	Oil Pollution Act of 1900
RANS	Reynolds-averaged Navier–Stokes
SHT	single-hull tank
VLCC	very large crude carrier
VOF	volume of fluid

Abstract

It is well understood that the spilled oil from damaged oil tankers poses a severe threat to the marine environment. Although great efforts have been devoted to studying the oil spilling from damaged oil tankers, especially double hull tanks (DHTs), the majority is subjected to an ideal condition (e.g., fixed tanks in still water; simple damage conditions) and adopts hydrostatic theories or quasi-steady models with over-simplified assumptions on data analysis or analytical prediction. These conditions or assumptions may not stand in the complex dynamic spilling process in the real spilling accident. This study brings a step further on the knowledge of oil spilling from a damaged tank by combining experimental and numerical investigations, with a focus on the dynamic spilling process from damaged oil tankers which is either fixed or subjected to motion, which have not been systematically investigated.

In the experimental investigation, the submerged oil spilling from DHTs under different accidental scenarios including grounding and collision is studied. Two new sets of laboratory tests are carried out, where the damaged tank is fixed in still water. In the first set, the axial offset between the internal and the external holes on two hulls of the grounded DHT is considered to widen the scope of damage conditions which the tanker may suffer from during grounding accidents. Although all cases in this set are subjected to the same hydrostatic conditions, completely different dynamic spilling processes are observed. In the second set, the initial water thickness inside the ballast tank of the collided DHT is considered. This aims to represent the real scenarios that the external hull is generally damaged prior to the internal hull and, therefore the ballast space is partially filled by the water flowing from the surrounding environment before the internal hull is damaged. These experiments do not only advance the state of the art of the experimental study in this field, but also provide a reference for validating the numerical models developed in this study. Based on the experimental data, the correlation analysis for the discharge through the internal hole by using quasi-steady Bernoulli's equation is presented, contributing to the development of an improved analytical model for predicting the oil spilling from damaged oil tankers.

The numerical study is carried out using a numerical model developed in OpenFOAM framework, where the VOF is applied to deal with the air-oil-water multiphase flow. This model enables the users: (1) to consider air, oil and water three phases of fluid and their interaction with solid tanker hull using dynamic mesh technologies; (2) to model turbulence associated with the oil spilling process using various available turbulent models; and (3) to investigate the effects of the compressibility of the fluid. The oil spilling from damaged DHTs is simulated and validated by the experimental data. Intensive investigations are carried out to clarify uncertainties in existing

numerical modelling of the oil spilling from damaged DHTs. These include (1) the associated turbulence behaviours and selecting an appropriate approach to turbulence modelling; (2) the role of fluid compressibility during the oil spilling; and (3) the effect of tank motion on the oil spilling process. For the turbulence modelling, various approaches to model the turbulence, including the large eddy simulation (LES), direct numerical simulation (DNS) and the Reynolds average Navier-Stokes equation (RANS) with different turbulence models are attempted. It is concluded that the oil spilling from DHTs is more sensitive to the turbulence modelling than that from SHTs. For DHT cases, the effective Reynolds number (*Re*) considering both oil outflow and water inflow is suggested to classify the significance of the turbulence and to correspondingly select the appropriate turbulence model. The investigation on the role of the air compressibility in the oil spilling from damaged DHTs reveals that the air compressibility may be considerable in a small temporal-spatial scale (e.g., jet-jet and jet-structure impact pressure), but plays an insignificant role in the macroscopic process of the oil spilling (e.g., spilling discharge and volume). In order to approach the spilling phenomena in the more realistic environment, a systematic numerical study is carried out to investigate the effect of the periodic ship motion on the oil spilling from the damaged tank. Different tank designs (i.e., SHTs and DHTs), accidental scenarios (i.e., grounding and collision) and tank motion parameters (i.e., types, frequencies and amplitude) are considered. The result indicates that the tank motion does not only cause a periodic oscillation of the oil/water flow through the broken hole, but also induces a second long-duration stage of spilling after a quasi-hydrostatic-equilibrium condition occurs, resulting in the more significant amount of spilled oil.

By using both the experimental data and numerical results produced in this research, an improved prediction model for oil spilling from damaged DHTs in still is formulated. This model considers the case-dependent hydrodynamic interaction between the oil and water jet flows inside the ballast tank and its effect on the spilling process. The result using the improved model is compared with the numerical result indicating its superiority over the existing model.

Chapter 1 Introduction

1.1   Background

Marine pollution is regarded as one of the global issues and generally comes from different sources including direct discharge, fertilizers runoff, ship pollution, atmospheric pollution and deep sea mining. Ships can pollute waterways and oceans in many ways, accidentally or intentionally. Typically, the ship accidental oil pollution may happen due to a vessel accident or during the transfer of oil to and from a vessel. While, the ship intentional pollution is operational dumping, e.g., the discharge of cargo residues from bulk carriers or dumping the dirty ballast water (a water-in-oil mixture) prior to or on arrival at a cargo-oil loading port. As shown in Figure 1.1, the statistical database provided by ITOPF (2016) suggests that the majority of medium or large-scale tanker spills are attributed to vessel accidents caused by grounding and collision, the proportion of which totally accounts for nearly half of the likelihood of accidental spilling and increases with the spilling size.
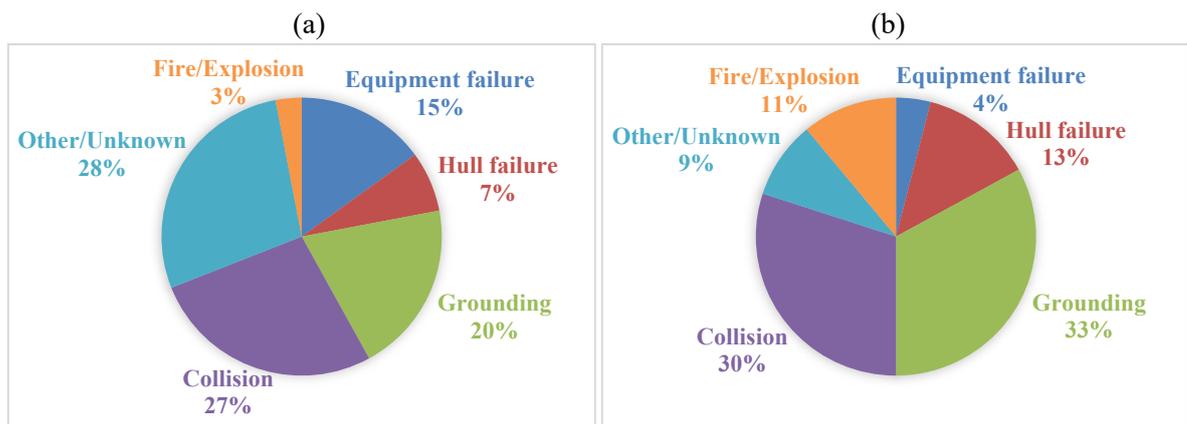
Figure 1.1 Incidence of spilling (a) 7-700 tonnes (medium scale) and (b) >700 tonnes (large scale) by cause, 1970-2016. (data is duplicated from ITOPF, 2016)

Over the past several decades, with the great increase in oceanic transportation of crude oil in large super-tankers, the subsequent occasional accidental episodes of disastrous oil spilling from these vessels leading to wide spread damage of marine environments raises worldwide public concerns. For instance, Patrick (2010) reported the disaster of the tanker Torrey Canyon which spilled her entire cargo of about 120,000t of crude into the sea while entering the English Channel resulting in huge economic losses and adversely affecting the environment for a significant duration. Moreover, the worldwide average cost of oil clean-up ranges from $20 to $200 per litre, depending on the oil type and its spilling location as mentioned by Fingas (2013). The cleaning up becomes trickier and is usually more expensive when the spilled oil reaches shorelines.

One important part of protecting the marine environment is to minimise the spilling. In order to reduce the potential risk of oil spilling, strict legislation and stringent operating codes have been introduced by governments and marine industries. One of the representative examples of the ship structure optimization is the double-hull tank (DHT) technology which was first mandated by OPA-90 in 1990 and then adopted by the UN's International Maritime Organization (IMO) in 1992 following the Exxon Valdez oil spilling in 1989. The DHT was implicitly regarded as one of the best solutions to preventing future catastrophic oil spilling, despite the fact the construction, operation and maintenance costs are much higher than those for conventional single hull tanks (SHTs).

Since the double hull space provides the barrier to minimize the damage on the internal hull, the double-hull tanks are less likely to spill oil than single-hull tankers from minor groundings and low energy collisions. Its impact on reducing historical spilling incidents was confirmed by historical studies (e.g., Yip *et al.*, 2011), which is also demonstrated in Figure 1.2 indicating the total number of tanker spills has dropped significantly for both medium and large-scale spills since the 1990s. However, Figure 1.2 also reveals that although the number of reported oil spills has been declining, marine pollution due to tanker spills remains a major threat. In some cases, the spilling incidents from DHTs is inevitable when the ship suffering from the severe damage. Due to the different ship configurations, the spilling process of the DHT is obviously more complicated and different from that of SHTs. Recently, this advanced ship design has frequently been doubted as some incident reports stated that the double-hull tanker performance may be no better than its predecessor of single-hull tanker (Terhune, 2011; John, 2014).
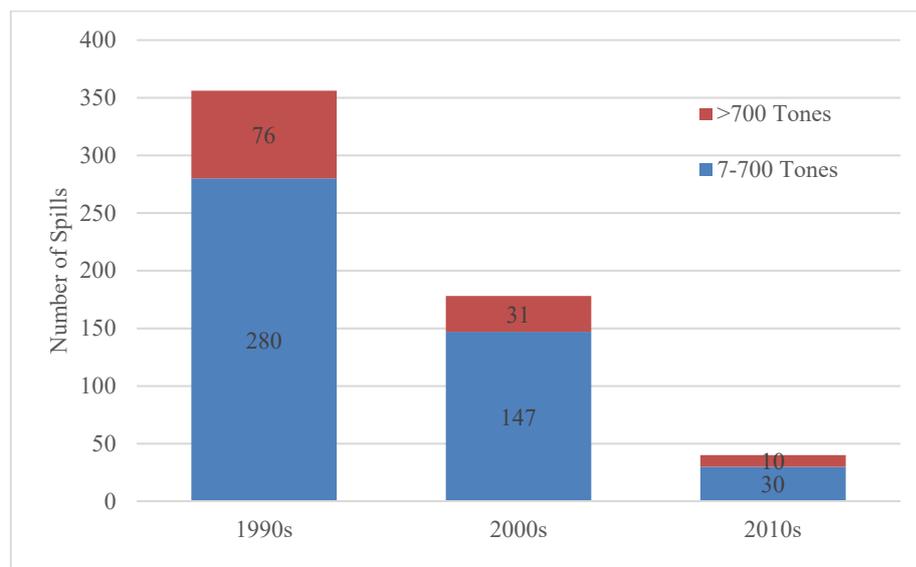
Figure 1.2 The number of medium (7-700 tonnes) and large (>700 tonnes) spilling per decade from 1990 to 2016. (data is duplicated ITOPF, 2016)

In the view of emergency planning, the most efficient and cost-effective response option is often to 'control at source' of potential ship spills (Gilbert and Nawadra, 2003), which is largely dependent upon a deep understanding of the associated mechanism of oil spilling from damaged oil tankers. Great efforts have been devoted to exploring the mechanism of oil spilling during a ship accident over the past several decades.

In the industrial community, the commonly used approach to estimate the accidental spilling performance of a new or existing ship is based on the hydrostatic theory associated with over-simplified or conservative assumptions (e.g., whole tank capacity spilled), from which only the final state information (e.g., ultimate spilling volume) may be provided. However, experimental observations have suggested that the oil spilling from a damaged ship is essentially a dynamics-dominated multi-phase flow problem with typical features of orifice flows, mixing, impact and interfacial shear layer, even for a fixed tank in still water (e.g., Karafiath, 1992; Yamaguchi and Yamanouchi, 1992). The parametric study in the previous experimental investigations (i.e., Yamaguchi and Yamanouchi, 1992; Simecek-Beatty *et al*., 2001; Tavakoli *et al*., 2011) also pointed out that the dynamic spilling procedures may be significantly affected by different accidental scenarios and tank designs yielding different spilling rates and durations, though they may reach a similar final state. It means that the final state information based on the hydrostatic theory is insufficient to comprehensively and accurately estimate an accidental oil spilling.

In order to reasonably/accurately predict the dynamic spilling process from a fixed tank under different accidental scenarios, many researchers (i.e., Fthenakis and Rohatgi (1999); Tavakoli *et al*., 2008; Tavakoli *et al*., 2012) analytically characterized the oil flow through the rupture as the orifice flow governed by the quasi-steady Bernoulli's equation. Although their models can quickly provide some important time-varying variables (e.g., discharge), many assumptions are embedded to simplify the complex spilling process especially when dealing with the flow motion inside the ballast tank of DHTs. Some of the assumptions, such as no oil spilling out of the DHT before filling up the ballast tank regardless of the hydrodynamic or rupture conditions, may be questionable and difficult to be justified.

As a cheaper and more efficient approach, the numerical modelling provides an alternative way for the further investigation through the extensive case study, providing more detailed results, comparing to experimental studies. The multiphase flow modelling is generally employed in the relevant studies to simulate the air-oil-water flow interaction during the spilling process. As mentioned by many experimental and numerical studies (e.g., Yamaguchi and Yamanouchi, 1992; Peter and Lin, 1994), due to the presence of the ballast tank, the DHT spilling involves more violent jet-jet and flow-structure interactions, impact and complex mixing inside the ballast tank, becoming a very challenging topic in the numerical investigation. So far, there are still many

uncertainties about model configurations. For example, when considering the jet impact and flow-structure interaction during the spilling process, the compressibility effect is always treated as a potential issue to investigate; another important issue is the turbulence effect as it exists during the flow through the rupture, on the interface between different fluids or during the fluid mixing inside the ballast tank (Peter and Lin, 1994).

It remains challenging to fully understand the dynamic behaviour of oil spilling out of a damaged ship in the real ocean environment. Generally speaking, when an oil tanker is subjected to a damaged condition due to collisions or groundings, the oil spilling affects the loads on the oil tankers and thus their instability, which mutually affects the behaviour of the spilled oil. Furthermore, in some cases, the external dynamic ocean conditions, such as tide, current, wave and any combinations, play an important role in the spilling process as preliminarily discussed by Karafiath (1992). Thus, the systematic investigation in this field should not only consider the hydrodynamic feature of multiphase flows but take into account the interaction among external environmental factors (such as tide, current and wave), ship motions and oil leakage. The issue becomes more complicated when incorporating different accidental scenarios and tank hull configurations. Although the phenomena of oil spilling from damaged tankers have received much attention from academic circles, most relevant studies are confined to the fixed model tank in the still water environment, while investigating the oil spilling in the dynamic environment is rarely seen to the best of the author's knowledge.

1.2   Aims and Objectives

The aim of this study is to advance the understanding of oil spilling from a damaged tank through physical and numerical approaches, and to answer the following research questions:

(1) How significant the dynamic effect on the oil spilling from DHTs which are either fixed or in motion? Do the damaged DHTs subjected to the same hydrostatic condition result in the same oil spilling process? How the tank motion affects the dynamic spilling process?

(2) What is the effect of fluid turbulence and fluid compressibility on the oil spilling from damaged DHTs?

(3) How to select an appropriate turbulence model for the DHT spilling problem?

(4) What is the limitation of existing analytical model and how to improve it?

Specific objectives listed below have been completed to achieve the aim:

- Design and carry out new laboratory tests to examine some important accidental factors, from which the significance of dynamic spilling process from a fixed damaged DHT is emphasized and discussed.

- Develop a numerical model for simulating the oil spilling from damaged oil tanks (including DHTs and SHTs) subjected to motions, with the capacity of dealing with the fluid compressibility and turbulence modelling.

- Carry out numerical investigations using the developed model to study the effect of turbulence modelling, fluid compressibility and tank motions on the oil spilling process, with the assistance of experimental data.

- The criterion of selecting proper turbulence models for the DHT spilling problem is proposed, considering both computational accuracy and robustness.

- Develop an improved quasi-steady prediction model for DHT spilling to overcome the limitation of the existing model.

1.3   Thesis Outline

The thesis starts with the introduction chapter which briefly introduces the accidental oil spilling from damaged tanks, outlines the current industrial and academic progress and their limitations, describes the complexity of real accidental spilling processes and states the aim and objectives of the study. In Chapter 2, a systematic literature review divided by different approaches is presented. Chapter 3 describes the experimental study on the oil spilling from a fixed DHT with different accidental conditions and scenarios, from which the significance of the dynamic spilling feature is highlighted. The numerical simulation in terms of SHT and DHT cases is carried out in Chapter 4. In this chapter, various approaches to model turbulence behaviours are employed in the DHT cases. According to the numerical results, Chapter 5 discusses the effect of turbulence modelling on the oil spilling from damaged DHTs. The associated turbulence features are characterized and a criterion of selecting proper turbulence models is proposed. Then, the compressibility effect on the DHT spilling process is examined in the following Chapter. Chapter 7 employs the correlation analysis to analyse the dynamic spilling process using the numerical results and proposes an improved quasi-steady analytical model to predict the different DHT spilling process under different damage situations. In Chapter 8, the numerical simulation is extended from the static case to a more realistic situation, where the oil spilling from a damaged tank subjected to periodic motions is addressed. Finally, Chapter 9 summarises the study and recommends future works.

Chapter 2 Literature Review

Over the past several decades, many academic and industrial efforts have been devoted to gaining better understanding of the oil spilling from damaged tanks. Many related researches have been presented by using different approaches (such as historical and probabilistic, experimental, analytical and numerical approaches). In this chapter, the review starts from the existing historical studies and common-used probabilistic approaches, which analysed spilling trends or assessed the accidental spilling performance of new or existing tanker design based on the actual/hypothetical database. Then, the preceding experimental investigations classified in the form of similarity criteria are presented, where the prototype is scaled down to the model and the intuitive observation of spilling behaviours for each representative accidental case can be obtained. Finally, in order to predict/investigate spilling processes specifically, the detailed review of the previous analytical models and numerical studies are conducted based on the different approaches.

2.1 Historical and Probabilistic Studies

Based on the spilling database, the historical approach is to statistically analyse the trend of oil spilling accidents or assess the impact of tank design (such as DHT) on the spilling consequence. In the industry, the probabilistic approach is usually employed to measure the spilling performance of a new tanker design or existing tanker design under various damage conditions described as probability density functions, where the final oil spilling volume is regarded as the key factor in the calculation.

2.1.1 Historical approaches

In response to the Exxon Valdez incident in 1989 (Morris and Loughlin, 2013), the largest vessel-accident oil spilling in US history, the US congress passed the Oil Pollution Act of 1900 (OPA-90) to reduce the occurrence of oil spilling and the resultant impact of potential future spilling through increased preparedness. According to the statistic study of Card (1975), it implicitly assumed that double-bottom hulls would reduce the vessel damage to tanker ships and tank barges involved in grounding accidents, thereby also reducing the oil cargo spilling from these vessel accidents. Thus, the Act mandates tankers operating in U.S. waters must be fitted with double hulls by 2015 with the phase-in schedule. Two year later, the double hull design was first executed by International Maritime Organization (IMO) for global oil tankers.

The consequent impact of OPA-90 on the U.S. or global historical spilling pattern resulting from the tank accident was investigated by several researchers (e.g., Kim, 2002; Burgherr, 2007; Homan and Steiner, 2008; Glen, 2010) based on different databases. A similar conclusion that the number and volume of oil spilling from tanker vessel in U.S. or global waters have fallen

considerably since enactment of the Act was drawn. An empirical analysis of the effectiveness of the double-hull design in decreasing the oil spilling of double-hull versus single-hull oil cargo vessel accidents was presented by Yip *et al*. (2011) using Tobit regression model and empirical data set of individual oil-cargo vessel accidents investigated by the US Coast Guard from 2001 to 2008. The results indicated that the double-hull design reduces the size of oil spilling during tanker ship accident by 62% and that for tank-barge accident oil spilling by 20%, comparing with the comparable single-hull design. Moreover, Liu *et al*. (2015) utilized the historical data from 1973 to 2002 together with the satellite images to identify the spilling risk zone due to ship accidents and oil drilling in Bohai Sea, China. They demonstrated that ship accidents still dominate the risk in the Bohai Sea and the high risk zones are distributed along the coast.

2.1.2 Probabilistic approaches

OPA-90 gave the impetus to the International Maritime Organization (IMO) for the worldwide adoption of double-hull standards for tanker ships. Moreover, IMO accepts alternatives which may not satisfy the OPA-90 requirements as long as the performance of impeding oil outflow is proven to be equivalent to the double-hull tanker (Paik, 2003). Based on this concept, IMO (1994a) (revised version: IMO, 2003) formulated a widely-used probabilistic approach which of purpose is to measure outflow performance of a new tanker design against an IMO specified reference double hull design in terms of a 'pollution prevention index'. This index includes three characteristics of the oil outflow performance of any tanker, namely, probability of zero outflow, mean outflow and extreme outflow.

There are four main steps when applying the IMO Guideline (mentioned in Sirkar *et al*., 1997). First, assemble damage cases based on several probability density functions (pdfs) describing the location, extent and penetration of side or bottom damage derived from historical damage statistic data. Second, regarding each unique side damage or bottom damage case, the oil outflow is calculated based on the hydrostatic pressure balance principle associated with some arbitrary conservative assumptions. Third, the aforementioned oil outflow parameters are computed as their definitions. Finally, calculate the 'pollution prevention index'. A representative application of this IMO guideline was recorded by Michel and Moore (1995). Rawson *et al*. (1998) concluded some specific deficiencies in the IMO Guidelines including the limited single hull tanker database and arbitrary manner of defining damage extents, and modified the IMO (1994a) by introducing a theoretical model to predict damage extents rather than historical data. It also recommended using the mean outflow parameter as the best single outflow risk index. With the purpose of simplification, IMO (2004a) and IMO (2004b) revised and approved the IMO's probabilistic approach (IMO, 2003). Smailys and Česnauskis (2006) further proposed a modification of IMO

(2004a), in which the input data is reduced several times with some main information of tanker types, operating and design characteristics for the expeditious applications in particular sea region.

With respect to the estimation of the accidental oil outflow for existing ships, a simplified deterministic model was developed by IMO (1994b); then revised by IMO (2001). In this method, damage extents are applied to determine the likelihood that a given cargo oil tank is breached, either alone or in combination with any other tanks without considering the pdfs. The weighted average of the probability of damaging the tank (60% for grounding and 40% for collision) and the associated oil outflow yield a hypothetical or average outflow value (mentioned by Michel *et al.*, 1996). Daidola *et al.* (1997) demonstrated that the absolute difference between the average outflows calculated utilizing IMO (1994b) and the mean values of IMO (1994a) are minimal. Following the similar methodology involved by IMO (1994b), Michel *et al.* (1996) further developed a simplified probabilistic methodology by including the pdfs and many of the assumptions contained in IMO (1994a). In this study, many simplifications were suggested. For example, the probability of damaging each cargo tank was calculated rather than determining each unique damage case and its associated probability done by IMO (1994a). Following this approach, the pdfs were converted into a table. Later, Sirkar *et al.* (1997) discussed the differences between IMO (1994a) and the method formulated by Michel *et al.* (1996) in details. Also, based on the simplified method of Michel *et al.* (1996), they presented a rational framework of evaluating tank design considering the costs of pollution oil outflow characteristic and enhanced structural performance.

Alternatively, the concept of energy conservation could be adopted to estimate the ship damage and the resulting oil outflow associated with the energy generated by ship accidents. By using this idea, Samuelides (1999) presented an oil outflow analysis following collision damage to tankers. In this study, a probability density function for the impact kinetic energy was formulated based on 176 collision accidents that occurred in the first semester of 1995. Then, using a simple model for determining the collision damage and oil outflow damage, the author derived probability density functions for the oil outflow of a 'basis' tanker and of a tanker with an extra stringer deck. Although some of the intermediate assumptions are rather simplistic, as mentioned in Kaminski *et al.* (2000), the methodology illustrates the necessary steps in rational and probabilistic design against collision accident.

Van de Wiel (2008) established a probabilistic oil outflow model to assess the potential oil spilling volume of an oil tanker in a collision or grounding accident scenario for both single-hull and double-hull tankers. According to a total of 80,000 random accident scenarios, the accidental damage extent inflicted on a tanker was simulated using the programs SIMCOL and DAMAGE developed by Brown (2001) and Tikka (2001) respectively based on the kinetic energy

conservation. After that, the binary logistic regression was employed to determine the probability of rupture and the resulting quantity of cargo oil that was spilled was estimated. When calculating the oil spilling volume given a set of rupture variables, a simplified or worst assumption was made e.g., all oil in a collided compartment was lost; the amount of oil that is lost under grounding is based on the principle of hydrostatic pressure equilibrium principle between the oil in damaged tank and the surrounding seawater. Later, this approach was further developed by coupling with the Maritime Transportation System (MTS) simulation by Van de Wiel and Dorp (2009) and by applying the Bayesian networks (BNs) in Goerlandt and Montewka (2014) and Montewka *et al.* (2014).

2.1.3 Summary and limitation

Although the historical approach is relatively convenient and extensive, Eide *et al.* (2007) pointed out that it was suspected that the older historical data were not necessarily proper representative for current accident scenarios when considering changes in ship construction or tanker arrangement. In other words, the new concepts cannot be evaluated on the basis of historical analysis alone (Michel and Winslow, 1999). Also, the worst-situation or simplified assumptions and pdfs embedded in the IMO's approach appear to be questionable, especially for the specific structural design and tank arrangement of ships operating in a given sea region. Moreover, according to Krata *et al.* (2012), the aforementioned historical and probabilistic methods are unable to provide the vital information (e.g., the leak rate or the spilling duration) which is regarded as the decisive factor to the appropriate spilling assessment and prompt emergency activities.

2.2 Experimental Studies

When simply characterizing the oil flow through a rupture, the orifice flow theory is generally employed. However, the oil spilling from a damaged tank is a more complex dynamic process, where the spilling rate and duration can be changed substantially depending on the environment, tank designs and damage conditions. With the purpose of gaining better understanding of accidental oil spilling from damaged tanks, several experimental investigations had been carried out over the past three decades, where the model-scale tests associated with different ship designs and representative damage scenarios were proposed, focusing on the hydrostatic and hydrodynamic spilling behaviours.

2.2.1 Orifice flow problems

Massey (1968) defined an orifice as: "an aperture through which fluid passes and its thickness (in direction of flow) is very small in comparison with its other measurements". As mentioned by Wang *et al*. (2016), the maritime structures are mostly made of steel plate which varies from

10mm to 30mm but where the total length is often greater than 100m. Thus, oil spilling from a rupture of the damaged tanker or pipeline can be catalogued as an orifice flow problem. The gravity-induced free jet flow through a circular orifice of the diameter D_0 is illustrated in Figure 2.1. In practice, due to the vena contracta ($A_j < A_0$) and the energy loss due to friction, turbulence, etc. ($U_j < U_0$), the actual discharge through the orifice ($Q_j = U_j A_j$) is usually less than the ideal discharge ($Q_0 = U_0 A_0$), where the ratio of the actual discharge and the ideal discharge is defined as the discharge coefficient, C_d. This value highly depends on the viscosity, turbulence and the geometry of orifice, which has attracted much researchers' attention.
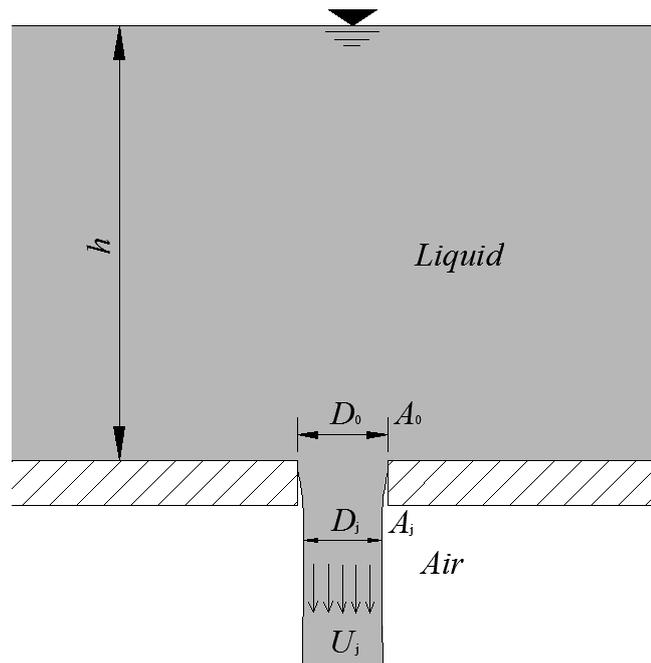
Figure 2.1 A cross-section of the gravity-induced free jet flow through a circular orifice of the diameter D_0 (A_j is the area of the exit jet flow; A_0 is the orifice area; D_j is the diameter of the exit jet flow; U_j is the average velocity of the exit jet; U_0 is the average theoretical velocity calculated by $\sqrt{2gh}$, where g is the gravitational acceleration and h is the liquid height).

A simplified physical model including venting-rate tests and a set of small-scale air and water ingestion tests were conducted by Dodge *et al.* (1980). In this study, a series of tests were conducted to determine the discharge coefficients (C_d) for different types of punctures and fluids in a range of Reynolds numbers (*Re*:1275-96000). The fluids used in this test were water, glycerine mixture and hydraulic oil. The value of the discharge coefficient which was depended upon the geometry and orientation of the hole was widely used by following researches for demonstrating the characteristic of orifice flows. Li *et al.* (2013) performed a systematic analysis of water flooding model that highlighted the change in discharge coefficient between flat orifices and these containing more realistic petalling edges. Following the similar procedure of Li *et al.* (2013), Wang *et al.* (2016) further investigated the oil spilling under collision scenarios by

categorising flows with immiscible oil and water fluids. Comparing with the results presented previously by Li *et al*. (2013), they found a similar trend for the discharge coefficient due to different orifice geometries, but the C_d value for the same shape and area of the orifice is larger for the water flooding into an empty compartment than for oil leaking into the water.

2.2.2 Froude scale physical models

Generally, full-scale experimental test on oil spilling is difficult and model scale is used instead. Hence, it is important to verify that the cargo properties and release condition are modelled in an acceptable way. When the prototype is scaled down to the model keeping the geometric similarity, Simecek-Beatty *et al*. (2001) demonstrated that the equivalent Froude number (*Fr*), which relates the inertial force to the gravitational force, is achieved between the full-scale and lab-test models, since it is assumed that the spilling velocity in both models is mainly dominated by the gravitational head by ignoring other forces (e.g., viscous force and surface tension force) which likely influence the dynamic spilling behaviour. Based on this principle, many Froude-scale physical models were built in the early works.
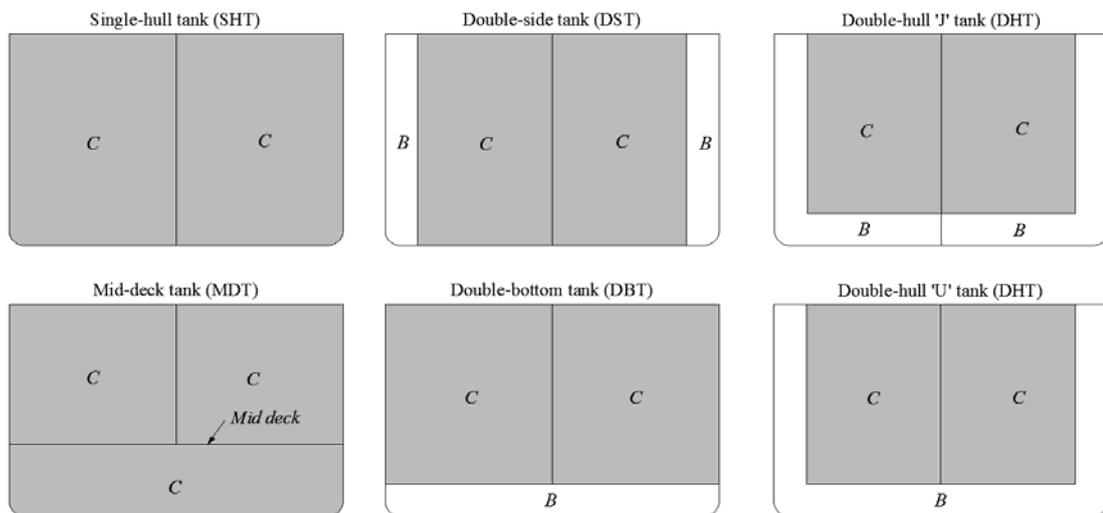
Figure 2.2 Different tank arrangements of oil tanker design (*C* is cargo tanks; *B* is ballast tanks).

Karafiath and Bell (1992) and Karafiath (1992) summarised a series of IMO sponsored preliminary model tests for accidental oil spilling of grounded double-hull tanks (DHTs) and mid-deck tanks (MDTs), the result of which was used by IMO in their probabilistic oil outflow analysis. The corresponding tank arrangements are sketched in Figure 2.2. They defined the total oil loss due to grounding composing of two parts: one is called instantaneous exchange loss at the time of grounding which was depended on the initial velocity, grounding conditions and the structural strength of the tank modelled by the 'rupture and stop' model tests; another is the additional oil loss subsequent to the grounding caused by the environmental conditions (e.g., current, sea state and tide drop).

With respect to the double-hull design, only the oil loss that occurred at the time of grounding (namely, instantaneous exchange loss with zero forward speed) was investigated based on the two groups of rupture tests conducted for 'J' tanks and 'U' tanks respectively (sketched in Figure 2.2). Although some of the differences in effectiveness between 'J' and 'U' tanks' capability to capture oil was attributed to the differences in testing procedures, it was confidently concluded that the 'U' tanks are far superior in terms of capturing the oil because they provided more volume for the oil to occupy. These studies also deduced that since the 'U' tank would have a greater resultant water layer, it provided greater resistance to oil loss due to current, sea state and further tide drop. Moreover, the internal structural details in the ballast tanks were regarded as a determining factor for preventing oil spilling outside, which directed the design guidance with respect to the improved arrangement of double hull voids to minimize oil loss in case of severe accident scenarios.

As for the mid-deck design, the effect of different ship speeds and cargo loadings on the amount of instantaneous loss was examined. Moreover, this experimental study also considered the additional oil loss resulting from the dynamic environment (i.e., current, sea state and tide drop) subsequent to the instantaneous loss at the time of grounding. The complex oil loss mechanism that appeared to change with the extent of the water layer inside the cargo tank and the amount of oil loss caused by the steady current or heaving motion was observed. It was found that the MDT oil loss due to current was greatly increased. The oil lost was sensitive to the combined effect of current and heaving oscillation, because the effect of the current was to sweep away the oil that emerged from the tank on the upward oscillation and very little oil was recaptured on the downward oscillation, but small additional oil loss was observed under the heave motion alone. In this study, the scale effect was examined based on the MDT models with different scale factors (λ=15 and 30). The inconsistent extrapolation of oil loss curves questioned the reliability of the current Froude-scaled similarity criteria. This paper also analysed different kinds of forces acting on a fluid particle (including gravitational forces, inertial forces, viscous forces and surface tension forces) which are considered important to the dynamic feature of oil spilling phenomena.

Furthermore, Yamaguchi and Yamanouchi (1992) carried out a Froude-scaled experimental investigation for quantitatively evaluating the effectiveness of the double-hull tanker in reducing oil spilling under groundings and collisions. The model tank was fixed in an initially still water basin. The effects of various parameters including tanker configurations (e.g., double bottom heights, double side widths and tank sizes) and ship and accident scenarios (e.g., the extent and the position of the rupture, the initial thickness of the water layer in the double hull space, the drafts and the cargo levels) on oil spilling under grounding scenarios were studied in terms of final state quantities, and some snapshots showing the dynamic behaviours of oil spilling were presented in this study. Similar to Karafiath and Bell (1992), a conclusion that the oil containment

in the double hull space is proportional to the double hull space was also drawn for groundings. With regard to the collisions, all amount of oil below the top of rupture spilled and replaced by water as the side hole was below the water line. While, whole oil was spilled through a side rupture located on the water line. Based on the balance of hydrostatic head at the rupture and the mass balance concept, the researchers proposed a formula to predict the final state of oil leakage from a grounded double-hull tank model, where a non-dimensional final thickness of water layer inside the double-hull space (ζ) was derived. The experimental data was organized in the form of non-dimensionlised variables which revealed that the draft condition significantly affects the relationship between the ζ value and other variables: at the lower water draft condition, ζ value was the only function of both double-bottom height and the rupture diameter; while for a higher water draft condition, the ζ value was the only function of the water draft and cross-section area of cargo tank. Only the latter correlation was confirmed by the proposed analytical solution associated with zero oil spilling volume assumption.

2.2.3 Froude and Reynolds scale physical models

When the dynamic process of the oil spilling is concerned, the flow motion may be affected by different forces (e.g., gravitational forces, inertial forces, viscous forces and surface tension forces). A severe scale effect in the time history of the oil outflow was mentioned by Karafiath and Bell (1992), since only the inertial force was properly scaled in their Froude scale experimental works. Peter and Lin (1994) also pointed out that the small-scale flow in the ballast tank between two hulls and/or near the broken holes shows significant viscous effects, which means that the viscous force should be appropriately scaled in the physical model in order to accurately predict the dynamic spilling features.

For this purpose, Simecek-Beatty *et al.* (2001) further proposed a more comprehensive scale analysis to address the oil spilling problem incorporating the viscous effect. Considering the oil release from a punctured, vented and single-hull tanker (SHT), the primary forces likely governing this process were gravitational, inertial and viscous forces and, therefore this study recommended two non-dimensional parameters, namely Froude number (inertial force/ gravitational force) and Reynolds number (inertial force/viscous force). It was supposed that the whole dynamic process of oil spilling can be considered dynamically similar, if these two numbers regarding to the oil flow were respectively equivalent for both the prototype and the model. Based on these similarity criteria, a set of tests was performed using Canola oil that was suitable to simulate petroleum products released from the prototype. However, the unique characteristic of Orimulsion (i.e., heavy stuff and surface slick) required to conduct a series of small-scale experiments with this product. Thus, the two types of oil products were used in this study to investigate oil leaking from a side puncture above or below the waterline. However, it should be

noticed that the Reynolds similarity law did not apply to the water media due to the material limitation. According to the results, the author deduced that the difference of drainage time simply accounts for the density differences but ignoring the effect of viscosity differences.

Following the similar similarity principle, two physical models were established recently by Lu *et al*. (2010) and Tavakoli *et al.* (2011), respectively. Lu *et al.* (2010) studied the accidental side release from an underwater circle orifice experimentally and numerically. The model test was carried out in the still water, and the gross volume and duration of leakage with different hole sizes and locations were measured. It was found that the duration of oil spilling was prolonged by the smaller hole, and the gross volume of leakage from a larger hole could rise up slightly as the upper side of the broken hole located higher. As for the different hole elevations, the gross volume and duration increased with higher elevation. However, this experimental study did not provide any time history of key variables reflecting the dynamic features involved.

Subsequently, in order to gain better understanding of the unsteady behaviour of oil spilling processes, the oil leaking from damaged ships with different tank designs during collision and grounding incidents were investigated by Tavakoli *et al.* (2011). Different tank designs including single-hull (SHTs), double-bottom (DBTs), double-side (DSTs) and double-hull (DHTs) tanks (sketched in Figure 2.2) were considered and the test was conducted under the still-water condition. The dynamic feature of oil spilling from ruptured tanks being either below or above the waterline was investigated by some time-dependent variables. Some important characteristics of spilled oil captured by the double-hull space were obtained and the effectiveness of these spaces in terms of retaining oil was influenced by the tank designs and breached hole conditions. From the point of view of reducing oil spilling and prolonging the oil spilling period, the double-hull design had been proved as the optimal solution. However, this study also mentioned that the oil began to spill into the surrounding water as long as the double hull space had become full, regardless of the oil loading and draft condition, which is inconsistent with the snapshots provided or the formula formulated by Yamaguchi and Yamanouchi (1992).

2.2.4 Summary and limitation

Undeniably, experimental investigations can provide some essential knowledge that is useful for exploring the oil spilling phenomena. Table 2.1 lists the relative literatures mentioned above with key details. Generally, the early physical models, which are merely based on the Froude scale similarity, could appropriately reflect the prototype if the area of the interest is located at the ultimate situation. However, such lab model may not be acceptable if the dynamic process of the oil spilling is considered, since the viscous effect on the dynamic spilling behaviour is significant and should be properly scaled (Peter and Lin, 1994). By introducing the Reynolds similarity law to the test oil, the viscous effect on the dynamic spilling process is theoretically and partially

considered in the following physical studies. But, as mentioned by Karafiath and Bell (1992), the examination of these proposed similarity laws governing the extrapolation of oil loss data from the model test was highly encouraged for the future work. This issue becomes more complicated when dealing with the DHT cases, where water plays a more important role when the passage of oil and water travels through the narrow double hull space along with the violent oil-water impact and mixing process.

Table 2.1 A summary of previous experimental studies on the oil spilling problem.

Studies	Similarity criteria	Scale factor	Accidental scenarios	Tank types	Rupture geometry
Karafiath and Bell (1992) and Karafiath (1992)	Froude scaling	15 & 30	Grounding	MDTs and DHTs	Simplified strip punctures (1.5cm*15cm)
Yamaguchi and Yamanouchi (1992)	Froude scaling	50	Grounding & collision	DHTs	Simplified circular punctures (Diameter=2.3~7.1cm)
Simecek-Beatty *et al*. (2001)	Froude & Reynolds scaling	16	Collision	SHTs	Simplified circular punctures (Diameter=2.2cm)
Lu *et al*. (2010)	Froude & Reynolds scaling	40	Collision	SHTs	Simplified circular punctures (Diameter=1.5~3.5cm)
Tavakoli *et al*. (2011)	Froude & Reynolds scaling	30	Grounding & collision	SHTs, DBTs, DSTs and DHTs	Simplified circular punctures (Diameter=1.05~2.2cm)

Due to the presence of ballast tanks, the DHT spilling process contains many dynamic features, such as the oil releasing from the internal cargo tank, traveling through the ballast tank and finally spilling out of the tank. They may be significantly affected by different rupture conditions (e.g., rupture size and locations) and accidental scenarios (e.g., grounding and collision). Although the previous physical studies have carried out parametric studies including many accidental factors, there are still some important accidental factors to be investigated. Moreover, the inconsistent discussions about the dynamic spilling features, especially inside the ballast tank, may cause confusion. A series of model tests are highly required to consider some new accidental factors, from which the different dynamic spilling processes from damaged DHTs can be highlighted providing more detailed observations and hydrodynamic analysis. More importantly, the experimental data can be used for validating the numerical simulation.

Furthermore, all the aforementioned experimental studies are confined to a damaged model tank fixed inside the initially still water tank ignoring the influence of the external dynamic environment and resultant ship motions on the oil spilling process, except for the study of Karafiath (1992) about a grounded mid-deck tanker (MDT). Actually, considering the oil leaking from a damaged tanker in the real ocean environment, the oil spilling affects the loads on the oil tankers and thus their motion, which mutually affects the dynamic behaviour of the spilled oil and

eventually the ultimate oil outflow. This systematic investigation should be regarded as an integrated system covering the external environment (tide, current and wave), the ship motion and the oil leakage. Therefore, it is necessary for researchers to carry out more advanced physical models considering the dynamic behaviour of oil spilling under more realistic dynamic surroundings.

2.3 Analytical Studies

Analytical model can quickly provide some basic information but requires the fundamental knowledge of the oil spilling behaviour. Based on the analysis of the hydrostatic pressure balance across the rupture, the early model yields the necessary final state result. In order to predict the dynamic gravity-induced spilling process, most investigations applied the quasi-steady Bernoulli's principle to simplify the unsteady spilling behaviour from a fixed damaged tank as the continuous steady process in the discrete time domain with the assumption that the flow is steady within the discretised time step and follows the steady Bernoulli's principle. Moreover, some assumptions were made in these models to simplify the complex oil-water interaction inside the ballast tank of DHTs during the spilling process.

2.3.1 Hydrostatic approaches

As the dominant driven force, the hydrostatic-pressure difference across the break is regarded as the key factor in analysing the final state of the oil spilling from a damaged tank. Apart from the employment of the hydrostatic pressure balance principle in the probabilistic studies mentioned above, Yamaguchi and Yamanouchi (1992) derived a formula to predict the final state of oil leakage from a grounded double-hull tank model by introducing a non-dimensional thickness of water layer inside the double-hull space (ζ) based on the balance of hydrostatic head at the rupture and the mass balance concept. The comparison between the experimental and analytical results suggested that the ζ value can be determined from the proposed formula under the deep water draft condition with the assumption of zero oil spilling volume. But due to the uncertainty of variables, this formula had not been employed under the shallow water draft condition. Devanney *et al*. (2006) further systematically explained the physics of tank spilling based on the hydrostatic theory. The different mechanism between the oil leaking through a bottom rupture and a side rupture was discussed. Considering the additional exchange flow induced by the density difference across a side break, the side damage was much worse than the bottom damage.

2.3.2 Hydrodynamic approaches

In order to analytically describe the dynamic spilling process, Fannelop (1994) introduced fundamental principles of unsteady oil outflows driven by the gravity and density difference which occurred in oil leakage from submerged vessels. Some basic assumptions, such as the

volume equivalent flow rates, the determination of flow velocity governed by the hydrostatic pressure difference and the constant flow area, were applied in the following researches.

Fthenakis and Rohatgi (1999) developed an analytical model to calculate the leakage of fluid from a side-damaged vessel submerged in a river, in which the movements of a vessel induced by recovery activities, ocean waves or river current were considered. In this study, two types of vessels, non-vented and vented vessels, were considered, besides, two phases of discharge: (1) the initial phase which lasts until equilibrium of hydrostatic pressures is established across the break ignoring the following exchange flow process, and (2) the following fluid discharge due to pressure variations caused by the tank movements were determined by the analytical model. During the second phase, the complex tank motion associated with the wave-structure interaction was simplified as the periodic vessel movement represented by the oscillation of the break depth which disturbed the hydrostatic equilibrium around the break without considering the sloshing inside the cargo tank or non-linear wave condition in the surrounding water. The quasi-steady Bernoulli equation was adopted with the assumptions that isothermal discharge; incompressible liquid; and liquid and water do not mix inside the vessel. Also, the discharge coefficient (C_d) was employed to consider the energy loss, and the final discharge quantities measured in the laboratory by Dodge *et al*. (1980) were used to verify the model prediction for the first phase. In the case study, the model was applied to a real incident of the release of APG (aromatic pyrolysis gasoline) in the Mississippi River and the oil outflow caused by the gravity and the vessel's movements was predicted. It was noted that as the side break was located at the bottom of the vessel, no water layer was formed inside the vessel during the first gravity-induced discharge phase, in other words, no exchange flow occurred for this collision case. In the sensitivity analysis, the interconnections were studied among the model's parameters, such as the vessel movement (amplitude and period of the barge's movement), puncture location and area, liquid density, discharge coefficient, gas-phase pressure and the fluid saturation pressure under non-vented condition. It is shown that the predictions for both the stagnant and the moving vessel were physically reasonable.

A comprehensive model for predicting the dynamics of spilling from LNG (liquefied natural gas) and oil product tankers in collision accidents was developed by Fay (2003) based on fluid mechanics principles and empirical properties of oil and LNG spilling on the water. This study included both the discharge process and the pool spread behaviours, expressing the significant results (pool area, pool fire duration, heat release rate) in terms of the tanker hold and rupture variables, covering the entire practical range. As for the time-dependent gravity-driven outflow through a side puncture, the discharge was estimated from the inviscid quasi-steady Bernoulli's equation where the phenomena of friction and vena contracta were ignored. For cargo hold punctures that are completely or partially below the sea surface, additional exchange outflow driven by the imbalance of pressure across the rupture due to the different density ensued,

accompanied by sea water intrusion into the cargo hold. But, the corresponding flow rates were not well determined in this paper.

Tavakoli *et al*. (2008) presented an analytical prediction of oil spilling from grounded cargo tankers associated with different configurations including the single-hull, double-bottom and double-hull designs (sketched in Figure 2.2). The quasi-steady Bernoulli's equation was used along with the discharge coefficient (C_d). The analytical result of single-hull tanks was verified against the 2D numerical simulation in terms of the final spilling volume and period. In order to describe the complicated air-oil-water convection motion inside the ballast space between inner and outer shells occurred during the oil leaking from grounded double-bottom and double-hull tanks, the whole spilling process was divided into two steps, i.e., the filling ballast tank step and the outflow or inflow from the tank step. In the first step, it was consistently assumed that the flow of water and oil convected through and filled the empty ballast space without any spilled oil. Two different assumptions about the oil-water mixture state had been embedded, namely, immiscible oil and water flows or a perfectly-mixed oil-water flow. In the second step, after the ballast tank was filled up, the pressure difference across the breaks can determine whether the oil leaked from the tank, or seawater flowed into the ballast. With regard to a high oil loading case, the cargo oil would further spill into the ballast tank through the internal hole. If oil and water were considered to be completely separated, they would be stratified into two layers inside the ballast tank. The underlying water layer delayed the oil drainage and effectively reduced the oil spilling for the double-hull tanker. If the oil and water were assumed to be perfectly mixed, the oily water flowed into the sea and caused larger spilling volume. The difference due to the mixture assumption could be more obvious in analysing the double-hull tank.

Later, based on the similar principle, Tavakoli *et al.* (2009) further developed the previous model proposed by Tavakoli *et al*. (2008) to incorporate the interaction between oil spilling and hydrostatic changes. They indicated that the hull damages can affect the buoyancy of the ship which can also change the draught, trim and heel conditions affecting the pressure distribution around a damaged ship. This would lead to more oil outflow which was called as 'the secondary oil spilling'. In this study, the hydrostatic changes in terms of the draught, trim and heel were determined by 'added/lost weight method' proposed by Schneekluth and Bertram (1998). To eliminate the time lag between the buoyancy changes and oil loss volume, the time domain analysis was applied. Different tank configurations (i.e., single-hull, double-bottom and double-hull, sketched in Figure 2.2) were studied with the immiscible mixture assumption and the result was compared with the study of Tavakoli *et al.* (2008). It was demonstrated that the hydrostatic changes gave a significant rise in the oil outflow rate and the final spilling volume, and the resulting additional oil spilling was dependent upon the damage location. Moreover, the double-hull design had the smallest potential for oil outflow due to groundings.
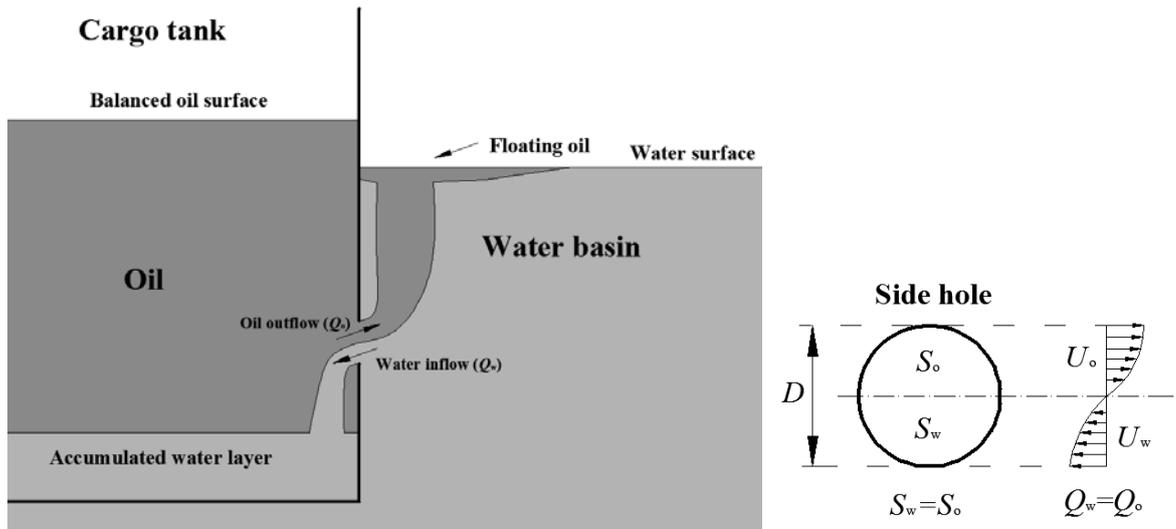
Figure 2.3 The sketch of the exchange flow through the side circular hole after the gravity outflow process and the corresponding flow state through the hole based on the assumptions introduced by Fannelop (1994) (Q_o is the volume flow rate of the oil outflow; Q_w is the volume flow rate of the water inflow; S_o is the hole area occupied by the oil outflow; S_w is the hole area occupied by the water inflow).

Tavakoli *et al.* (2012) conducted an analytical solution for a damaged oil tank during ship collisions. With respect to the gravity outflow, the quasi-steady Bernoulli's equation with discharge coefficient (C_d) was employed for non-vented and vented vessels. The application of the ideal gas law to the ullage pressure in a non-vent vessel derived by Fthenakis and Rohatgi (1999) was adopted. After the gravity outflow process, a combination of water inflow and oil outflow through the side hole resulting from the local pressure imbalance due to the different densities of the fluids, namely exchange flow, was simply described by using basic assumptions introduced by Fannelop (1994), such as the equivalent volume flow rates and the constant equivalent flow areas. Figure 2.3 illustrates the sketch of the exchange flow through a side circular hole (with the diameter of D) and the corresponding flow state through the hole based on the assumptions introduced by Fannelop (1994). The significant effect of puncture height on the final oil spilling volume was indicated for the side-damaged single-hull tanker. Different tank configurations including single-hull and double-side designs (sketched in Figure 2.2) were considered. Similar to the study of Tavakoli *et al.* (2008), no oil leaking into the surrounding water during the early stage was also supposed when dealing with the ballast filling process and the immiscible oil-water mixture assumption was applied. With the C_d value calculated from the two-dimensional numerical model, the analytical solutions for a single-hull and double-side tankers were validated by the corresponding numerical results in terms of time-dependent variables. Based on the results obtained from the proposed analytical model, it was found that a proportion of oil that leaked from the cargo tank may be retained by the ballast tank provided by

the double-side design, and the oil-water mixture in the ballast tank delayed the oil drainage and effectively increased the duration of the oil spilling.

Later, Sergejeva *et al.* (2013) comprehensively modelled the submerged oil spilling from a single-hull or double-hull tankers under collisions or groundings. An internal hydraulics theory proposed by Laanearu and Davies (2007) was employed to demonstrate that the assumption embedded in the study of Tavakoli *et al.* (2012) for the exchange flow from a side hole under the balanced internal and external hydrostatic-pressure situation was reasonable and regarded as the critical-flow solution. With the similar assumption that the hydrostatic overpressure was associated with the initial uni-directional oil outflow that can fill the ballast tank in the case of double-hull tank without any oil spilling out of the tank, some non-dimensional parameters related (e.g., the volume and duration of spilled oil from damaged tanker) were calculated with the inviscid flow ($C_d \approx 1$). The final spilled oil and retained oil volumes predicted by the model were compared with the experimental data provided by Tavakoli *et al.* (2011). A satisfactory agreement was achieved.

2.3.3 Summary and limitation

Table 2.2 lists the previous analytical studies with some key features of the corresponding model. In order to capture the hydrodynamic features of oil spilling from a damaged tank, all the aforementioned investigations applied the quasi-steady Bernoulli's equation, and some of them employed the discharge coefficient (C_d) to consider the vena contracta and energy loss during the spilling process. In these models, the unsteady gravity-induced spilling is regarded as the continuous steady process in the discrete time domain with the assumption that the oil flow is steady within the discretised time step governed by the steady Bernoulli's principle, by which the velocity head of oil flow is related to the potential and pressure heads.

However, it should be noted that when dealing with the oil leaking from a fixed double-hull tanker, some assumptions or simplifications proposed by these studies are probably questioned and need to be verified. For example, according to the lab images provided by the study of Yamaguchi and Yamanouchi (1992), it was clearly shown that the oil began to spill into the secondary water basin at the instant of opening the ruptures. In other words, the processes of oil leaking and filling the ballast tank happened simultaneously. As a result, it can be inferred that the assumption of commencing oil leaking after filling up the ballast tank embedded in Tavakoli *et al.* (2008), Tavakoli *et al.* (2009), Tavakoli *et al.* (2012) and Sergejeva *et al.* (2013) is inappropriate for all cases. Moreover, if the cases are under the same hydrostatic condition initially and finally, this assumption seems to yield the closed spilling curve, which cannot reflect the different dynamic spilling procedures due to different damage conditions as observed by experimental studies (e.g., Yamaguchi and Yamanouchi, 1992). Future works are required to correct this assumption.

Table 2.2 A summary of previous analytical studies on the oil spilling problem.

Relative studies	Governing equations	Tank types and accidental scenarios	Model description and highlights
Yamaguchi and Yamanouchi (1992)	Hydrostatic pressure balance and mass conservation	Grounded DHTs	Only the final state considered; Introduce the variable α; α can be predicted only under limited certain conditions;
Fthenakis and Rohatgi (1999)	Quasi-steady Bernoulli's equation with C_d	Collided SHTs	C_d is custom; Additional spilling occurs due to ship motion expressed by the oscillation of break depth; Ignore the exchange flow through side hole;
Fay (2003)	Quasi-steady Bernoulli's equation without C_d	Collided SHTs	Consider both the discharge process and the pool spread behaviours; Fail to describe the exchange flow through the side hole;
Tavakoli et al. (2008)	Quasi-steady Bernoulli's equation with C_d	Grounded SHTs, DBTs and DHTs	C_d is custom; No oil leaking into water during the ballast filling process at early stage; Different assumptions for oil-water mixture inside the ballast tank;
Tavakoli et al. (2009)	Quasi-steady Bernoulli's equation with C_d	Grounded SHTs, DBTs and DHTs	C_d is custom; Consider the effect of hydrostatic change due to the change of draught, trim and heel conditions on the spilling;
Tavakoli et al. (2012)	Quasi-steady Bernoulli's equation with C_d	Collided SHTs and DSTs	Calculate C_d based on corresponding 2D numerical results; No oil leaking into water during the ballast filling process at early stage; Describe the exchange flow through the side hole;
Sergejeva et al. (2013)	Quasi-steady Bernoulli's equation with $C_d=1$	Grounded or collided SHTs, DSTs, DBTs and DHTs	No oil leaking into water during the ballast filling process at early stage; Use the internal hydraulic theory to describe the exchange flow;

2.4 Numerical Studies

Generally, the experimental studies can provide some macroscopic parameters to reflect the dynamic spilling process, but fail to measure the micro-scale flow fields, especially inside the ballast tank of DHTs. With the purpose of obtaining more detailed unsteady features involved in the oil spilling process, the numerical approach is regarded as a cheaper and more efficient way. Considering the fact that the oil spilling process involves violent impact and complex fluid motion associated with jets, mixing and fluid-structure interaction, the numerical modelling could shed some light on hydrodynamic characteristics, such as fluid viscosity, turbulence and compressibility. Moreover, in order to further develop the knowledge of oil spilling to the more realistic situation, the investigation of interaction among the dynamic external environment (e.g., wave, current and tide), ship motion and the oil spilling could be conducted by the numerical modelling. This section focuses on the related numerical studies and reviews the previous works

in the form of different numerical methods. Finally, the aforementioned concerns will be summarised.

2.4.1 VOF-based methods

As one of the most popular methods, the Finite Volume Method (FVM) incorporated with the interface capturing method, namely, the Volume of Fluid (VOF), had been widely-used for the oil-leaking modelling (Jeong *et al.*, 2012). Peter and Lin (1994) might be the pioneer in the field of performing the numerical simulation of oil leaking from grounded double-hull tankers. A two-dimensional numerical model was established using Flow-3D, which can simulate flows with two densities and interfaces. But, the effects of viscosity and turbulence were ignored in their simulations. Two double-hull configurations: the first one was a 1/30 scale model with or without longitudinal web frames in the ballast tank, which was similar to the model used by Karafiath and Bell (1992); the second one was a full-scale Advanced Double Hull with the U-tank completely open or closed, which was similar to the physical model of Rodd and McCampbell (1994), were investigated. The limitation of the two-dimension assumption, neglecting the viscosity and turbulence effects and zero time lag between the initial oil and water flow were discussed in this paper. Only the instantaneous loss (solely driven by the gravity) was considered by ignoring the additional loss caused by forward speed, tide or sea state. The numerical results shown that the geometry of inner and outer ruptures, the longitudinal web frames inside the ballast tank and the volume of the cargo tank with respect to the U-tank were important factors. Moreover, the cargo tank resonance sometimes led to the suction event which was responsible for forming a water layer in the cargo tank and U-tank reducing further oil ejection.

Recently, using a similar numerical approach, several researches were carried out by using the commercial software 'FLUENT'. Xiao *et al.* (2010) developed a two-dimensional numerical study on the oil spilling from a wrecked (sunken) single-hull ship to explore the motion law of oil leaking from damaged ships and the variation tendency of spilling velocity and volume. Two side holes, respectively located close to the top or the bottom of the tank, were considered. The current, viscosity and turbulence (modelled by the standard k-ε model) effects were incorporated and the numerical result explained the similar dynamic features described in the previous experimental observation (Lu *et al.*, 2010). Subsequently, Lu *et al*. (2010) further established a three-dimensional comparable numerical model to investigate the oil leakage from a side broken opening on a single-hull tanker in still water. The numerical model was verified by comparing with the experimental snapshot at the corresponding instant. The dynamic behaviour of oil spilling was captured in terms of the residue oil volume and mass flow rate through the broken hole. A new variable, namely, the instantaneous oil ratio of the flow through the broken hole was

introduced to specify the different two spilling stages (i.e., the gravity-driven and density-driven stages) in cases of collision.

In order to verify their simplified analytical models, Tavakoli *et al.* (2008) presented a two-dimensional numerical analysis of the oil spilling from a grounded single-hull tanker. The laminar flow was assumed and only the final spilling states (i.e., duration and final oil loss) were compared between the numerical and analytical results. Later, Tavakoli *et al.* (2012) built a similar two-dimensional numerical model for oil spilling from collided tanks. The oil outflow from single-hull and double-side tankers was simulated and compared with the corresponding analytical solutions.

Furthermore, Krata *et al.* (2012) proposed a preliminary three-dimensional model to address the bunker oil spilling problem of a fixed single hull tanker in grounding accidents. Considering the relatively low Reynolds number associated with the oil outflow through the hole, the laminar flow was applied. The effect of different rupture length estimated by the IMO methodology on the oil outflow process and its duration were investigated. It was found that the leaking rate would be significantly decreased with a smaller damaged hole. Moreover, the authors also revealed that the fluctuation of oil discharge rates was attributed to the bubble-like character of the oil outflow.

2.4.2 Particle-based methods

Using the MPS (Moving particle semi-implicit) method introduced by Koshizuka and Oka (1996), Cheng *et al.* (2010) carried out a two-dimensional study to investigate the interaction between the transient process of the oil leakage and the damaged stability of a single-hull crude oil carrier due to collisions. The oil-water multiphase flow with the interface was modelled incorporating the viscosity and surface tension. It was found that the rolling motion of the oil carrier was induced by the leakage at the beginning of the process, when a relatively large amount of oil is released suddenly. Also, the effect of filling ratio and damage height above the keel on the oil leakage and the resultant hull motion was investigated. Based on the comparison between the numerical and analytical results in terms of final list angles, it was clear that the numerical approach was very effective in dynamic conditions where the filling ratio is large and the height of the damaged is low. The limitation of the two-dimensional model and the MPS method was also discussed in this study.

Alternatively, Jeong *et al*. (2012) conducted a two-dimensional numerical study using the PNU-MPS approach (i.e., Pusan-National University-modified Moving Particle Simulation) developed by Lee *et al.* (2011). The phenomena of oil leaking from a puncture in a side or bottom hull of a single-hull tank model were simulated. The viscous effect was included in the current model test and the numerical results agreed well with the analytical solution obtained by the quasi-steady

treatment of Bernoulli's equation (namely, Torricelli's equilibrium equation in this paper) with the experiment-measured discharge coefficient (namely, Torricelli's factor in this paper).

2.4.3 Summary and limitation

The numerical simulation can provide more spatial-temporal details than experiments, giving further insight into the unsteady oil leaking mechanism. Based on the foregoing investigations, a brief summary is presented in Table 2.3.

However, most of the aforementioned studies were trapped in the two-dimensional condition or over-simplified models. Although the two-dimensional model can shed some light on the hydrodynamic spilling features from which the related analysis can be provided, many researchers (e.g., Peter and Lin, 1994; Cheng *et al*., 2010) pointed out the unlimited longitudinal extension of the opening without considering dimension variations and no flow longitudinally in the two-dimensional simulation may not properly reflect the flow motion through the broken hole or inside the three-dimensional ballast space of DHTs. Also, the two-dimensional condition narrows the comparability between the numerical and experimental results, since most of the previous experiments simplified the puncture as a circular broken hole with a significant three-dimensional effect (see Table 2.2).

In the framework of the model establishment, it is important to recognize the importance of every potential physical issue which may affect the spilling behaviour under different situations. As mentioned by Peter and Lin (1994), it should be noticed that a wide range of physical flow scales with complex geometries could change the predominant force widely during the spilling process. Due to the different tank configurations, the unique features of fluid state in the DHT cases, particularly in the ballast tank of DHTs, where both jet flows and free shear layers appear as observed in the lab tests mentioned in the previous section, are considerably different from that in the SHT cases and show the presence of turbulence characteristics. However, few studies have discussed the turbulence modelling and behaviour for the DHT cases. Moreover, due to the different spilling features, the previous numerical studies on the case of SHTs cannot guide a reliable criterion for implementing an appropriate turbulence model in the DHT cases.

Furthermore, considering the sudden fluid-fluid or fluid-structure impacts associated with the jets of oil outflow and water inflow (either strikes on the walls of the ballast tank or the interaction between them occurs during the spilling processes) and the interaction between entrapped air bubbles in the oil/water mixture and fluid states (such as velocity, vorticity and turbulent kinetic energy) in the ballast tank of DHTs, the effect of the air compressibility may play important role in the dynamic spilling process, but this issue has not be addressed so far.

Table 2.3 A summary of previous numerical studies on the oil spilling problem.

Relative studies	Numerical approaches	Model validation	Model description
Peter and Lin (1994)	FVM-VOF	None	2D condition; Fixed double-hull tankers under groundings; Neglect viscosity, turbulence and surface tension effects;
Xiao *et al.* (2010)	FVM-VOF	The oil jet pattern was compared with the experiment of Lu *et al.* (2010)	2D condition; Fixed wrecked single-hull tankers under collisions; Consider current, viscosity and turbulence effects; Use standard k-ε model;
Lu *et al.* (2010)	FVM-VOF	The oil jet pattern was compared with their own experimental snapshots	3D condition; Fixed single-hull tankers under collisions; Consider the viscosity and turbulence effect; Use standard k-ε model; Specify different spilling stages;
Tavakoli *et al.* (2008)	FVM-VOF	Comparing with the proposed analytical model in terms of the final state variables	2D condition; Fixed single-hull tankers under groundings; Neglect turbulence and surface tension effects;
Tavakoli *et al.* (2012)	FVM-VOF	Comparing with the proposed analytical model in terms of the time-dependent variables	2D condition; Fixed single-hull and double-side tankers under collisions; Neglect turbulence and surface tension effects;
Krata *et al.* (2012)	FVM-VOF	None	3D condition; Fixed single-hull bunkers under combination of groundings and collision; Neglect turbulence and surface tension effects;
Cheng *et al.* (2010)	MPS	The final list angle was compared with the one obtained from the quasi-static calculation using the software 'SSTAB'	2D condition; Single-hull tankers under collisions incorporating the ship stability; Consider viscosity and surface tension effects;
Jeong *et al.* (2012)	PNU-MPS	Comparing with the analytical solution in terms of the time-dependent variables	2D condition; Fixed single-hull tankers under collisions and groundings; Neglect turbulence and surface tension effects;

To reflect the real spilling in the open sea, estimating the interaction among the dynamic external environment (e.g., wave, current and tide), ship motion and the oil spilling is necessary. However, the advanced numerical simulation accounting for this issue is rarely found.

2.5 Summary

According to the relevant researches in the preceding sections, although the oil spilling from damaged tankers has been investigated extensively for several decades, there are still many gaps to be filled.

Generally speaking, the oil spilling from a damaged ship is essentially a dynamics-dominated multi-phase flow problem with typical features of orifice flows, mixing, impact and interfacial shear layer, even for a fixed tank in still water. Moreover, the dynamic spilling procedures may be significantly affected by different accidental scenarios and tank designs yielding different spilling rates and durations. It may be more complicated to address a real oil tanker subjected to a damaged condition due to collisions or groundings. The oil spilling affects the loads on the oil tanker and thus its motion, which may mutually influence the behaviour of the spilled oil and eventually the ultimate oil outflow. This implies that the dynamic process of the oil spilling should be considered properly in order to comprehensively and accurately estimate the accidental spilling problem. If the area of the interest is in the ultimate oil outflow from damage tanks, the existing probabilistic/hydrostatic approach based on the hydrostatic pressure balance is a relatively convenient and extensive way to estimate this complicated issue. But they may not be acceptable if the dynamic process of the oil spilling is concerned.

Researchers advanced the understanding of oil spilling mechanism by using the experimental, analytical and numerical models. The physical model was improved by considering the Reynolds scale similarity to the test oil. Although previous experimental studies have carried out parametric studies including many accidental factors to investigate the hydrodynamic spilling features for DHT cases, there remains some important accidental factors to be investigated. Furthermore, considering the inconsistent discussions of the dynamic spilling features for DHT cases, a series of new DHT model tests are required to provide more detailed observation, measurement and hydrodynamic analysis.

Using hydrodynamic analytical models, the whole unsteady spilling process was simplified as the continuous steady process in the discrete time domain governed by the quasi-steady Bernoulli's equation. In order to describe the more complicated spilling process from advanced tank configurations (e.g., DHT, DBT and DST), some simplifications/assumptions (i.e., no oil spilling out of the DHT at the first filling ballast tank stage regardless of the hydrodynamic condition) were introduced, but questioned according to the experimental observation (Yamaguchi and Yamanouchi, 1992). Moreover, these simplifications/assumptions may affect the capability of the current analytical model to accurately predict different dynamic spilling procedures under different damage conditions. Future improvement is required.

The numerical model can provide more spatial-temporal details involved in the oil spilling process, from which the knowledge can be advanced by investigating the importance of different physical features (e.g., turbulence and compressibility) and considering the oil spilling in the more realistic environment. Many numerical studies concentrated on this topic using different numerical methods. However, considering the more complex flow motion (including jet interactions, impact and mixing) during the oil spilling from damaged DHTs, many uncertainties of numerical modelling, such as how to implement turbulence models and whether to consider air compressibility, should be examined. Besides that, there are few comprehensive numerical models considering the interaction among the dynamic external environment, ship motion and oil spilling.

Chapter 3 Experimental Investigation on Oil Spilling from Fixed Damaged DHTs

As mentioned in the previous chapter, previous experimental studies generally described the violent dynamic features during the oil spilling from damaged tanks and found that the dynamic spilling process was affected significantly by the different tank configurations and accidental situations. However, there are still inconsistent discussions about the dynamic spilling process in DHT cases to be clarified through detailed observations and hydrodynamic analysis. In this study, a series of physical cases are conducted at the laboratory centre of Zhejiang Ocean University, China to investigate the oil spilling from a fixed damaged DHT. The purpose of current lab tests is not only to further explore dynamic behaviours of oil spilling from a damaged double-hull tank, but to extend the knowledge on some important accidental factors which haven't been studied by the previous parametric studies. Besides that, the experimental measurement is used as the reference data for the model validation in the following numerical investigation.

One may agree that the selection of new accidental factors shall not only reflect the real accidental situation, but also lead to different hydrodynamic processes ideally under the same initial and final hydrostatic conditions. Based on this concept, the effect of different axial offsets of the bottom openings under groundings and initial water thicknesses inside the ballast tank under collisions on the oil spilling process is discussed, respectively. In grounding scenarios, the change of axial offsets between the inner plating and outer plating holes simply represents different damage situations associated with the ship bottom impact. With respect to the collisions, since the rupture on the inner hull plating could be initiated later comparing to that on the outer hull plating in some accidental collisions, the surrounding water could flow into the ballast space forming a water layer prior to the beginning of oil releasing from the cargo tank. Thus, in this study, this time lag between the initiation of the water and the oil flows is represented by different initial thicknesses of water layer inside the ballast tank. Following this assumption, the oil and water jets occur simultaneously in each case. According to the different spilling features, the whole spilling process in each case is divided into several stages and the corresponding observation, hydrodynamic explanation and correlation analysis are provided.

3.1 Similarity Criteria

Similar to the previous works of Karafiath (1992) and Simecek-Beatty *et al.* (2001), since the full-scale experiment is infeasible, the current cargo model is simplified as a small-sized,

stationary and vented tank. It is important to demonstrate that the oil leakage from the model tank is caused by the same hydrodynamic mechanism that results in the oil spilling from a prototype. Simecek-Beatty *et al*. (2001) introduced some conventional similarity criteria including both geometric and dynamic similarities, which are employed herein.

3.1.1 Geometric similarity

The geometric similarity was established when all body dimensions in all three coordinates have the same linear-scale ratio (λ) between a model and prototype (White, 1998). To achieve this, a model tank was built at 1/40 scale of a wing cargo tank section of a reference double-hull Very Large Crude Carrier (VLCC) (Thomae, 1995; Karafiath, 1992; Papanikolaou *et al*., 2010) with simplified middle part ignoring details of the internal support structures inside the ballast space. However, due to the restriction of craftsmanship and materials, the correct scale factor failed to be applied to the hull thickness (the average real hull thickness for VLCC is around 2cm (Gaspar *et al*., 2016)), which may affect the discharge rate and thus, the wall thickness of the model tank (t_g) is kept as thin as possible to be a constant (1cm).

3.1.2 Dynamic similarity

Based on the geometric similarity, the dynamic similarity exists simultaneously with the kinematic similarity, if the model and prototype force and pressure coefficients are identical (White, 1998). Considering the oil releasing from a punctured and vented tank, the dominated forces shall be gravitational, inertial and viscous forces ignoring the effect of surface tension (Simecek-Beatty *et al*., 2001; Karafiath, 1992). Some non-dimensional parameters that are useful for scaling these forces in fluid flows are employed thereafter:

The Froude number, *Fr*, relates the inertia force to the gravity force:

$$Fr = \left(\frac{u}{\sqrt{gh}}\right)_p = \left(\frac{u}{\sqrt{gh}}\right)_m \qquad (3\text{-}1)$$

where u is the outflow velocity; g is the acceleration due to gravity; h is the fluid level and the subscripts p and m refer respectively to the prototype and model. Because the velocity in both prototype and model is mainly driven by the gravitational head (i.e., the kinematic similarity), i.e., $\frac{u_p}{u_m} = \sqrt{\lambda}$, then equation (3-1) is trivially satisfied.

The Reynolds number, *Re*, relates the inertia force to the viscous force:

$$Re = \left(\frac{\rho u D}{\mu}\right)_p = \left(\frac{\rho u D}{\mu}\right)_m \qquad (3\text{-}2)$$

where ρ is the density of the fluid; D is the hole diameter and μ is the dynamic viscosity. Considering the much smaller μ and D for model test than an actual catastrophic spilling from the

prototype, a dramatic change in the physical properties of the test fluid would be required to achieve a similar *Re* condition for both prototype and model. Therefore, the above equation can be expressed in terms of the kinematic viscosity ($v=\mu/\rho$)

$$\frac{v_m}{v_p} = \frac{u_m D_m}{u_p D_p} = \frac{1}{\sqrt{\lambda}}\frac{1}{\lambda} = \frac{1}{\lambda^{3/2}} \tag{3-3}$$

which implies that for a scale factor of 40, the required kinematic viscosity of the test fluid should only be approximately 1/253 of the real fluid. It should be noticed that the DHT spilling is a multiphase flow problem including both oil and water flows. Ideally, both fluids shall follow the Reynolds scaling law. As for choosing the test oil, according to Tavakoli *et al.* (2011) and Udeagbara (2009), the kinematic viscosity of extra heavy crude oil ranges 1.73×10^{-3}-5.75×10^{-3}m^2/s (with the dynamic viscosity ranging 1.5-5Pa·s and the density larger than 870kg/m^3) corresponding to the kinematic viscosity of the test oil ranging 6.84×10^{-6}-2.27×10^{-5}m^2/s. It is also important to ensure the test oil has the similar density to the extra heavy crude oil, because the density ratio may be critical for multiphase flow. Moreover, an added benefit would be if the product is relatively innocuous in the laboratory environment with the relatively cheap product and waste disposal costs. Based on these criteria, the canola oil is chosen as the most suitable test oil. However, the Reynolds scaling law does not work on the water since it is hard to choose a replacement test fluid (Simecek-Beatty *et al.*, 2001). The physical properties of fluids used in the experiment are listed in Table 3.1.

Table 3.1 Physical properties of fluids at 15 ℃.

Fluids	Density (ρ, kg/m^3)	Dynamic viscosity (μ, Pa·s)	Kinematic viscosity (v, m^2/s)
Water	998	1.0×10^{-3}	1.0×10^{-6}
Canola oil	915	2.93×10^{-2}	3.2×10^{-5}

3.2 Experimental Setup
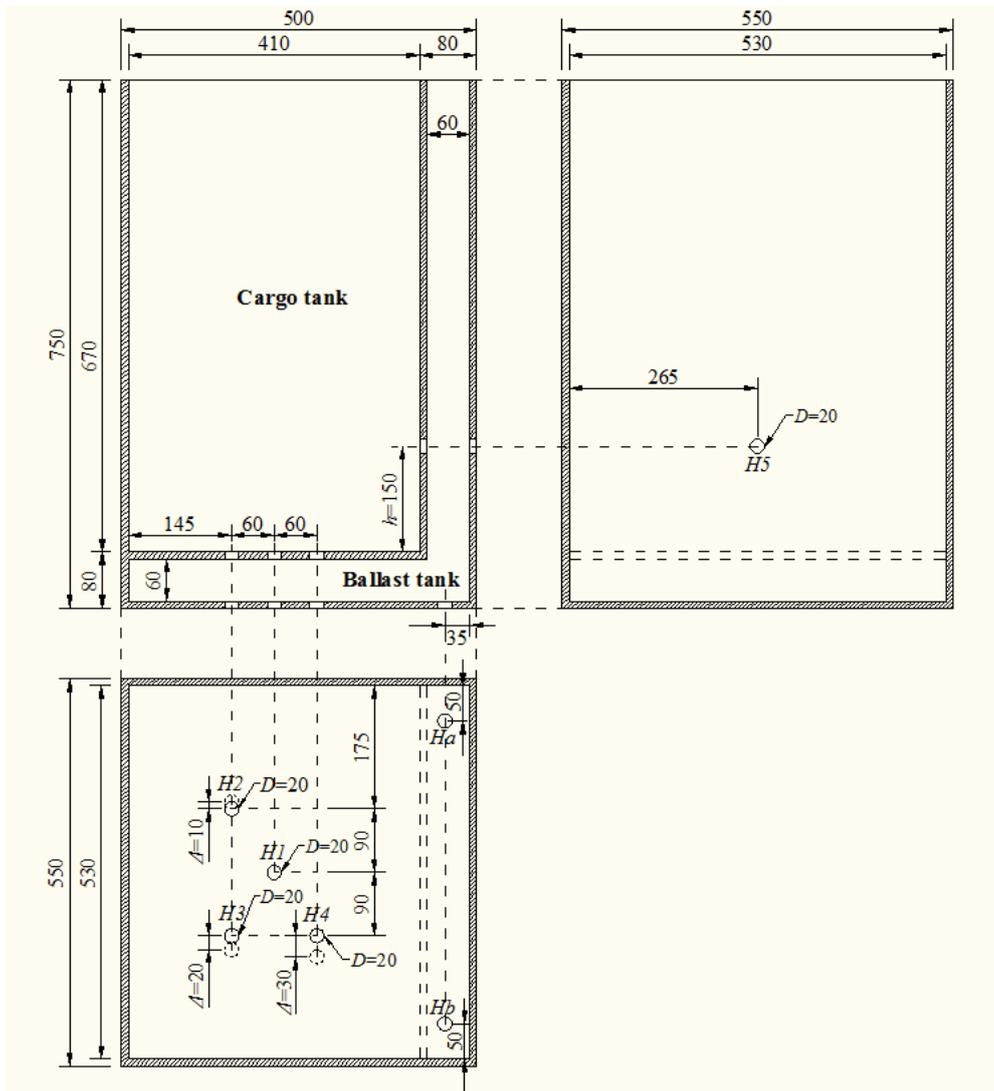
Figure 3.1 Dimensions of double-hull tank model and the location of broken holes (unit: mm).
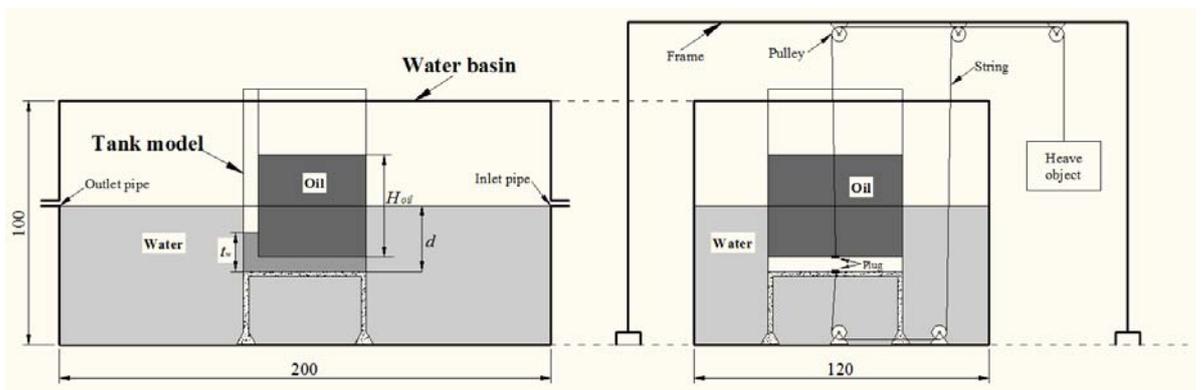
Figure 3.2 Sketch of the experiment configuration (unit: cm).

Similar to the work done by Karafiath (1992), one individual wing cargo compartment associated with a J-shape double-hull space is used in this study (sketched in Figure 3.1). The height, breadth and length of the external hull are 0.75m, 0.5m and 0.55m, respectively. The J-shape double-hull

50

space consists of the bottom ballast space with 6cm in height (H_b) and the side ballast space with 6cm in width (H_s). The model is made of watertight plywood and glass for visual observations and the thickness of the glass wall (t_g) does not follow the exact geometric similarity as mentioned above, but is taken as 1cm. For simplification, the tank model is initially fixed on a supporting frame inside a secondary water basin with dimensions of 2m*1.2m*1m as illustrated in Figure 3.2. The water in the water basin is initially at rest. Inlet/outlet pipes are connected to the water basin, which along with the relatively large free surface of the secondary tank ensure a thin oil layer formed by the spilled oil maintaining a constant draft during the experiment.

Since the instantaneous destruction process and the resultant damage extent due to ship groundings and collision are far beyond the scope of the present study, the grounded and collided damage is simply specified by a smooth-edge circular puncture (2cm in diameter, D) drilled into the tank bottom plates and the tank side plates, respectively (Karafiath, 1992; Yamaguchi and Yamanouchi, 1992; Tavakoli *et al*., 2011). The corresponding rupture size in the prototype is one of the most representative damage samples (IMO, 2004a). Any structural deflections and potential blockage effects caused by the obstacles creating the ruptures in full scale are not modelled. The hole distribution can be found in Figure 3.1. Each case composes of one hole on the external hull (referred to as the external hole and marked by solid circles in Figure 3.1) and one hole on the internal hull (referred to as the internal hole and marked by dashed circles in Figure 3.1). In the existing experimental and numerical studies, these groups of holes are restrictedly configured to be coaxial and orthogonal to the hull surface (Lu *et al*., 2014). In this study, four grounding cases with different axial offsets (Δ=0, 1, 2 and 3cm corresponding to H_1, H_2, H_3 and H_4, respectively) between the centres of the internal and external holes are considered. Compared to the existing coaxial configuration, the consideration of the axial offset widens the range of the application, bringing the experiment a step further to the reality. The space between the bottom of the double-hull model tank and the water basin is 30cm representing the narrow space underneath the double-hull tank in real grounding accidents. As for the collision scenarios, in this study, one set of punctures is attached coaxially on the side plate of the tank model (i.e., H_5). Due to the time lag between the initiation of the water and the oil flows in some incidents, the effect of the different initial thicknesses of water layer inside the ballast tank (t_w=0, 6 and 26cm) on collided spilling is first investigated. In order to simulate the oil spilling due to collisions in open waters, the water basin wall keeps far away from the side hole as sketched in Figure 3.2.

Both the inner and outer punctures are sealed tightly by small plugs before starting each test. For each case the corresponding holes are opened simultaneously and the others remain closed. As illustrated in Figure 3.2, an opening apparatus associated with cables and pulley assembly can ensure that the external and internal plugs are removed simultaneously. The test starts from opening holes via pulling plugs driven by a heavy falling body and terminates when the oil level

in the cargo tank has been kept constant for two minutes. However, due to the time limitation, the exchange flow caused by local pressure differences is excluded in collision tests.

PTP703 level sensors, which continuously convert the measured pressure signal (at a frequency of 5.0 Hz) into the liquid level output (with a resolution of 0.2mm and an accuracy of ±0.4mm) with the pre-defined liquid density, are used in the lab tests. The level sensors are located logically and used to measure the mean level of the oil surface in the cargo tank and that of the oil/water mixture in the ballast tank (illustrated in Figure 3.3). The sensitivity and the accuracy of the sensors have been initially tested and calibrated in an oil tank to ensure an accurate reading. For each case, the time histories of the level of water/oil mixture in the ballast tank, H_{mixture} (measured from the bottom of the ballast tank), and the height of the oil in the cargo tank, H_{oil}, are recorded and the whole spilling process is recorded by two HD cameras.

Different accidental factors considered in this study may cause different dynamic fluid motions inside the ballast tank, which may lead to a large amount of water flowing into the ballast tank in some cases and, thus the density of the oil/water mixture inside the ballast tank changes with time. This may cause faults in the measuring instrument and affect the accuracy of the oil/water mixture measurement in the ballast tank (i.e., H_{mixture}). To deal with this systematic uncertainty, two metric rulers (with a resolution of 1mm) attached to different locations of the tank model are used to manually record the surface elevations instead. All the tests are carried out in a controlled environment with the temperature of 10±3°C to mitigate the systematic uncertainty caused by the temperature. With respect to the random uncertainty, tests on all cases have been duplicated and the mean differences in terms of the time history of the measured data are within 1%.

As mentioned by Tavakoli *et al.* (2008) and Devanney *et al.* (2006), most crude carriers are loaded such that the internal oil pressure at the ship bottom level is greater than the external sea pressure. Thus, in this study, the initial oil level in the cargo tank ($H_{\text{oil}(t=0)}$) is set as 42cm for grounding cases and 38cm for collision cases respectively with constant 27cm water draft (*d*). Table 3.2 summarises the tests considered in this study.

Figure 3.3 Details of experimental facilities.

Table 3.2 Summary of the test cases.

Tests	Scenarios	Spilling hole group	Initial oil height; $H_{oil(t=0)}$ (cm)	Axial offsets; Δ (cm)	Initial water thickness in ballast tanks; t_w (cm)
G1	Grounding	H1	42	0	0
G2	Grounding	H2	42	1	0
G3	Grounding	H3	42	2	0
G4	Grounding	H4	42	3	0
C1	Collision	H5	38	0	0
C2	Collision	H5	38	0	6
C3	Collision	H5	38	0	26
Note: The diameters of the holes (D) are all 2cm; the drafts of the DHT (d) are all 27cm.					

3.3 Result Analysis and Discussions

Considering the fact that the dynamic behaviours of spilling processes under the different accidental scenarios are quite different, the following discussion consists of two parts: grounding scenarios and collision scenarios.

3.3.1 Observation of oil leakage in grounding scenarios

In order to understand the dynamic process of oil leaking from a double-hull tank under groundings, the Case G1 with coaxial holes ($\Delta=0$) is selected as an illustration case and some snapshots recorded near the puncture area at different time instants are shown in Figures 3.4, 3.5 and 3.6. Also, the time histories of the oil height in the cargo tank (H_{oil}) and the oil-water mixture height in the ballast tank ($H_{mixtrue}$) are shown in Figure 3.7(a), together with the corresponding

volume variables (Figure 3.7(b)) calculated directly using the measured data (H_{oil} and H_{mixtrue}). Through the analysis of the process from the instant the holes are opened to the instant the hydrostatic pressure equilibrium is achieved, the whole spilling process is characterized as three typical stages associated with different features involved:

At the moment when opening both the ruptures of internal hull and external hull simultaneously, water flows into the ballast space against the opposing oil outflow, and then these two opposite jets impact with splashing, as shown in Figure 3.4(a). Considering the higher potential head difference between the internal hole and the oil-air interface in the cargo tank than that between the external hole and the air-water interface in the water basin, the resulting velocity of and the momentum carried by the oil flow are greater than these of the water flow. Moreover, the gravity may accelerate the downward oil flow meanwhile decelerate the upwelling water flow. Therefore, the impact position is moved towards the external hole from the first instant of impact, and eventually oil begins to spill into the water basin when the impact point travels across the external hole (Figure 3.4(b)). It is consistent with the experimental observation provided by Yamaguchi and Yamanouchi (1992), but in contrast with the assumption embedded in the analytical model of Tavakoli *et al*. (2008). In this study, the aforementioned process is referred as the transient stage including the transition from static to dynamic conditions with violent water-oil jet impacts.
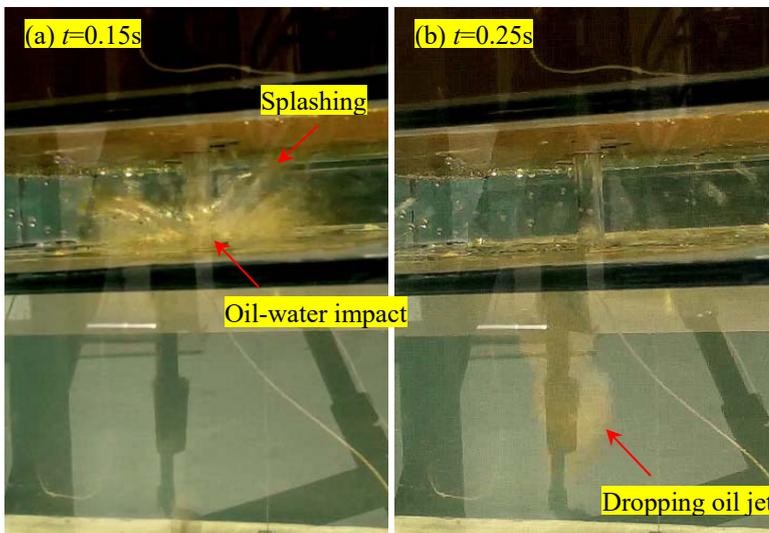
Figure 3.4 Flow states near the puncture at transient stage (Case G1).
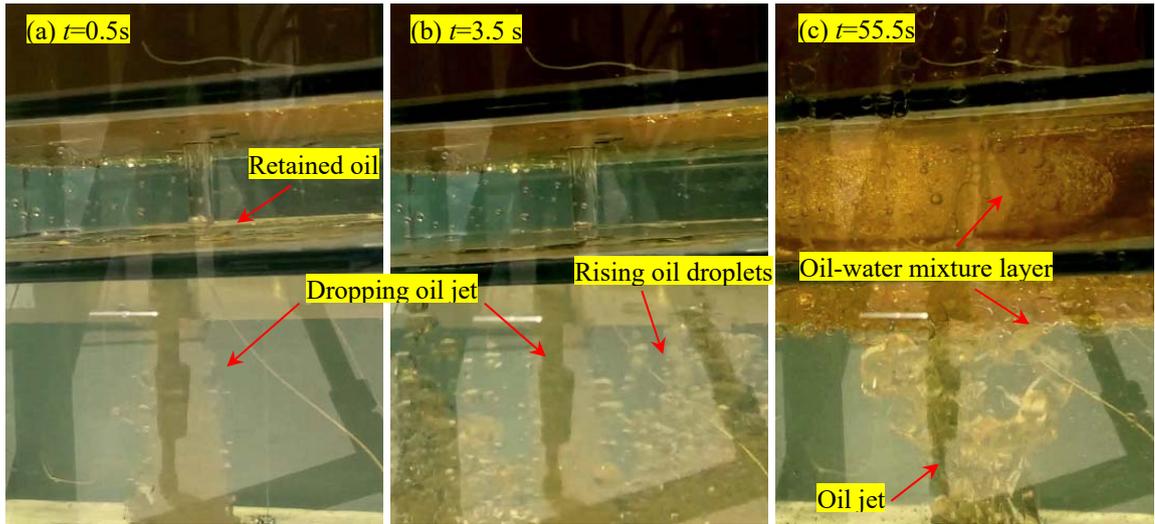
Figure 3.5 Flow states near the puncture at second stage (Case G1).
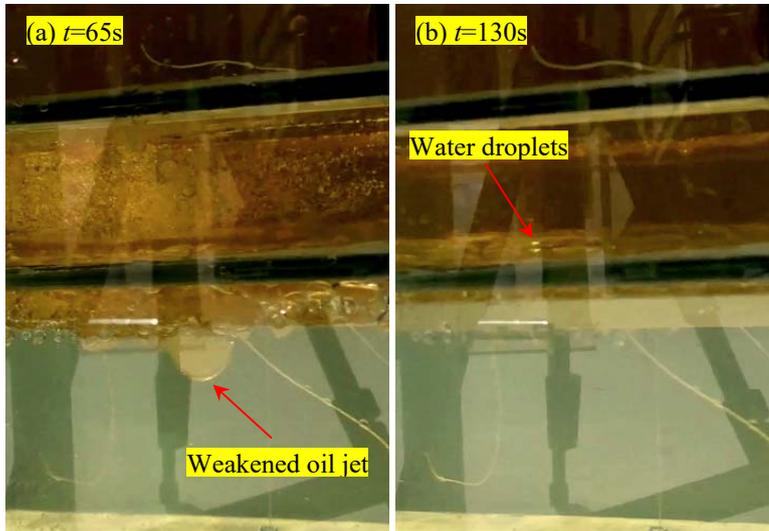
Figure 3.6 Flow states near the puncture at third stage (Case G1).
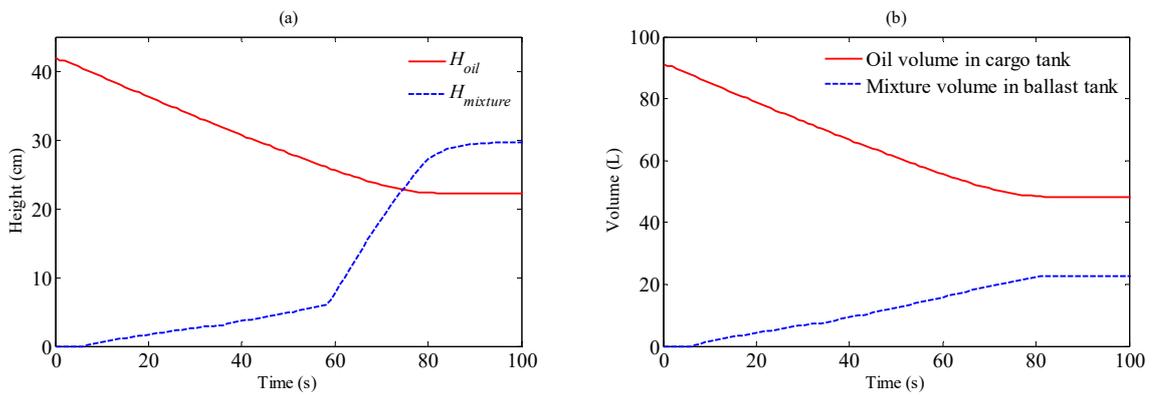
Figure 3.7 Time histories of (a) the oil height in the cargo tank (H_{oil}) and the oil-water mixture height in the ballast tank ($H_{mixtrue}$) and (b) the oil volume in the cargo tank and the oil-water mixture volume in the ballast tank for the Case G1.

The second stage lasts around 58s from the instant that oil begins to spill into the water basin to the situation that the oil-water mixture fills the bottom ballast space (namely, $H_{\mathrm{mixtrue}}=H_{\mathrm{b}}$). Figure 3.5 illustrates flow states near the puncture at some typical instants. During this stage, since both the internal hole and the oil surface in the cargo tank are exposed to the atmosphere, the oil jet releasing from the internal hole manifests as the free orifice flow dominated by the oil height in the cargo tank. This can be further demonstrated by the correlation between the average velocity head across the internal hole (i.e., $\frac{u_i^2}{2g}$, where g is the gravitational acceleration; u_{i} is the average velocity through the internal hole calculated by H_{oil}) and the hydraulic head difference between the oil-air interface of the cargo tank and the centre of the internal hole ($\varDelta H_{\mathrm{i}}$) presented in Figure 3.8. The proposed hydraulic head difference consists of the pressure head difference (i.e., $\frac{\varDelta p}{\rho_o g}$, where ρ_{o} is the density of oil; $\varDelta p$ is the pressure difference between the oil-air interface of the cargo tank and the centre of the internal hole. For the free orifice flow, $\varDelta p$=0) and the potential head difference (i.e., H_{oil}) between the oil-air interface of the cargo tank and the centre of the internal hole. There is a strong linear relationship between these two variables over this stage (with R^2=0.99). This means that the instantaneous average velocity head of the orifice flow can be predicted by the corresponding hydraulic head with a constant ratio, based on which the time history of flow velocity can be solved over this period.

When the oil jet is travelling through the external hole, part of the leaving oil from the cargo tank is captured by the ballast tank forming an oil-water mixture layer at the bottom of ballast space as shown in Figure 3.5(a) and Figure 3.7. But, no water entering the ballast tank is observed. As more oil spilling into the water basin, the exit oil jet extends downward and is shattered into small oil droplets resulting from the large velocity gradient and the resultant shearing stress on the oil-water interface (Figure 3.5(b)). These oil droplets in the water column decelerate, suspend and float governing by combined effects of buoyance force, self-weight, viscous drag force/added mass force and surface tensions. Finally, it can be seen in Figure 3.5(c) that certain amount of oil is accumulated underneath the bottom of the double-hull model tank. Also, with the falling oil height in the cargo tank and rising mixture level, the pattern of exit oil jet changes from small droplets to large blocks. Based on the above observation, the assumption proposed in the work of Tavakoli *et al*. (2008) that there is no oil spilling out during filling the ballast tank may be questioned.

When the internal hole is submerged by the oil-water mixture (H_{mixtrue} exceeds H_{b} in Figure 3.7(a)), the spilling process enters a new stage. The oil jet from the internal hole switches to the submerged orifice flow affected by both the oil height in the cargo tank and the mixture level in the ballast tank. This is reflected by another linear relation (with R^2=0.99) in Figure 3.8, before which one short nonlinear-correlation transitional period lasting about 5s is found although. For this

submerged orifice flow, the mixture above the cargo bottom contributes the pressure head difference of the hydraulic head difference (i.e., $\frac{(H_{mixture}-H_b)\rho_m g}{\rho_o g}$, where ρ_m is the density of mixture. Here, it is assumed $\rho_m = \rho_o$ considering the fact that the vast majority of the mixture is oil). It is also clearly shown in Figure 3.7(a) that the time history of $H_{mixture}$ has a sudden rising when $H_{mixture}$ reaches the height of the bottom ballast space (H_b). This is caused by a sudden change of the horizontal cross-sectional area of the ballast tank at this position (see Figure 3.1 for details). But the mixture volume in the ballast tank still experiences a smooth ascent indicated in Figure 3.7(b). Figure 3.6 displays the corresponding flow state at two instants. It is observed that the exiting oil stream mitigates and finally disappears as the oil height in the cargo tank decreases (Figure 3.6(a) and (b)). At the end of the process, it can be clearly found that the most majority of the mixture inside the ballast space is oil with some droplets of water lying on the ballast tank bottom as shown in Figure 3.6(b). The whole spilling process of case G1 took around 90s resulting in 43.03L oil (47.15% of total oil) spilled from the cargo tank. If neglecting the final volume contribution of small water droplets inside the ballast tank, there are 22.71L oil (52.8% of spilled oil from the cargo tank) left in the ballast tank and 20.32L (47.2% of spilled oil from the cargo tank) oil spilled into water basin (Figure 3.7(b)). It supposes that the double-hull tank design is very effective under the current condition in terms of the capability to capture oil outflow from the cargo tank.
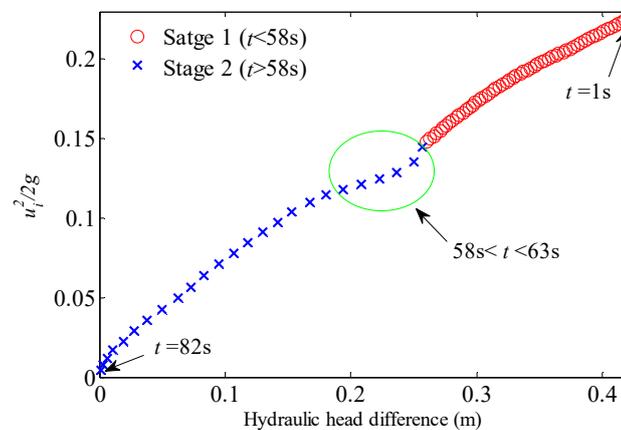
Figure 3.8 Correlation between the average velocity head across the internal hole and the hydraulic head difference between the oil-air interface of the cargo tank and the centre of the internal hole in Case G1.

It is interesting to find that the two linear relationships in Figure 3.8 reveal the possibility of empirical formulas for describing the oil discharge through the internal hole using the Bernoulli's principle. To do so, considering the presence of the mixture flow inside the ballast tank, the whole process should be divided into two stages if the short transitional period between them is ignored. One is characterized as the free orifice flow process lasting until the oil-water mixture in the

ballast tank reaches the bottom of the internal plate (t <58s). The other is treated as the submerged orifice flow as the $H_{mixture}$ exceeds H_b (t >58s).

The quasi-steady Bernoulli's principle shall be employed to calculate the outflow rate from the internal hole. In order to consider the vena contracta and the energy loss on the orifice flow, the discharge coefficient (C_d) is introduced to relate the real discharge ($Q_i=u_iA_h$, where A_h is the hole area) to the ideal discharge ($Q_{i0}=u_{i0}A_h$, where u_{i0} is the theoretical average velocity through the internal hole) through the internal hole, i.e., $C_d=Q_i/Q_{i0}=u_i/u_{i0}$. Considering the Bernoulli's principle for the flow through the internal hole ($\frac{u_{i0}^2}{2g} = \Delta H_i$) and the definition of the discharge coefficient, the discharge coefficient can be determined from the slope of linear correlation displayed in Figure 3.8. Moreover, based on the previous discussion, two individual constant C_d values corresponding to the two linear relationships (with different slopes) should be applied to the two stages respectively.

As for the first free orifice flow stage, the time-dependent oil height in the cargo tank can be expressed as (Tavakoli *et al*., 2008):

$$H_{oil}(t) = \frac{u_{i0(inital)}^2}{2g} - \frac{C_{d1}A_h t}{S_c} u_{i0(initial)} + \frac{C_{d1}^2 A_h^2 g t^2}{2S_c^2}$$ (3-4)

where C_{d1} is the discharge coefficient for the first stage; A_h is the hole area; S_c is the cross-section area of the cargo tank; t is the time; and $u_{i0(initial)}$ is the theoretical initial velocity through the internal hole which can be calculated by the Bernoulli's equation:

$$u_{i0(initial)} = \sqrt{2gH_{oil}}\big|_{t=0}$$ (3-5)

After the $H_{mixture}$ exceeds H_b (6cm), the oil outflow from the internal hole is characterized as the submerged orifice flow. As a result, the mixture height above the internal hole level in the ballast tank (expressed as $H_{mixture(t)} - H_b$) should be considered in the above quasi-steady Bernoulli's equation:

$$H_{oil(t+\Delta t)} = \frac{\rho_m(t)}{\rho_o}[H_{mixture(t)} - H_b] + \frac{u_{i0(t)}^2}{2g} - \frac{C_{d2}A_h\Delta t}{S_c} u_{i0(t)} + \frac{C_{d2}^2 A_h^2 g \Delta t^2}{2S_c^2}$$ (3-6)

where C_{d2} is the discharge coefficient for the second stage; $\rho_{m(t)}$ and ρ_o are the oil-water mixture and oil density; H_b is the height of the ballast bottom space; Δt is a small time interval. However, considering the time-dependent mixture height in the ballast tank ($H_{mixture(t)}$) as shown in Figure 3.7(a) during the period of 58-90s, the theoretical velocity ($u_{i0(t)}$) is also varied with time and determined as:

$$u_{i0(t)} = \sqrt{2gH_{oil(t)} - \frac{2\rho_{m(t)}}{\rho_o}g[H_{mixture(t)} - H_b]}$$

(3-7)

According to the observation mentioned above, the mixture in the ballast tank is composed mainly of the oil captured by the ballast tank. Thus, the $\rho_{m(t)}$ is approximately equivalent to ρ_o for this case. The experimental data (i.e., $H_{mixture}$) and time-domain analysis (time-stepping technique) are employed to solve these equations.

Figure 3.9 compares the oil height in the cargo tank measured in the experiment and that predicted based on Equation (3-4) and Equation (3-6) for the whole spilling process. It is surprised to notice that the whole process of the oil spilling from the internal hole can be satisfactorily predicted by the two proposed empirical formulas, if two different constant discharge coefficients are estimated from the curves in Figure 3.8. This good agreement implies that the dominated factor driving the oil flow through the internal hole is mainly the proposed hydraulic head difference between the oil free surface in the cargo tank and the internal hole. In other words, the mixture level plays a significant role in the internal hole discharge.
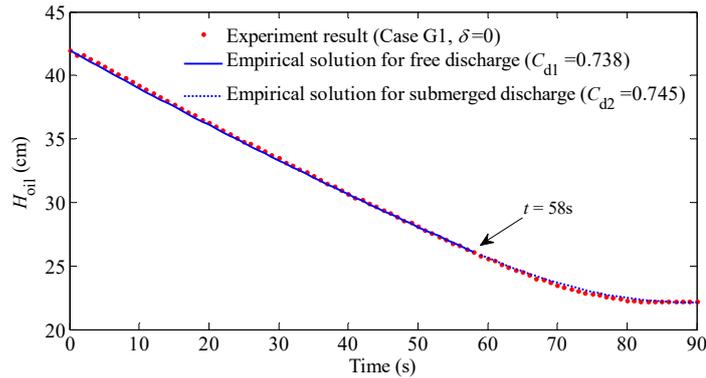
Figure 3.9 The comparison of H_{oil} between the experiment data and the empirical solution for Case G1.

3.3.2 Effect of axial offsets between external and internal bottom holes

In this section, the new accidental factor, the axial offsets between external and internal bottom holes, is considered. Its effect on the dynamic spilling process is discussed. Four different cases (G1-G4) with different axial offsets represented by a non-dimensioned variable ($\delta=\Delta/D$) are conducted with the same initial hydrostatic conditions (i.e., H_{oil} and d). Figure 3.10 indicates the time histories of the oil-water mixture level in the ballast tank ($H_{mixture}$) and the oil height in the cargo tank (H_{oil}) for these cases. It is clearly shown that dynamic spilling process is significantly affected by the different rupture offsets yielding distinct level profiles. Moreover, one may also notice that all the grounding cases finally reach the same levels of H_{oil} and $H_{mixture}$ after the ultimate hydrostatic equilibrium is resumed, which yield the same final oil volume spilled from the cargo tank (43.03L). Considering the similar curves for Cases G3 and G4 in Figure 3.10, only two

typical cases (i.e., Case G2 and G3) are selected for the illustration and some corresponding snapshots of the flow state near the rupture hole at different time instants are shown in Figure 3.11.
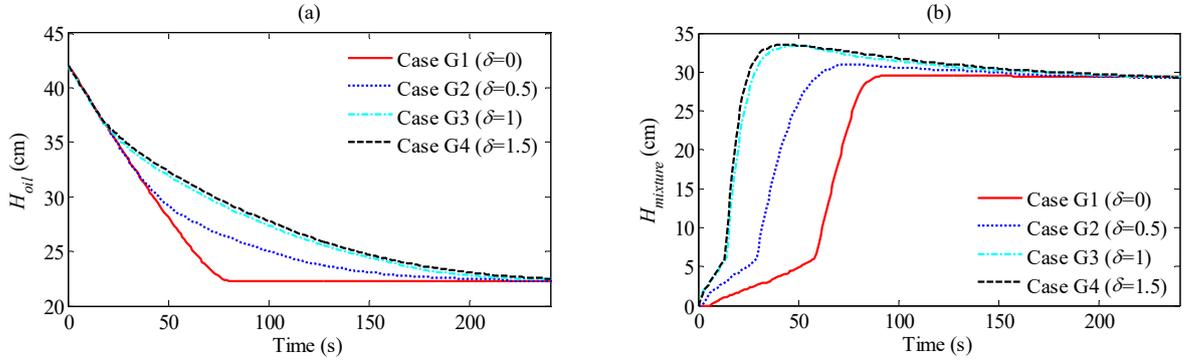
Figure 3.10 Time histories of (a) oil height in the cargo tank (H_{oil}) and (b) the oil-water mixture height in the ballast tank ($H_{mixture}$) for grounding cases.

Figure 3.11(a) gives the snapshots of the violent jet interaction between the downward oil flow and the upward water flow inside the bottom ballast space at t=0.5s. It is clearly indicated that due to the non-coaxial ruptures the flow state inside the ballast tank is quite different to the one in the Case G1 in Figure 3.5(a). There is a clear upwelling jet releasing from the external hole, although the measures data may fail to justify its fluid composition. It is interesting to notice that with regard to the Case G3 and G4, where the overlap area between the internal and external holes being zero, the oil starts to spill into the water basin through the external hole until the moment of the mixture level exceeding the draft (around t=22s illustrated in Figures 3.11(b) and 3.11(c)). But, as for the case G1 and G2, the oil begins spilling into the water basin in considerably short time after opening the hole (as illustrated in Figure 3.11(b)). Furthermore, with the increasing axial offset (particularly in Case G3 and G4), this upwelling jet seems to enhance admitting larger fluid inflow and in turn, more oil could be captured by the ballast tank before t=22s, which causes a more rapidly rise in the mixture height in the ballast tank (Figure 3.10(b)). Thus, the period of the free orifice flow from the internal hole is significantly shortened with a larger δ value (shown in Figure 3.10(b) and 3.11(c)). This implies that the H_{oil} curves in Figure 3.10(a) differ from each other after the mixture height in the ballast space reaches the internal hole. Specifically, the increasing δ value could lead to a much longer spilling period associated with a slower spill rate at the internal hole because of the earlier peaked $H_{mixture}$ as illustrated in Figure 3.10(b). One may also found from the Figure 3.10(b) the $H_{mixture}$ peaks at a higher level with a larger axial offset. It is attributed to the higher oil head in the cargo tank at the corresponding instant (shown in Figure 3.10(a)). However, these above influences of axial offsets on the H_{oil} and $H_{mixture}$ are limited when the δ value goes up from 1 to 1.5 as shown in Figure 3.10.

Based on the experimental observation, it can be supposed that the vast majority of the mixture captured by the ballast tank in Case G2 (δ=0.5) seems to be oil considering the mixture property (similar to the oil property) and no final stratification inside the ballast tank (Figure 3.11(d)). As a result, the final spilling state of Case G2 is similar to that of Case G1, but with a longer spilling period (approximately 185s). The spilling period is further prolonged as the offset becomes larger (approximately 230s for Case G3 and G4). It is also deduced that with the offset increasing from 0.5 to 1.5, there may be a slightly larger amount of oil leaking into the water basin, since a larger proportion of water is finally retained by the ballast tank forming the mixture with the lighter colour as shown in Case G3 (Figure 3.11(d)). In other words, the effectiveness of the double-hull space on capturing spilled oil could be undermined with higher δ. However, due to the fully-mixed mixture (perhaps oil emulsification occurs during the experiment), it is very difficult to detect a clear oil-water interface inside the ballast tank at the end of Case G3 and G4 evidenced in Figure 3.11(d). As a result, the correlation between the oil amount left in the ballast tank or spilled into surroundings and axial offsets at the final state may not be analysed through the limited experimental data.

Since the height of the oil left in the cargo tank (H_{oil}) still reflects the discharge through the internal hole, it is reasonable to use the empirical model applied for the Case G1 to describe the oil discharge from the internal hole with different δ values. The coinciding H_{oil} curves in Figure 3.10(a) before the instant the mixture level reaching the cargo tank bottom suggest the upward jet inside the ballast tank has very little impact on the downward oil jet which could still be considered as the free orifice flow over the period. The oil density may be still used for the mixture density when dealing with the submerged orifice flow. Considering the similar geometry and orientation of the hole and discharge characteristics in each case, it is reasonable to adopt the C_d values for the different two stages of Case G1 to predict the H_{oil} in other grounding cases (Dodge *et al.*, 1980; Tavakoli *et al.*, 2011). Figure 3.12 presents the performance of the empirical model for different grounding cases. A satisfactory agreement is achieved in Case G2, but the empirical model somewhat over predicts the oil discharge rate over the submerged orifice flow stage for the Case G3 and G4, resulting in a more rapidly dropping H_{oil} comparing against the experimental one. This may because that the assumption of $\rho_{m(t)}=\rho_o$ in Equations (3-6) and (3-7) are no longer valid as the axial offset causes much water filling into the ballast tank during the spilling process shown in Figure 3.11.

(a) *t*=0.5s
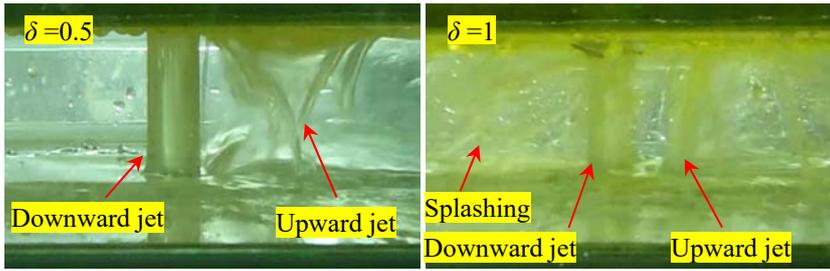
(b) *t*=1s
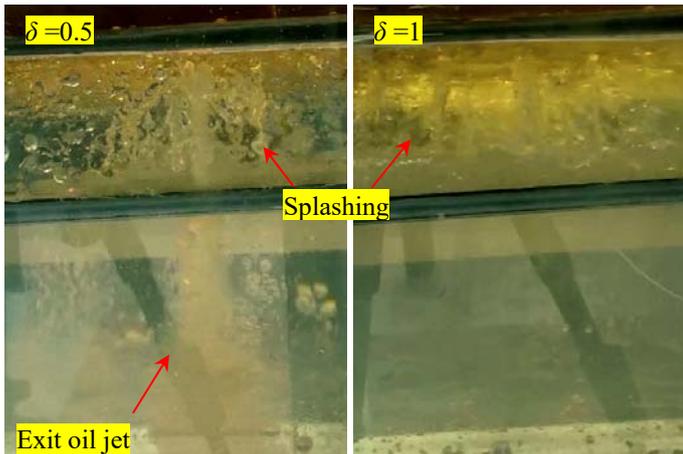
(c) *t*=22s
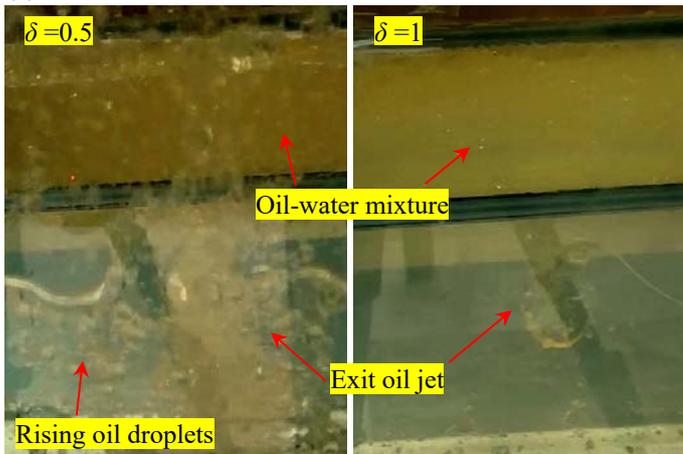
(d) *t*=240s
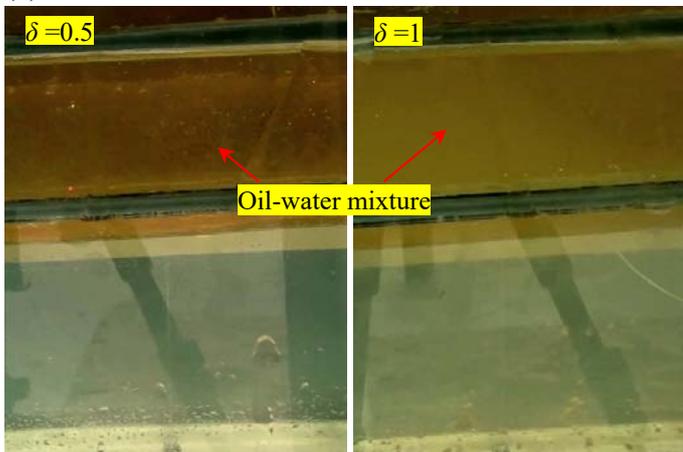
Figure 3.11 Flow states near the rupture holes at different instants for Case G2 and G3.
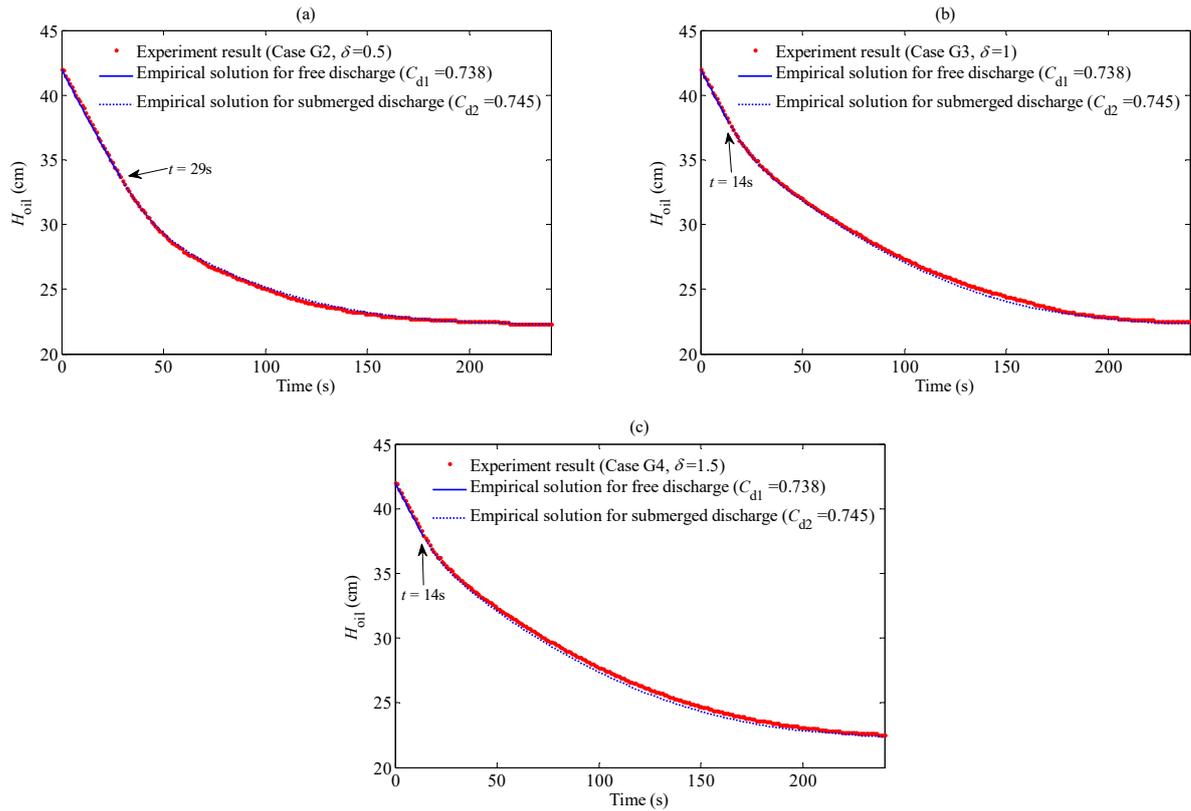
Figure 3.12 The comparison of H_{oil} between the experiment data and the empirical solution for (a) Case G2 (δ=0.5), (b) Case G3 (δ=1) and (c) Case G4 (δ=1.5).

3.3.3 Observation of oil leakage in collision scenarios

The oil leakage from a double-hull tank in collision scenarios is considered. With the purpose of discussing the involved dynamic spilling characteristics, the Case C1 with zero initial thicknesses of water layer inside the ballast tank (t_w=0) is chosen as the benchmark case in this section. The analysis covers the process from the moment that the holes being opened to the instant when the final hydrostatic pressure equilibrium is built. Some snapshots illustrating the flow state near the side holes at different time instants are shown in Figures 3.13, 3.14 and 3.15. Also, Figure 3.16 illustrates the time-histories of the oil height in the cargo tank (H_{oil}) and the mixture height in the ballast tank ($H_{mixture}$) along with the oil volume in the cargo tank and the oil-water mixture volume in the ballast tank calculated directly from the data H_{oil} and $H_{mixtrue}$.
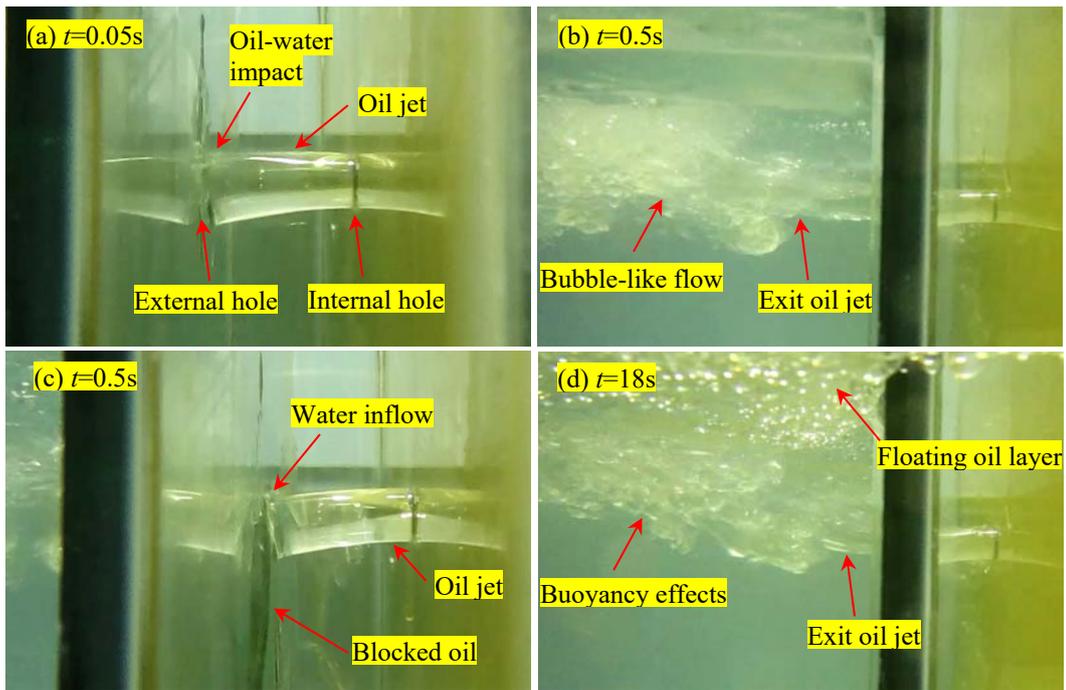
Figure 3.13 Flow states near the puncture at first stage (Case C1).
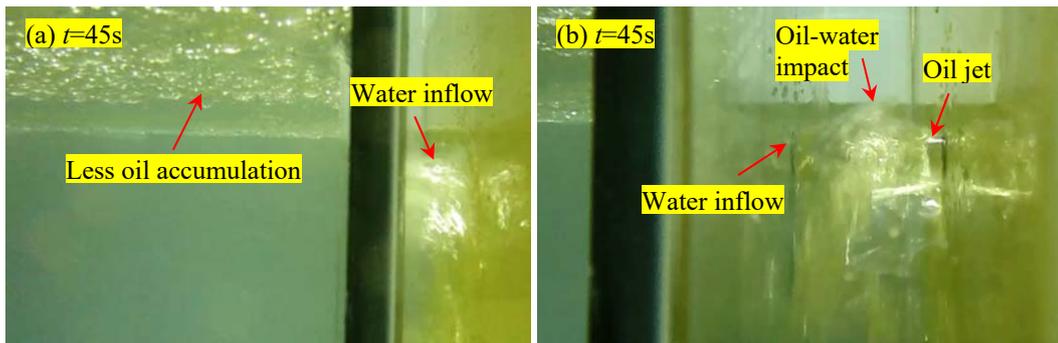
Figure 3.14 Flow states near the puncture at second stage (Case C1).
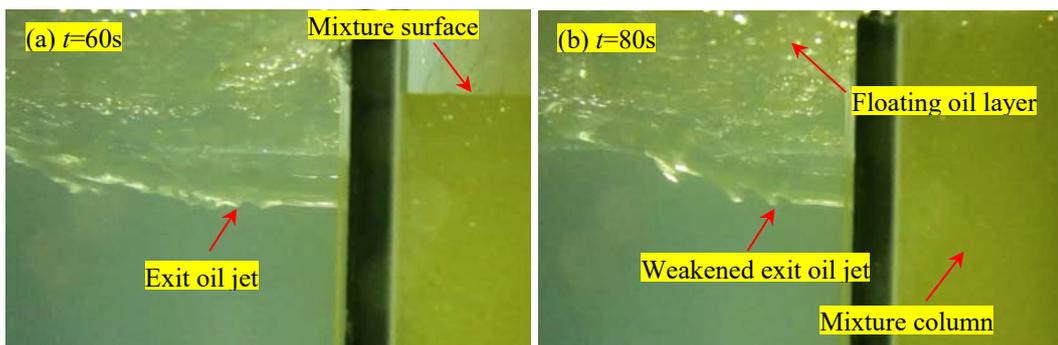
Figure 3.15 Flow states near the puncture at third stage (Case C1).
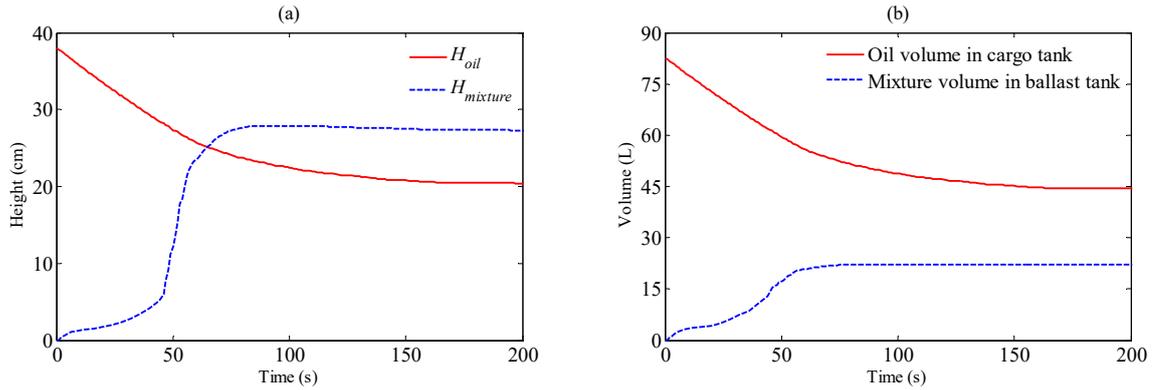
Figure 3.16 Time histories of the (a) the oil height in the cargo tank (H_{oil}) and the oil-water mixture height in the ballast tank ($H_{mixtrue}$) and (b) the oil volume in the cargo tank and the oil-water mixture volume in the ballast tank for the Case C1.

Similar to the Case G1, there are three typical stages with different spilling features. In the instant that the holes are opened, both the oil in the cargo tank and the water in the water basin begin flowing into the ballast space through the internal hole and the external hole, respectively, showing typical free orifice flow behaviour. Since the hydraulic head difference between the internal hole and the oil-air interface in the cargo tank is significantly higher than that between the external hole and the air-water interface in the water basin, the initial velocity and the momentum carried by the oil flow are higher than these of the water flow. Thus, the water and oil jets hit each other and the water stream is pushed backward by the oil stream as illustrated in the Figure 3.13(a).

The oil flow reaches the external hole after a very short time and oil starts to spill into the water basin preventing the water pouring into the ballast space as shown in Figure 3.13(b) at $t=0.5$s. Meanwhile, Figure 3.13(c) provides a snapshot from another viewing angle at the same time ($t=0.5$s). It is also noticed that due to the effect of self-weight, the oil jet turns downwards near the external hole. Therefore, part of oil spilled from the cargo tank is retained in the ballast tank. Moreover, since the oil jet cannot cover the whole cross-section of the external hole, some water could escape to the ballast tank through a narrow space on the top of the external hole. This stage sustains for a quite long duration, approximately up to $t=30$s, and the mixture level inside the ballast tank increases gradually as indicated in Figure 3.16. During this period, the spilled oil in the water basin shows a feature of buoyance-drive and bubble-like flow with convection behaviours and finally floats on the water surface as demonstrated in Figure 3.13(b) and (d).

At the second stage, because of the dropping of the oil level in the cargo tank, the velocity and momentum carried by the oil flow decrease. As a result, the oil jet cannot withstand the opposing water jet at the external hole allowing more water to flow in through the external hole. In other words, the oil outflow through the external hole attenuates and eventually becomes water inflow

65

instead as shown in the Figure 3.14(a) and (b). Both the flows through the internal and external holes pour into the ballast tank bringing a quicker mixture accumulation over this stage shown in Figure 3.16. Moreover, it is found that the decreasing oil outflow into the water basin causes a less oil concentration near the external hole due to the convection-diffusion effect and floatation mechanism, which further promotes the water inflow. This stage lasts from t=30s to t=57s.
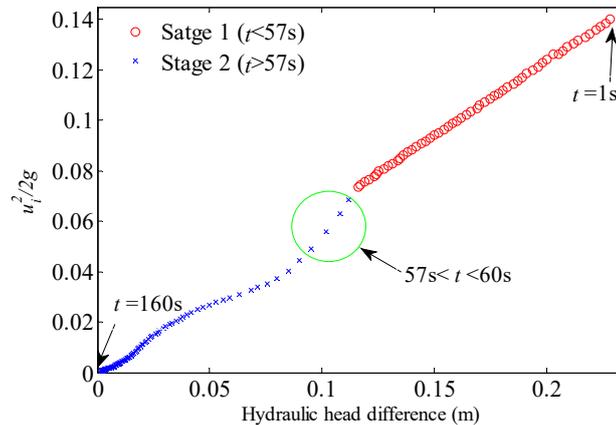
Figure 3.17 Correlation between the average velocity head across the internal hole and the hydraulic head difference between the oil-air interface of the cargo tank and the centre of the internal hole in Case C1.

Similar to what has done for the oil jet from the internal hole in the Case G1, Figure 3.17 presents the correlation between the average velocity head across the internal hole and the hydraulic head (the sum of pressure head and potential head) difference between the oil-air interface of the cargo tank and the centre of the internal hole, from which a strong linear relationship (R^2=0.999) over these two stages is found representing the free orifice flow.

When the mixture-height reaches the hole, (around t=57s), the third stage launches. The spill feature is different due to the presence of the oil-water mixture between the internal and external holes. The internal hole is submerged in the mixture and a jet flow releasing towards the water basin is observed as shown in Figure 3.15 (a) and (b). Though it is impossible to tell the accurate fluid component of the outflow through the external hole due to the lack of details about the flow field, it can be concluded that the ballast space shows the negligible contribution to the prevention of the oil spilling during this stage at least. According to Figure 3.17, With the assumption of $\rho_{m(t)}$=ρ_o, the oil discharge from the internal hole experiences a short transitional period (57s<t<60s) with nonlinear correlation, but after which another weakened linear relationship is formed with R^2=0.982 suggesting the submerged orifice flow is mainly dominated by the considered hydraulic head. Finally, the gravity-induced spilling ceases as long as the average net pressure difference across the internal and external holes is zero. The following spilling driven by the exchange flow due to the local density difference is excluded in this study.

The whole gravity-induced spilling process takes around 200s and the final oil volume spilled out of the cargo tank is 38.03L (46.06% of total oil). Based on the stratified mixture inside the ballast tank at t=200s, there are approximately 18.47L oil (48.6% of spilled oil from the cargo tank) spilled into water basin and 19.56L oil (51.4% of spilled oil from the cargo tank) left in the ballast tank.

Ignoring the short transitional period between these two linear correlations, the proposed empirical model (Equations 3-4, 3-5, 3-6 and 3-7) is applied for the oil discharge from the internal hole with two linear-correlation stages. As shown in Figure 3.17, the two linear relationships indicate two individual constant C_d values which should be respectively applied to the two stages. Similar to the grounding case, the oil discharge from the internal hole during the first two stages manifests as the free orifice flow using the Equations (3-4) and (3-5). When the oil spilling enters the third stage (at around t=57s), the H_{oil} profile is governed by the submerged orifice flow. The mixture height above the rupture hole (expressed as $H_{mixture(t)} - H_b - h$) in the ballast tank shall be considered in Equations (3-6) and (3-7). But, one may concern that since certain amounts of the water and oil have entered the ballast space, the mixture density (ρ_m) may locate between ρ_o and ρ_w and is hardly estimated. Herein, considering the lighter oil density, the ρ_m is directly assumed to be ρ_o, namely, the mixture above the rupture level is mainly consisted of oil. Figure 3.18 compares the oil height in the cargo tank measured in the experiment and that predicted by the proposed empirical model for the whole spilling process.
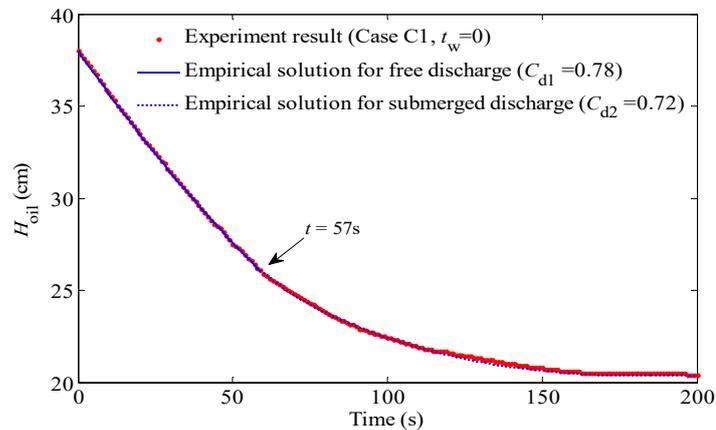
Figure 3.18 The comparison of H_{oil} between the experiment data and the empirical solution for Case C1.

The constant C_d values of 0.78 and 0.72 are applied respectively to the two empirical formulas. A good agreement between the experimental data and the empirical solution is achieved, which extends the proposed empirical model to the collision case. The situation is comparable to the grounding case, where the oil releasing from the internal hole is mainly dominated by the hydraulic head difference between the oil free surface in the cargo tank and the internal hole, and

the energy loss can be appropriately evaluated by a constant discharge coefficient during each orifice process.

3.3.4 Effect of initial thicknesses of water layer in the ballast tank of collided DHTs

Two new additional collision cases are carried out to investigate the effect of the initial thickness of the water layer in the ballast tank. The 6cm and 26cm water layers are introduced inside the double hull space, respectively, which stand for different time lags of the rupture initiation between the external and internal holes. Figure 3.19 gives some snapshots near the spilling hole at different instants for Case C2 (t_w=6cm) and C3 (t_w=26cm). The time histories of the height of the oil-water mixture in the ballast tank ($H_{mixture}$) and that of the oil in the cargo tank (H_{oil}) are shown in Figure 3.20.

(a) t=0.5s
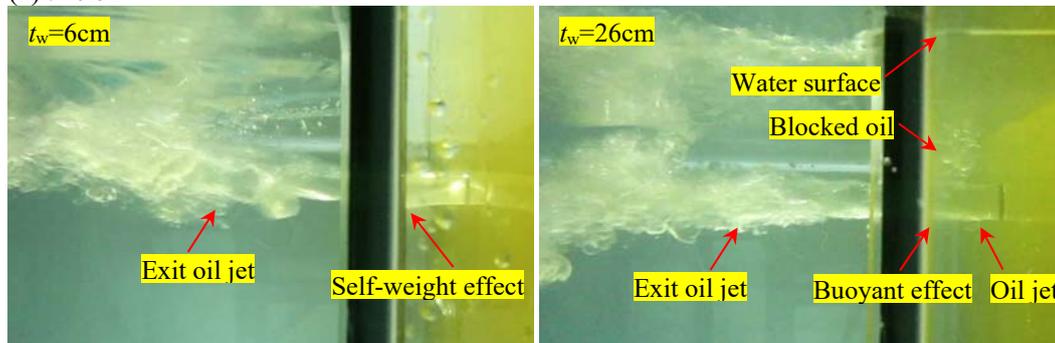
(b) t=18s
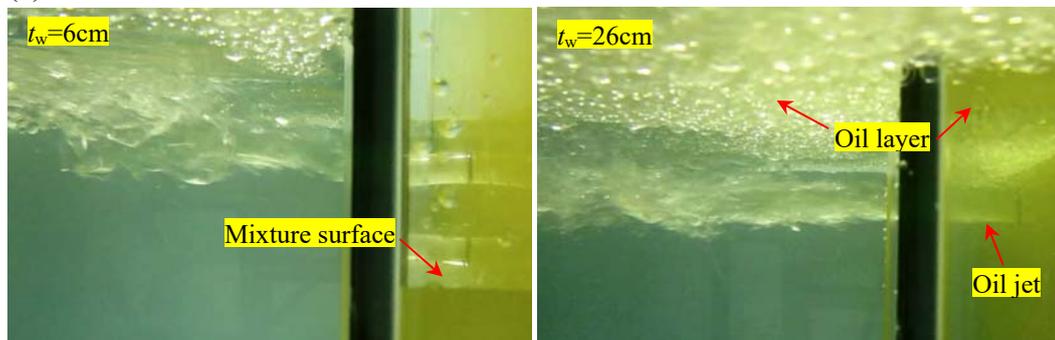
(c) t=180s
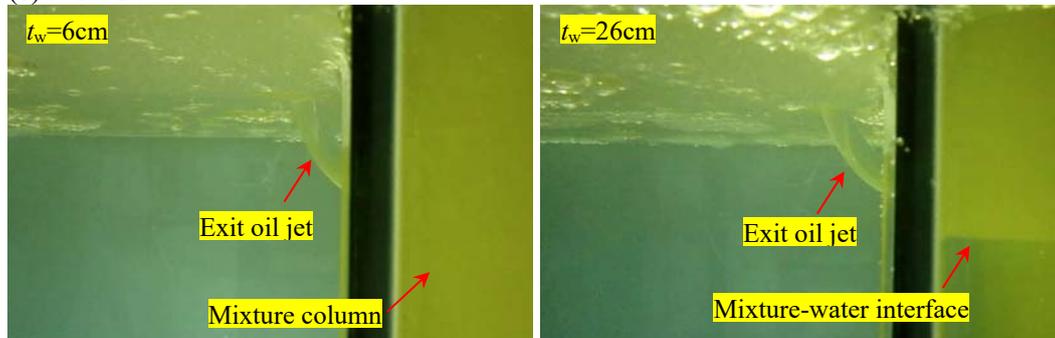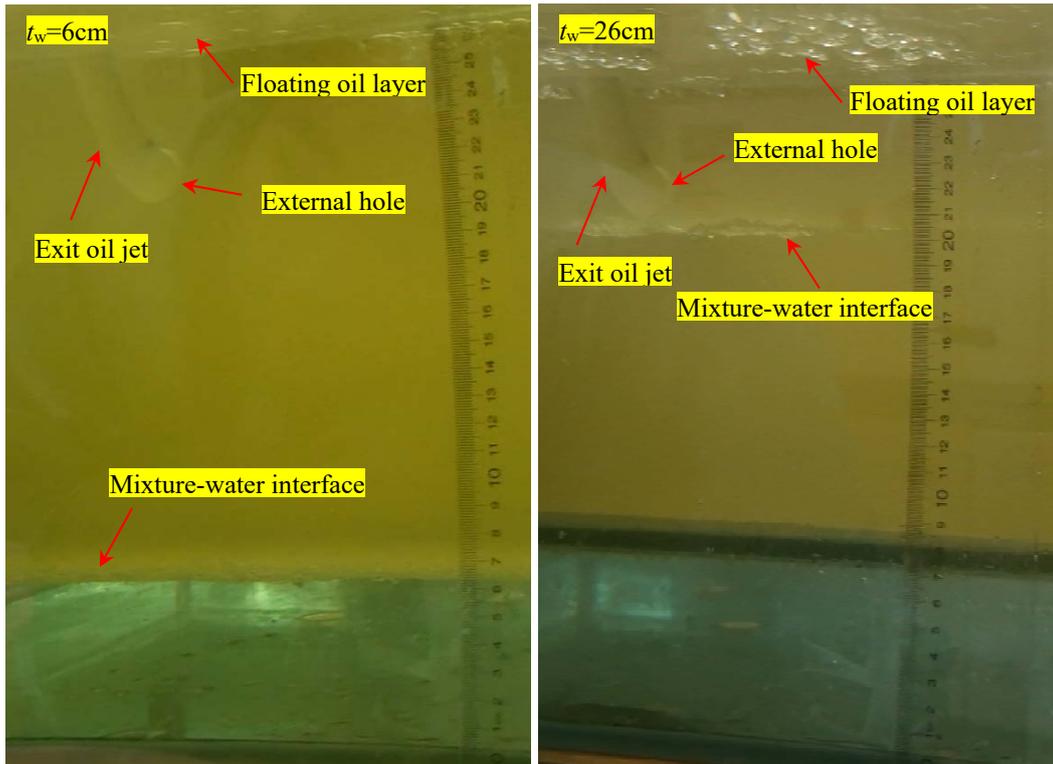
Figure 3.19 Flow states near the rupture holes at different instants for Case C2 and C3.
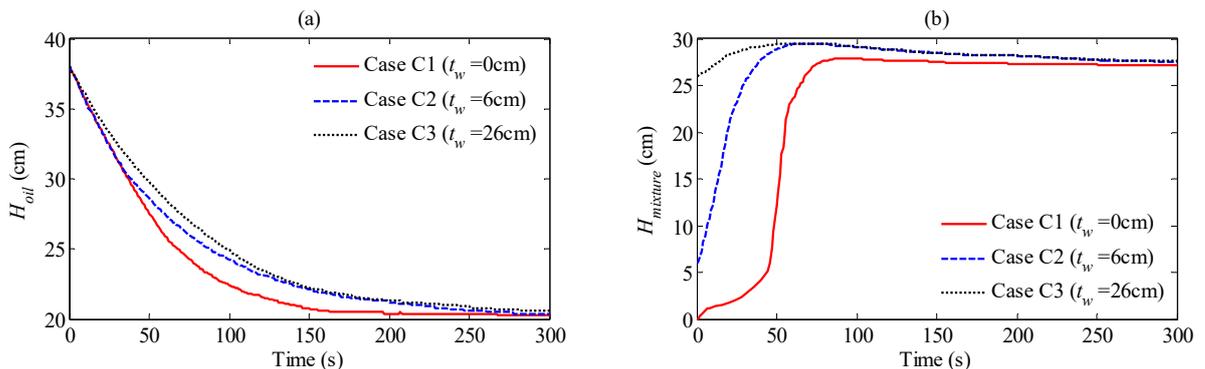
Figure 3.20 Time histories of (a) oil height in the cargo tank (H_{oil}) and (b) the oil-water mixture height in the ballast tank ($H_{mixture}$) for collision cases.

As illustrated in Figures 3.19 and 3.13, the oil spill processes for the Case C1 and C2 look very similar during the first stage. However, due to the initially water-filled bottom ballast space, the mixture level reaches to the side hole earlier in the case with t_w=6cm than that in the case of no initial water thickness. Thus, the second stage associated with the water inflow is omitted in Case C2 and the early arrival of the third stage (i.e., submerged discharge process) mitigates the oil outflow from the internal hole forming an obvious gap in H_{oil} (Figure 3.20(a)). The $H_{mixture}$ peaks earlier and higher with the t_w increased from 0 to 6cm, which is attributed to the relatively higher H_{oil} at the corresponding instant. Moreover, the whole process of oil spilling for Case C2 takes approximately 265s which is longer than Case C1.

As for the case C3 with a 26cm initial water thickness, the side oil spilling process directly enters the submerged orifice stage. Based on the Figure 3.19, it is clearly shown that because of the buoyancy effect, the oil flow travels through the water column in the side ballast space and turns upwards near the external hole and thus, some oil could be blocked by the external hull and accumulated on the water surface in the ballast tank. The resulting oil layer inside the ballast tank stops increasing when it totally covers the side holes. Considering the absence of the free orifice flow stage, a slow submerged discharge from the internal hole happens from the beginning yielding a bigger H_{oil} gap between Case C1 and C3 (shown in Figure 3.20(a)). However, the difference on H_{oil} between the Case C2 and C3 is not quite evident. This is because the period spent in Case C2 for mixture level rising from the cargo bottom to the side hole is short (around 23s), due to which the accumulated effect on the oil level in the cargo tank is limited. The overall spilling period for Case C3 (approximately 285s) is slightly longer than C2 as indicated in Figure 3.20.

In addition, as shown in Figure 3.20, the final levels of $H_{mixture}$ and H_{oil} are independent of the different initial water layers, which yield the same final oil volume spilled from the cargo tank (38.03L) in each case. With the increasing t_w value, a larger amount of the spilled oil could leak into the water basin with less oil retained in the ballast tank finally. This is because the initial water layer inside the ballast tank still exists at the end of the spilling process (shown in Figure3.19(c)), which decreases the double hull space being available to capture the spilled oil from the internal hole. Therefore, the effectiveness of the double hull space on capturing the spilled oil could be reduced by introducing the initial water layer. If the mixture above the initial water layer inside the ballast tank is assumed to be oil, the whole spilling processes of Case C2 and C3 finally result in 31.19L and 36.28L oil (82% and 95.4% of spilled oil from the cargo tank) spilled into water basin and 6.84L and 1.75L oil retained by the ballast tank (18% and 4.6% of spilled oil from the cargo tank), respectively.
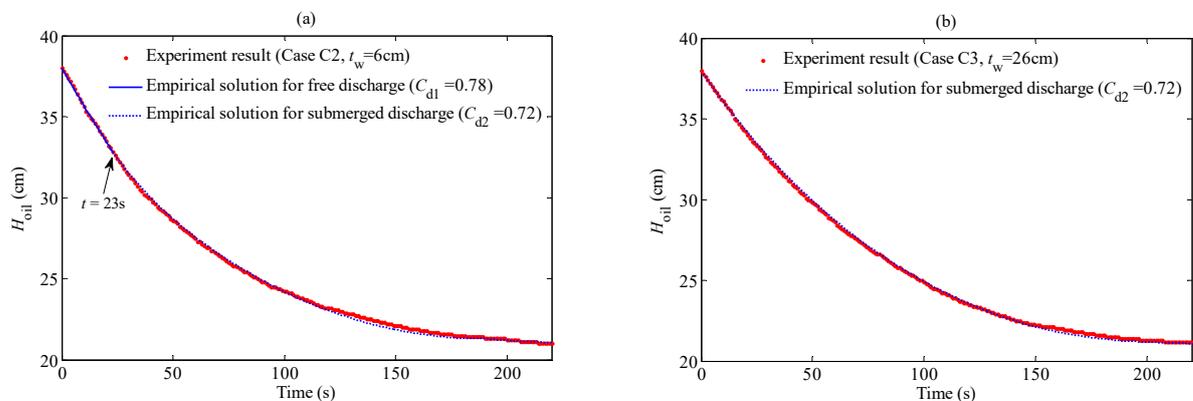

Figure 3.21 The comparison of H_{oil} between the experiment data and the empirical solution for (a) Case C2 (t_w=6cm) and (b) Case C3 (t_w=26cm).

Similar to the grounding cases, the empirical model applied for the Case C1 is employed to the other collision cases with different t_w values. According to the different discharge features, it should be noticed that the different t_w conditions may only affect the transition point between the different stages. As a result, the C_d values used for the Case C1 are applied to the other cases. The oil density may be still used for the mixture density in Equations (3-6) and (3-7). Figure 3.21 presents the performance of the empirical model for different collision cases, where the empirical solution matches the experimental data well.

3.4 Summary

The dynamic behaviours of oil spilling from a fixed grounded or collided double-hull tank is investigated using different lab cases. The new accidental factors, i.e., the axial offsets between the internal and external holes under grounding scenarios and the initial thickness of water layer inside the ballast tank under collision scenarios, are considered. The result indicates that these factors could significantly affect the dynamic spilling process yielding different spilling durations and flow states, although all the grounding cases are under the same initial or final hydrostatic conditions. Different to the previous studies, the current work does not only emphasize the importance of dynamic spilling characteristics when estimating the effectiveness of DHT design on reducing the oil spilling into the sea, but also provides experimental data used to validate the numerical models. Moreover, the experimental observation indicates that the oil spills out of the DHT from the beginning of the spilling process under either collision or grounding condition, for which the hydrodynamic explanations are presented.

Table 3.3 Statistics of the final spilling state.

Cases	Oil spilled from the cargo tank	Oil spilled into the water basin	Oil retained inside the ballast tank	Spilling durations
G1	43.03L	20.32L (47.2%)	22.71L (52.8%)	90s
G2	43.03L	20.32L (47.2%)	22.71L (52.8%)	185s
G3	43.03L	More than 20.32 L (47.2%)*	Less than 22.71 L (52.8%)*	230s
G4	43.03L	More than 20.32 L (47.2%)*	Less than 22.71 L (52.8%)*	230s
C1	38.03L	18.47L (48.6%)	19.56L (51.4%)	200s
C2	38.03L	31.19L (82%)	6.84L (18%)	265s
C3	38.03L	36.28L (95.4%)	1.75L (4.6%)	285s
* Due to the unstratified mixture inside the ballast tank, the data was not measured.				

Based on the current case study, Table 3.3 summarises the available measurement of the final spilling state in terms of the oil spilled from the cargo tank, the oil spilled into the water basin, the oil retained inside the ballast tank and spilling durations. The corresponding percentages of the oil spilled into the water basin and the oil retained inside the ballast tank in the oil spilled from the cargo tank are also indicated. It is clearly shown that the accidental factors considered in this

study significantly affect the DHT effectiveness on preventing oil spilling. The increasing axial offsets and initial thicknesses of water layer inside the ballast tank reduce the final oil retained inside the ballast tank and conversely enhance the oil spilled into the water basin with a prolonged spilling duration.

Considering the different spilling features, the oil spilling process is divided into several stages. The correlation analysis suggests the possibility of proposing a modified empirical model using the quasi-steady Bernoulli's equation with constant custom discharge coefficient to estimate the oil discharge from the internal hole. The oil discharge through the internal hole is characterized as the free orifice flow or submerged orifice flow, depending on the mixture level inside the ballast tank. Based on the comparison, the empirical solution accurately coincides with the measured data in all the cases. However, due to the limited available measurements it is temporarily incapable of analysing the oil discharge through the external hole or carrying out the final state assessment for some cases (e.g., Case G3 and G4). Further analysis needs the assistance of numerical modelling from which more detailed data, especially for the fluid state through external hole, can be obtained.

Chapter 4 Numerical Modelling on Oil Spilling from Fixed Damaged Tanks

The aforementioned experimental observation indicates that the dynamic spilling behaviours could be significantly affected by different accidental situations and tank configurations yielding different fluid characteristics. For example, Peter and Lin (1994) emphasized the presence of turbulence features of the flow emerging inside the ballast tank of DHTs, which is quite different from the SHTs. However, the existing numerical studies did not systematically investigate the turbulence modelling and, thus fail to provide a comprehensive discussion on this aspect. Moreover, the most previous numerical investigations on the oil spilling problem are restricted by the two-dimensional condition, which would hide the comparability between the numerical and experimental results due to the dimensional limitation. In this chapter, the three-dimensional numerical study is organized in the form of different accidental situations (e.g., grounding and collision) and tank configurations (e.g., SHTs and DHTs), from which the numerical configuration, especially for turbulence modelling, to each group can be determined separately.

4.1 Model Formulation

Considering the insufficient data captured by the experimental study, the numerical investigation is necessary to provide more hydrodynamic details which may shed more light on the spilling features. Recently, an open-source CFD package OpenFOAM, which benefits users with ready-to-use and customized applications, has been widely-used to deal with different engineering problems involving the complex multiphase flow. It integrates diverse solvers and packages in forms of a bundle of C++ libraries and codes. In this study, all the numerical cases are carried out in OpenFOAM platform, where the multiphase technology VOF with a new multiphase MULES functionality is applied to identify different phases involved (usually, air, oil and water) and the FVM is used to solve the governing equations. The phases are treated as Newtonian fluids with the hypothesis of incompressibility and immiscibility. The viscosity, turbulence and the surface tensions are considered as well. The compressibility effect will be considered in the following chapter. Some brief descriptions of governing equations used in the OpenFOAM are presented below (Ubbink, 1997):

Mass continuity equation:

$$\frac{\partial \rho}{\partial t} + \nabla \cdot (\rho \boldsymbol{U}) = 0 \qquad (4\text{-}1)$$

Momentum equation:

$$\frac{\partial \rho \boldsymbol{U}}{\partial t} + \nabla \cdot (\rho \boldsymbol{U} \otimes \boldsymbol{U}) = \nabla \cdot \boldsymbol{T} + \rho \boldsymbol{g} + \boldsymbol{F_s} \tag{4-2}$$

where $\boldsymbol{U}$ is the fluid velocity; ρ is the bulk density of the fluid; $\boldsymbol{T}$ is the stress tensor for a Newtonian fluid in local thermodynamic equilibrium, which is not exposed to very high temperatures or pressure ranges, which is defined as: $\boldsymbol{T} = -\left[p + \frac{2}{3}\mu_{eff}\nabla \cdot \boldsymbol{U}\right]\boldsymbol{I} + \mu_{eff}[\nabla \otimes \boldsymbol{U} + (\nabla \otimes \boldsymbol{U})^T]$ where μ_{eff} is the effective dynamic viscosity, which takes into account the molecular dynamic viscosity μ and the turbulent dynamic viscosity μ_t; $\boldsymbol{I}$ is the unit tensor; p is the pressure; $\boldsymbol{F_s}$ is the surface tension force being active in the interfacial region, which is formulated by the Continuum Surface Force (CSF) method as:

$$\boldsymbol{F_s} = \kappa\sigma(\nabla\alpha_i) \tag{4-3}$$

where κ is the mean curvature of interface expressed as $\kappa = -\nabla \cdot \left(\frac{\nabla\alpha_i}{|\nabla\alpha_i|}\right)$, where α_i is the volume fraction of the phase i; σ is the surface tension coefficient. For each interface between two different phases, typical constant is used (i.e., $\sigma_{\text{air-oil}}$=0.032N/m (Flingoh and Chong, 1992); $\sigma_{\text{air-water}}$=0.072$N/m$ (Dean, 1999); $\sigma_{\text{oil-water}}$=0.026$N/m$ (Konno and Izumiyama, 2002)).

In the VOF approach, the transport of α_i is written as (Weller, 2008):

$$\frac{\partial \alpha_i}{\partial t} + \nabla \cdot (\alpha_i \boldsymbol{U}) = -\nabla \cdot [\alpha_i(1 - \alpha_i)\boldsymbol{U_c}] \tag{4-4}$$

where α_i is strictly bounded between 0 and 1, and $\sum_{i=1}^{n} \alpha_i = 1$. Here, i=1, 2…n denote n phases respectively; $\nabla \cdot [\alpha_i(1 - \alpha_i)\boldsymbol{U_c}]$ is the artificial compression term, embedded into the OpenFOAM multiphase solvers. The artificial compression velocity is given by:

$$\boldsymbol{U_c} = \frac{\nabla\alpha_i}{|\nabla\alpha_i|}\min(C_\gamma|\boldsymbol{U}|, max(|\boldsymbol{U}|)) \tag{4-5}$$

where c_γ is an adjustable coefficient which set to 1.5 as recommended.

The variables ρ and μ used in the momentum Equation (4-2) are substituted with weighted averages based on the α_i distribution:

$$\rho = \sum_{i=1}^{n} \alpha_i\rho_i \tag{4-6}$$

$$\mu = \sum_{i=1}^{n} \alpha_i\mu_i \tag{4-7}$$

More model information can be referred to Suponitsky *et al.* (2014); Deshpande *et al.* (2012); Higuera *et al.* (2013).

Since the VOF requires an explicit solution and is considerably sensitive to the Courant number (C_o) (Wardle and Weller, 2013), a self-adapted time step is applied to satisfy the Courant

condition. The solver implements the robust transient PIMPLE (merged PISO-SIMPLE) algorithm for the pressure-velocity coupling. The post-processing and visualization of numerical results are achieved through utilities within the OpenFOAM distribution and an open-source visualization package ParaView 4.0.

It should be noted that the VOF model may not reflect the nonlinear behaviour of the viscosity associated with the emulsified oil as mentioned in McNaught (2011) due to their inherent limitation that the viscosity of the mixture varies linearly following the volumes of the fraction of the fluids (as shown in Equation 4-7). To avoid this issue, the cases where the oil emulsion is insignificant in the corresponding experimental studies are selected.

4.2 Oil Spilling from Damaged SHTs

The oil spilling from a damaged single-hull tank (SHT) is considered firstly to examine the convergence property and accuracy of the current model considering the available experimental data. Although the spilling process and related hydrodynamic features for SHTs are different from these of DHTs, one may agree that the comparison between the numerical results and the experimental data available in the public domain in such case could shed some light on the performance of the present numerical approach.

4.2.1 Model results and discussions

Considering the fact that none of the previous numerical investigations mentioned in Chapter 2 conducted the model validation by comparing against the experimental data in terms of the time-dependent variables, when focusing on the hydrodynamic spilling features, however, it is important to validate the numerical result of the time history of the spilling process rather than the final state variables. For this purpose, the time histories of the height of the oil inside the cargo tank (H_{oil}) measured in the experimental study of Tavakoli *et al*. (2011) are used. In this study, a SHT model tank was built at 1/30 scale. The similarity criteria introduced by Simecek-Beatty *et al*. (2001) including geometric, kinematic and dynamic aspects were used to determine the viscosity of the oil and other related parameters. The density and kinematic viscosity of the water are 998 kg/m^3 and 1.0×10^{-6} m^2/s, respectively. Those of the oil are 920 kg/m^3 and 8.1×10^{-5} m^2/s, respectively. The grounding and collision scenarios are simplified by specifying smooth-edge circular punctures located on the bottom and the side walls, respectively.

Four cases (corresponding to N3, N4, N8 and N9 in Tavakoli *et al*., 2011) are considered in the numerical investigation with the same configuration as the experiment. These cases cover the oil spilling from either submerged (Case 2 and 4) or un-submerged holes (Case 1 and 3), and consider both the grounding (Case 1 and 2) and collision scenarios (Case 3 and 4). Related parameters of

these cases are summarised in Table 4.1. More details of the configurations can be found in Tavakoli *et al*. (2011).

Table 4.1 Related case configurations.

Cases	Scenarios	Surrounding conditions	Initial oil height ($H_{oil(t=0)}$, cm)	Hole diameter (D, cm)	Water draft (d, cm)
1	Grounding	Air	70	2.2	0
2	Grounding	Water	80	2.2	47
3	Collision	Air	70	2.2	0
4	Collision	Water	80	2.2	50

As for modelling the turbulence behaviours, the previous experimental observations (Lu *et al*., 2010; Simecek-Beatty *et al*., 2001) suggested that the spilling from an unsubmerged or submerged hole of a fixed SHT is dominated by the oil outflow through the broken hole, which behaves similarly to a jet flow through an orifice. Thus, referring to the definition of *Re* number of the orifice flows (Dabiri *et al*., 2007; Arun *et al*., 2010; Hollingshead *et al*., 2011), the *Re* numbers with the length scale specified by the diameter of the hole are approximately 1100, 760, 930 and 752 initially in Case 1 to 4, respectively, implying a laminar regime (for orifice flow, the upper limit of *Re* for the laminar regime is 2000).

As reviewed in Section 2.4, Krata *et al*. (2012) established a model to address the bunker oil spilling problem of a grounded SHT. In their study, considering the similar low *Re* numbers, the flow is assumed as laminar and the direct numerical simulation (DNS) approach in which the NS equation is solved directly without any turbulence models was applied. But the numerical result was not validated by the experimental data. Furthermore, the oil spilling from a collided SHT was simulated by Lu *et al*. (2010) and Xiao *et al*. (2010). Although the *Re* number associated with the oil outflow through the hole was in the laminar regime, the RANS standard k-ε model was employed to deal with the complex flow motion of the exit oil jet in the water basin. The model was demonstrated to deliver the oil jet patterns close to the experimental snapshots. Considering the completeness of model validations, both the DNS and standard k-ε models are employed for each case. The numerical results are validated by the experimental time-dependent variables, which is not involved in the previous studies. The discussion of model applicability is carried out based on these validations and comparisons.

In the numerical simulation, a three-dimensional computational domain consistent with the experimental configuration is adopted. The heights of the air layers above the water surface in the water basin and the oil surface in the oil tank are determined based on numerical tests to ensure the boundary on the top of the computational domain does not affect the numerical results. On the walls of the water basin and the SHT, a non-slip boundary condition (i.e., the 'fixedValue' boundary type for the velocity) is employed and the appropriate wall functions (i.e., the

'kqRWallFunction' boundary type for the turbulent kinetic energy (k); the 'epsilonWallFunction' boundary type for the turbulent dissipation (ε); the 'nutkWallFunction' boundary type for the turbulent kinematic viscosity (v_t)) are chosen for the turbulence models with the $y+$ requirement (i.e., $30<y+<200$ located in the logarithmic region). On the top boundary, a pressure outlet condition (i.e., the 'totalPressure' boundary type for the pressure) is imposed. More details of the boundary condition implementation in OpenFOAM can be referred to Hedlund (2014) and Liu (2016). The computational mesh is unstructured hexahedral as shown in Figure 4.1.
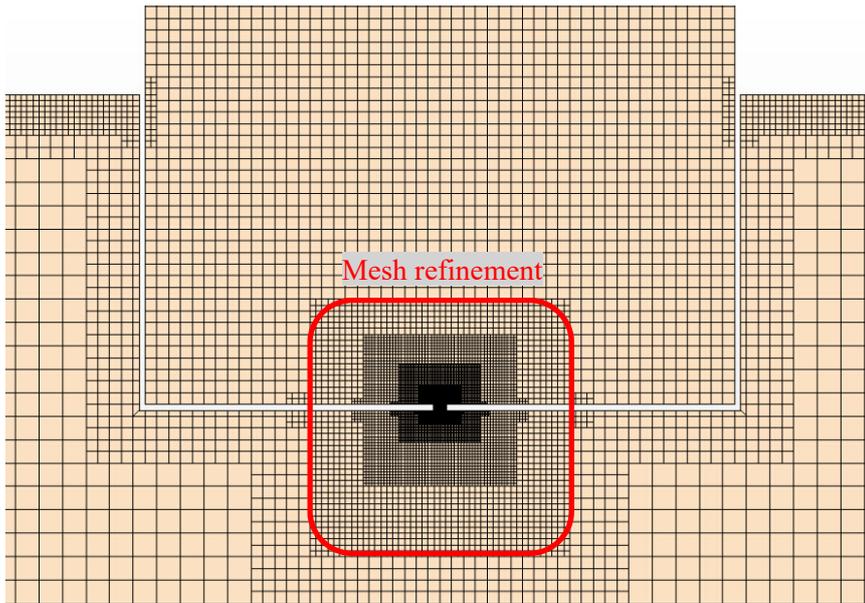
Figure 4.1 Illustration of the mesh distribution at the central plane near the rupture in the Case 2.

The convergence test is proposed for all the cases in prior. A reference cell size of 2cm is used, which represents the maximum cell size in the computational domain. Broadly speaking, the cell size shall be sufficiently small near the holes (Stringer *et al.*, 2010) and shall be also sufficient to resolve the interface between different phases and minimise the numerical diffusion (Yan and Ma, 2010). A spatially hierarchical mesh refinement is adopted in such areas to provide sufficient mesh resolutions. By using this approach, the ratio (α_{ds}) of the minimum cell size to the maximum cell size (constantly 2cm for all cases) may be used to reflect the overall mesh resolution in the convergence investigation. As the self-adapted time step satisfying the Courant condition ($C_o< 0.5$) links the convergence and stability properties associated with the time step size to the cell size (Wardle, 2011), only the convergence property against the cell size is required in this test. Different mesh resolutions, specified by using α_{ds}, are used. Figure 4.2 indicates the time history of the oil height inside the cargo tank (H_{oil}) and the corresponding discharge through the broken hole (Q, a positive value indicates an outflow from the cargo tank towards the water basin tank) for each case with different mesh solutions, together with the experimental data duplicated from Tavakoli *et al.* (2011). For convenience, the time, the height of the fluids and the discharge are

non-dimensionlised by using $\sqrt{H_{oil(t=0)}/g}$, the initial height of oil in the SHT tank ($H_{\text{oil}(t=0)}$) and $\sqrt{2g\Delta H_{(t=0)}}A_{\text{h}}$ where $\Delta H_{(t=0)}$ is the initial hydraulic head difference between the oil surface in the SHT tank and the broken hole and A_{h} is the hole area.

(I) Case1
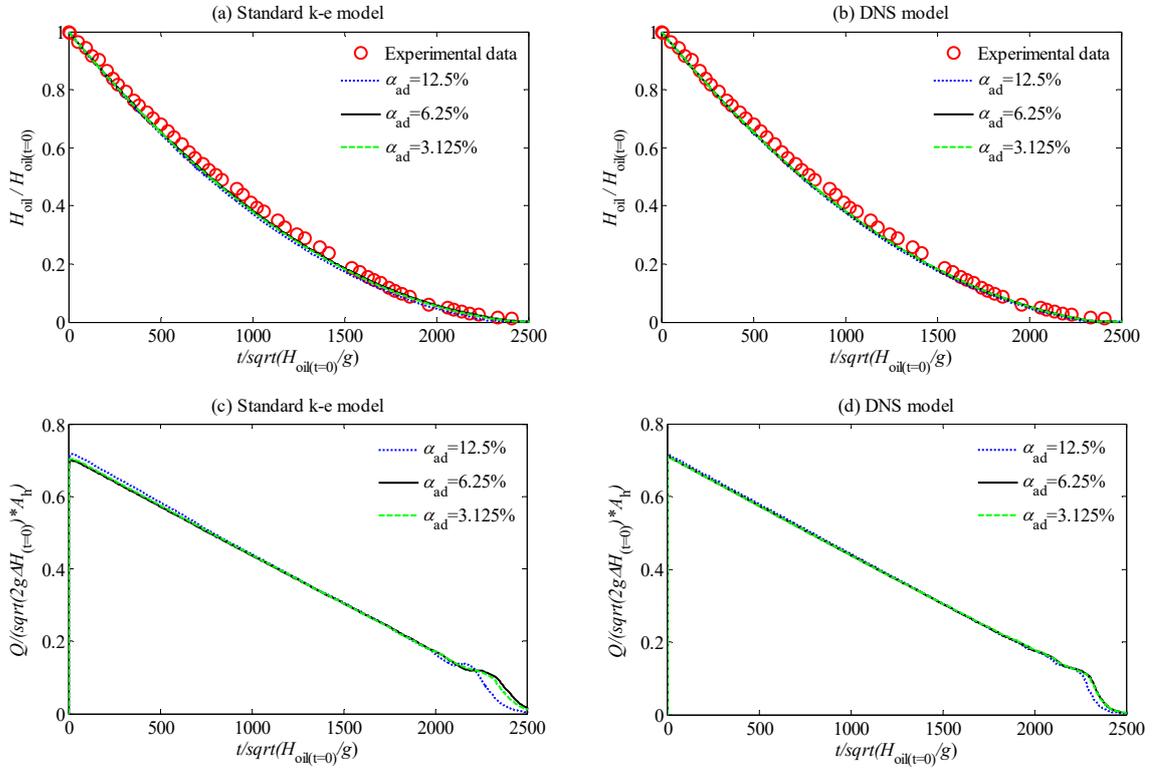
(II) Case2
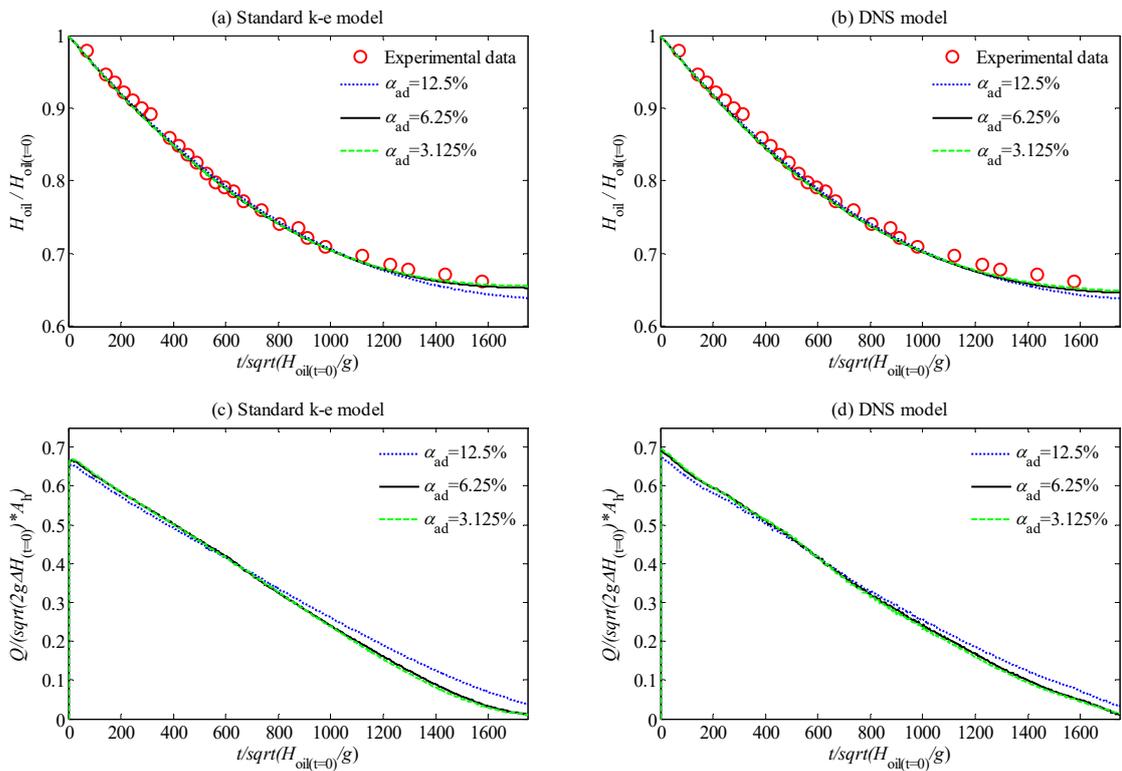
(III) Case 3
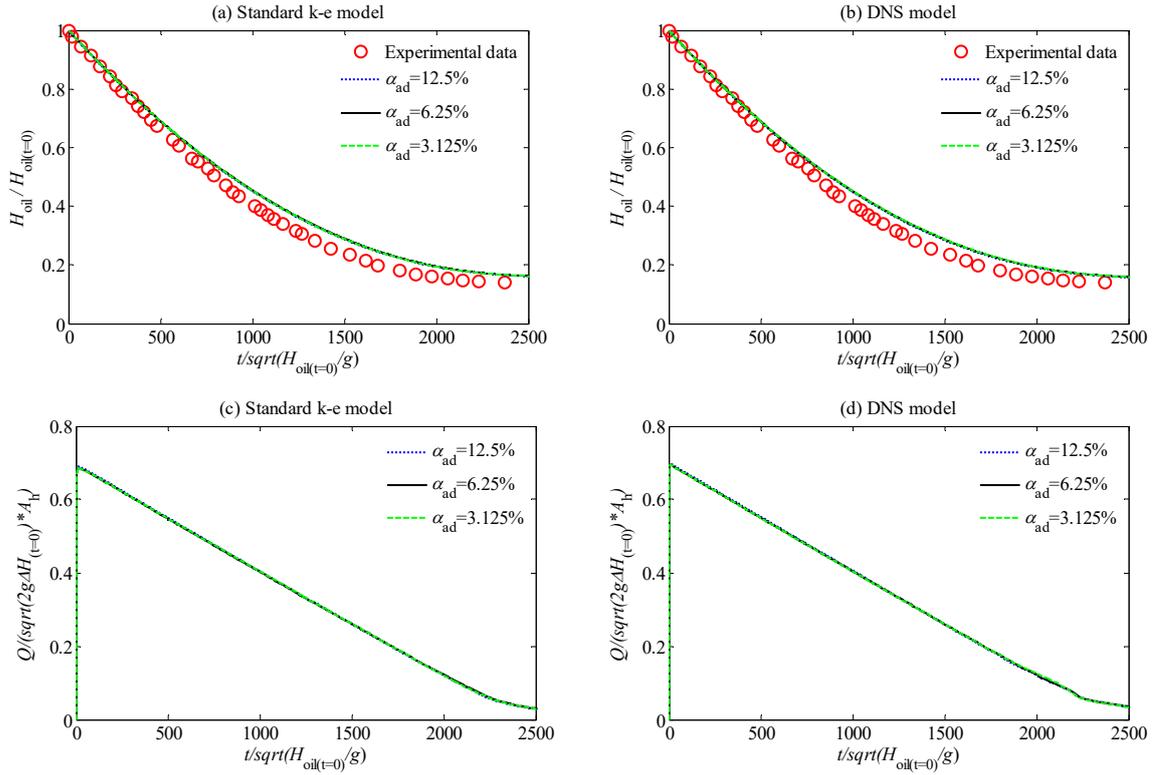
(IV) Case4
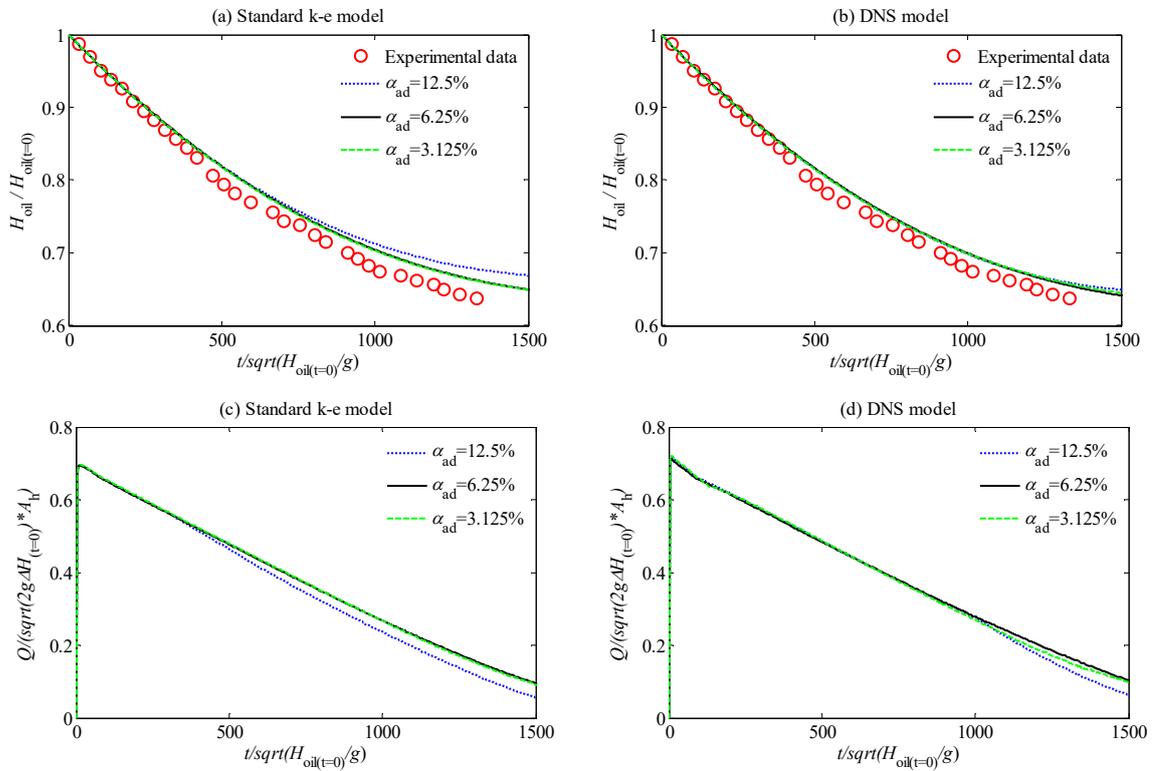
Figure 4.2 The time histories of the oil height inside the cargo tank (H_{oil}) and the corresponding discharge through the broken hole (Q) in the cases with different cell sizes.

It is clearly shown that both DNS and standard k-ε models lead to a similar convergence behaviour using the same group of cell sizes. The curves become closer as the α_{ds} drops. The relative difference between the results with α_{ds}=6.25% and the corresponding result with α_{ds}=3.125% is less than 1.8%, which may mean that the mesh with α_{ds}=6.25% is sufficient fine for the purpose of this model. Moreover, the results of DNS and standard k-ε models with α_{ds}=6.25% match the experimental data well in all four cases, confirming the model applicability. The conclusion about SHT cases using the DNS and standard k-ε models also further completes the model validation on this topic.

4.3 Oil Spilling from Damaged DHTs

The previous studies focusing on numerically investigating oil spilling from DHTs are relatively rarely seen in literatures, considering the complexity caused by the presence of the narrow ballast tank of DHTs. Most relevant studies mentioned in the literature review part were restricted to the two-dimensional condition, which may yield the numerical result failing to validate against the existing experimental data (Cheng *et al.*, 2010). Moreover, despite the fact that the turbulence plays an important role in the ballast tank in the cases of DHTs as pointed out by Peter and Lin (1994), the turbulence modelling was consistently ignored in these numerical studies, partially due to its extra computing cost, which are not only spent on solving extra differential equations of turbulence models but also caused by the requirement of denser mesh resolutions and smaller time steps to resolve much smaller-scale turbulent behaviours.

4.3.1 Model results and discussions

In this study, a three-dimensional model is established following the similar model setup of SHT cases. The current experimental data is used for validation purpose, from which two cases (i.e., Case C1 and G1) are first selected covering the oil spilling behaviours from a DHT under collision and grounding scenarios. With regard to turbulence modelling, it is not clear which turbulence model is proper to such DHT case, due to lack of guidelines targeting similar multiphase flow pattern in literature. Also, considering the fact that modelling turbulence influence inside the ballast tank may lead to considerably expensive mesh resolutions when using the DNS model, thus the preliminary attempt for the DHT case starts from the standard k-ε model. The convergence test similar to the SHT case is conducted for all the two cases and the Case G1 is selected as a demonstration case here.

Figure 4.3 presents the time histories of the oil height inside the cargo tank (H_{oil}), the mixture height in the ballast tank ($H_{mixture}$) comparing with experimental data and the corresponding discharges through the internal and external holes (Q_i and Q_e) in the case G1 with different cell sizes. Here, Q_i and Q_e are non-dimensionlised by $\sqrt{2g\Delta H_{i(t=0)}}\,A_h$ and $\sqrt{2g\Delta H_{e(t=0)}}\,A_h$

respectively, where $\Delta H_{i(t=0)}$ is the initial hydraulic head difference between the oil surface in the cargo tank and the internal hole, $\Delta H_{e(t=0)}$ is the initial hydraulic head difference between the oil surface in the cargo tank and the external hole and A_h is the hole area.
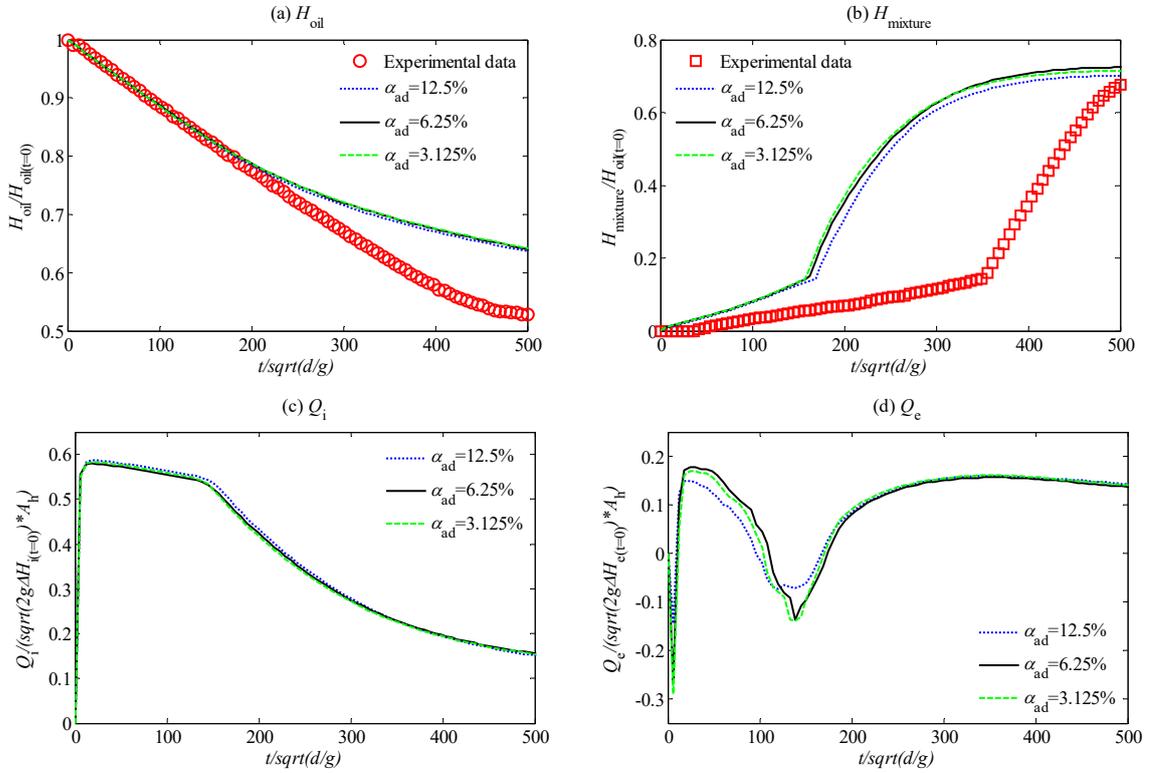
Figure 4.3 The standard k-ε model results in terms of the time histories of (a, b) the oil height inside the cargo tank (H_{oil}) and the mixture height in the ballast tank ($H_{mixture}$) comparing with the experimental data and (c, d) the corresponding discharge of the oil/water mixture through the internal hole (Q_i) and the external hole (Q_e) in the case G1 with different cell sizes.
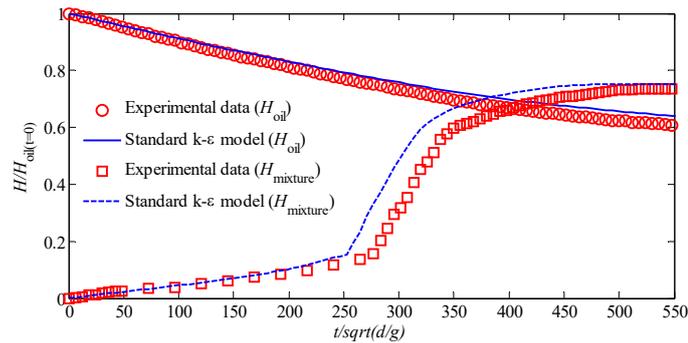
Figure 4.4 The standard k-ε model results in terms of the time histories of the oil height inside the cargo tank (H_{oil}) and the mixture height in the ballast tank ($H_{mixture}$) comparing with the experimental data in the case C1.

Although all the considered variables in Figure 4.3 trend to be convergent and the mesh with $\alpha_{ds}=6.25\%$ is supposed to be sufficient fine, the difference between the numerical results and the

experimental data is considerably large, especially for the mixture height inside the ballast tank as shown in Figure 4.3(b). It should be noticed that the height of the oil left in the cargo tank (H_{oil}) reflects the discharge through the internal hole, meanwhile, the height of the oil/water mixture in the ballast tank ($H_{mixture}$) is determined by the discharges through both the internal and external holes. Different from the perfect prediction in the submerged or un-submerged SHT spilling cases confirmed by Figure 4.2, the standard k-ε model fails to accurately simulate turbulence features in the Case G1 yielding a significantly different spilling process as shown in Figure 4.3. This implies that the conclusion about the turbulence effect on the height of the oil left in the cargo tank drawn based on the previous studies of the oil spilling from SHTs (Lu *et al*., 2010; Xiao *et al*., 2010) and the discussion in the previous section claiming that the standard k-ε model yields promising accuracy for predicting the oil spilling from SHTs, may not be fully extended to the problems associated with DHTs. However, the corresponding comparison of Case C1 shown in Figure 4.4 indicates an opposite conclusion that the numerical results using the standard k-ε model agree satisfactory with the experimental data. This suggests that the applicability of the standard k-ε model is case-dependent and the turbulence model selection is crucial for the DHT case, which need to be investigated further. In the following sections, several turbulence models will be selected and their performance on the DHT spilling problem will be compared in Section 4.3.2; the systematic investigation of turbulence features modelled by different turbulence models and their effects on the DHT spilling process will be presented in the next chapter.

4.3.2 Performance of different turbulence models

When carrying out the numerical investigation on one engineering problem, applying an appropriate turbulence model to simulate the turbulence features is one of the curial issues for accurate and efficient modelling. This issue is raised seriously according to the above discussion on the DHT cases and there is a lack of guidelines targeting similar multiphase flow patterns in literature. Thus, in this section, in order to find a suitable turbulence model, a group of common-used turbulence models are selected and their performance is examined.

Different approaches to resolving the turbulence, including the RANS with different turbulence models, LES and DNS, are considered in this section. It is worth noting that the LES (Hunt *et al*., 2006; Reboux *et al*., 2006) and the DNS (Pan and Suga, 2006) are generally known to be able to resolve the interfacial turbulence and the transition turbulence associated with free shear layers. Nevertheless, they have not yet been attempted in the DHT oil spilling problems. The LES with the one-equation sub-grid eddy viscosity model, which has been examined in a wide range of turbulent problems and shows a superiority over the Smagorinsky's eddy viscosity model especially if the flow is highly complex and has shear flows as described by Gebreslassie *et al*. (2013) and Menon *et al*. (1996), is utilized. This model accounts for the sub-grid scaling stress

using a Boussinesq type assumption to captures the small-scale eddies, which are isotropic in nature (Gebreslassie *et al.*, 2013; Gourdain, 2015; Taghinia *et al.*, 2015).

On the other hand, the RANS uses time-averaged Navier-Stokes (NS) equations, through which the unsteady flow-field is ensemble-averaged, and the effects of turbulence are represented by the Reynolds stress tensor, which is usually solved by using appropriate turbulence models, such as the well-known k-ε and k-ω models, tuned and calibrated for specific flow features excluding the situations concerned with DHTs. Therefore, various RANS approaches, including the standard k-ε, Launder-Sharma low-*Re* k-ε, RNG k-ε, realizable k-ε and k- ω SST models are employed in this study.

Generally speaking, the RANS approaches normally require relatively coarser mesh resolution with shorter CPU time to get convergent results. However, the LES requires a much higher mesh resolution and much smaller time steps to achieve convergent results and, therefore is more time-consuming, compared to the RANS approaches. Compared to the LES and the RANS approaches, the DNS requires much denser mesh to get a convergent solution but can fully resolve the turbulence. This means that by using the same computational mesh as the one required by the LES, the results of the DNS may be under-resolved. When taking the model efficiency into account, the fully-solved DNS model is too time-consuming to be carried out. Nevertheless, one may agree that for a specific mesh resolution, the difference between the result of the under-resolved DNS and that of the LES may reflect the overall effect of the sub-grid stress. Considering this, an under-resolved DNS is also employed in this investigation to shed some light on the significances of the sub-grid stress in the LES. More detailed discussion is presented in Chapter 5.

As a result, a comprehensive convergence test with regard to the LES model is presented in order to demonstrate the mesh resolution meets its strict requirements. All the related cases are examined in prior and the Case G1 with initial H_{oil} is set as 42cm and the draft of the tank d is kept as a constant value of 27cm is selected as the demonstration case. Following the similar procedures of SHT cases, the spatially hierarchical mesh refinement for the LES model is redistributed with a significantly increase of the total cell number. A sample of the computational domain and mesh distribution are illustrated in Figure 4.5. Different mesh resolutions, specified by using α_{ad} ranging from 1.5625% to 6.25%, are used, yielding that the number of the cells per diameter of the holes in horizontal direction varies from 64 to 16 and the number of cells along the vertical axis through the centres of the holes ranging 224-56; the total number of cells varies from approximately 4.1 to 0.7 million.

(a)

(b)
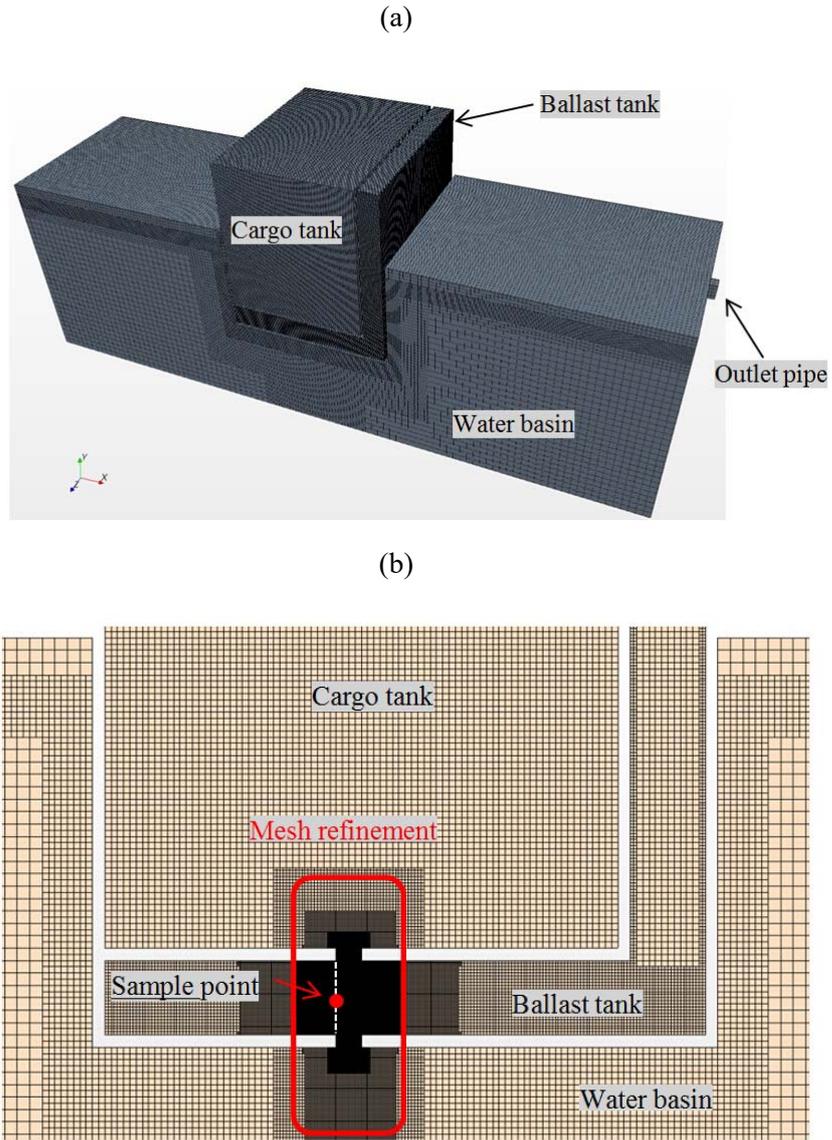
Figure 4.5 Sketch of the computational domain and mesh.
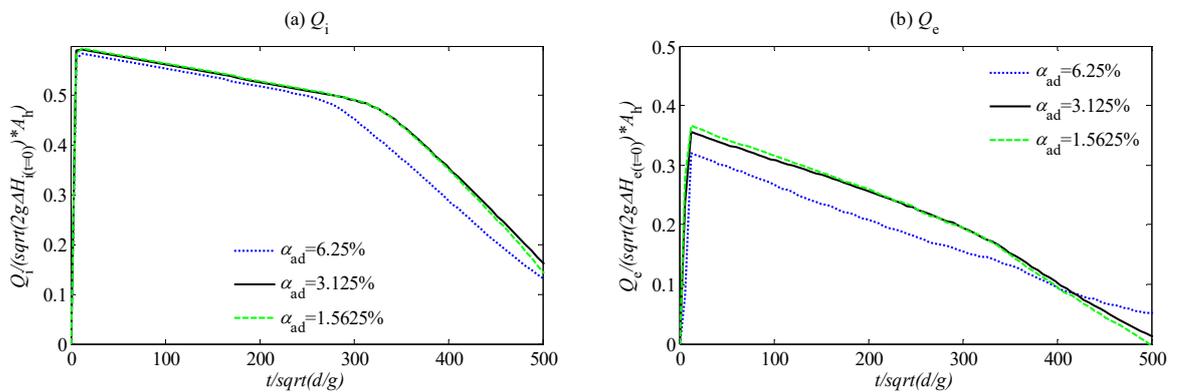
Figure 4.6 The time histories of the volumetric flow rate through the internal (Q_i) and external hole (Q_e) for the LES model with different cell sizes (Case G1).
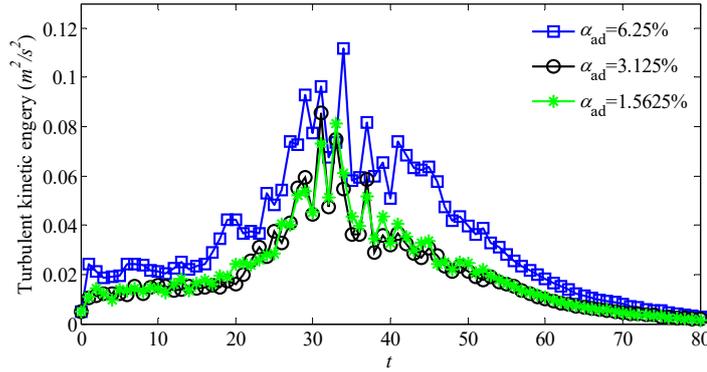
Figure 4.7 The time histories of the turbulent kinetic energy (k) at the sample point (in Figure 4.5(b)) for the LES model with different cell sizes (Case G1).

Figure 4.6 shows the time histories of the non-dimensionlised discharge of the oil/water mixture through the internal hole, Q_i, and the external hole, Q_e in the cases with different cell sizes for the LES model. It is observed that the results with α_{ad}=3.125% agree well with those using a finer mesh, i.e., α_{ad}=1.5625% but are visually different from those using a coarser mesh, i.e., α_{ad}=6.25%. Considering the fact that the discharge indicates a spatially averaged velocity through the holes and may not represent the feature of the turbulent flow in a smaller scale, other turbulence-related parameters, e.g. the turbulent kinetic energy (k), is also examined at some specific locations of interest. These include the locations inside the boundary layers attached to the solid wall near the holes and near the interfaces between different phases, where the turbulence is expected to be either more significant or more sensitive to achieve correct results (Hunt *et al*., 2006). Figure 4.7 compares the turbulent kinetic energy (k) in the case G1 with different cell sizes at the midpoint between left bottom corner of the internal hole and the left top corner of the external hole on the central vertical plane (as illustrated in Figure 4.5(b)), which is mainly located on the interfacial region between oil and air phases in the ballast tank before it becomes submerged. For clarity, corresponding results with a time interval of one second are plotted, although the actual time step size used in the numerical simulation reaches the level of 10^{-5}s. A similar convergence property can be achieved. The time-averaged relative difference, which is defined in the same way as Ma and Yan (2006), of turbulent kinetic energy (k) between α_{ad}=3.125% and α_{ad}=1.5625% shown in Figure 4.7 is approximately 1.6%, which can be considered as acceptable.

One may find from Figures 4.3 and 4.6 that different turbulence models lead to significantly different results. As discussed above, the standard k-ε fails to model the spilling flow in grounding Case G1 but yields acceptable result in other collision case Case C1. It is necessary to carry out a systematic investigation in order to address the appropriate turbulence modelling with the consideration of model accuracy and robustness. In this study, the LES-based one equation eddy viscosity model (refer to as the LES model), RANS with the standard k-ε model, Launder-Sharma

low-*Re* k-ε, RNG k-ε, realizable k-ε and k-ω SST models, and the DNS are employed for this purpose. Considering the limit of the laboratory model tests on measuring micro-scale flow fields, two macroscopic parameters, i.e. H_{oil} and $H_{mixture}$, are examined. The mesh resolution used in the RANS model is determined based on the convergence test as shown in Figure 4.3. As the Launder-Sharma low-Re k-ε model adopts the empirical treatment of the flow near the wall with local low turbulent Reynolds number effects and the wall damping effects (Seyedein *et al*., 1994; Cho and Goldstein, 1994) rather than the wall function applied by other conventional turbulence models, the mesh near the hull wall, especially in the rupture region, is further refined to reach the *y*+ requirement, i.e., down to the viscous sublayer (Igci and Arici, 2016). For the case with DNS, the cell sizes used are the same as the one used by LES according to relevant convergent investigation shown in Figures 4.6 and 4.7, although the mesh resolution required by the DNS may be under-resolved.
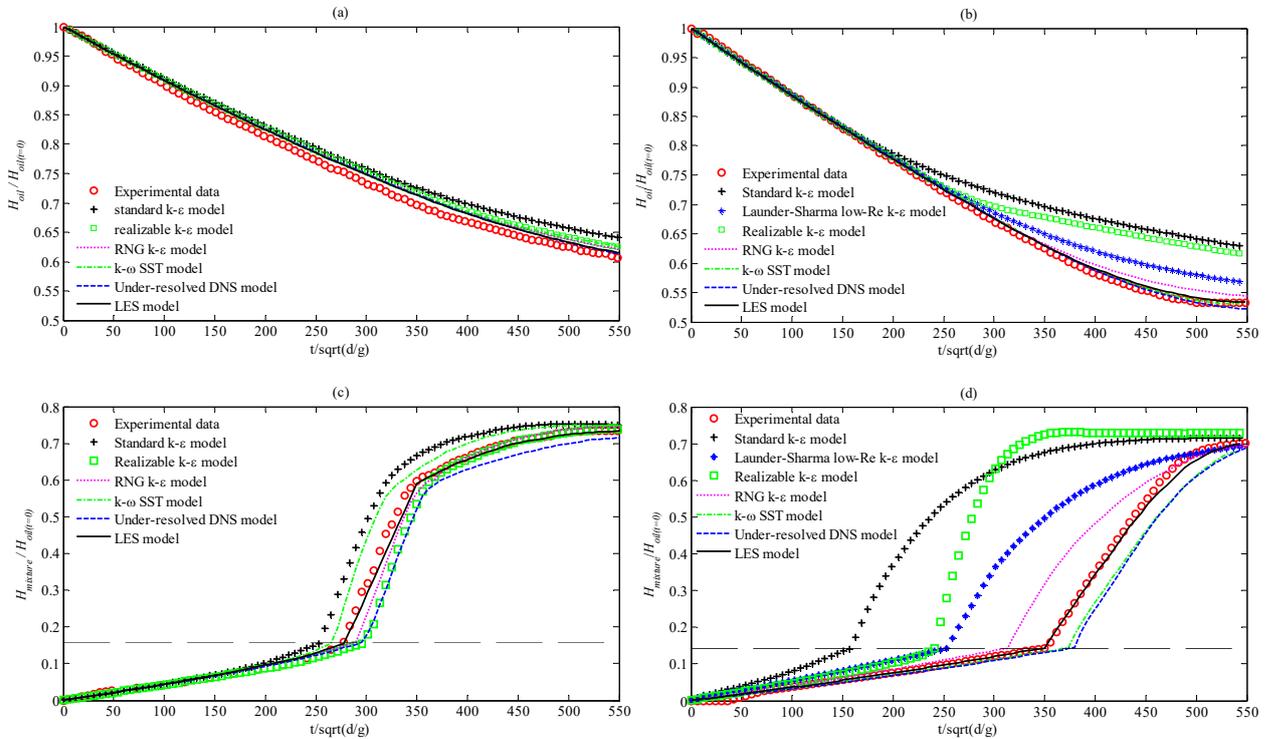
Figure 4.8 The comparison of turbulence model performance in terms of the time histories of (a, b) the oil height inside the cargo tank (H_{oil}) and (c, d) the mixture height in the ballast tank ($H_{mixture}$) for Case C1 and Case G1.

The model performance in terms of two macroscopic parameters, i.e., H_{oil} and $H_{mixture}$ for Case C1 and Case G1 is compared in Figure 4.8. The height of the oil left in the cargo tank (H_{oil}), reflecting the discharge through the internal hole, is firstly considered. The time histories of H_{oil} in the Case C1 and Case G1 with different turbulence modelling approaches are plotted in Figure 4.8(a) and (b), respectively. Similar to Figure 4.3, the time and H_{oil} are non-dimensionlised by

using $\sqrt{d/g}$, the initial height of oil in the cargo tank ($H_{oil(t=0)}$), respectively. As observed from this Figure, all numerical results agree well with the experimental data in Case C1 (Figure 4.8(a)) no matter which turbulence modelling approaches are used. However, in Case G1(Figure 4.8(b)), most of the approaches lead to a satisfactory agreement with the experimental data, except the standard, realizable and low-*Re* k-ε models, whose results seem to diverse from others at the dimensionless time larger than approximately 160, 240 and 250 respectively. For example, at $t/\sqrt{d/g} \approx 160$, the internal hole becomes fully submerged ($H_{mixture}/H_{oil(t=0)} > 0.143$) in the case using the standard k-ε model but not in other cases as shown in Figure 4.8(d). It is understandable that the hydrodynamic features or the hydraulic head difference dominating the flow through the internal hole (reflecting the change of H_{oil}) are different before and after such instant. This may directly explain the diversion of the time history of H_{oil} at $t/\sqrt{d/g} \approx 160$ between the standard k-ε model and others. Similar mechanism can be used to explain the diversion of the H_{oil} result by the realizable k-ε model or the low-*Re* k-ε model at $t/\sqrt{d/g} \approx 240$ or 250. This implies that the height of the oil in the cargo tank during spilling may be considerably affected by the characteristics of the flow in the ballast tank, which will be discussed below.
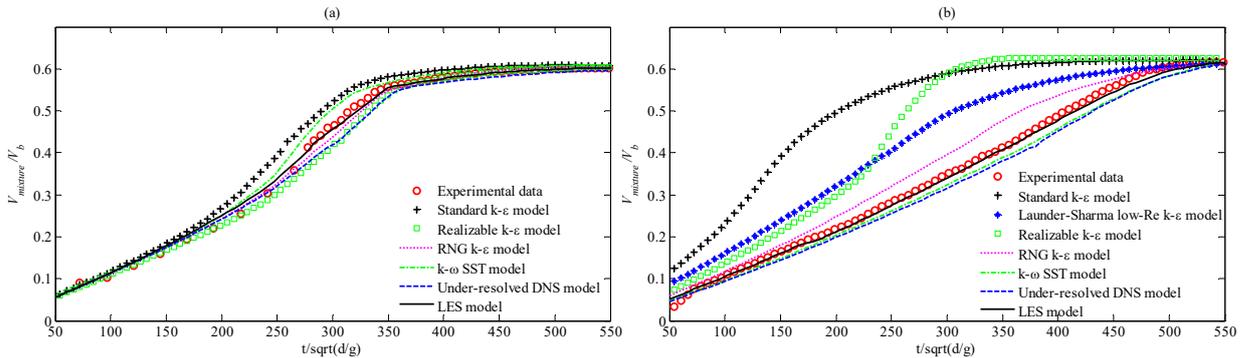
Figure 4.9 Time histories of the volume of the mixture in the ballast tank ($V_{mixture}$) in the Case C1 and Case G1 with different turbulence models.

The height of the oil/water mixture in the ballast tank ($H_{mixture}$) for both cases, which is determined by the discharges through both the internal and external holes, is examined then. The profiles using different turbulence modelling approaches and measured in the laboratory are presented in Figure 4.8(c) and (d). Considering the sudden transition when $H_{mixture}$ reaches the height of the bottom ballast space (H_b) representing by a horizontal dash-dotted line in Figure 4.8(c) and (d), the corresponding results of the volumes of the oil/water mixture ($V_{mixture}$) in the ballast tank are illustrated in Figure 4.9 for clarity, in which $V_{mixture}$ is non-dimensionlised by the volume of the ballast tank, V_b. From Figures 4.8 (c) and (d) and Figure 4.9, it is observed that the numerical results are sensitive to different turbulence modelling approaches. In both cases, the standard k-ε model results in a much quicker increase of the mixture in the ballast tank, whereas the under-

resolved DNS underestimates the rate of the increment of the mixture. It is also interesting to find that the realizable k-ε model, RNG k-ε model and k-ω SST model do not only produce values of H_mixture or V_mixture considerably different from the experimental data, but show different trends of error in different cases. For example, the k-ω SST model overestimates the rate of the increase of the mixture level in Case C1 but underestimate that in Case G1. This implies uncertainties in estimating the errors caused by these models. The low-Re k-ε model seems to produce a better result compared to the realizable k-ε model, as observed from Figure 4.8(b) and (d) and 4.9(b), which shows that the results by the low-Re k-ε model are close to that by the realizable k-ε model before $t/\sqrt{d/g}\approx240$ and then shifts towards the one by the RNG k-ε model. The RNG k-ε model seems to yield the best profiles among all mentioned k-ε models in both cases, but an obvious gap between the experimental and numerical results remains as shown in Figure 4.8(d) and Figure 4.9(b). The comparison double-confirms that employing the standard k-ε model, or even k-ε models to simulate the DHT cases, one would obtain wrong results for the height of the oil/water mixture in the ballast tank.

Furthermore, it has been found that the results of the under-resolved DNS agree well with the experimental data in terms of H_oil (Figure 4.8(a) and (b)). However, Figure 4.8 (c) and (d) and Figure 4.9 show that the corresponding results for H_mixture are considerably different from the experimental data. This is due to the different characteristics of the flows influencing them. H_oil corresponds to the oil discharge through the internal hole and is dominated by the oil motion inside the cargo tank and driven mainly by the gravity. The flow state through the internal hole with the initially Re numbers approximately 1200 and 1800 in Case C1 and Case G1, respectively, is similar to that in SHT cases and, thus the performance of under-resolved DNS is consistent to that in SHT cases. On the other hand, H_mixture reflects an overall effect of the flows through the internal/external holes and the motion of fluids in the ballast tank, which shows complex features of multiple phase flows and may involve violent fluid impacts, broken interfaces between different phases and entrapped air bubbles. The associated turbulence behaves differently and plays a more important role. The present under-resolved DNS model fails to properly capture the turbulence characteristics to achieve satisfactory results in the ballast tank. The turbulence behaviour will be discussed in the next chapter. Overall, as expected, the LES leads to the most accurate results, which agree well with the experimental data for both macroscopic parameters (H_oil and H_mixture) in both cases.
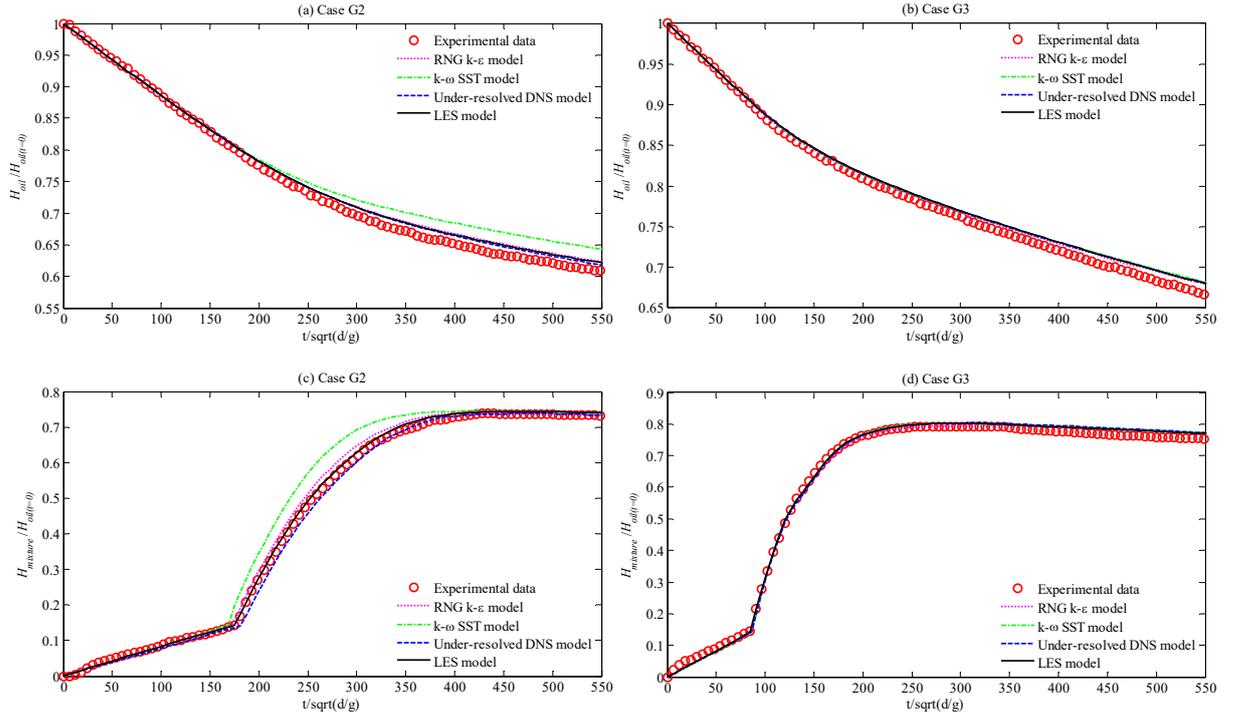
Figure 4.10 The comparison of turbulence model performance in terms of the time histories of (a,b) the oil height inside the cargo tank (H_{oil}) and (c,d) the mixture height in the ballast tank ($H_{mixture}$) for Case G2 and Case G3.

Considering the spilling features described in Chapter 3, two additional grounding cases with a different offset (Δ) between the internal and the external holes, i.e., Case G2 and Case G3, are considered. Due to the fact that these cases are under the grounding scenario, four different models including RNG k-ε model, k-ω SST model, LES model and under-resolved DNS model are applied, considering the worse performance of other k-ε models involved in the Case G1. The corresponding comparison of the time histories of the oil height in the cargo tank (H_{oil}) and the mixture height in the ballast tank ($H_{mixture}$) is presented in Figure 4.10. Overall, the H_{oil} and $H_{mixture}$ predicted by using the LES model agree well with the experimental data in these two cases similar to the previous discussion for Case G1 and C1. With the increase of offset, the differences among the concerned models on H_{oil} and $H_{mixtrue}$ become smaller. The difference is highlighted via the discharges through the internal and external holes (Q_i and Q_e) displayed in Figure 4.11. It is clearly shown that the k-ω SST model delivers underestimated discharge curves (shown in Figure 4.11 (a) and (c)) and fails to match the experimental data in Case G2 (shown in Figure 4.10(a) and (c)). While the discharge difference among the models is little in Case G3 (shown in Figure 4.11 (b) and (d)), except at the early stage. According to the Figure 4.10 (b) and (d), the curves of three models are similar and match the experimental data very well in Case G3.
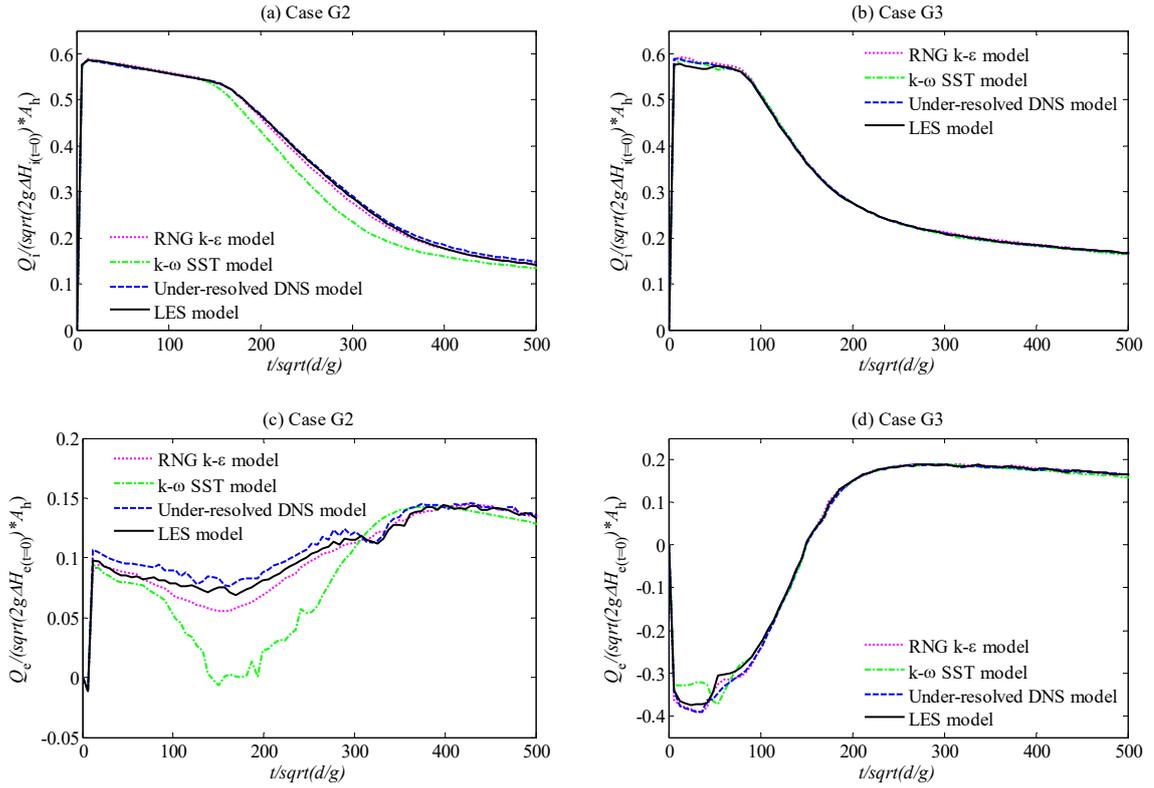
Figure 4.11 The time histories of the volumetric flow rate through the internal (Q_i) and external hole (Q_e) with different turbulence modelling in (a), (c) Case G2 and (b), (d) Case G3 (positive value means outflow).

4.4 Summary

The comprehensive three-dimensional numerical simulation on the oil spilling from damaged tanks is carried out using the open source software OpenFOAM. The VOF-based multiphase solver is solved using FVM method incorporated with the viscosity and surface tension effect. Different tank configurations (SHTs and DHTs) and accidental scenarios (grounding and collision) are considered. Since the turbulence behaviours of the fluids motion during the spilling process are significantly different between the SHT and DHT cases, this numerical study is focusing on the performance of the turbulence modelling, which has not been studied in the previous study.

For the SHT cases, both the DNS and standard k-ε models show similar convergence properties and yield accurate results comparing with the published experimental data. This is consistent to some previous conclusions. With respect to the DHT cases, the three-dimensional model makes it possible to compare numerical results with the experimental data. The measured data from the current physical models is applied for the model validation. The preliminary attempt for the DHT case starts from the standard k-ε model and the significant gaps between numerical and experimental data are observed in grounding Case G1, but it becomes insignificant in collision Case C1. This demonstrates the necessity to examine the performance of different turbulence

models for different DHT cases. Thus, different common-used turbulence models, including k-ε, k-ω, LES and DNS models, are selected. The different convergence properties of these models are discussed and the corresponding mesh sensitivity test is tailored. The comprehensive model comparison in terms of H_{oil} and $H_{mixture}$ for the Case G1 and C1 indicates that the accuracy of turbulence model is case-dependent. Moreover, based on the model comparison of Case G1, a group of turbulence models is selected to further simulate the grounding cases with different offsets (Δ). Overall, the LES model leads to the most accurate results, which agree well with the experimental data in each case included in this Chapter. However, the higher mesh resolution is required by the LES model leading to higher computational consumptions. With the increase of Δ, the difference among different models on the concerned variables decreases. The corresponding discussion about the turbulence behaviours for DHT cases and the criteria of implementing appropriate turbulence modelling will be presented in the following chapter.

Chapter 5 Turbulence Effect on the Oil Spilling from Fixed DHTs

According to the previous model comparison, the differences in the H_{oil} and $H_{mixture}$ profiles are attributed to the different turbulence behaviours modelled by different turbulence models. It is beneficial to investigate/summarise the turbulence features of the spilling process from a damaged DHT, based on which the criteria of selecting proper turbulence models shall be suggested.

5.1 The Effect of Turbulence Simulation on Spilling Processes

It is worthy of noting that all numerical results displayed in Figures 4.3, 4.4, 4.8, 4.9 and 4.10 are convergent, except the under-resolved DNS, as demonstrated in the previous section and the differences are caused by different turbulence modelling approaches. As expected, the LES leads to the most accurate results, which agree well with the experimental data for both macroscopic parameters (H_{oil} and $H_{mixture}$) in both cases. The relevant results from the LES modelling are considered as correct solutions for further comparisons on the kinematic and dynamic characteristics of the flow inside the ballast tank, due to the lack of experimental data on these parameters.
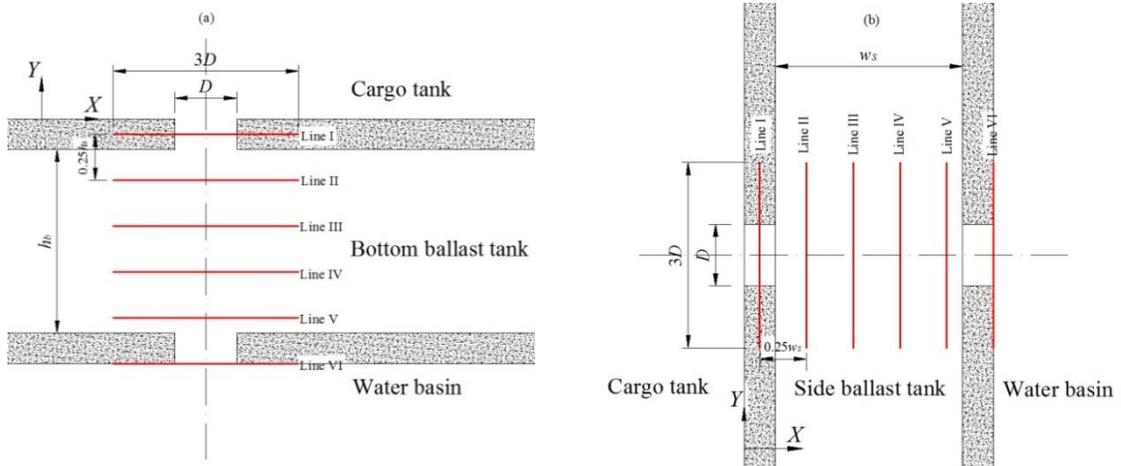
Figure 5.1 Sketch of the sampling lines at the central vertical plane near the holes for (a) Case G1 and (b) Case C1.

Such model comparison aims to shed some light on why different turbulence models lead to significantly different results in Figures 4.8 and 4.9. To do so, some sampling lines at different cross-section between holes on internal and external hulls in Case G1 and Case C1 are introduced as shown in Figure 5.1. Relevant distributions of the parameters have been compared.

We firstly focus on Case G1, where the corresponding results are more sensitive to the selection of the turbulence modelling (Figure 4.8(b) and (d)). Figure 5.2 shows the velocity head ($U^2/2g$) and the pressure (p) distributed at different sampling lines at $t/\sqrt{d/g} \approx 12$ in Case G1. For convenience, they are normalised by using $H_{oil(t=0)}$ and the atmospheric pressure (p_{atm}). As observed from Figure 5.2, near the internal hole (Line I), the velocity head and the pressure predicted by using different turbulence modelling approaches are close to each other, except for the slightly underestimated velocity head profile delivered by standard k-ε model. However, as the location of the observation moves further towards the external hole, more significant difference can be observed. This suggests a considerable underestimation of the outflow through the external hole, due to the overestimation of the turbulent energy loss by the standard and realizable k-ε models.
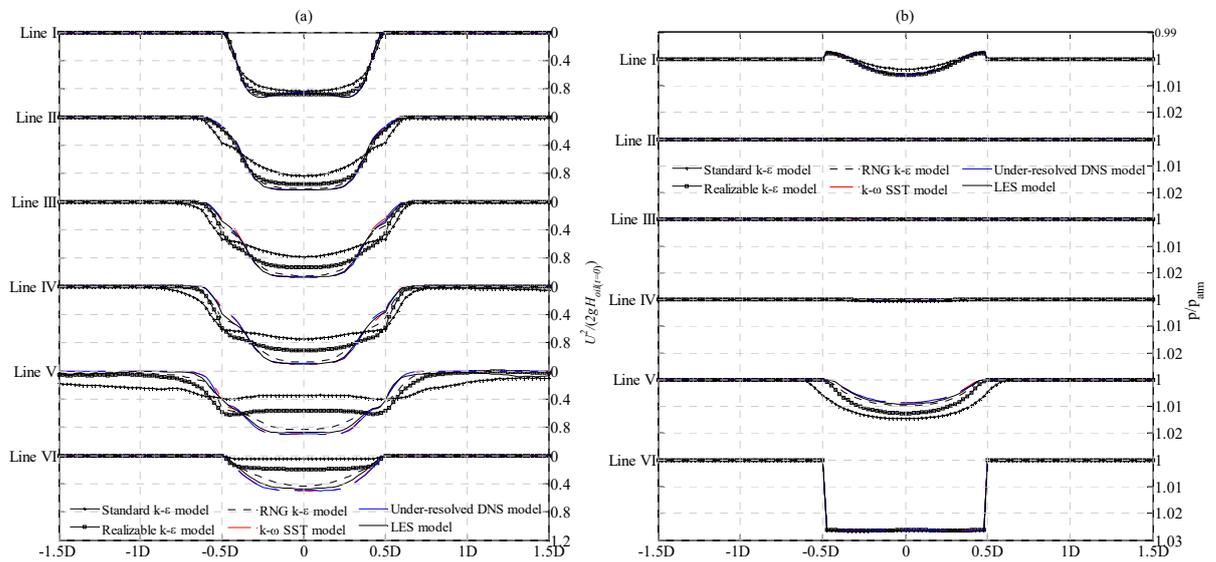
Figure 5.2 Distribution of (a) the normalized velocity head $U^2/(2gH_{oil(t=0)})$ and (b) the normalized pressure (p/p_{atm}) along the horizontal sampling lines at $t/\sqrt{d/g} \approx 12$ in the cases with different turbulence modelling in Case G1.

It is clearer in Figure 5.3 which illustrates the turbulent kinetic energies (k) in the region near the broken holes obtained by using different turbulence modelling. From Figure 5.3, a significantly higher level of the turbulent kinetic energy (k) is observed in the main body of the oil jet inside the ballast tank given by the standard, low-Re and realizable k-ε models. The low-Re k-ε model performs better than the standard k-ε model, partially attributing to the empirical treatment of the flow near the wall with local low turbulent Reynolds number effects and the wall damping effects (Seyedein *et al.*, 1994; Cho and Goldstein, 1994). Compared to the standard, low-Re and realizable k-ε models, the RNG k-ε model shows a dramatic improvement, perhaps attributing to its special concern on smaller scales of the fluid motion, making it more feasible to deal with the

turbulence associated with the interface between different phases and triggered by convective shearing layers. The conclusion on the poor performance of the k-ε models also conforms to the comments by Höhne and Mehlhoop (2014), i.e. without special treatment of a turbulence damping, the differential eddy viscosity models, such as the k-ε models, generate levels of turbulence that are too high throughout the interface of the multi-phase flow. It is also found from Figure 5.2(a) that the k-ω SST model leads to a better estimation of the velocity head (and turbulent energy loss) compared to the k-ε models, conforming to existing conclusion on the suitability of the k-ω SST model on dealing with low Reynolds problems without any extra damping functions (Karim *et al.*, 2009; El-Behery and Hamed, 2011).

Only the LES model yields reasonable turbulence distribution associated with the fluid motion. Firstly, the turbulence occurs during oil/water mixture passing through the damaged holes on the DHTs including the internal hole and external hole, which may behave similarly to jet flows through an orifice. Secondly, the turbulence takes place near the interface between different phases, e.g. the oil/water/air interface inside the ballast tank, where the transition turbulence triggered by the free-shear layers may play an important role.

| (a) Standard k-ε | (b) Realizable k-ε | (c) Low-Re k-ε |
| (d) RNG k-ε | (e) k-ω SST | (f) LES |
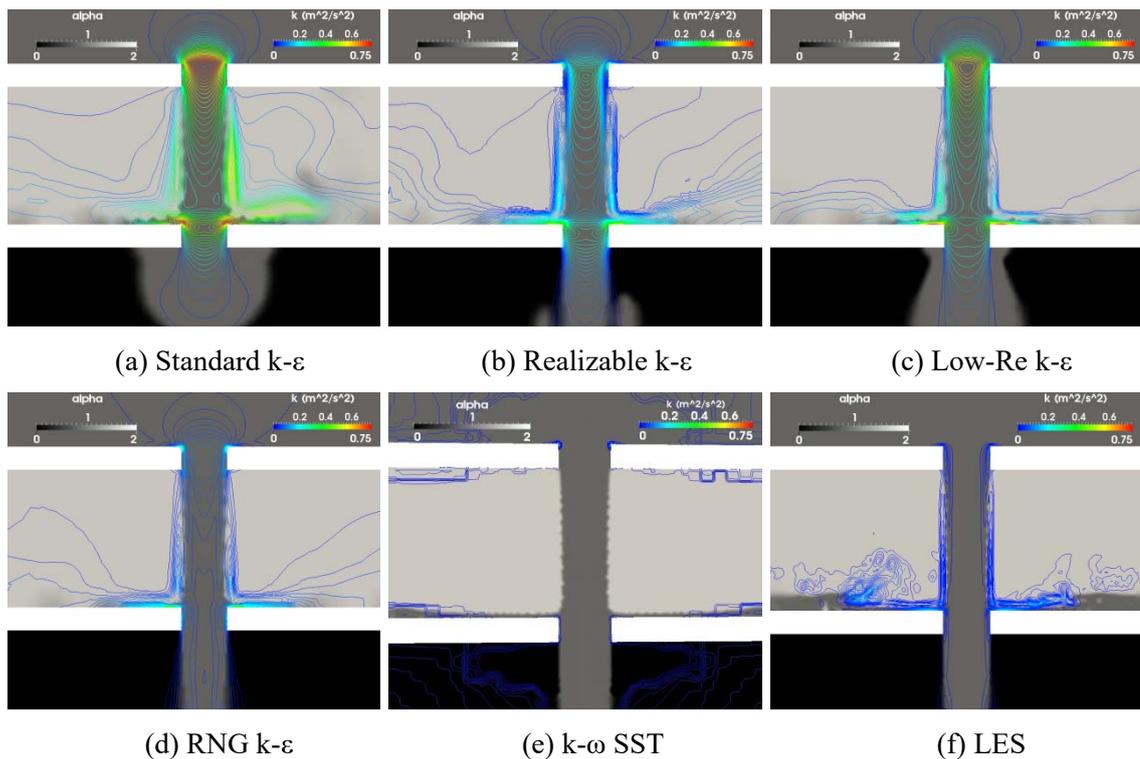
Figure 5.3 Spatial distribution of the turbulent kinetic energy (k) at $t/\sqrt{d/g} \approx 12$ in the cases with different turbulence modelling in Case G1 (the volume fraction, i.e. α, are 0, 1 and 2 for water, oil and air phase).

Figure 5.4 highlights some supplementary LES results regarding to spatial variation of velocity vector, vorticity distribution and 3D oil jet around the ruptures at the corresponding instant. As

mentioned by Eggers and Villermaux (2008), the slip velocity difference between the jet and its air surroundings as shown in Figure 5.4(a) produces shear motion at the jet interface and forms the intensive eddy structure around the air-oil interface inside the ballast tank as shown in Figure 5.4(b). More specifically, the oil jet traveling through the ballast tank with accelerating velocity and drives more intensive vortex as indicated in Figure 5.4(a) and (b), respectively. With the combined effect of interfacial shear motion, gravity, surface tension, turbulence etc., the surface of the oil jet fluctuates with a wave length at the scale of 0.25-0.3D as demonstrated by Figure 5.4(a) and (c), which is similar to the rippled/wavy pattern categorized by Brocchini and Pjeregrine (2001). However, the relatively thick jet and its short falling time to reach the external hole are insufficient to launch breakup, namely Rayleigh-Taylor instability (Eggers and Villermaux, 2008).

| (a) | (b) | (c) |
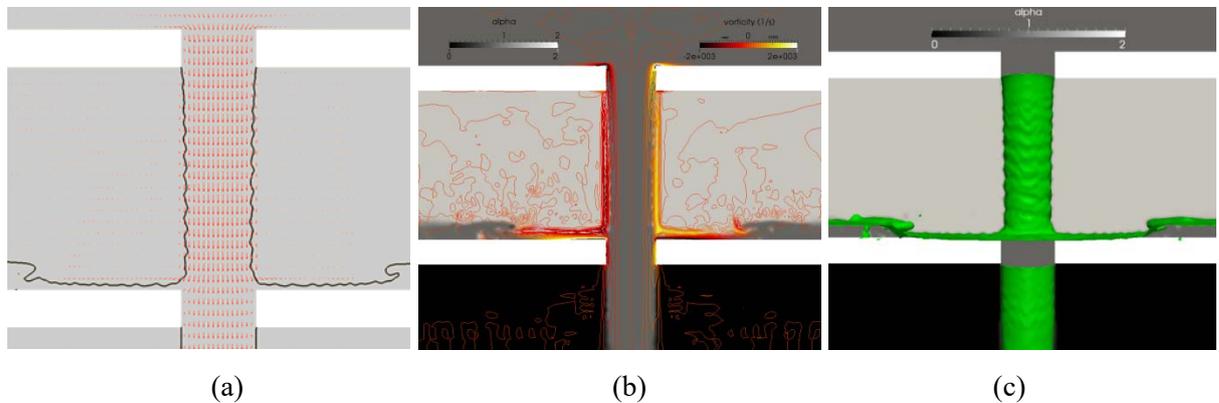
Figure 5.4 Snapshots of (a) the spatial variation of velocity vector, (b) the vorticity distribution and (c) the 3D oil jet interface around the ruptures at $t/\sqrt{d/g} \approx 12$ using the LES simulation for Case G1 (the volume of fraction, i.e. α, are 0, 1 and 2 for water, oil and air phase, the interfaces of the oil jet and water jet are marked by the green iso-surfaces)

The effect of the turbulence modelling on the discharge through the internal hole (Q_i) and external hole (Q_e) lasts throughout the spilling process as demonstrated in Figure 5.5. During the early stage, the difference in Q_e yielded by the turbulence models forms different $H_{mixture}$ profiles as indicated in Figure 4.8(d). Since the instants that mixture level reaches the bottom of the cargo tank are different among these turbulence models, the discharge through the internal hole (Q_i) differs from each other significantly afterwards. It highlights the importance of the turbulence modelling on the oil spilling from grounded DHTs.
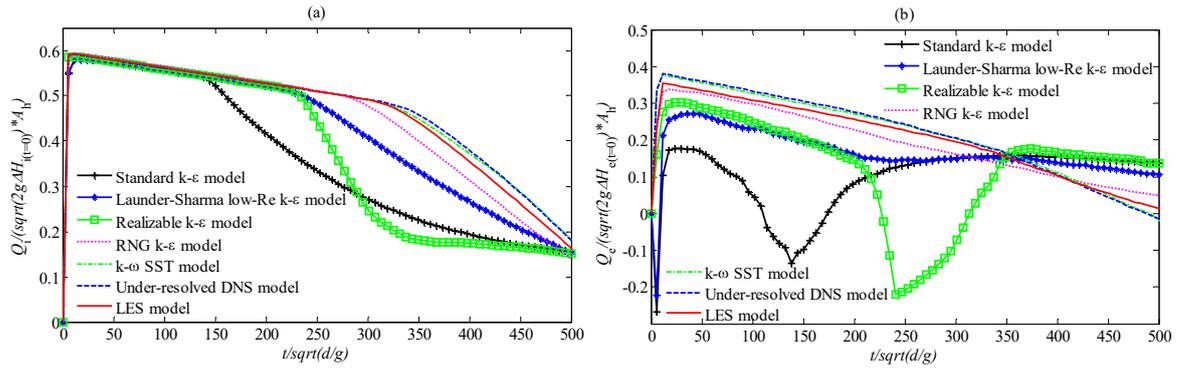
Figure 5.5 The time histories of the volumetric flow rate through the internal (Q_i) and external hole (Q_e) with different turbulence modelling in Case G1 (a positive value means outflow).
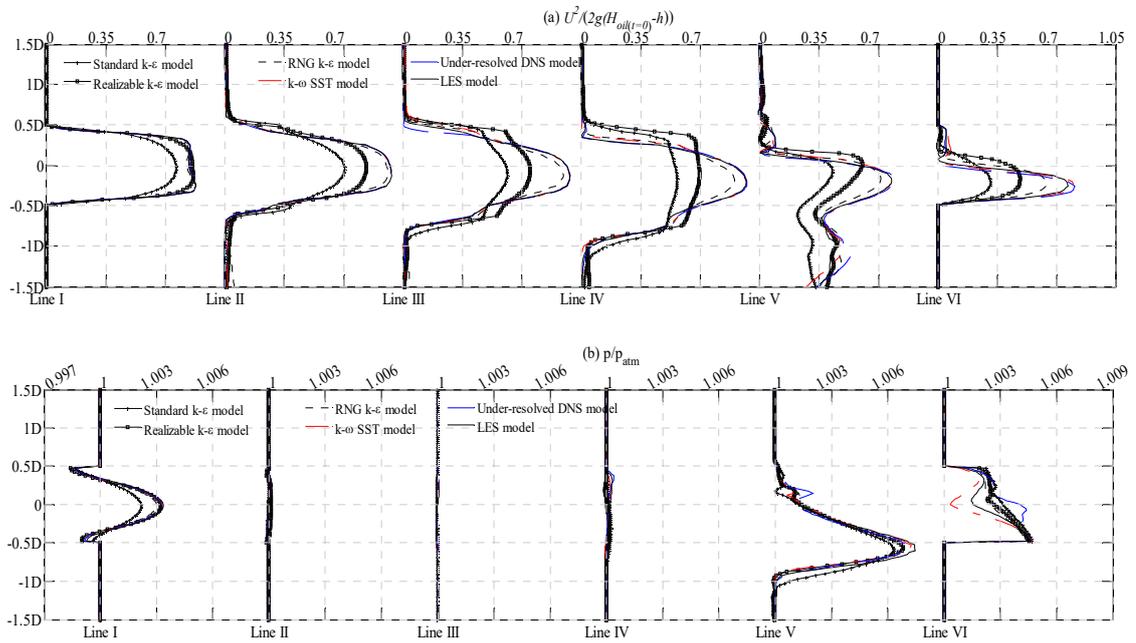
Figure 5.6 Distribution of (a) the normalized velocity head $U^2/(2g(H_{oil(t=0)}-h))$ and (b) the normalized pressure (p/p_{atm}) along the horizontal sampling lines at $t/\sqrt{d/g} \approx 12$ in the cases with different turbulence modelling in Case C1.

Figure 5.6 shows the velocity head ($U^2/2g$) and the pressure (p) distributed at different sampling lines at $t/\sqrt{d/g} \approx 12$ in Case C1. The turbulence performance on the oil discharge through the internal hole is similar in Case C1, where the standard k-ε model underestimates the velocity head more significantly than the one in Case G1. As the jet travelling towards the external hole, the difference on the velocity head among different turbulence models becomes greater, from Line II to Line IV. This is mainly attributed to the different turbulent kinetic energies (k) (illustrated in Figure 5.7), in which the standard k-ε and realizable k-ε models delivery high k value attached to the oil jet body inside the ballast tank.

(a) Standard k-ε   (b) Realizable k-ε   (c) RNG k-ε

(d) k-ω SST   (e) LES
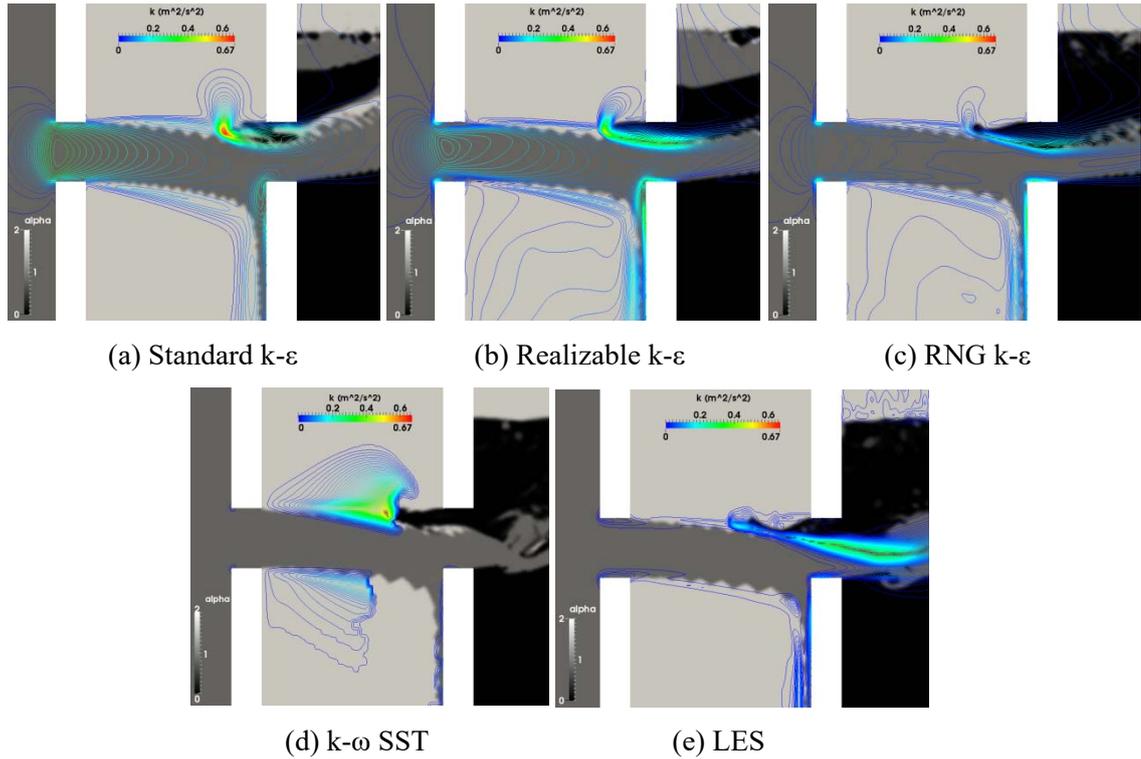
Figure 5.7 Spatial distribution of the turbulent kinetic energy (k) at $t/\sqrt{d/g} \approx 12$ in the cases with different turbulence modelling in Case C1 (the volume fraction, i.e. α, are 0, 1 and 2 for water, oil and air phase).

Based on the experimental observation, the flow features around the external hole in Case C1 are more complicated and different at each spilling stage, which introduces some water inflow during the first and second stages as mentioned in Section 3.3.3. For clarity, the comparison of flow patterns between the experimental and numerical results at some representative instants is shown in Figure 5.8. More specifically, the corresponding velocity vectors and the corresponding distribution of water, oil and air (represented by using the volume fraction, α) in the central vertical plane by using the LES modelling illustrated in Figure 5.8(a) for $t/\sqrt{d/g} \approx 12$ shows that the water inflow from the environment and the oil outflow occur at the external hole simultaneously indicating a typical shear flow. However, Figure 5.7 displays different turbulence behaviours around the shear flow interface delivered by different turbulence models, which significantly affects the fluid state, such as air-oil-water portions, velocity and pressure fields (at Line V and VI in Figure 5.6).

It is also found from Figure 5.8(b) that such convective motion of the oil outflow and the water inflow also occurs at other time instants at the second stage. It is clearer in Figure 5.9, which displays the time histories of discharges of the oil (Q_{eo}) and water (Q_{ew}) through the external hole in Case C1 (positive value of the discharge indicates an outflow). It should be noticed that both the oil flow blocked by the external hole (Q_i-Q_{eo}) and the water inflow through the external hole

(Q_{ew}) contributes the mixture inside the ballast tank during the early stage ($t/\sqrt{d/g} < 350$). Though different turbulence models bring different Q_{eo} and Q_{ew} profiles as shown in Figure 5.9, the closer $H_{mixture}$ curves indicated in Figure 4.8(c) reveal that the combined influence on the mixture accumulation inside the ballast tank in Case C1 is not as significant as the one in Case G1 shown in Figure 4.8(d).
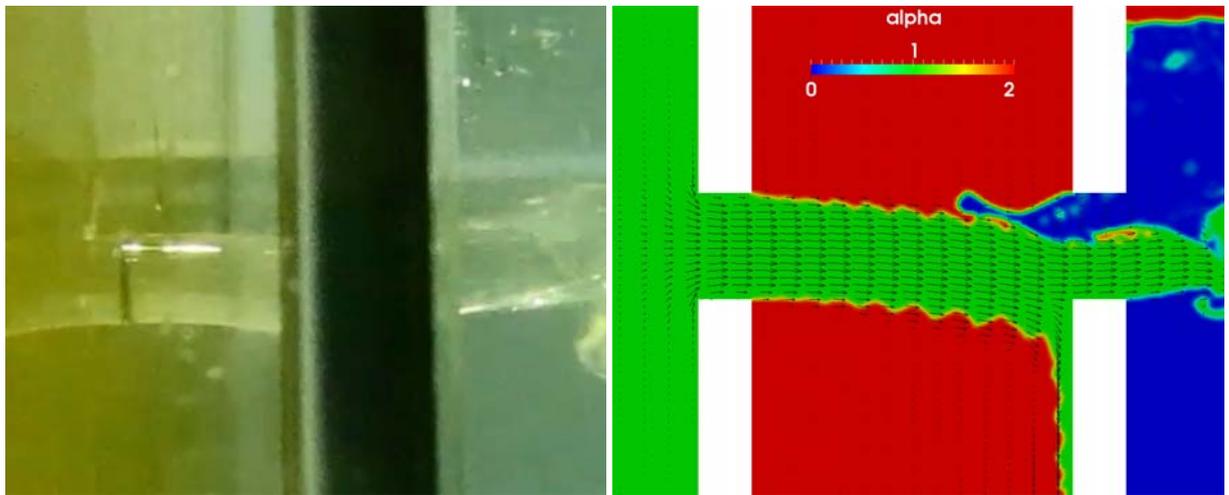
(a) $t/\sqrt{d/g} \approx 12$
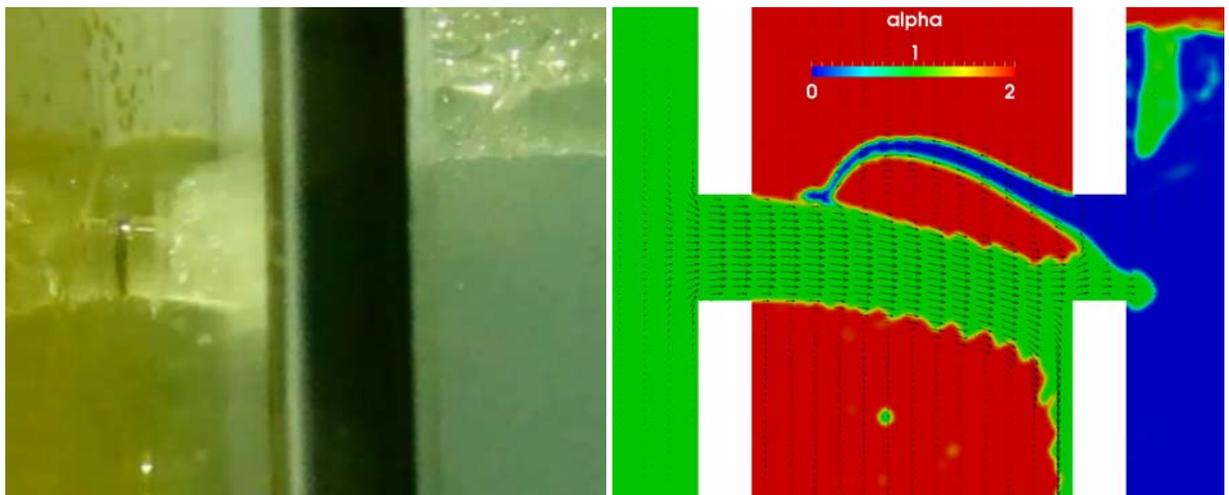
(b) $t/\sqrt{d/g} \approx 300$

Figure 5.8 Flow pattern at different time instants in Case C1. (Left: experimental snapshots; Right: the velocity vector and distribution of the fluids in the central vertical plane in the LES modelling, the volume fraction, i.e. α, are 0, 1 and 2 for water, oil and air phase)
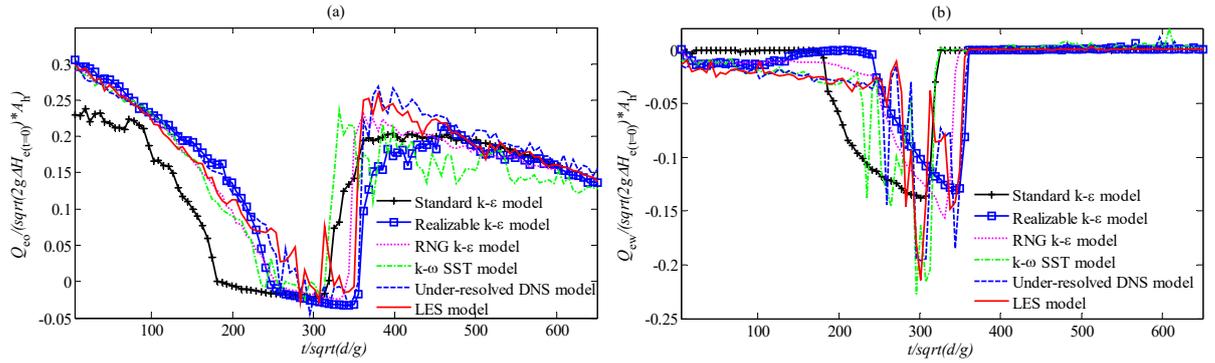
Figure 5.9 Time histories of discharges of the oil (Q_{eo}) and water (Q_{ew}) through the external hole in Case C1. (a positive value means outflow)

5.2 Criteria of Selecting Proper Turbulence Models

Based on the previous experimental and numerical results, it can conclude that the water jet appears during the oil spilling from either grounded or collided DHTs, and its importance is case dependent. For example, the water jet occurs in form of convective oil-water flow around the external hole in Case C1 as demonstrated in Figure 5.8 and the resultant Q_{ew} changes with time as indicated in Figure 5.9(b). The instantaneous Reynolds number of the water inflow (calculated by using $\tilde{U}2\sqrt{\tilde{A}/\pi}/\nu$, where ν is the kinematic viscosity, $\tilde{U}$ and $\tilde{A}$ are the areal averaged flow velocity and the cross-sectional area occupied by the fluid) through the external hole may reach the level of 10^4 (Figure 5.10), which is much larger than the Reynolds number corresponding to the oil flow (around 1200 as shown in Figure 5.10) and indicates a typical turbulence regime.
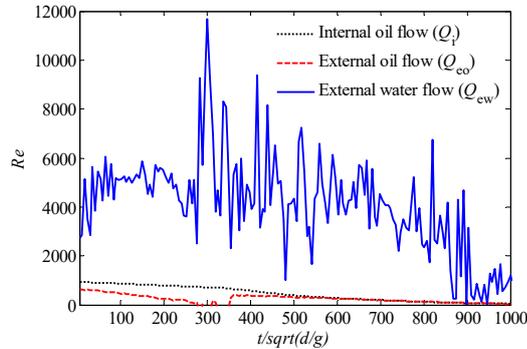
Figure 5.10 Instantaneous Reynolds numbers corresponding to the water and oil flow in Case C1 by using LES modelling (the instantaneous Reynolds number is calculated by using $\tilde{U}2\sqrt{\tilde{A}/\pi}/\nu$, where ν is the kinematic viscosity, $\tilde{U}$ and $\tilde{A}$ are the areal averaged flow velocity and the cross-sectional area occupied by the fluid)

As for the grounding cases, the presence of the water flow in each case is quite different producing different characterised Reynolds number corresponding to the water inflow, while the characterised Reynolds number corresponding to the oil flow remains approximately the same due to the same hydrostatic condition in each grounding cases. Due to the lack of experimental

data, Figure 5.11 plots the time histories of the discharges of the oil and water through the external hole (Q_{eo} and Q_{ew}) in the grounding cases with different axial offsets (Case G1, G2 and G3) simulated by the LES model. One can see that discharges are significantly affected by the different offset (Δ). For example, in the cases with Δ=0 and Δ=0.5D, no significant water inflow is detected but the considerable amount of water enters the ballast tank from the beginning of the case with Δ=D. Another interesting point is that the water will be expelled out by oil in the later stage in the case with Δ=D.
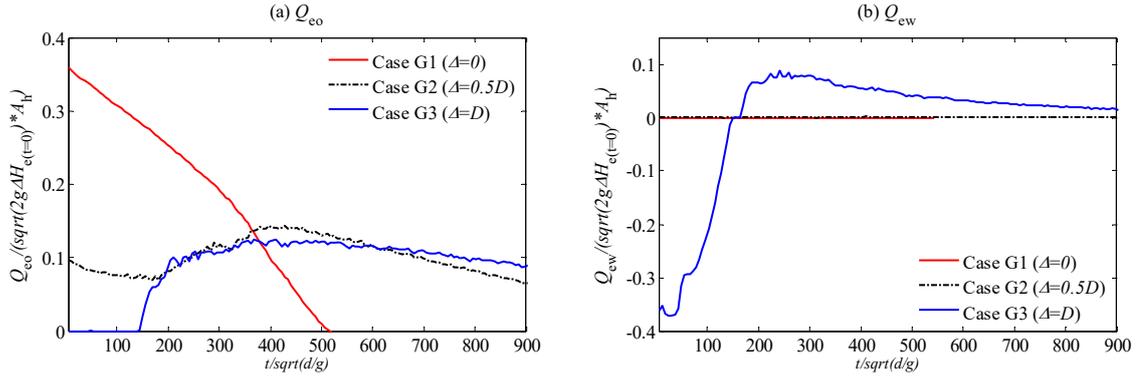
Figure 5.11 The comparison of the time histories of the discharges of the oil and water through the external hole in the grounding cases with different axial offsets by LES modelling (a positive value means outflow).

(a) $t/\sqrt{d/g} \approx 0.16$ (b) $t/\sqrt{d/g} \approx 0.19$ (c) $t/\sqrt{d/g} \approx 0.57$
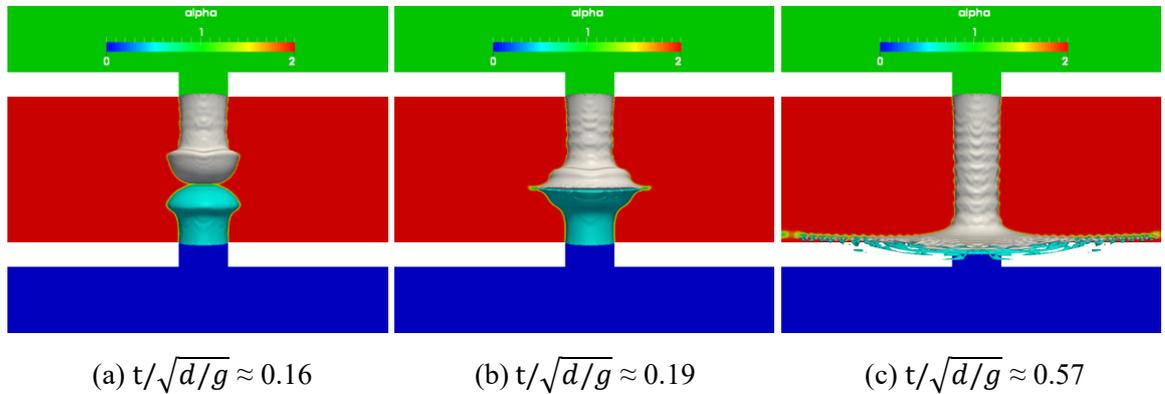
Figure 5.12 Snapshots of the oil jets in the ballast tank at different stages using the compressible LES simulation for Case G1. (the volume fraction, i.e. α, are 0, 1 and 2 for water, oil and air phase, the interfaces of the oil jet and water jet are marked by the grey and light blue iso-surfaces)

To explain why water inflow is not significant for the case with small offsets, such as in Case G1 and Case G2, Figure 5.12 is plotted for G1, from which one can see that the amount of water flow through the external hole in the short period of the spilling from the start, e.g. $t/\sqrt{d/g} < 0.5$. However, due to the strike of the downward oil jet from the internal tank carrying higher momentum than the water jet, the upwelling water is pushed down. The similar phenomenon is

found in Case G2 and the oil outflow through the external hole occupies the spilling process afterwards without the significant water inflow, which fails to be recognized from the experimental snapshots (Figure 3.11). In Case G3 ($\mathit{\Delta}=D$), where the oil-water opposite jets do not overlap vertically, such strike becomes insignificant and, therefore in the early stage before the mixture level in the ballast tank reaches a maximum value ($t/\sqrt{d/g} < 150$), the water inflow with Reynolds number at the level of 46000 occupied the entire external hole and the downwards oil jets and the upwards water jets exist at the same time. It is clearer in Figure 5.13 which compares the flow pattern obtained using the LES modelling and experimental data. The numerical result provides more details indicating the distribution of the fluids with velocity vectors.
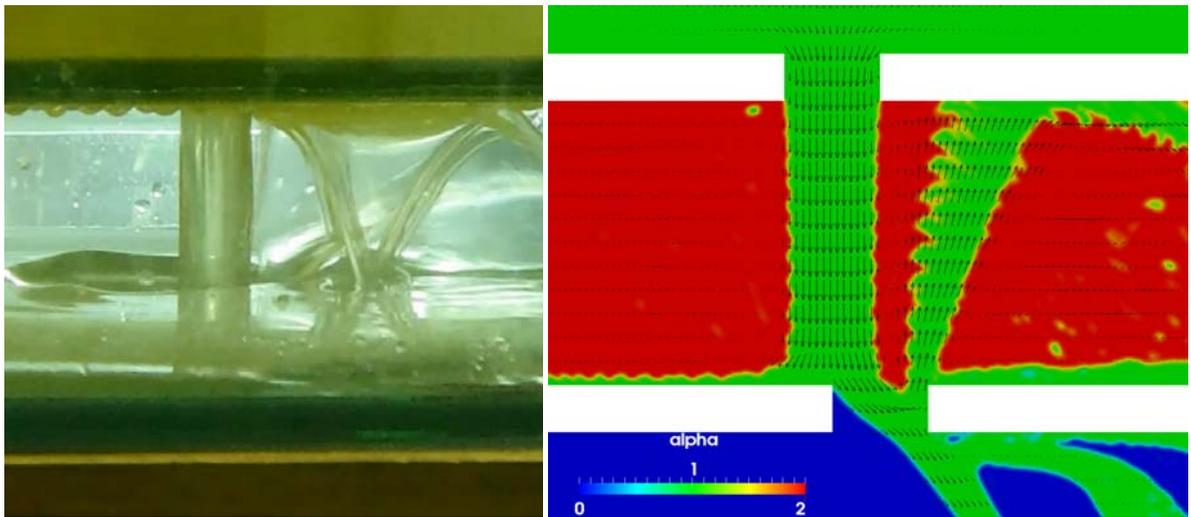
(a) Case G2
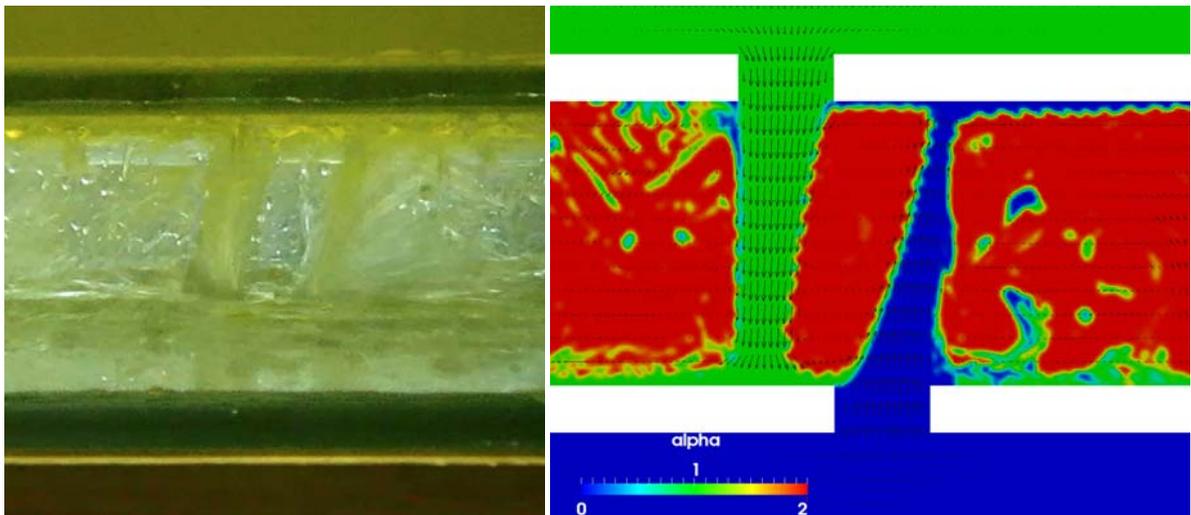
(b) Case G3

Figure 5.13 Flow pattern at $t/\sqrt{d/g} \approx 12$ in Case G2 and G3. (Left: experimental snapshots; Right: the velocity vector and distribution of the fluids in the central vertical plane in the LES modelling, the volume fraction, i.e. α, are 0, 1 and 2 for water, oil and air phase)

According to the analysis of the water flow in different cases, effectively, in some cases, such as Case G1 and G2, the Reynolds number indicating the turbulence may be taken as that corresponding to the oil flow through the internal tank, i.e. ~1800, since the water inflow plays the insignificant role in the spilling process. Nevertheless, the flow state in Case G3 and C1 is more complex due to the axial offset of the spilling hole and horizontal hole location, respectively. In these cases, the water flow associated with Reynolds number approximately 46000 in Case G3 and 17000 in Case C1 participates in the spilling process and reacts violently with the oil flow around the rupture region. This means the definition of the Reynolds number in Case G1 and G2 may be inappropriate to the Case G3 and C1.

From the above case studies, one may agree that both the turbulence associated with the jet flow through the broken hole and the transition turbulence near the interface between different phases associated with the oil spilling from a damaged DHT shall be considered. Generally, the Reynolds number shall reflect the turbulence behaviour in different situations. The significance of the former may be indicated by using the Reynolds number corresponding to the orifice flow. The latter is commonly classified by a sheared Reynolds number (Lombardi *et al*., 1996; Fulgosi *et al*., 2003; Reboux *et al*., 2006), which largely depends on the kinematics and the dynamics of the interface between different fluids and is not easy to be identified before the numerical simulations or laboratory experiments. Considering the complex and unsteady free-shear layers, the former Reynolds number is used to classify the appropriate turbulence models for the oil spilling from DHTs in terms of computational robustness. Reynolds number corresponding to the water flow and to the oil flow shall be employed.

Considering the fact that both the oil outflow and the water inflow are dominated by the gravity, we define the Reynolds numbers corresponding to the water flow and the oil flow, respectively, as $Re_o = \frac{\sqrt{2g\Delta H_{pi(t=0)}}D}{\nu_o}$ and $Re_w = \frac{\sqrt{2g\Delta H_{pe(t=0)}}D}{\nu_w}$ where subscripts 'o' and 'w' corresponds to the oil flow and water flow, respectively; $\Delta H_{pi(t=0)}$ is the initial potential head difference between the oil surface in the cargo tank and the internal hole; $\Delta H_{pe(t=0)}$ is the initial potential head difference between the external water surface and the external hole. These two Reynolds numbers may well indicate the turbulence associated with the water jet and oil jet detected in the early stage of the spilling (e.g. Figure 5.12(a) for Case G1). Nevertheless, the water jet may not always significant, as shown in Figure 5.12(c) where it disappears due to the strike with the oil jet that contains considerably larger momentum. Thus, the convective oil/water or water flow in the external hole becomes insignificant. The similar phenomenon is also found in Case G2. For the cases where the significant water flow through the external hole is observed, e.g. Case C1 and Case G3, the effective Reynolds number for the classification is taken as max(Re_o, Re_w), otherwise, it is assigned to be Re_o.

By using such definition of the effective Reynolds number, the comparison of relative errors in all cases considered in the numerical simulation is displayed in Figure 5.14. The relative error in this Figure is defined as $\int_t |f_n - f_e| dt / \int_t |f_e| dt$ for parameter f to be considered; the subscript n represents the numerical results, and e represents the experimental data for H_{mixture} in Figure 5.14(a) but the LES results for discharge in Figure 5.14(b). For clarity, the corresponding results by the standard, low-Re and realizable k-ε models are not included due to their significantly larger errors compared to RNG k-ε, k-ω SST and under-resolved DNS models, and only the corresponding maximum errors/difference at each Reynolds number column are included in Figure 5.14.
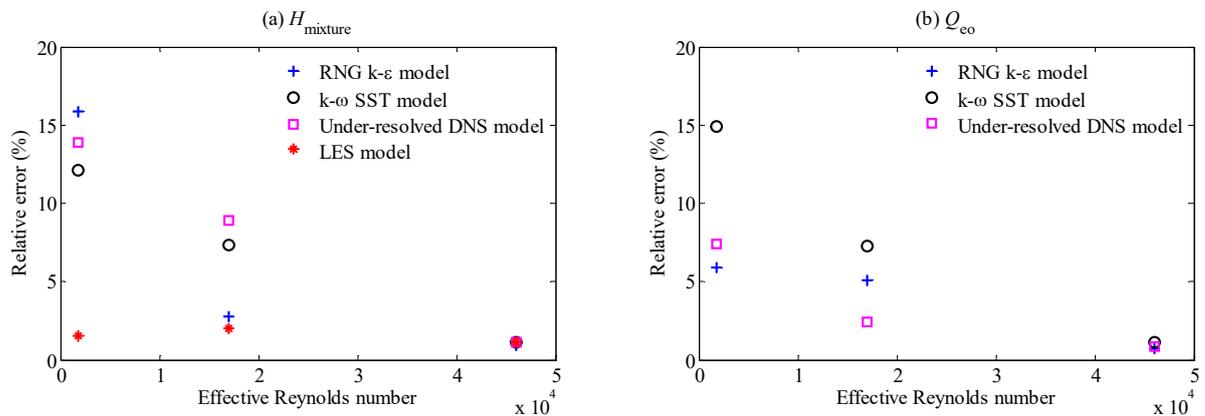
Figure 5.14 Relative errors in the cases with different turbulence models in terms of the effective Reynolds number.

It is found that for a smaller effective Reynolds number, e.g. Case G1 and Case G2, the k-ε and k-ω SST models lead to considerable large errors, though depending on which quantities (H_{miture} or Q_{eo}) are concerned with. For example, at effective Re ~1800, the relative errors of H_{mixture} are 16% and 12% (Figure 5.14(a)) for RNG k-ε and k-ω SST models, respectively, both are much larger than the error (1.5%) of LES results; while the relative difference for discharge from the LES results are 6% and 15% (Figure. 5.14(b)) for RNG k-ε and k-ω SST models. If the errors at effective Re ~17000 are examined, one may find that the result of RNG k-ε model for H_{mixture} is very close to that of LES (Figure 5.14(a)) and the result of k-ω SST models is quite different from the LES results. However, if one examines Figure 5.14(b) for discharge, one finds that the results from both models are significantly different from the LES results. Moreover, as observed from Figure 5.14, with the increase of the effective Reynolds numbers the errors of RANS models trend to be reduced. For the high-Re case (i.e., Case G3 where effective Re ~ 46000), the k-ω SST model and RNG k-ε models yield the result matching well with the experimental data and the results from LES in terms of H_{mixture} and Q_{eo}, respectively. It is also remarked that the agreement between the results by the under-resolved DNS and the corresponding results by the LES becomes better as the increase of the effective Reynolds number. Considering the fact that they used the

same mesh, this phenomenon implies that the effect of the sub-grid stress relative to the large eddy decreases as the increase of the effective Reynolds number.

Based on the numerical results of these cases, one may conclude that for low-*Re* cases with effective Reynolds number smaller than 17000, the LES shall be only used, although the higher computational consumption is required; whereas if the effective Reynolds number is greater than 40000, one may use the RANS approach, e.g. the k-ω SST and RNG k-ε models, which generally requires less computational efforts compared to the LES as demonstrated in the previous section. As for the middle range, it is inferred that the LES model is suggested if the high accuracy is required. It should clarify that the 'low-*Re*' used in this conclusion is termed of the effective Reynolds number suggested above. In fact, in the low-*Re* cases, e.g. Case C1, the instantaneous Reynolds number may be high as demonstrated by Figure 5.10.

Furthermore, in the present cases, the flow in the ballast tank does not only rely on the near-wall turbulence but also, perhaps more significantly, influenced by the turbulence associated with the interfaces between different liquid phases. This means that the low-Reynolds-number extensions of the commonly used RANS approaches (whose performance is improved mainly through imposing empirical functions near wall regions with fine grids, as a replacement of the wall function (Seyedein *et al.*, 1994; Cho and Goldstein, 1994)) may not be suitable for so-called low-Re cases. This has been confirmed by our numerical results using the Launder-Sharma k-ε model, as demonstrated in Figures 4.8 and 4.9.

One may notice that such classification system depends on a reliable assessment of whether the water inflow through the external hole is significant. It is feasible to qualitatively address this issue through analysing the momentum brought by the water jet and the oil jet in the initial stage of the spilling. In the collision scenario with coaxial configurations (e.g. Case C1), the water inflow is usually considerable, because the self-weight of oil jets leads to a vertical fluid velocity component which leads to the situation that at the external hole, the oil jet does not cover the entire cross-sectional area. In the grounding scenario with coaxial configurations (e.g. Case G1), whether the water inflow is significant largely depends on whether the momentum brought by the upwards water jets is more significant than that by the downwards oil jets (as shown in Figure 5.12). As the offset between the internal and external holes (Δ) increases to (at least) the situation that the vertical overlapping area between internal and external hole reaches zero, the water inflow has to be taken into account as shown in Case G3. However, further investigations are required in the future to identify the exact critical offset condition from which the water inflow has to be considered.

5.3 Summary

In this chapter, the different turbulence behaviours and their effects on the DHT spilling process modelled by different models are discussed. It is noticed that the H_{oil} is only dependent on the flow through the internal hole, but both the flows through the internal hole and external hole contribute H_{mixture}. The result indicates that different models simulate significantly different turbulence features associated with the complex and dynamic flow motion inside the ballast tank, which greatly affects H_{mixture} profiles. The LES can deliver the most accurate result because it can properly model the turbulence distribution associated with the flow through the rupture behaving similarly to jet flows through an orifice and the transition turbulence attached around the oil/water/air interface inside the ballast tank triggered by the free-shear layers as the oil jet travels through the ballast space with mixing and separation.

Since different accidental conditions cause different dynamic fluid motions around the external hole, for instance, the convective oil-water flow through the external hole in Case C1 does not occur in the Case G1, the combined effect of turbulence modelling simulated by different models on the H_{mixture} is case-dependent. That means it is difficult to propose a conventional criterion of selecting a proper turbulence model only based on the flow through the internal hole.

In some DHT cases (e.g., Case G3 and C1), the water inflow through the external hole emerges and plays a dominant role in the spilling process. The numerical result indicates that the instantaneous Reynolds numbers corresponding to the water and oil flow indicate significant difference covering the typical regime from laminar to turbulence. An effective Reynolds number corresponding to both the oil outflow and the water inflow is introduced to classify the importance of turbulence in each case. All the cases can be organized based on the effective Reynolds number and the corresponding model performance is judged in terms of computational accuracy and robustness. The criterion of selecting a proper turbulence model is proposed.

The criterion concludes that at the low effective Reynolds number (<17000), one should not use the RANS models as they do not yield sufficiently accurate results and one must choose the LES modelling. When the effective Reynolds number is large enough (>40000), one may choose to use RANS models as they can give similar results to LES but costing much less CPU time. As for the middle range, it is inferred that the LES model is suggested if the high accuracy is required, but further demonstration for the RANS models is needed.

Considering the fact that the criterion proposed in this study is based on the model performance of the selected common-used turbulence models in which the conventional wall function with the default parameters is implemented, there still remains some uncertainties in the turbulence modelling, such as different types of wall functions, boundary initial conditions, other advanced

turbulence models and tuning of the free parameters in certain turbulence models. Their effects on the oil spilling from DHTs need to be investigated in the future work, from which the criterion shall be improved further.

Chapter 6 Compressibility Effect on the Oil Spilling from Fixed DHTs

As mentioned by Weller (2008), in some multiphase flow cases, only considering the incompressible flow system is far from enough. Sometimes, the gas compressibility plays an important role in the fluid dynamics and needs to be taken into account. For example, the gas-liquid systems in which the hydrostatic pressure of the liquid is great enough to cause significant compression of the gas or high-speed injection in which the liquid speed is great enough to cause significant compression of the gas into which it issues or in extreme cases even shock-waves in the gas. It is well-known that because of the relatively sparse molecular distribution, the gas is considered as a much more compressible medium than liquids. As for the multiphase flow problems (e.g., wave breaking, slamming and sloshing), many researches have emphasised the significant influence of the air compressibility in form of air bubbles on flow motion, short-time impact force and interface or free-surface deformation (e.g., Seiffert *et al.*, 2015; Zou *et al.*, 2015; Yang *et al.*, 2016).

As for the oil spilling from DHTs, considering the sudden fluid-fluid or fluid-structure impacts associated with the jets of oil outflow and water inflow (either strikes on the walls of the ballast tank or the interaction between them occurs during the spilling processes) and the interaction between entrapped air bubbles in the oil/water mixture and fluid states (such as velocity, vorticity and turbulent kinetic energy) in the ballast tank, it is necessary to examine how significant the effect of the air compressibility on the dynamic spilling process. However, due to the fact that no existing numerical works in this field have considered the compressibility of the fluids to the best of author's knowledge, this issue is unclear so far.

6.1 Model Formulation and Validations

6.1.1 Model formulation

According to the available libraries and solvers provided in the OpenFOAM platform, a solver named 'compressibleThreePhaseInterFoam' is developed to deal with the current three-phase flow problem (oil, air and water) by combining the compressible medium library with the existing VOF-based algorism. The governing equation in this solver is extended from the one in the compressible two-phase solver ('compressibleInterFoam') referenced by Suponitsky *et al.* (2014). Here, some basic derivations for the three-phase solver are listed:

Mass continuity equation:

Based on the Equation (4-1), continuity equation for each of the phases (Lakehal *et al*., 2002; Weller, 2008):

$$\frac{\partial \alpha_i \rho_i}{\partial t} + \nabla \cdot (\alpha_i \rho_i \boldsymbol{U}) = 0 \tag{6-1}$$

where the subscript i denotes the phase (i=1,2 and 3) and α is the volume fraction.

Momentum equation:

The momentum equation is consistent with Equation (4-2).

Energy equation:

According to the compressibleInterFoam solver discussed in Miloshevsky and Hassanein (2013) and Calderón-Sánchez *et al*. (2015), the energy conservation equation is achieved by simulating the temperature field (thermal energy) with a specific heat capacity (C_v) for reach phase translating the temperature into internal energy ($C_{v(\text{water})}$=4190J/kgK, $C_{v(\text{air})}$=1005J/kgK and $C_{v(\text{oil})}$=1970J/kgK). Based on the definition of total energy for multiphase flows in Ma *et al*. (2014), the thermal energy equation for the three-phase flow can be written as (Ma *et al*., 2016):

$$\frac{\partial \rho T}{\partial t} + \nabla \cdot (\rho T \boldsymbol{U}) + S = \frac{1}{C_v}[\nabla \cdot (K \nabla T)] \tag{6-2}$$

where T is the temperature field; the effective thermal conductivity of mixture (K) takes into account the volume fraction sum of thermal conductivity of each phase K_i (i.e., $\sum_{i=1}^{3} \alpha_i K_i$, where $K_{(\text{water})}$=0.57J/msK, $K_{(\text{air})}$=0.026J/msK and $K_{(\text{oil})}$=0.16J/msK) and the turbulent thermal conductivity K_t (Vakhrushev *et al*., 2010); the specific heat capacity for mixture (C_v) is calculated as $\frac{1}{C_v} = \sum_{i=1}^{3} \frac{\alpha_i}{(C_v)_i}$ where $(C_v)_i$ is the specific heat capacity for phase i; S is the source term accounting for the kinematic energy and product of pressure, which can be expressed as:

$$\frac{1}{C_v}\left(\nabla \cdot (\boldsymbol{U}p) + \frac{\partial \rho e^K}{\partial t} + \nabla \cdot (\rho e^K \boldsymbol{U})\right) \tag{6-3}$$

where ρe^K is the kinematic energy defined as $\frac{1}{2}\rho \boldsymbol{U}^2$.

Equation of state:

As each phase is assumed to be isothermal and a barotropic equation of state is implemented as:

$$\rho_i = \rho_{ni} + \psi_i p \tag{6-4}$$

108

where ψ is the compressibility, $\psi = \frac{1}{c^2}$ with c being the speed of sound; ρ_{ni} is the nominal density and p is the pressure.

For a gas (compressible phase) the nominal density (ρ_{ni}) is set to zero, which results in an ideal gas equation of state:

$$\rho_{\mathrm{i}} = \frac{1}{\bar{R}T}p \qquad (6\text{-}5)$$

where $\bar{R} = R/\dot{m}$, R is ideal gas constant (8.314472 J/(mol·K)) and $\dot{m}$ is the unit molar weight (for air: 28.97g/mol); T is absolute temperature in Kelvin.

For a liquid (low compressible phase) the nominal density (ρ_{ni}) is defined as:

$$\rho_{ni} = \rho_{0i} - \psi_{\mathrm{i}}p_0 \qquad (6\text{-}6)$$

where ρ_{0i} is the liquid density under the normal condition with the normal pressure of p_0.

The Equation (6-4) can rewrite as (Suponitsky *et al.*, 2014):

$$\frac{D\rho_i}{Dt} = \psi_i \frac{Dp}{Dt} \qquad (6\text{-}7)$$

Phase fraction transport equation:

With respect to the VOF system of equations, in order to avoid smearing the interface, care must be taken to the discretization of the convective term (Weller, 2008 and Ferziger and Perić, 2002). In the OpenFOAM platform, this equation is modified in such a way that it includes an additional 'compression' term that helps to ensure the interface remains sharp. The modified fraction transport equation is mentioned before and here no repeat is required.

However, in the compressible VOF scheme, handling compressibility effects in this manner is problematic because generally the density variations due to compression effects are likely to be small compared to the difference in the phase densities and so the density variation must be handled separately for each phase rather than together via the mixture density (Weller, 2008). Therefore, for compressible flow, Equation (6-1) can be re-written as:

$$\frac{\partial \alpha_i}{\partial t} + \nabla \cdot (\alpha_i \boldsymbol{U}) + \frac{\alpha_i}{\rho_i}\frac{D\rho_i}{Dt} = 0 \qquad (6\text{-}8)$$

Equation (6-7) can be inserted into Equation (6-8) yielding:

$$\frac{\partial \alpha_i}{\partial t} + \nabla \cdot (\alpha_i \boldsymbol{U}) = -\frac{\alpha_i \psi_i}{\rho_i}\frac{Dp}{Dt} \qquad (6\text{-}9)$$

The L.H.S. of Equation (6-9) is identical to the L.H.S. of Equation (4-4), while the R.H.S. of Equation (6-9) representing the compressibility effects is treated as the source term.

By adding equations for each phase in Equation (6-9), the divergence of the volumetric velocity U can be calculated as:

$$\nabla \cdot \boldsymbol{U} = -\frac{Dp}{Dt} \sum_{i=1}^{3} \frac{\psi_i \alpha_i}{\rho_i} \tag{6-10}$$

The VOF interface compression term can be included in exactly the same way as it was for the incompressible solver, since it is clearly conservative and maintains boundedness of progress variable α_i between 0 and 1 (Weller, 2008). Thus, the equation of phase continuity ($\frac{\partial \alpha}{\partial t} + \nabla \cdot (U\alpha) = \alpha \nabla \cdot U$ for the original fraction material derivative) is modified for the compressible flow in form of Equation (4-4) as:

$$\frac{\partial \alpha_i}{\partial t} + \nabla \cdot (\alpha_i \boldsymbol{U}) + \nabla \cdot [\boldsymbol{U_c} \alpha_i (1 - \alpha_i)] = \alpha_i \nabla \cdot \boldsymbol{U} + \alpha_i \sum_{j=1, j \neq i}^{3} \alpha_j \left(\frac{\psi_j}{\rho_j} - \frac{\psi_i}{\rho_i}\right) \frac{Dp}{Dt} \tag{6-11}$$

As for the two-phase flow case, Equation (6-11) can be expressed as:

$$\frac{\partial \alpha_1}{\partial t} + \nabla \cdot (\alpha_1 \boldsymbol{U}) + \nabla \cdot [\boldsymbol{U_c} \alpha_1 (1 - \alpha_1)] = \alpha_1 \nabla \cdot \boldsymbol{U} + \alpha_1 (1 - \alpha_1)\left(\frac{\psi_2}{\rho_2} - \frac{\psi_1}{\rho_1}\right) \frac{Dp}{Dt} \tag{6-12}$$

which is consistent to the expression in Suponitsky *et al*. (2014) for the two-phase solver.

The overall numerical procedure for solving governing equations is similar to that used in the 'compressibleInterFoam' solver, detailed description of which can be found in Suponitsky *et al*. (2014).

6.1.2 Model validations

Dam break

The flow originated by the dam break and the impact of the water front against a vertical wall has been widely used for a classic validation test. The laboratory experiment conducted by Hu and Kashiwagi (2004), in which the impact pressure data was recorded, is used here and the schematic view of the computational domain is shown in Figure 6.1. The point A denotes the point where the pressure sensor is installed.
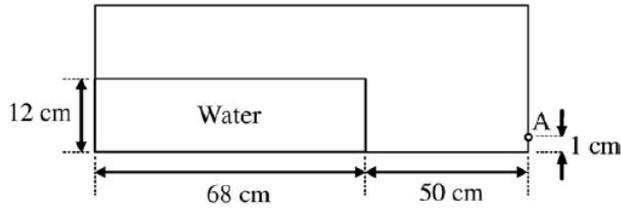
Figure 6.1 Schematic sketch of the dam break simulation.

In the compressible model, the typical air compressibility with $\bar{R}$=287 J/(kg·K) and T_{inital}=293K and the water compressibility with the speed of sound 1483 m/s (Yebra *et al.*, 2017) are considered. The structure mesh is applied and according to the mesh sensitivity test, the uniform cell size of 1.25mm is used. The computed pressure at point A obtained by the two-phase incompressible solver (interFoam), two-phase compressible solver (compressibleInterFoam) and three-phase compressible solver (compressibleThreePhaseInterFoam) are compared with experimental data illustrated by Figure 6.2. In this Figure, the solid line indicates the mean value of the measure pressure data in 8 repeated tests and the scatter of all measured data is represented by the lower and upper bank lines. The upper and lower lines indicate a range of uncertainty associated with the experimental measurement. Based on the comparison, it is clearly shown that all the solvers well estimate the two peak impact instants with accurate duration. Moreover, the compressible flow yields the peak value better matching the measured average data. The compressibility effect is more obvious after the second peak with large oscillation, since the overturned flow hit the free surface causing breaking as well as air entrapment near the wall (Hu and Kashiwagi, 2004). The coincided curves delivered by the two different compressible solvers indicate the reliability of the proposed solver.
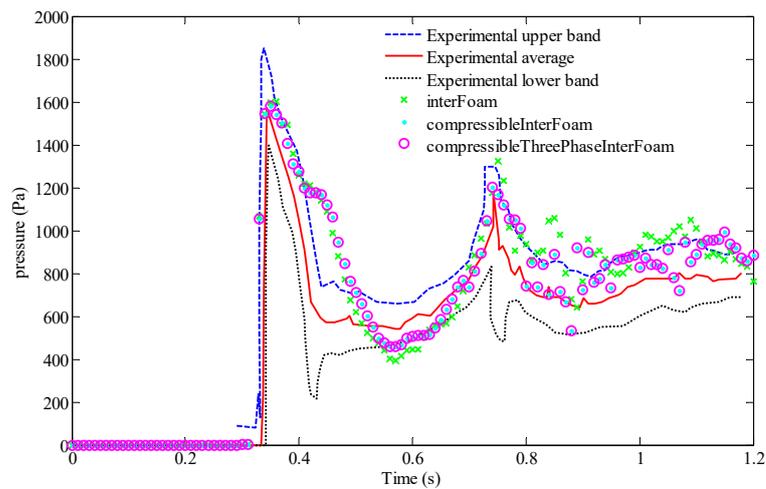
Figure 6.2 Comparison of the pressure at Point A between the measured data and numerical results using different solvers.

Solitary wave-induced uplift force on horizontal plate

As mentioned in Gaeta and Lamberi (2015), loading on maritime structures are strictly correlated, in magnitude and duration, with the air content that characterizes the impacting wave front. Many researchers (e.g., Gaeta and Lamberti, 2015; Peregrine *et al*., 2005; Gao *et al*., 2015) have been investigating the influence of air modelling on the computation of extreme wave-induced forces on the structure.

The laboratory case of solitary wave-induced uplift force on horizontal platforms carried out by French (1969) is numerically replicated using the incompressible and compressible solvers. The two-dimensional numerical model configuration is illustrated in Figure 6.3. The dimensions of the tank are 14*0.6 m². The initial water depth (*d*) at the wave maker boundary is 0.381m. The width of rectangular structure (*L*) is 4*d* (1.524m) and the distance from the bottom of the rectangular structure to the still water surface (*s*) is 0.2*d* (0.0762m). The simulated solitary wave with amplitude (*H*) of 0.241*d* (0.0918m) is generated imposing at the left boundary the velocity components and the fraction coefficient corresponding to the surface elevation using the GroovyBC utility. More details of wave generation using OpenFOAM could be referred to Aydogan and Kobayashi (2014) and Seiffert and Ertekin (2012). The top and right boundaries are set to open allowing air and water to escape out, respectively.
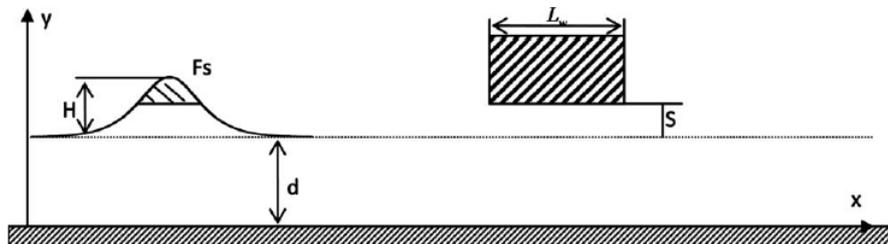
Figure 6.3 Experimental setup for the simulation of wave impact on the deck by French (1969).

Wave force acting on the rectangular structure (*F*) is normalized by the weight (*F_s*) of the generated wave volume above the deck bottom, marked as the shaded water area in Figure 6.3. Also, the time (*t*) is normalized by $\sqrt{d/g}$ as τ. The positive sign is adopted for the uplift force values.

The unstructured mesh where the finest size is located around the space between the free surface and the plate bottom is generated. Based on the recommendation provided by Afshar (2010), certain mesh refinement is necessary around the free surface as the wave propagation. The convergence test is conducted under different grid resolutions specified by using the ratio of the smallest cell size to the constant largest cell size of 2cm (α_{ds}=25%, 12.5% and 6.25%). It is found

that the result of α_{ds}=12.5% and α_{ds}=6.25% indicates no significant differences in wave forces. Therefore, the mesh density of 12.5% is selected with the total number of cells of 150,000.

The comparison between the experimental and numerical results is indicated in Figure 6.4. Three solvers are included and all of them deliver satisfactory results compared with the laboratory data. Specifically, including the fluid compressibility can better predict the extreme values of the uplift and the downlift loads (i.e., 27.9% drop of peak uplift load and 20.4% rise of peak downlift load obtained from the compressible solver). Moreover, the two curves solved by the 'compressibleInterFoam' and 'compressibleThreePhaseInterFoam' are properly overlapped.
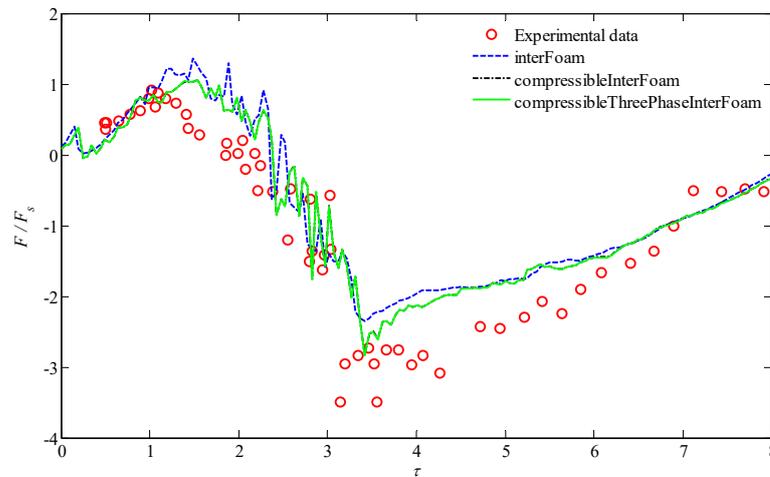
Figure 6.4 Comparison of experimental data and numerical results in terms of normalized force F/F_s on the horizontal desk against the normalized time τ.

Water entry problems
A classic three-dimensional water entry case is chosen for model validation with the assistance of dynamic mesh package available in the OpenFOAM. Considering this violent impact phenomenon, the compressibility effect, especially the compressible air, may be the dominant factor on the impact pressure and Ma *et al*. (2015) demonstrated their numerical model called 'AMAZON-CW' incorporating the air compressibility could be competent.

The experimental work was carried out in the Ocean Basin at Plymouth University's COAST Laboratory. The ocean basin is 35m long by 15.5m wide and has an adjustable floor allowing the operation at different water depths up to 3m. The falling block includes a rigid impact plate connected to two deriver plates and the total mass (m_{plate}) can be varied from 32kg (plate 1) to 52kg (plate 2). The impact plate is 0.25m long and 0.25m wide with a thickness of 0.012m. The impact velocity can vary between 4m/s and 8m/s by adjusting the initial position of the plate. Force and pressures were measured during the impact by an S-type load cell and five miniature

pressure transducers installed on the impact plate as illustrated in Figure 6.5. Further information could be referred to Ma *et al.* (2015).
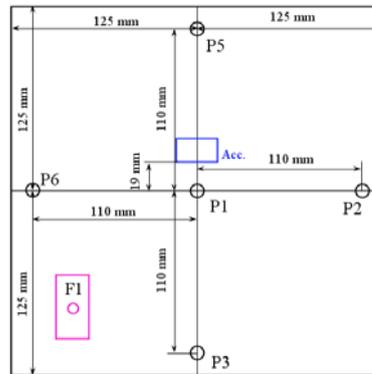
Figure 6.5 Configuration of the instrumentation on the flat plate. (P1-P6 are pressure transducers; F1 is the load cell and Acc. is the accelerometer)

With the purpose of validation, one benchmark case with V_{impact}=5m/s and m_{plate}=32kg is selected. The proposed 'compressibleThreePhaseInterFoam' and original 'compressibleInterFoam' solvers coupled with the dynamic mesh package are implemented. Both the air and water are considered as a compressible medium with the typical properties as mentioned in the dam break case. The incompressible solver 'interFoam' is also applied for this case to shed some light on the significance of compressibility effects.

Since this impact problem is inertia-dominant and lasts for a very short period, the flow can be appropriately assumed to be symmetric about the central section planes (x-y and y-z planes) of the plate. Under these considerations, only a quarter of the domain covering a quarter of the flat plate with the assistance of symmetry boundary conditions embedded in OpenFOAM is modelled.

The hexahedral mesh is used and the mesh refinement mainly locates in the area between the plate and free surface. The convergence test is completed with different mesh densities with the smallest mesh ($\varDelta_{min}$) from 0.625mm with 2.8 million cells to 0.15625mm with 6.8 million cells. The convergence results obtained from the 'compressibleThreePhaseInterFoam' solver with the condition of V_{impact}=5m/s and m_{plate}=32kg in terms of P1 and P2 are plotted in Figure 6.6. The pressure peaks are correlated to time zero. With the decreasing of cell size, the relevant variables are convergent and the time-averaged relative difference (defined in the same way as Ma and Yan, 2006) of 1.7% and 1.9% between the meshes of 0.3125mm and 0.15625mm for P1 and P3 curves respectively suggest the mesh with the finest size of 0.3125mm is acceptable for this case.
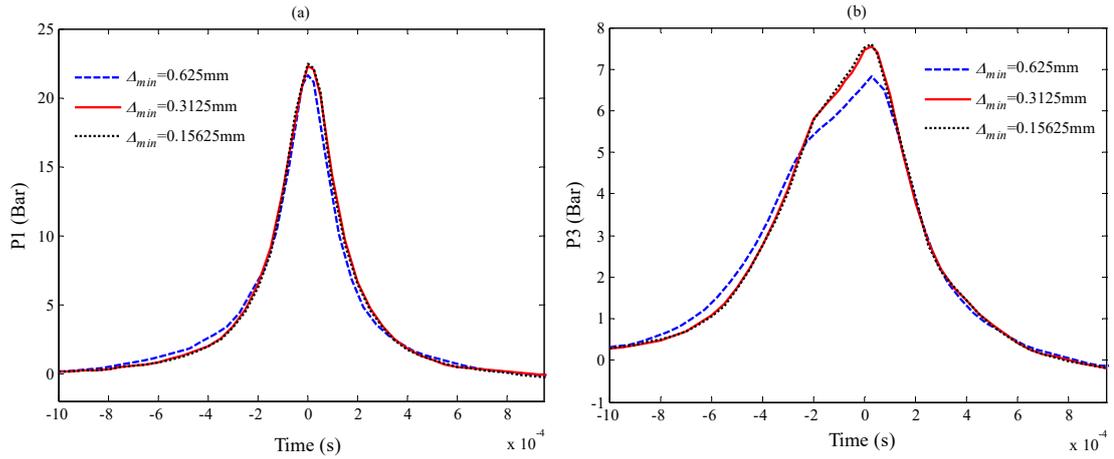
Figure 6.6 Convergence test of the 'compressibleThreePhaseInterFoam' solver in terms of (a) P1 and (b) P3 with different cell sizes for the slamming case with V_{impact}=5m/s and m_{plate}=32kg.

The comparison among different solvers and experimental data is indicated in Figure 6.7 in terms of P1 and P3 and F2, where F2 is the force calculated based on the pressure at the five points as illustrated in Figure 6.5 (Ma *et al*., 2015). Here, it should be noticed that the peak values recorded around the plate edges (i.e., P2, P3, P5 and P6) are not as identical as the numerical ones due to the uncertainty associated with experimental measurement sensitivity and resolution. Therefore, the range of recorded peak values is also plotted in Figure 6.7(b).
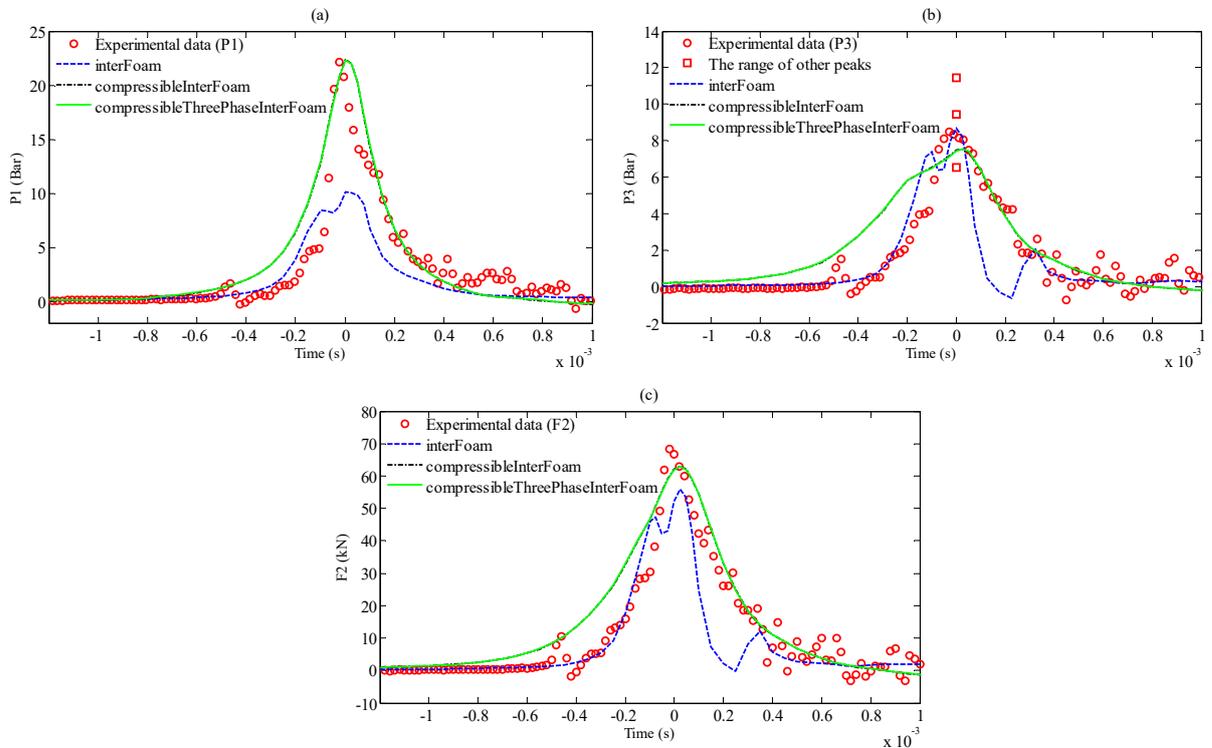
Figure 6.7 The comparison between the experimental and numerical results in terms of (a) P1, (b) P3 and (c) F2 for the case with V_{impact}=5m/s and m_{plate}=32kg.

It is clearly shown that the compressible solver matches the experimental data much better providing obviously more accurate peak values (especially for P1) and the resultant impact force (F2) than the incompressible solver. The incompressible solver yields obvious oscillation near the peak point and afterwards, which fails to track the measured curves. This may be attributed to the significant compressible effect on the interaction between the pressure evolution and the free surface deformation. Also, one may also notice that the compressible solver stretches the impact pressure with a longer rising period and poses a negative pressure region after the impact. More discussion can be found in Yang *et al*. (2016). The consistent profiles of 'compressibleInterFoam' and 'compressibleThreePhaseInterFoam' in Figure 6.7 further indicate the applicability of the current proposed compressible three-phase solver. Moreover, the feasibility of integrating the dynamic mesh package in these solvers is also preliminary demonstrated. The comprehensive discussion will be presented in the 'Oil Spilling from Tanks under Motions' section.

6.2 Air Compressibility Effect on Oil Spilling Processes

As discussed in the previous Section, the entire process of the oil spilling includes several typical phenomena on which the compressibility may play an important role.   The role of the compressibility of the fluids on the oil spilling from the damaged DHTs is discussed in this section. To do so, the proposed three-phase compressible solver, in which the air phase is considered to be compressible, is used for all cases considered in this study. The results are compared with those achieved in the previous section using the incompressible solver. The LES model is employed in the compressible solver, considering the accurate prediction discussed in Chapter 5. The similar convergence tests are also carried out and it suggests that the consistent mesh distribution of the incompressible case is acceptable.

Based on the validation cases above, we are aware that the compressibility of the fluids on the dynamics/kinematics of the fluids may be significant in a small spatial-temporal scale, e.g. the water and oil jets interaction inside the ballast tank at some typical instants in a short duration near the occurrence of a violent fluid impact as illustrated in Figure 5.12 for Case G1. Some corresponding results are shown in Figure 6.8 and Figure 6.9 for demonstration. Figure 6.8 compares the profiles (the front) of the oil jet at different time instants characterizing the occurrence of its impact with the upwelling water jet as illustrated in Figure 5.12, among which the maximum pressure occurs at t=0.026s shown in Figure 6.9(b). It is found from Figure 6.8 that the profiles of the oil jet obtained using the incompressible solver agree well with the corresponding results by the compressible solver at t=0.026s (Figure 5.12(a)) and t=0.031s (Figure 5.12(b)). At t=0.095s, when the main body of the oil jet reaches the external hole (y/D =-3.0), part of the oil jet hits the wall of the external hull and leads to oil splashing on the ballast bottom plate (Figure 5.12(c)). At this moment, the profile of the oil jet from the compressible

solver largely agrees with that by the incompressible solver, except the shape of splashing oil droplets. Further examinations of the location of the tip of the oil jet (at $x = 0$ in the central vertical plane) and its pressure are illustrated in Figure 6.9. Again, a good agreement has been observed in terms of the location of the tip of the oil jet (Figure 6.9(a)). However, from Figure 6.9(b), where the pressure is normalised by the atmosphere pressure (p_{atm}), one may notice that the peak value of the pressure obtained by using the compressible solver (1.071) is slightly higher than that by the incompressible solver (1.068), although the overall time histories of the pressure by both solvers look very similar.
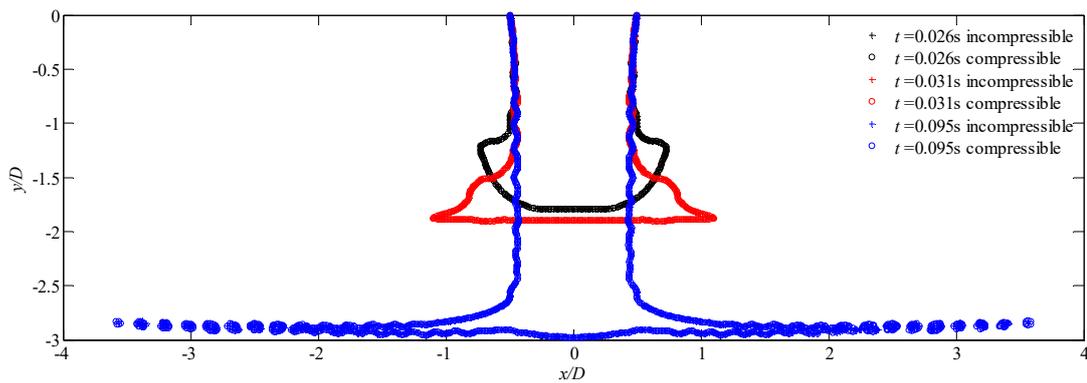
Figure 6.8 Surface profiles of the oil jets at the central vertical plane in the transient stage of Case G1. (y axis origins from the bottom of the internal hole)
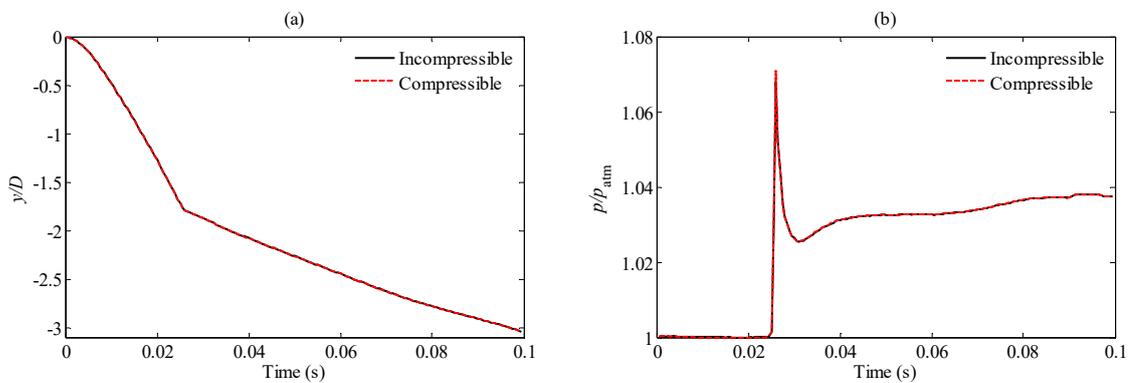
Figure 6.9 Time history of (a) the location of the tip of the oil jet and (b) the pressure on the tip in the transient stage of Case G1. (y axis origins from the bottom of the internal hole)

The previous chapter specifically discusses the different dynamic spilling processes caused by different accidental conditions (e.g., rupture and scenario conditions) associated with fluid-structure impact phenomena. One may agree that the air compressibility may lead to different impact loadings when the jet flow hits the hull wall, which in turn affects the fluid motion around or through the rupture potentially yielding different spilling curves. This may be more significant at the early spilling stage considering the relative larger jet velocity. In order to investigate the air

compressibility effect on the fluid-structure impact during the spilling process, some sample points are located at the region where the fluid-structure impact takes place in Case G2 and Case C1 (shown in Figure 6.10(a) and (b)) and the time histories of the pressure recorded at the corresponding sample point obtained by the incompressible and compressible solvers are compared in Figure 6.10(c) and (d). It is clearly shown from Figure 6.10(c) that the pressure oscillates obviously in Case G2 at the early stage ($t<0.5s$), which is affected significantly by the air compressibility, but this phenomenon does not happen in Case C1 (Figure 6.10(d)). This may be attributed to the fact that the larger jet velocity of Case G2 enhances the compressibility effect. The compressible solver delivers earlier peak pressure in both cases, although the air compressibility seems to have limited effect on the peak value. The difference of pressure is diminished as the spilling proceeds, which indicates the weakened compressibility effect on the impact loading.
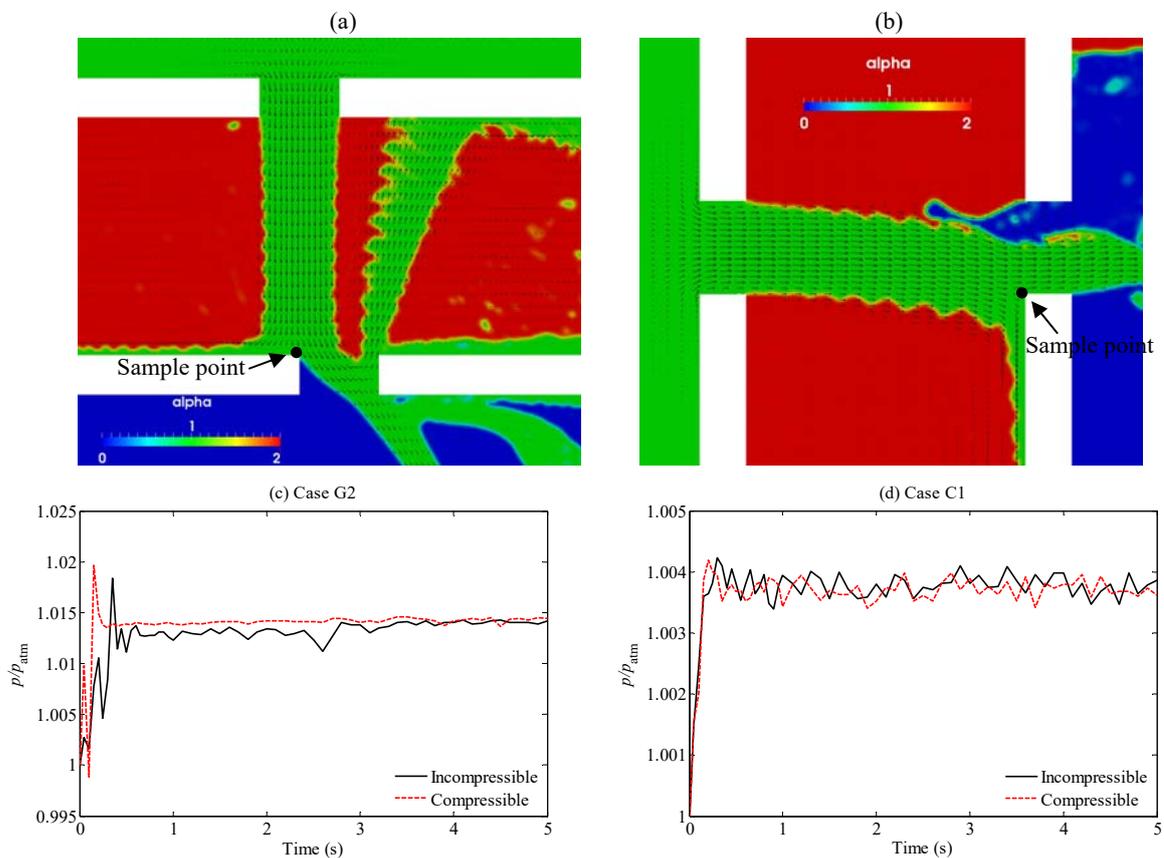
Figure 6.10 (a, b) the sample point locations of Case G2 and Case C1 and (c, d) the time histories of pressure at the sample points during the early spilling period of Case G2 and Case C1.

As the difference between the results by the compressible and incompressible solvers occurs in very short impact duration, the role of compressibility of the fluid may be insignificant in the longer term. To examine how the compressibility of fluids influences the macroscopic process of the oil spilling, the time histories of H_{oil}, $H_{mixture}$ and the discharge of the oil/water mixture through

the internal (Q_i) and external (Q_e) holes are focused. Figure 6.11 compares the corresponding results obtained by the compressible solver and the incompressible solver. For the purpose of comparison, the corresponding experimental data is also plotted together.
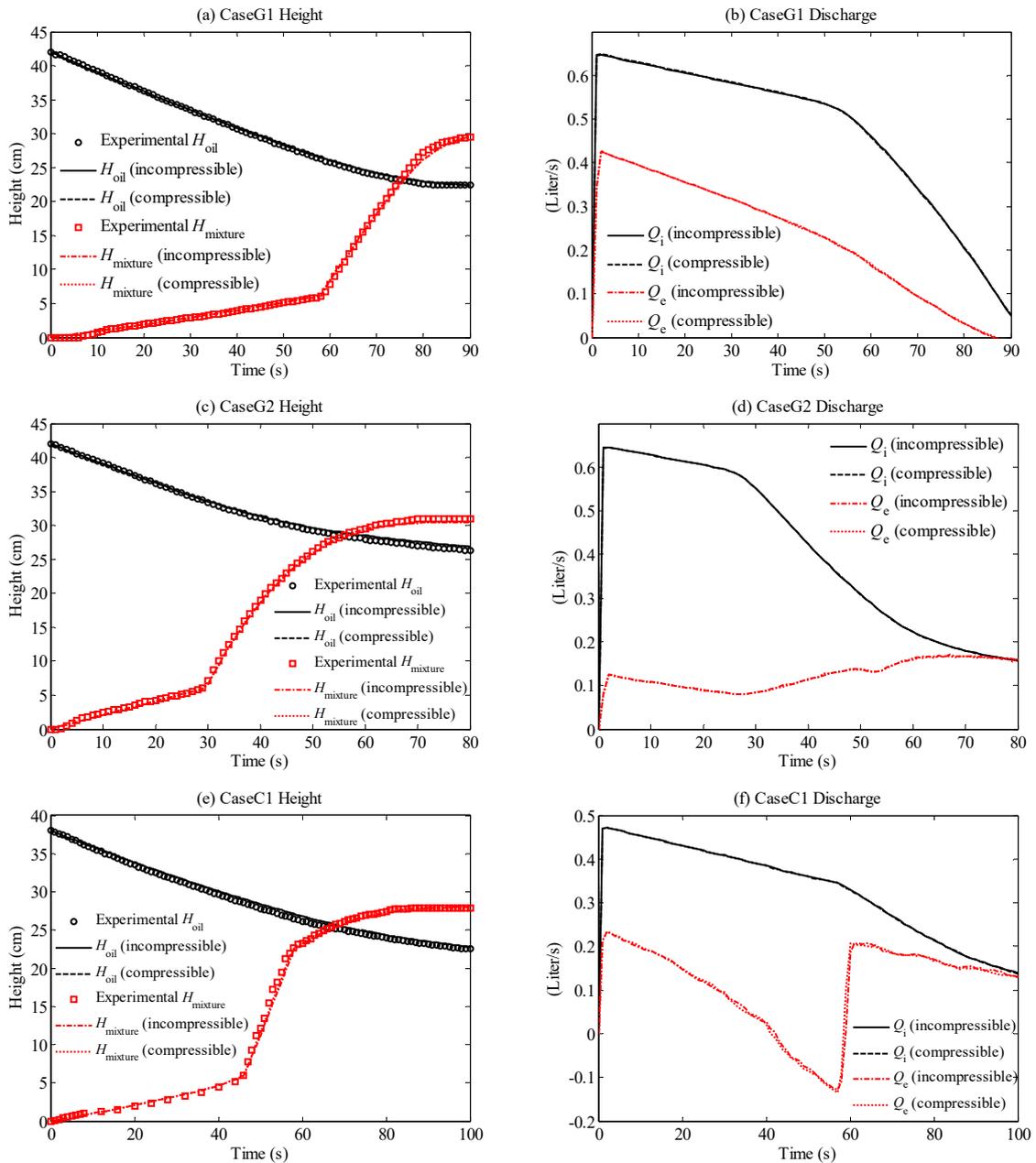
Figure 6.11 Time histories of the oil height in the cargo tank (H_{oil}), the mixture height in the ballast tank ($H_{mixture}$) and the discharge of the mixture through the internal (Q_i) and external hole(Q_e) in the cases with or without considering the compressibility of the fluids.

For these macroscopic parameters, the results obtained by using the compressible and incompressible solvers are observed to be very close. Based on this observation, one may conclude that the air compressibility may only play an important role in a short duration of the

impact and may be ignored logically in the numerical modelling of the oil spilling from damaged fixed DHTs, especially if the macroscopic process is simply considered.

6.3 Summary

The fluid-fluid or fluid-structure impacts involved in the dynamic spilling process implies the necessity of examining the fluid compressible effect on the spilling process. There is no existing research on this topic. To do so, a new three-phase compressible solver is developed by combining the compressible medium package and the VOF algorithm on the OpenFOAM platform. Three different validation cases are proposed. The compressible solver is applied to simulate the different fixed DHT cases considered in the previous chapter and the result obtained from the compressible and incompressible solvers are compared in short and long terms. It concludes that the compressibility of the fluids may play an important role in a short duration of the impact, leading to a higher jet-jet impact pressure and different fluctuations of jet-structure impact pressure, but does not significantly influence the macroscopic process of the oil spilling in terms of discharge and height. It also suggests that applying the incompressible solver is acceptable to analyse the dynamic spilling process from damaged tankers.

Chapter 7 Analysis of Dynamic Spilling Characteristics and Prediction Models

Although the correlation analysis for the flow through the internal hole is carried out using the experimental data, the quasi-steady empirical model developed in Chapter 3 fails to further predict the flow through the external hole due to the lack of measurement. Generally speaking, the accurate numerical results can provide more comprehensive information on dynamic spilling characteristics than the experimental measurement or observation. From the comparison in Chapter 4, 5 and 6, one may agree that the current incompressible LES model is always sufficient for modelling the turbulence associated with the oil spilling in both grounding and collision scenarios and yields the curves coinciding well with the macroscopic experimental data. Thus, the numerical results by using the incompressible LES model will be used in this chapter to further analyse the dynamic behaviours of DHT spilling using the correlation analysis. Based on the discussion of the capability of the existing prediction models (Tavakoli *et al*., 2008 Tavakoli *et al*., 2009 and Tavakoli *et al*., 2012), an improved prediction model is developed and some validations are presented.

7.1 Discussions on Dynamic Characteristics of Spilling Processes

In practices, macroscopic outflows from both the internal hole and the external hole are of great concern, which mutually influences the flow regime in the ballast tank and external environment. The deeper understanding of the discharge mechanism through the internal hole or external hole shall contribute towards the development of analytical predictions.

Similar to the analysis in Chapter 3, the correlation analysis for the internal hole is carried out for each case including Case G1-G3 and Case C1. The corresponding correlation results are illustrated in Figure 7.1. It is indicated that the very strong linear correlation between the two concerned variables (i.e., the average oil velocity head and hydraulic head difference) are founded in each case, except for the transient stage at the very beginning and the transitional period between stages 2 and 3. One may find that the expected linear relationship at the stage 1 of Case G3 is disrupted as shown Figure 7.1(c), which is due to the impact of the upward water stream through the external hole as demonstrated in Figure 5.13(b). Considering the fact that this period is very short compared with the entire spilling period in Case G3, this non-linear relationship is

simplified as a linear one. Overall the correlation analysis based on the numerical results indicated in Figure 7.1 is similar to the one derived from the experimental data, which further demonstrates the feasibility of the empirical solution derived in Chapter 3.
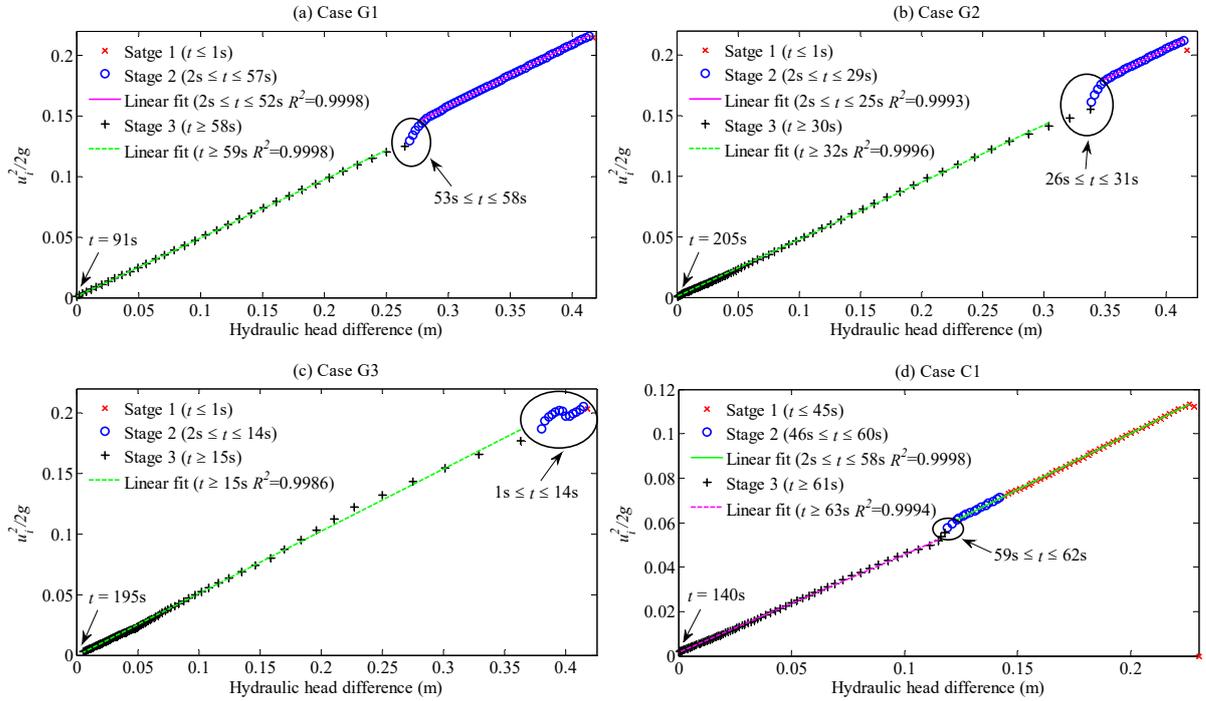
Figure 7.1 Correlation between the average velocity head across the internal hole and the hydraulic head difference between the oil-air interface of the cargo tank and the centre of the internal hole using the LES model results.

It should be noticed that the hydraulic head used in Figure 7.1 is composed of the potential head and the pressure head which are highly related to the $H_{mixture}$ after the internal hole is submerged as $H_{mixture} > H_b$ in grounding cases. As mentioned before, the $H_{mixture}$ is dominated by both the oil outflow from the cargo tank and water/oil flow releasing to the external environment. With respect to the characteristics of the discharge through the external hole (Q_e), the LES numerical result is beneficial for exploring the mechanism. Similar to Q_i, the corresponding correlation between the average mixture velocity head across the external hole and the hydraulic head difference between the oil-air interface in the cargo tank and the centre of the external hole is presented in Figure 7.2. It is clearly indicated that only the Case G1 achieves a good linear relationship similar to the one for the internal hole (Figure 7.1(a)). In other cases, the nonlinear effect dominates the violent discharge over the early period of the spilling, while the linear correlation only appears at the late spilling period afterwards. Moreover, the curves displayed in Figure 7.2 reveal that the characteristics of the discharge through the external hole are case-dependent and in some cases (e.g., Case G3 and C1) the discharge through the external hole (i.e., the water inflow) may be not fully driven by the current hydraulic head.

Figure 7.2 also clearly indicates that the oil spilled out the DHT occurs at the very beginning of the spilling process, except for the Case G3 due to the zero vertical overlapping area between the internal and external hole (shown in Figure 5.13(b)). Moreover, considering the water flowing into the ballast tank during the early stage in Case G3 and C1, the velocity head used in the late linear correlation period is the average oil-water mixture velocity across the external hole, while in the other cases, only the oil discharge contributes to the velocity head due to no significant water inflow took place. In order to conduct the accurate prediction, all of these findings need to be considered in the analytical model.
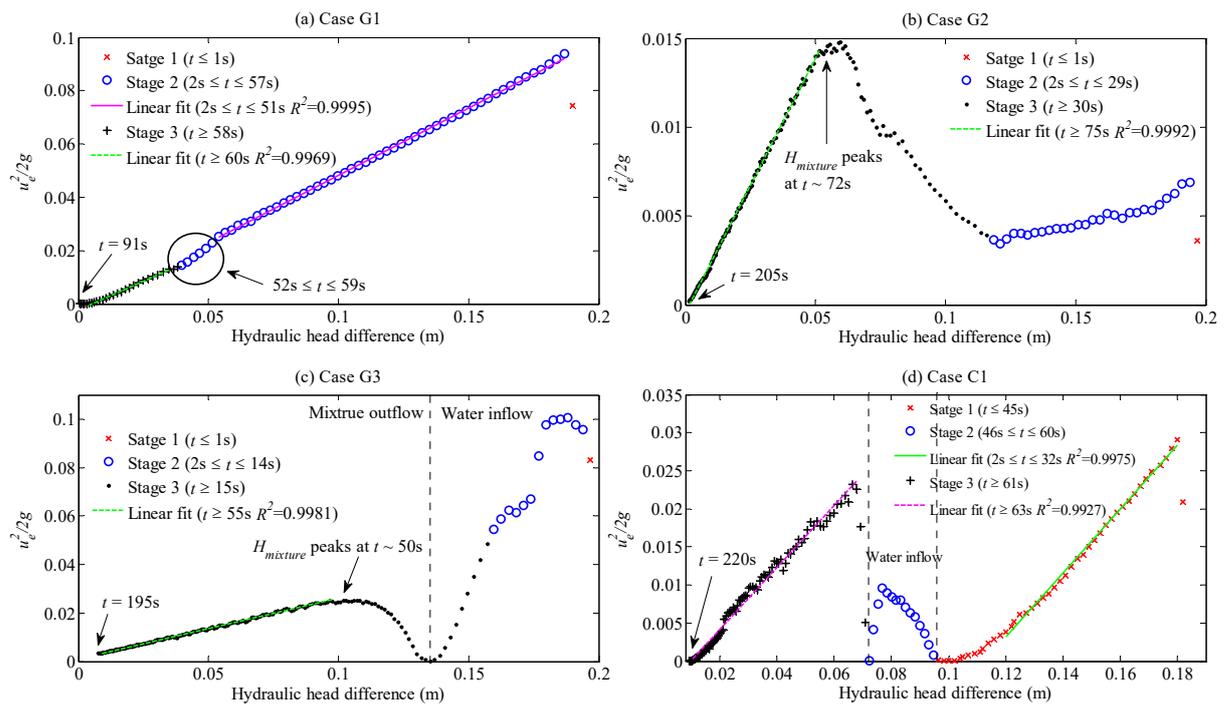
Figure 7.2 Correlation between the average velocity head across the external hole and the hydraulic head difference between the oil-air interface of the cargo tank and the centre of the external hole using the LES model results.

7.2 Tavakoli Analytical Models

In the existing works related to the oil spilling from DHTs, e.g., the quasi-steady prediction models of Tavakoli *et al*. (2008), Tavakoli *et al*. (2009) and Tavakoli *et al*. (2012), it is generally assumed that the oil and water convectively flow into the ballast tank without any oil spilled out of the DHT at the early spilling stage; before the ballast tank is fully filled, the cargo oil flows into the ballast tank and is dominated by the hydraulic head difference between the internal hole and the oil surface inside the internal tank; meanwhile the external water flows into the ballast tank and is dominated by the hydraulic head difference between the external hole and the external water surface; after the ballast tank is filled up and before the hydrostatic equilibrium of the system is recovered, the oil/water mixture may flow out through the external hole, the flow rate

of which is determined by the hydraulic head difference between the oil surface in the internal tank and the internal hole under different assumptions of the mixture states (e.g., immiscible oil-water fluid or perfectly-mixed oil-water fluid). Based on this simplified spilling process, Tavakoli *et al.* (2008) and Tavakoli *et al.* (2012) developed analytical solutions for predicting the spilling rate into the environment from grounded or collided double hull tankers, respectively. The flow chart of this prediction model is presented in Figure 7.3.
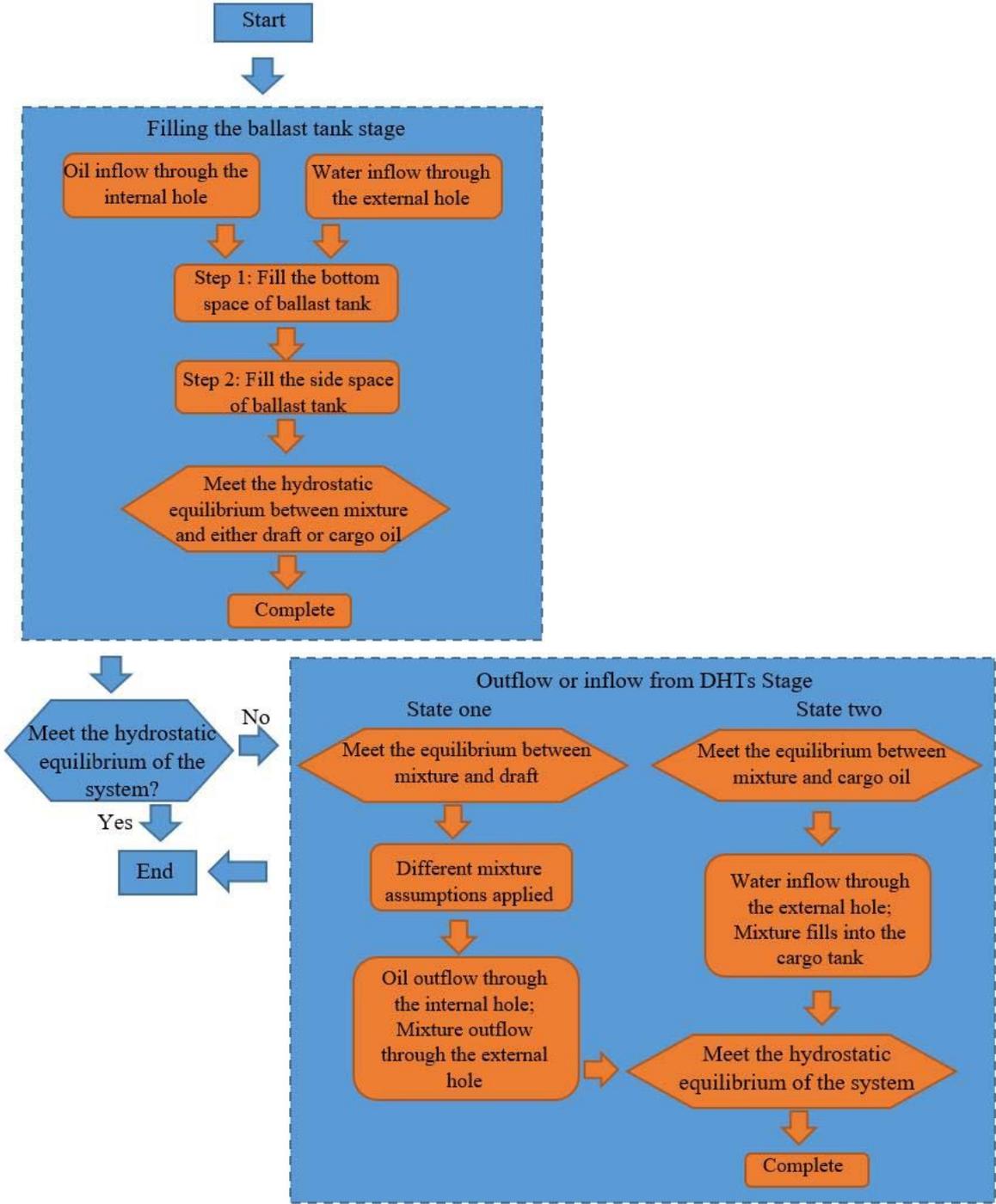
Figure 7.3 Flow chart of Tavakoli analytical model for oil spilling from DHTs.

Figure 7.4 illustrates the comparison between the existing prediction model with the custom C_d=0.65 and the LES numerical result for the four cases in terms of oil volume spilled out of the DHT (V_s) non-dimensionlised by the initial oil volume in the cargo tank ($V_{oil(t=0)}$). The two different mixture assumptions used in the prediction model yield two different spilling trends forming a shaded area between them. Based on the comparison, it is clearly indicated that this simplified solution fundamentally ignores the hydrodynamic interaction between the oil and water jet flows inside the ballast tank at the early spilling stage, which significantly underestimates the V_s over the early period. Despite the fact that the reasonable spilling duration is provided in some cases, the existing model is not suitable for most of the present numerical cases, such as Case G1 and G2 and C1. For example, since the total momentum brought by the oil flow through the internal hole is larger than that brought by the water flow through the external hole, the water inflow only appears at the short transient stage (as shown in Figure 5.12) and disappear afterwards in Case G1. As a result, V_s increases from the very beginning and terminates much earlier compared with the prediction. It is understandable that if the total momentum brought by the oil jet is initially lower than that by the water jet for the Case G1, the water inflow may happen at the early stage and prevent the oil spilling into the environment at the same time. This means that the corresponding hydrodynamic analysis on the interaction between the oil and water jets in the early spilling stage is required for more accurate predictions. Also, the numerical curves in Figure 7.4 reveal that the oil spilling into the environment is largely dependent upon the rupture conditions (such as Case G2 and G3) and the damage scenarios (such as Case C1). Overall, the existing model seems to fail to predict the case-dependent V_s curves.
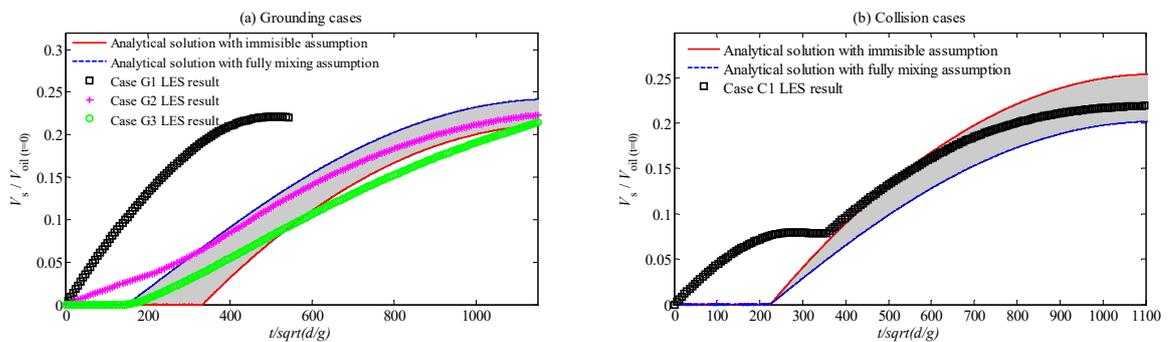
Figure 7.4 Comparison between the prediction model and the numerical results using LES model for different cases in terms of the oil volume spilled out of the DHT (V_s).

7.3 Improved Quasi-steady Analytical Solutions

Considering the previous discussion, the quasi-steady analytical models developed by Tavakoli *et al*. (2008) and Tavakoli *et al*. (2012) are improved to better predict the case-dependent spilling features, especially for the Case G1, G2 and C1.

In this model, it is assumed that:

- The DHT is fixed and the water draft is constant;
- The areas of the external hole and the external hole are equal;
- The ballast tank is initially empty;
- There is no time lag between the initiation of the flows through the internal and external holes;
- The transient stage is ignored;
- The properties of oil and water do not change with time;
- Two different mixture assumptions are applied: the first one is that the oil and water are mixing in a perfect manner (fully mixing) and the second one is that the oil and water are completely separated (immiscible);

The time-domain analysis (time-stepping technique) is employed to solve this model.

7.3.1 Grounding scenarios

The improved model for the spilling from grounded DHTs composes of three steps:

Step one: Filling the bottom space of the ballast tank

Based on the aforementioned discussion, the oil spilling out of the DHT from the very beginning should satisfy two conditions at the same time: the first one is the total momentum brought by the oil jet is higher than that by the water jet around the external hole (as demonstrated in Case G1); the second one is that the vertical overlapping area between the internal and external holes is not zero (at least $\lambda_A = A_o/A_{he} > 0.391$ as demonstrated in Case G2, where A_o is the vertical overlapping area between the internal and external holes, A_{he} is the external hole area). Otherwise, the down-rushing oil flow through the internal hole and the upwelling water flow through the external hole take place simultaneously (as indicated in Case G3).

As indicated by the correlation analysis based on either experimental or numerical results, at this step, the oil jet through the internal hole is regarded as the free discharge driven by the oil height inside the cargo tank and follows the quasi-steady Bernoulli's equation. Thus, the average oil velocity (u_i) and discharge (Q_i) through the internal hole can be calculated as:

$$u_{i(t)} = C_{di1}\sqrt{2gH_{oil(t)}} \qquad (7\text{-}1)$$

$$Q_{i(t)} = A_{hi}C_{di1}\sqrt{2gH_{oil(t)}} \qquad (7\text{-}2)$$

where the subscript i represents the internal hole; subscript 1 means step one; A_{hi} is the internal hole area; C_{di1} is discharge coefficient calculated from the correlation analysis for Case G1 indicated in Figure 7.1(a). The relationship between the $H_{oil(t)}$ and $Q_{i(t)}$ can be expressed as:

$$-S_c \frac{dH_{oil(t)}}{dt} = Q_{i(t)} = A_{hi} C_{di1} \sqrt{2gH_{oil(t)}} \tag{7-3}$$

where S_c is the cross-section area of the cargo tank.

If the above two conditions satisfied, the correlation analysis (indicated in Figure 7.2) suggests that the oil outflow through the external hole (Q_{eo}) can be simplified as the submerged orifice flow by using the quasi-steady Bernoulli's equation without considering the effect of the mixture inside the ballast tank. The discharge depends on the water draft, the height of the ballast tank and oil height inside the cargo tank. The λ_A factor is introduced to take the offset effect into account:

$$u_{eo(t)} = \lambda_A C_{de1} \sqrt{2g(H_{oil(t)} + H_b) - \frac{2\rho_w}{\rho_o} gd} \tag{7-4}$$

$$Q_{eo(t)} = A_{he} \lambda_A C_{de1} \sqrt{2g(H_{oil(t)} + H_b) - \frac{2\rho_w}{\rho_o} gd} \tag{7-5}$$

where u_{eo} is the average oil flow velocity through the external hole; the subscript o and e represent the oil and external hole respectively; C_{de1} is calculated from the correlation analysis for Case G1 indicated in Figure 7.2(a); H_b is the height of the ballast bottom space; d is the water draft; A_{he} is the external hole area; λ_A is the ratio of the vertical overlapping area between the internal and external holes (A_o) to the external hole area (A_{he}). The relationship between the mixture height in the ballast tank ($H_{mixture(t)}$) and $Q_{eo(t)}$ can be expressed as:

$$S_{bb} \frac{dH_{mixtrue(t)}}{dt} = Q_{i(t)} - Q_{eo(t)}$$
$$= A_{hi} C_{di1} \sqrt{2gH_{oil(t)}} - A_{he} \lambda_A C_{de1} \sqrt{2g(H_{oil(t)} + H_b) - \frac{2\rho_w}{\rho_o} gd} \tag{7-6}$$

where S_{bb} is the cross-section area of the ballast bottom space.

If either of the above conditions fails during the spilling process, the water inflow through the external hole occurs and no oil shall spill out of the DHT. This water inflow is characterized as the submerged orifice flow. It depends on both the water draft and the height of the mixture of oil and water in the ballast tank using the quasi-steady Bernoulli's equation (Tavakoli *et al.*, 2008):

$$u_{ew(t)} = C_{de1} \sqrt{2gd - 2g \frac{\rho_{m(t)}}{\rho_w} H_{mixtrue(t)}} \tag{7-7}$$

$$Q_{ew(t)} = A_{he} C_{de1} \sqrt{2gd - 2g \frac{\rho_{m(t)}}{\rho_w} H_{mixtrue(t)}} \tag{7-8}$$

where u_{ew} is the average water flow velocity through the external hole; Q_{ew} is water discharge through the external hole; the subscript w represents the water; Considering the similar flow state, the discharge coefficient (C_{de1}) takes the coefficient for the submerged oil discharge through the internal hole in Case G1 (stage 3 in Figure 7.1(a)). ρ_m is the mixture density in the ballast tank, which is computed as:

$$\rho_{m(t)} = \frac{h_{uo(t)}\rho_o + h_{uw(t)}\rho_w}{H_{mixtrue(t)}} \tag{7-9}$$

where $h_{uo(t)}$ and $h_{uw(t)}$ are the height of the oil and water inside the ballast tank, respectively (i.e., $H_{mixtrue(t)} = h_{uo(t)} + h_{uw(t)}$).

The relationship between the mixture height in the ballast tank ($H_{mixture(t)}$) and $Q_{ew(t)}$ can be expressed as:

$$S_{bb}\frac{dH_{mixtrue(t)}}{dt} = Q_{i(t)} + Q_{ew(t)}$$

$$= A_{hi}C_{di1}\sqrt{2gH_{oil(t)}} + A_{he}C_{de1}\sqrt{2gd - 2g\frac{\rho_{m(t)}}{\rho_w}H_{mixtrue(t)}} \tag{7-10}$$

When the $H_{mixture}$ reaches the bottom of the cargo tank, i.e., $H_{mixture}=H_b$, the step one terminates.

Step two: Filling the side space of the ballast tank

After the $H_{mixture}$ reaches the bottom of the cargo tank, the step two of filling the side space of the ballast tank is launched. This step ends until the hydrostatic equilibrium is achieved between the oil-water mixture and either oil in the cargo tank or water draft.

The oil discharge through the internal hole continues but changes to the submerged discharge. As mentioned in Chapter 3, the flow rate is a function of the height of the oil in the cargo tank (H_{oil}) and the height of the oil-water mixture in the side space of the ballast tank. One may also notice that the mixture assumptions have an influence on the discharge. For clarity, the derivations listed below are under the fully mixing assumption.

By linearizing the transitional period as indicated in Figure 7.1, the rate of the submerged oil flow through the internal hole can be calculated as:

$$u_{i(t)} = C_{di2}\sqrt{2gH_{oil(t)} - \frac{2\rho_{m(t)}}{\rho_o}g[H_{mixture(t)} - H_b]} \tag{7-11}$$

$$Q_{i(t)} = A_{hi}C_{di2}\sqrt{2gH_{oil(t)} - \frac{2\rho_{m(t)}}{\rho_o}g[H_{mixture(t)} - H_b]} \tag{7-12}$$

where C_{di2} is the discharge coefficient for the submerged discharge calculated from the correlation analysis of stage 3 for Case G1 indicated in Figure 7.1(a). Under the fully mixing assumption, $\rho_{m(t)}$ is calculated as:

$$\rho_{m(t)} = \frac{V_{uo(t)}\rho_o + V_{uw(t)}\rho_w}{V_{mixtrue(t)}}$$ (7-13)

where $V_{uo(t)}$ and $V_{uw(t)}$ are the oil and water volume captured by the ballast tank, respectively. (i.e., $V_{mixtrue(t)} = V_{uw(t)} + V_{uo(t)}$)

Thus, the relationship between the $H_{oil(t)}$ and $Q_{i(t)}$ can be expressed as:

$$-S_c\frac{dH_{oil(t)}}{dt} = Q_{i(t)} = A_{hi}C_{di2}\sqrt{2gH_{oil(t)} - \frac{2\rho_{m(t)}}{\rho_o}g[H_{mixture(t)} - H_b]}$$ (7-14)

If the two conditions justifying the oil outflow through the external hole are satisfied during this step, the oil outflow still occupies the external hole, which is similar to the submerged orifice flow in the previous step (Equations 7-4 and 7-5). Ignoring the nonlinear effect during this stage, its rate can be simplified as:

$$u_{eo(t)} = \lambda_A C_{de2}\sqrt{2g(H_{oil(t)} + H_b) - \frac{2\rho_w}{\rho_o}gd}$$ (7-15)

$$Q_{eo(t)} = A_{he}\lambda_A C_{de2}\sqrt{2g(H_{oil(t)} + H_b) - \frac{2\rho_w}{\rho_o}gd}$$ (7-16)

where the discharge coefficient of the oil outflow (C_{de2}) is calculated from the correlation analysis of the stage 3 for Case G1 shown in Figure 7.2(a). The relationship between the mixture height in the ballast tank ($H_{mixture(t)}$) and $Q_{eo(t)}$ can be expressed as:

$$S_{bs}\frac{dH_{mixtrue(t)}}{dt} = Q_{i(t)} - Q_{eo(t)}$$

$$= A_{hi}C_{di2}\sqrt{2gH_{oil(t)} - \frac{2\rho_{m(t)}}{\rho_o}g[H_{mixture(t)} - H_b]}$$

$$-A_{he}\lambda_A C_{de2}\sqrt{2g(H_{oil(t)} + H_b) - \frac{2\rho_w}{\rho_o}gd}$$ (7-17)

where S_{bs} is the cross-section area of the ballast side space.

If either of the above conditions fails during the spilling process, the water inflow through the external hole occurs and is regarded as the submerged water inflow, which is similar to one in the previous step (Equations 7-7 and 7-8):

129

$$u_{ew(t)} = C_{de2}\sqrt{2gd - 2g\frac{\rho_{m(t)}}{\rho_w}H_{mixtrue(t)}} \qquad (7\text{-}18)$$

$$Q_{ew(t)} = A_{he}C_{de2}\sqrt{2gd - 2g\frac{\rho_{m(t)}}{\rho_w}H_{mixtrue(t)}} \qquad (7\text{-}19)$$

Considering the similar flow state, the discharge coefficient of water inflow (C_{de2}) is same as the value of C_{de1} for the water inflow. The relationship between the mixture height in the ballast tank ($H_{\text{mixture(t)}}$) and $Q_{ew(t)}$ can be expressed as:

$$S_{bs}\frac{dH_{mixtrue(t)}}{dt} = Q_{i(t)} + Q_{ew(t)}$$

$$= A_{hi}C_{di2}\sqrt{2gH_{oil(t)} - \frac{2\rho_{m(t)}}{\rho_o}g[H_{mixture(t)} - H_b]}$$

$$+A_{he}C_{de2}\sqrt{2gd - 2g\frac{\rho_{m(t)}}{\rho_w}H_{mixtrue(t)}} \qquad (7\text{-}20)$$

The derivation under the immiscible assumption follows the similar procedure, which is not presented here.

Step three: Outflow or inflow from DHTs

According to the results obtained from the previous step, two different states may take place in the third step:

State one: If equilibrium occurs between the oil-water mixture in the ballast tank and water draft in the second step finally, the oil inside cargo tank continues flows into the ballast tank driven by the larger internal pressure. It pushes the oil-water mixture out from the ballast into the sea at the same rate of the oil outflow through the internal hole. The different mixture assumptions may cause significant difference on the mixture outflow during this stage (Tavakoli *et al.*, 2008). This stage stops when the oil height inside the cargo tank drops to the condition in which the equilibrium is built among the water draft, the cargo oil and the oil-water mixture inside the ballast tank.

Considering the good linear correlation for the oil discharge through the internal hole at the late spilling period shown in Figure 7.1, Equations (7-11) and (7-12) can be applied to the flow rate and discharge through the internal hole with the discharge coefficient C_{di3} calculated from the correlation analysis of stage 3 for Case G1 indicated in Figure 7.1(a).

According to the above discussion, the outflow rate through the external hole is assumed to be equal to the one through the internal hole during this step. But, in the case that some water is

captured by the ballast tank during the previous stages, the fluid composition of the outflow through the external hole is significantly influenced by the different mixture assumptions.

State two: If the equilibrium occurs between the oil-water mixture inside the ballast tank and the cargo oil in the second step, the water shall flow into the ballast tank through the external hole and pushes the oil-water mixture into the cargo tank. This step will terminate when the second equilibrium among the water draft, cargo fluid and the oil-water mixture inside the ballast tank. Since there is no further oil spilling in this state, the corresponding calculation of the water inflow is ignored in this study.
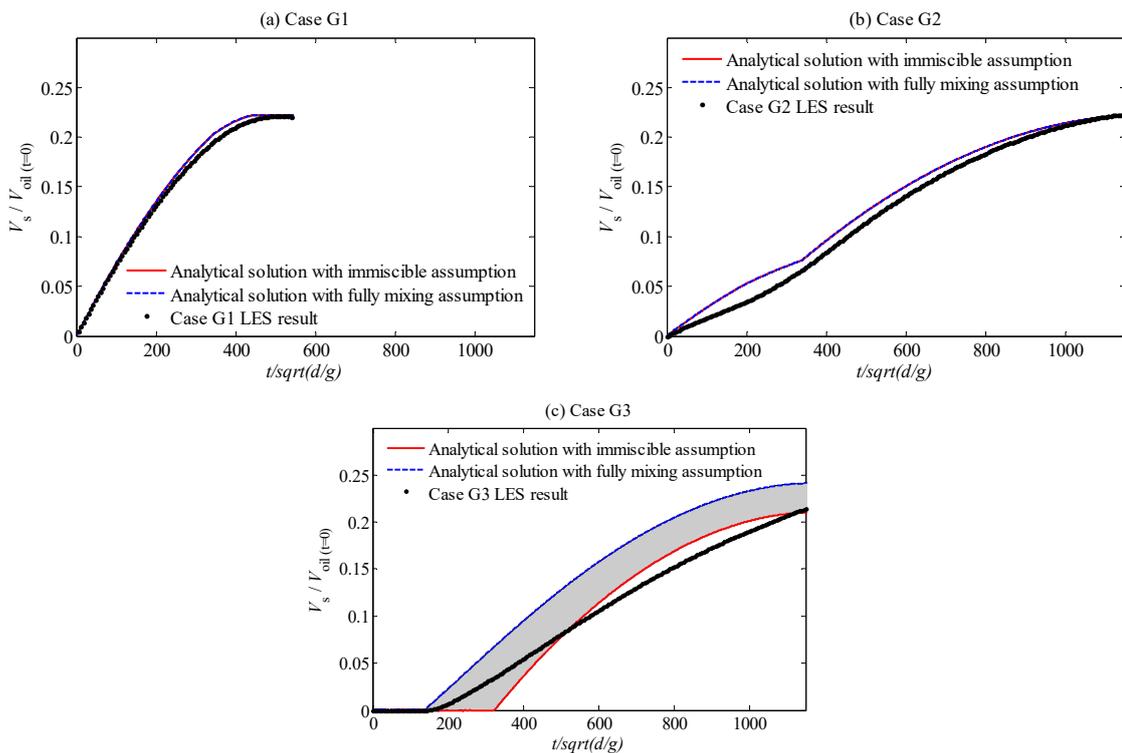
Figure 7.5 Comparison between the proposed prediction model and the numerical results using LES model for grounding cases in terms of the oil volume spilled out of the DHT (V_s).

Based on the above description, Figure 7.5 illustrates the comparison between the present prediction model and the LES numerical result. It is clearly found that the present model significantly better predicts the spilling trend than the previous one by considering some case-dependent spilling features under grounding scenarios.

7.3.2 Collision scenarios

Based on the study of Tavakoli *et al*. (2012), modelling the spilling from a DHT under the collision is similar to the one under the grounding. As the late two-way flow process driving by the pressure imbalance due to the different density of the fluids across the hole is excluded in the

present investigation, only the preceding gravity-driven spilling is considered and the spilling process is divided into three steps:

Step one: Filling the space of the ballast tank underneath the side hole

Considering the available cases in this study, only the coaxial situation is investigated under the collision scenario. Similar to the grounding case, the oil spilling from the DHT from the very beginning needs to satisfy the conditions that the total momentum brought by the oil jet is higher than that by the water jet around the external hole. Otherwise, only the water inflow occupies flow state through the external hole.

The governing equations of the oil jet through the internal hole at this step are similar to Equations (7-1) and (7-2) with the discharge coefficient (C_{di1}) calculated from the correlation analysis for Case C1 indicated in Figure 7.1(d). The relationship between the $H_{oil(t)}$ and $Q_{i(t)}$ can be expressed as Equation (7-3).

If the above conditions of the oil outflow through the external hole satisfied, the previous observation shows that due to the gravity effect, some oil shall travel through the lower part of the external hole finally spill out, meanwhile, the opposite water flow occupies the upper hole area. There is strong interaction between the oil outflow and water inflow around the external hole yielding violent discharge fluctuation as indicated in Figure 5.9. But, this convective oil-water flow through the external hole is ignored in the previous model. In this study, a new approach to deal with this convective flow is proposed, where the gravity-induced vertical distance of the oil jet when approaching the external hole (y) is a factor to determine the proportion of the hole area assigned to the oil and water flows. Based on the observation, due to the gravity effect, the oil outflow travels through the lower part and the water inflow occupies the remaining upper part. The details are shown in Figure 7.6.
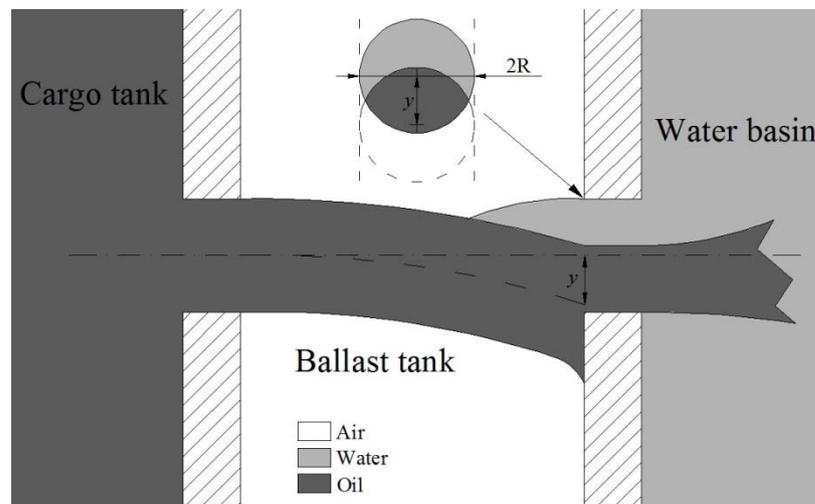
Figure 7.6 Illustration of the area assignment of the water-oil convective flow through the external hole under collisions.

Using this approach, the vertical distance (y) can be calculated as:

$$y_{(t)} = \frac{H_s^2}{4C_{di1}^2(H_{oil(t)} - h)}$$ (7-21)

where H_s is the horizontal space of the ballast side space; h is the vertical distance between the internal hole centre and the cargo tank bottom.

The area the external hole occupied by the oil and water flows (i.e., A_{heo} and A_{hew}) can be expressed as a function of factor y. Using the solution of A_{heo} and A_{hew} the oil outflow and water inflow can be characterized as the submerged and free orifice flows governed by the quasi-steady Bernoulli's equation, respectively:

$$u_{eo(t)} = C_{de1}\sqrt{2g\left(H_{oil(t)} - h\right) - \frac{2\rho_w}{\rho_o}g(d - h_e)}$$ (7-22)

$$Q_{eo(t)} = A_{heo}C_{de1}\sqrt{2g\left(H_{oil(t)} - h\right) - \frac{2\rho_w}{\rho_o}g(d - h_e)}$$ (7-23)

$$u_{ew(t)} = C_{de1}\sqrt{2g(d - h_e)}$$ (7-24)

$$Q_{ew(t)} = A_{hew}C_{de1}\sqrt{2g(d - h_e)}$$ (7-25)

where $A_{heo} + A_{hew} = A_{he}$; h is the vertical distance between the internal hole centre and the cargo tank bottom; h_e is the vertical distance between the external hole centre and the DHT bottom; a custom constant $C_{de1} = 0.65$ is used to simplify the dynamic process;

If the momentum condition fails during the spilling process, only the water inflow dominates the flow through the external hole and no oil spills into the environment. This flow is characterized as the free orifice flow using the steady Bernoulli's equation:

$$u_{ew(t)} = C_{de1}\sqrt{2g(d - h_e)}$$ (7-26)

$$Q_{ew(t)} = A_{he}C_{de1}\sqrt{2g(d - h_e)}$$ (7-27)

When the $H_{mixture}$ reaches the side hole (H_b+h), the step one terminates.

Step two: Filling the side space of the ballast tank above the side hole

This step starts when the $H_{mixture}$ reaches the side hole and ends until the hydrostatic equilibrium is achieved between the oil-water mixture and either oil in the cargo tank or water draft. Generally, this step lasts very short time due to the relatively small ballast space to be filled. Similar to the grounding case, the oil flow through the internal hole is regarded as the submerged orifice flow with a constant C_{di2} as demonstrated in Figure 7.1(d). As for the complex flow state through the external hole, it is assumed that only the water inflow occurs over this short step. The water inflow is modelled as submerged discharge flow with the custom discharge coefficient (i.e., $C_{de2} =$

0.65). The derivation of the governing equations for the aforementioned discharges follows the similar procedure as shown by Equations (7-11) to (7-20).

Step three: Outflow or inflow from DHTs

This step is same as the one under the grounding scenario, except for the fact that only the mixture above the side hole inside the ballast tank is involved in the determination of the fluid composition of the outflow through the external hole in State one under the immiscible assumption.

The comparison between the present model and the LES numerical result is shown in Figure 7.7. The present model can capture the spilling feature well predicting a more reasonable V_s profile.
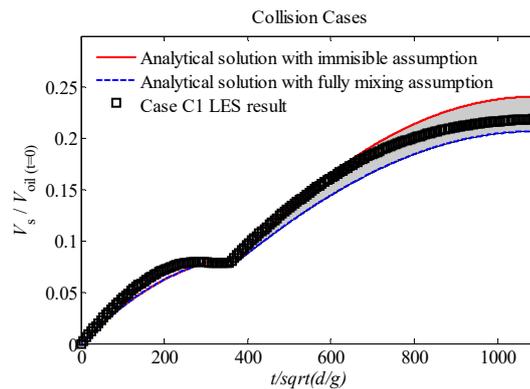

Figure 7.7 Comparison between the proposed prediction model and the numerical results using LES model for collision cases in terms of the oil volume spilled out of the DHT (V_s).

7.4 Summary

In this chapter, the correlation analysis of the discharge through the internal and external holes is carried out based on the LES numerical result. Different cases are considered. The result of the discharge through internal hole indicates the strong linear correlation similar to the one derived from the experimental data, which demonstrates the feasibility of the quasi-steady empirical model developed in Chapter 3. With the assistance of numerical modelling, the correlation analysis extends to the discharge through the external hole. It is suggested that there is much stronger nonlinear effect dominating the flow through the external hole. Moreover, the different complex flow motion around the external hole in each case makes the nonlinear effect case-dependent. Only the Case G1 achieves a good linear relationship similar to the one for the internal hole.

The numerical result is then employed to examine the capability of the analytical solutions developed by Tavakoli *et al*. (2008) and Tavakoli *et al*. (2012). Due to the assumption that no oil spills out of the DHT at the early stage regardless of different loading and draft, rupture location and accidental situations, the existing prediction cannot reflect the different hydrodynamic interaction between the oil and water jet flows inside the ballast tank at the early spilling stage.

As a result, in some cases, such as Case G1, G2 and C1, the analytical model fails to accurately predict the curve of oil volume spilled out of the DHT (V_s).
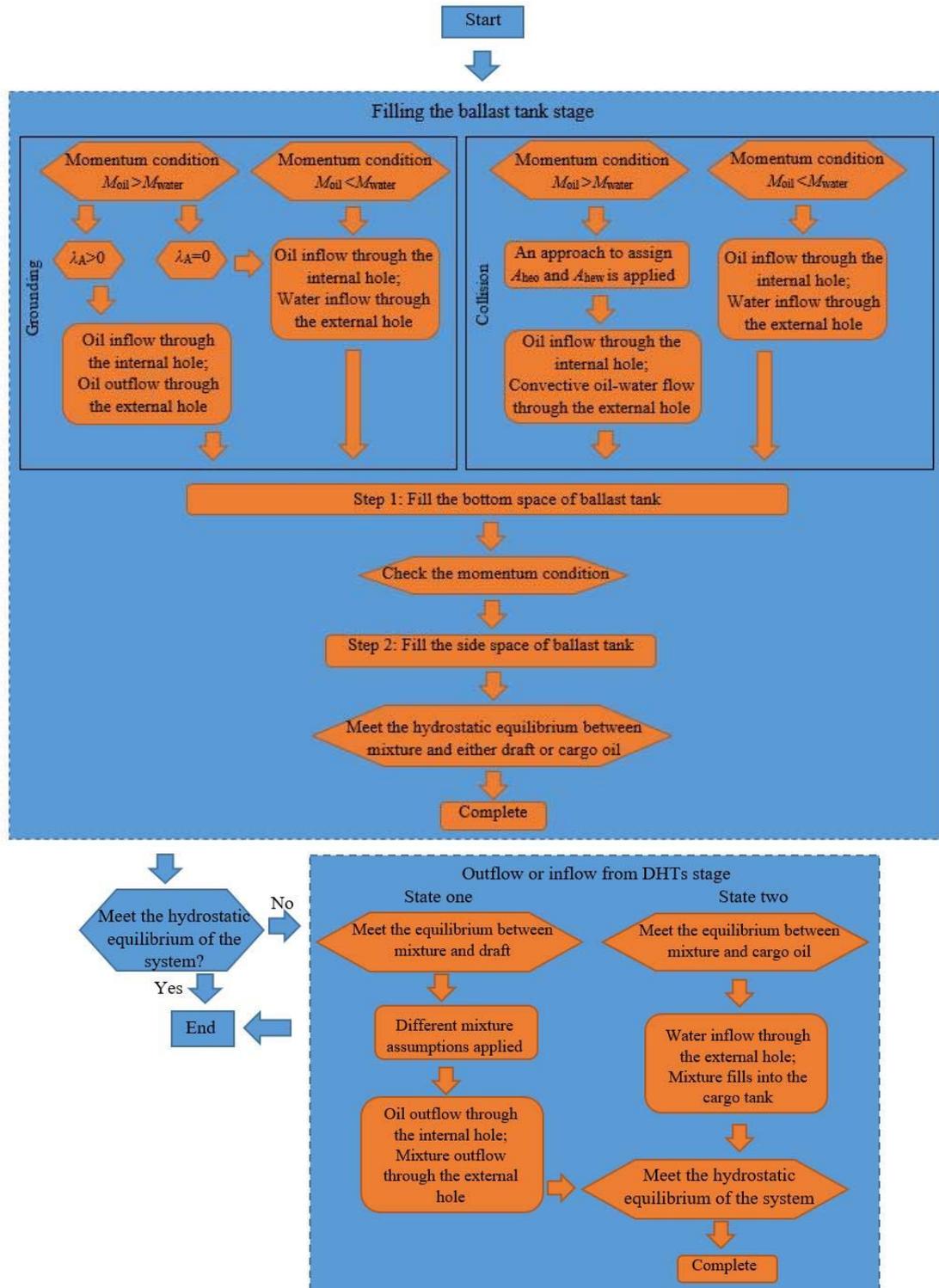
Figure 7.8 Flow chart of the improved analytical model.

An improved analytical model incorporating the interaction between the oil and water jet flows at the early spilling stage is proposed. Two conditions with respect to the momentum balance and

rupture situations are posed to identify whether the oil spills out of the DHT at the early stage of the spilling process under grounding situations. The ratio of the vertical overlapping area to the hole area is introduced to control the oil outflow through the external hole, by which the spilling process under different offset conditions can be predicted. The numerical discharge coefficient for each spilling stage is used. Apart from the momentum balance condition, to model the convective oil-water flow through the external hole under the collision condition, an approach to assigning the proportion of the hole area occupied by oil and water flows is adopted. Using this improved model, different V_s curves resulting from the different hydrodynamic interaction of oil and water flows can be predicted properly and the model applicability is greatly enhanced. The specific flow chart of the improved analytical model is presented in Figure 7.8.

Chapter 8 Oil Spilling from Tanks under Motions

One may notice that all the cases mentioned in this study previously are under the assumption of stationary and initially placed in the still water. However, in reality, the grounded or collided oil tankers are often subjected to motions caused by the ocean current, wave or tide, which excites the liquid sloshing inside the cargo tanks. As discussed based on the experimental and numerical results, the oil discharge through the rupture closely correlates with the oil height inside the cargo tank, particularly on the internal hole of DHTs. Thus, it can be expected that the tank-motion induced sloshing inside the cargo tank shall affect the dynamic spilling process. Though the fluid-ship interaction topic including the effect of liquid sloshing in the intact tank on the global ship motions or the effect of damaged ship sloshing and flooding on the ship instability has been inclusively studied recently (e.g., Zhang and Suzuki, 2010; Gao and Vassalos, 2012; Gao *et al.*, 2013; Manderbacka *et al.*, 2014; Manderbacka *et al.*, 2015), the relevant systematic studies on the oil spilling from damaged hulls under motion are rarely found in literature.

This issue becomes more complicated when considering different tank configurations and thus, in this chapter, the motion effect on the oil spilling is analysed in terms of the SHT and DHT sections. As for the SHT section, the relative spilling effect on the sloshing is also included conversely. A customized solver coupling the multiphase VOF method and the dynamic mesh technology is developed and the numerical results are validated against the existing sloshing lab tests. To simplify the problem, the two-dimensional model associated with pre-specified periodic tank motions (covering heaving, sway and rolling) with various frequencies and amplitude are considered in this study. Although the two-dimensional result may not well reflect the real situation, one may agree that the qualitative results help advance our knowledge and provide a good reference for future studies.

8.1 Model Formulation and Validations

8.1.1 Model formulation

A new solver named 'multiphaseInterDyMFoam' is established, where the package for the dynamic mesh technology which determines the mesh morphing in response to prescribed or free rigid object motions is embedded in the original multiphase VOF solver 'multiphaseInterFoam' used in the previous sections. The governing equations used in this model are same as the one discussed in Chapter 4 as the whole system is under the fixed coordinate. But, comparing to the solvers associated with fixed grids, one additional flux correction step after the mesh deformation

update is necessary prior to solve the discretised equation at each time step. More detailed discussion can be found in Higuera *et al*. (2013) and Devolder *et al*. (2015). In this study, considering the fact that the ship motion is confined to be periodic with small amplitude, the relevant library of 'dynamicMotionSolverFvMesh' is used to solve a Laplace's equation for the motion displacement or motion velocity without topological change. More information can be referred to Jasak and Tuković (2010).

8.1.2 Model validations

Considering the fact that experimental data in literatures for the oil spilling from damaged SHT subjected to a periodic motion is not available, two groups of alternatives for the validation may be adopted, i.e. (1) oil spilling from a fixed damaged SHT and (2) the liquid sloshing in a sealed intact container. The accuracy of the present model in the former has been demonstrated for both grounding and collision scenarios in the previous chapters. It will not be repeated here. For the latter, two sets of experimental data on two-dimensional liquid sloshing will be considered.

The previous discussion in Chapter 4 suggests that directly solving Navier-Stokes (NS) model without implementing turbulent modelling (i.e., DNS) using OpenFOAM may be sufficient for simulating the oil spilling from a SHT in terms of the macroscopic physical quantities, e.g. the discharges through the hole and the volume of the oil outflow from the SHT. But, as for the oil spilling case from DHTs, Chapters 4 and 5 reveal that the numerical results are sensitive to the turbulence models providing a criterion for selecting the turbulence model based on the effective Reynolds number. Thus, considering all the discussion above, some turbulence models which are the most suitable for the fixed DHT cases, i.e., the one equation LES model and the k-omega SST RANS models and the DNS model are applied in the above sloshing validations.

Two-layer sloshing
The first experiment involves the sloshing of multiple fluids and was carried out by Sciortino *et al*. (2009) using a squared tank with a length (*B*) of 0.5m and a height (*H*) of 0.3m. The tank is subjected to a periodic roll motion with a period of 5.78s and amplitude of 0.052rad. The tank is initially filled with fresh water up to a level of 0.057m (H_1) and a layer of Vaseline oil (density of 840kg/m^3) with a thickness of 0.024m (H_2) on the top of the water.

The present solver with turbulence models (i.e., the LES and k-omega SST models) and DNS are applied with a prior satisfactory convergence investigation. The comparisons of the locations of the oil surface ($H_2+\eta_2$) and the oil/water interface (η_1) at different horizontal locations between the present numerical predictions and the experimental data are plotted in Figure 8.1. A satisfactory agreement has been observed, except the k-omega SST model, which suggests that

the k-omega SST model may not be applicable to liquid sloshing cases. Moreover, it can be seen that the LES profiles coincide well with these obtained from the DNS model.
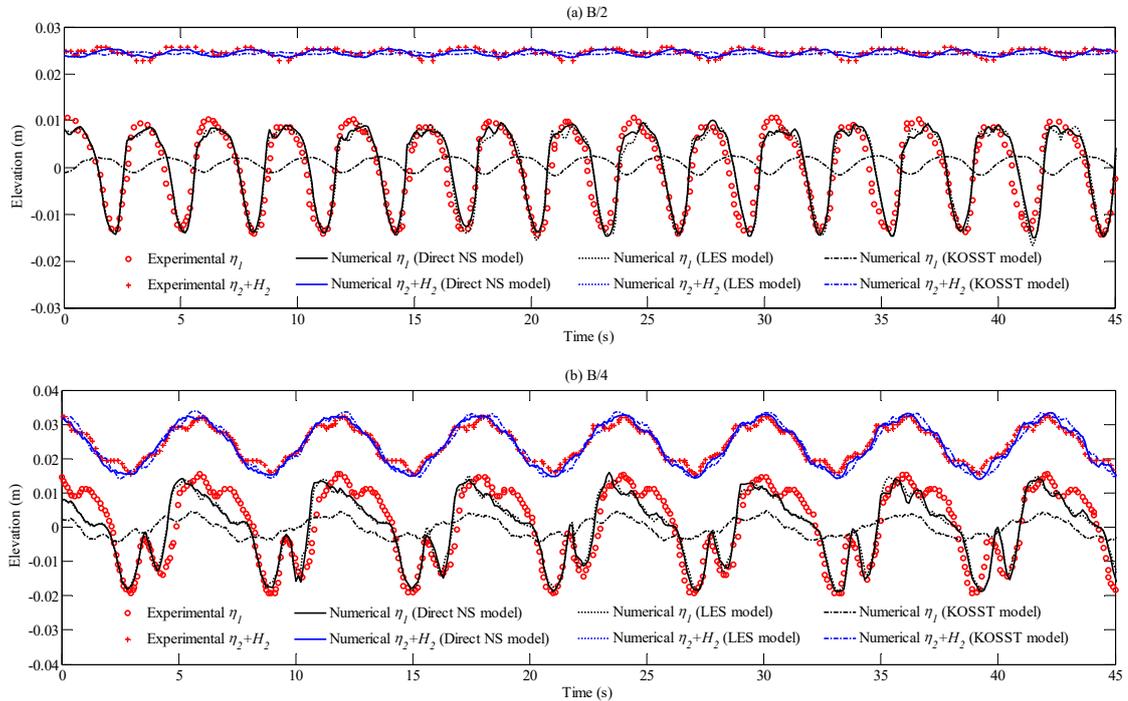
Figure 8.1 Comparisons of the locations of the free surface ($H_2+\eta_2$) and the interface between two fluids (η_1) at (a) the centre of the tank and (b) quarter of the tank length away from the centre. (experimental data is duplicated from Sciortino *et al*., 2009)

One-layer sloshing

The second experiment to be considered was carried out by Kishev *et al*. (2006). In this experiment, water with an initial depth of 0.12m is filled in a rectangular tank with a length of 0.6m and height of 0.3m, which is subjected to a periodic sway motion with a period of 1.3s and amplitude of 0.05m. A pressure sensor is installed on the side wall at 0.1m distance from the bottom of the tank.

The comparison of the time history of the pressure predicted by the different numerical models (LES, k-omega SST and DNS models) and the corresponding experimental data is illustrated in Figure 8.2(a). The similar conclusion to the previous two-layer case can be drawn. A significant difference between the k-ω SST model and lab data rises after the third pressure impulse. The other two models agree well with the experimental data, except the underestimated peak value in each cycle. According to the previous discussion about compressibility effect, the corresponding result considering the compressibility of fluids using the DNS model is also plotted in Figure 8.2(b). It is noticed that the compressibility of fluids slightly improves the accuracy especially during short windows of impulse, although the overall profiles between the compressible and incompressible solvers are similar. This resembles the conclusion in Chapter 6. Nevertheless,

considering the short duration of the impact, such differences on the impulse pressure generally does not lead to considerable error on predicting the macroscopic process of the oil spilling from a damaged oil tanker, e.g. the discharge and/or the volume of the spilled oil, as confirmed by our previous discussion.
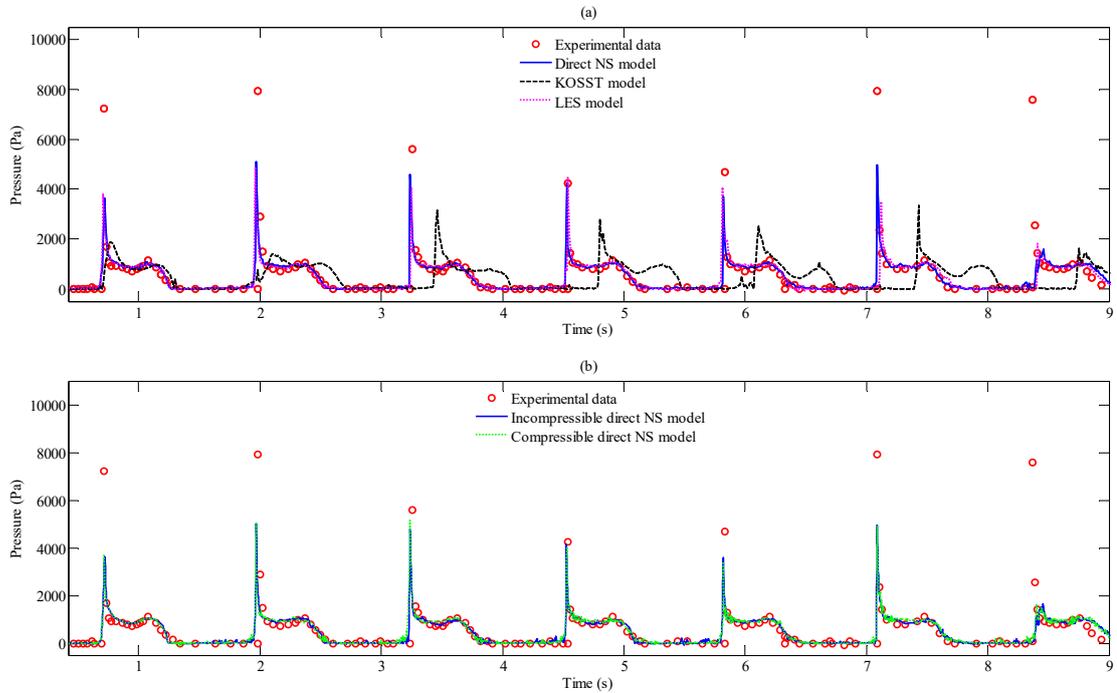
Figure 8.2 The comparison of time histories of the pressure on the wall of the tank subjected to a periodic sway motion for (a) different numerical models and (b) fluid compressibility effect. (experimental data is duplicated from Kishev *et al*., 2006)

8.2 Model Configuration and Convergence Tests

Based on the above validation cases, the incompressible DNS model is supposed to be a competent one for the spilling from SHTs under motions. In this study, it is assumed that the oil spilling from a damaged SHT occurs in the shallow open sea without considering any potential blockage effects caused by the obstacles creating the ruptures. Figure 8.3 illustrates the sketch of the numerical configuration. The numerical investigations are carried out in a two-dimensional rectangular basin with the water depth of W_d. A damaged SHT model tank is horizontally placed in the middle of the water basin with a draft of d, which is 0.47m for all grounding cases and 0.5m for all collision cases.

The geometry of the SHT model tank is taken from the cross-section of the 1/30 model tank used by Tavakoli *et al*. (2011). The breadth B and the height H of the SHT tank are all 1m. The thickness of the tank wall is 0.01m. The SHT tank is vented through an opening space on the top and the initial height of the oil in the tank ($H_{oil(t=0)}$) is 0.80m. Considering different spilling scenarios, a broken hole with dimension (D) of 0.022m (equivalent to the diameter of the hole

140

used by Tavakoli *et al*., 2011) is introduced at different locations, i.e. in the centre of the tank bottom (referred to O_G in Figure 8.3) to simplify grounding scenarios and on the side wall at 10cm above the tank bottom (referred to O_C in Figure 8.3) to simplify collision scenarios. Drain holes in line with the initial water level in the basin are used on both sides of the basin to avoid the rise of the mean fluid surface due to the oil spilling from the SHT tank.

Numerical damping zones with the length of *B* are employed on both sides of the basin. In the damping zone, an artificial damping term is introduced into the momentum equation to gradually damp the wave induced by the motion of the tank and avoid the reflection from the vertical walls of the basin. The details can be found in Zha (2011) and Xu and Duan (2013). The length of the water basin is taken as 30*B* according to our numerical test targeting that reflection wave is negligible in the near field of the tank during the entire oil spilling process. Following the similarity criteria explained in Chapter 3, the density and viscosity of the oil are chosen as 920 kg/m^3 and 8.1×10^{-5} m^2/s, respectively.
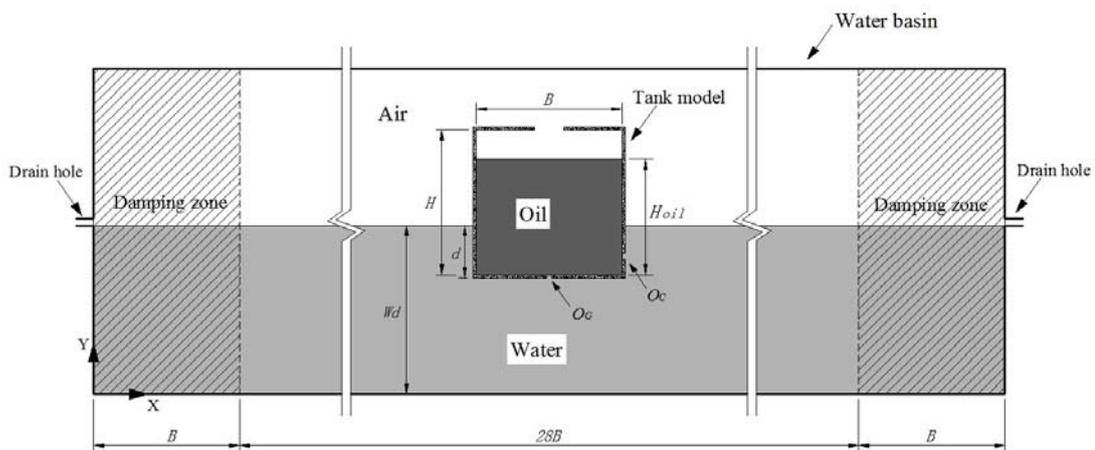
Figure 8.3 Sketch of the numerical configuration of SHT cases.

During the spilling process, the tank is subjected to a pre-specified periodic motion with a frequency of ω and amplitude of *A*. Different types of motions, including heaving, swaying and rolling, are considered. For the roll motion, the rotation centre is assumed to locate at the middle point of the tank bottom. Unlike the liquid sloshing in a sealed container, the mean fluid depth and the fluid properties in the damaged SHT continue changing during the spilling process, in particular in the early stage. As a result, the natural frequency of the damaged SHT is time dependent. Figure 8.4 illustrates the first-mode natural frequency of a sloshing tank with different oil depth according to Faltinsen (1978). The liquid depth in the SHT is initially 0.8m. By applying the hydrostatic analysis on the final state of the fixed tank, it drops to 0.52m and 0.537m in grounding and collision cases, respectively, when the hydrostatic equilibrium reaches. Considering the variation of the liquid depths, the first-mode natural frequency of the damaged

tank during the oil spilling may largely fall in the range from 5.35 rad/s (ω_2) to 5.5 rad/s (ω_1). This frequency range will be assigned to the motions of the SHT in the numerical investigation. In addition, various motion amplitude ranging from $0.01B \sim 0.03B$, $0.02 \sim 0.06$ rad are considered for translational and rotational motions, respectively. Table 8.1 summarises the motion frequencies and the amplitude employed in this investigation, where 'C' and 'G' in the Case No represent the collision and grounding scenarios, respectively.
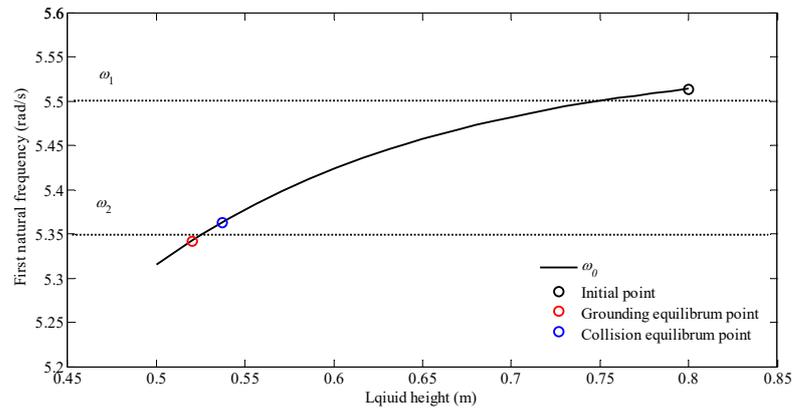
Figure 8.4 First-mode natural frequencies (ω_0) with different liquid heights evaluated using Faltinsen (1978).

Table 8.1 The case list of SHT spilling under different scenarios.

Case No	Motion types	Frequency (ω, rad/s)	Amplitude (A)
C0, G0	None	-	-
C1, G1	Heave	5.5	1 cm
C2, G2	Heave	5.5	2 cm
C3, G3	Heave	5.5	3 cm
C4, G4	Heave	5.35	2 cm
C5, G5	Sway	5.5	1 cm
C6, G6	Sway	5.5	2 cm
C7, G7	Sway	5.5	3 cm
C8, G8	Sway	5.35	2 cm
C9, G9	Roll	5.5	0.02 rad
C10, G10	Roll	5.5	0.04 rad
C11, G11	Roll	5.5	0.06 rad
C12, G12	Roll	5.35	0.04 rad

Following the previous discussion, the similar strategy of the mesh distribution and convergence test is applied. The unstructured hexahedral mesh with the spatially hierarchical refinement is used. Considering the violent flow near the hole and the liquid sloshing inside the tank, sufficiently refined mesh is not only distributed near the holes but also covers the entire tank to resolve the interface between different phases and minimize the numerical diffusion (Yan and Ma, 2010). In the regions far away from the tank a reference cell size of 0.02m is used. The ratio (a_{ds}) of the smallest cell size to the reference cell size is used to reflect the overall mesh resolution during the convergence test.

As an illustration case, the results in grounding Case G6 are presented below for demonstration. In this case, a_{ds} ranges from 1.5625% to 6.25% yielding a ratio of the largest cell size inside the tank to the reference cell size varying from 12.5% to 50%. The total number of elements varies from approximately 0.75 to 0.18 million. The closely related parameters, such as the volume and discharge of fluids, are adopted as indexes in the convergence tests. Figure 8.5 presents the time histories of the volume of the oil spilling into the water basin (V_s), the volume of the water flowing into the tank (V_f) and the discharge of the oil outflow (Q_o) in Case G6. For convenience, the time, the volume of the fluids and the discharge are non-dimensionlised by using $\sqrt{d/g}$, the initial volume of oil in the SHT tank ($V_{oil(t=0)}$) and $\sqrt{2g\Delta H_{(t=0)}}A_h$ where $\Delta H_{(t=0)}$ is the initial hydraulic head difference between the oil surface in the SHT tank and the broken hole and A_h is the hole area.
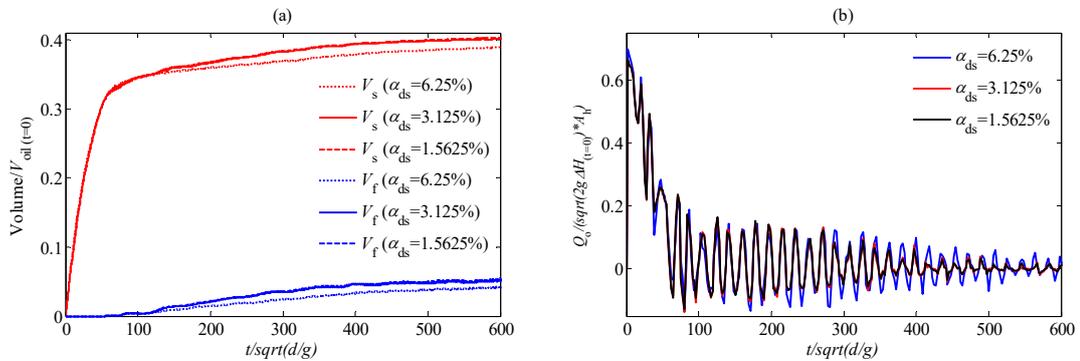
Figure 8.5 Time histories of the dimensionless (a) volume of oil spilling into the water basin (V_s), that of the water flowing into the tank (V_f) and (b) discharge of the oil through the broken hole (Q_o) (Case G6, sway motion with ω_1=5.5 rad/s and A=0.02m)

As observed from Figure 8.5 that with the decrease of α_{ds}, the corresponding results gradually become closer to each other. The time-averaged relative difference (Ma and Yan, 2006) of V_s, V_f and Q_o between α_{ds}=3.125% and α_{ds}=1.5625% are approximately 0.3%, 2.4%, and 0.3%, respectively, suggesting that the mesh with α_{ds} =3.125% can lead to convergent results in terms of macroscopic oil spilling.

8.3 Oil Spilling from SHTs under Tank Motions

8.3.1 The spilling effect on the liquid sloshing in the cargo tank

The sloshing inside a damaged tank is different to the one in an intact tank as the mean fluid depth and fluid properties in the damaged tank vary with time during the spilling process yielding a time-dependent natural frequency of the cargo liquid. In order to investigate this, some grounding cases under different modes of motions are selected (i.e., G2, G6 and G10) and some

corresponding intact tank cases (numbered as G2i, G6i and G10i) are also conducted for the purpose of comparison.

Due to no horizontal translations, the heaving motion does not excite obvious liquid sloshing in both damaged and intact cases as evidenced by the snapshot of the spatial distribution of the air, oil and water in Figure 8.6. In this Figure, different phases of fluid are represented by the contour of volume of fraction (α). Different from the intact tank sloshing case, the liquid height inside the damaged tank drops dramatically as the oil spills from the bottom hole (Figure 8.6(a)). It is also noticed that the heave motion introduces the water/oil convective flow through the hole during the later spilling stage, by which some amount of water accumulates on the bottom of the tank (Figure 8.6(c)). As a result, the dominant variables for calculating the natural frequency (i.e., the fluid depth and fluid property) vary with time in damaged tank cases.

(a) $t \approx 10T$ (Case G2)   (b) $t \approx 10T$ (Case G2i)

(c) $t \approx 35T$ (Case G2)   (d) $t \approx 35T$ (Case G2i)
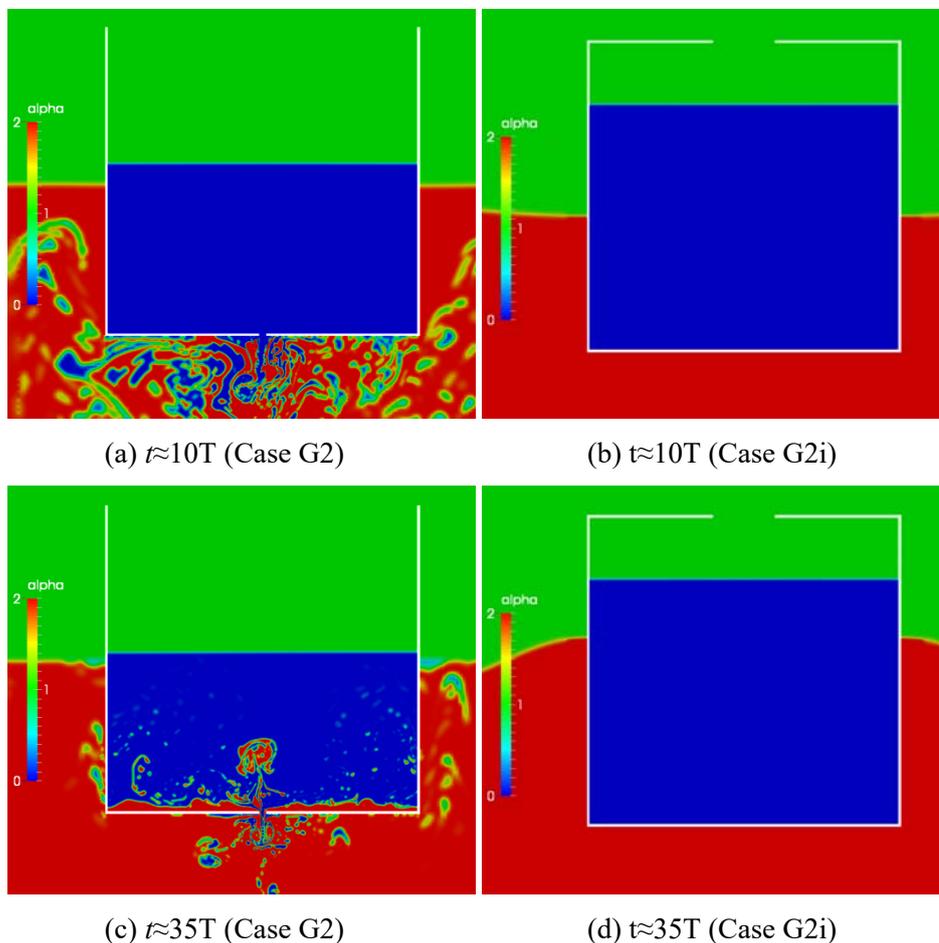
Figure 8.6 Snapshots of the spatial distributions of oil, water and air (volume of fraction α) at different instants in Case G2 and G2i (water: red ($\alpha=2$); air: green ($\alpha=1$); oil: blue ($\alpha=0$); Heave motion: $\omega_1=5.5$ rad/s and $A =0.02$m)

When the grounded tank is subjected to a forced sway motion with $\omega_1= 5.5$ rad/s and $A=0.02B$ (Case G6), an obvious liquid sloshing is excited as illustrated by the time histories of the wave

elevation recorded at different locations relative to the vertical central axis of the tank in Figure 8.7. It is observed that the oil surface elevation becomes more significant at the locations farther from the centre of the tank; the dominated oscillating frequency of the oil surface is the motion frequency, except in the centre where higher frequency harmonics becomes more significant. Furthermore, the dropping oil surface undermines the symmetry of the liquid sloshing with respect to x-axis in the early stage (<5T) which is expected in the intact tank. As the sloshing proceeding, the increasing oscillating amplitude leads to breaking of the oil surface in the tank associated with unsymmetrical elevation profiles in Figure 8.7. This is clearer in Figure 8.8 which displays snapshots of the spatial distribution of the air, oil and water in one motion period. The mean oil surface seems to become relatively steady after approximately 10 periods of the motion (Figure 8.7). Unlike the spilling from the fixed SHT, the spilling continues by means of water/oil exchange flow through the hole over a long period yielding time-dependent liquid properties inside the tank. Finally, a significant water layer on the bottom of the tank is formed and leads to a stratified liquid sloshing in the cargo tank as shown in Figure 8.16.
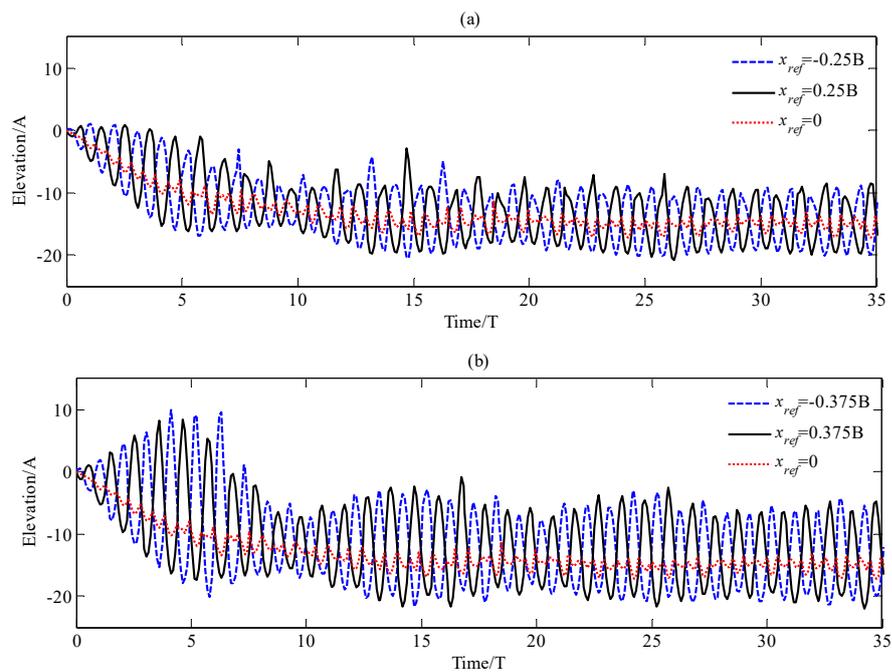
Figure 8.7 Time histories of the oil surface elevations recorded at different locations in Case G6 (Sway motion: ω_1=5.5 rad/s and A=0.02m, x_{ref}: horizontal coordinate relative to the vertical central axis of the tank).

(a) 7.25T   (b) 7.5T

(c) 7.75T   (d) 8T
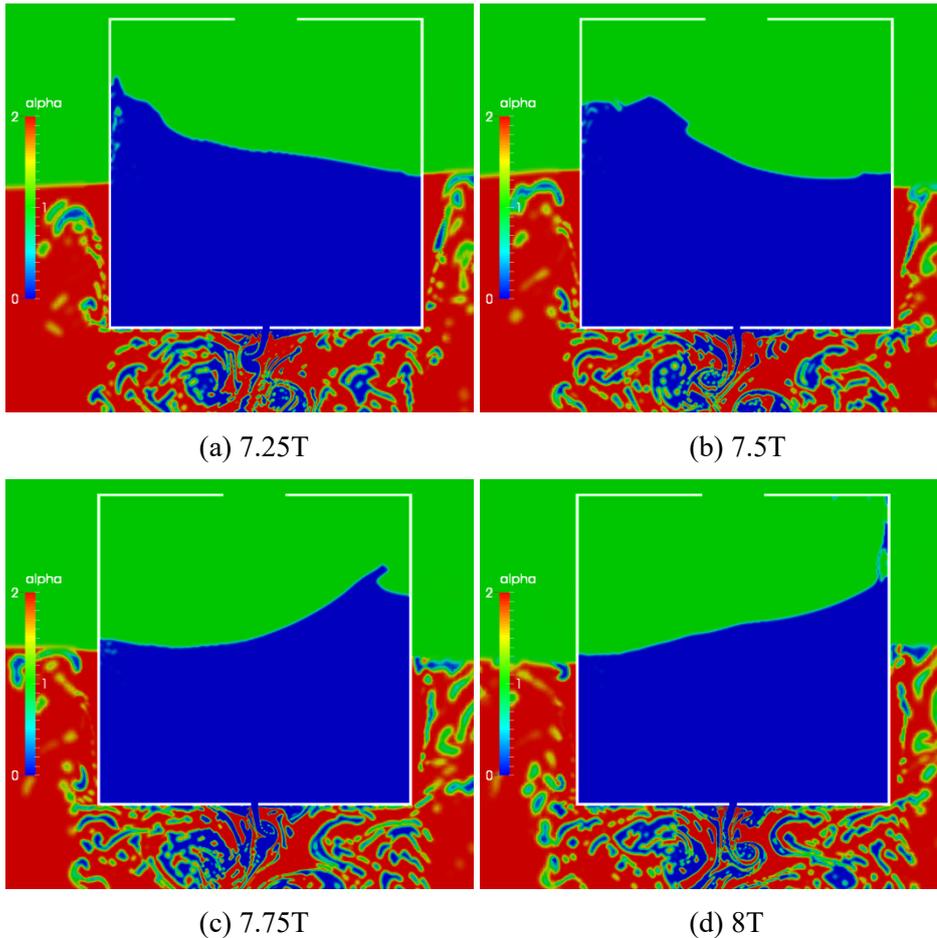
Figure 8.8 Snapshots of the spatial distributions of oil, water and air (volume of fraction α) at different instants in Case G6 (water: red (α=2); air: green (α=1); oil: blue (α=0); Sway motion: ω_1=5.5 rad/s and A =0.02m)

Investigating the pressure distribution at different locations is one of the interesting aspects for the sloshing in a partially-filled tank with or without spilling processes. Considering the fact that the motion frequency is close to the first-mode natural frequency of liquid inside the tank even taking the changing depth due to spilling into account as shown in Figure 8.4, the violent sloshing associated with the breaking free surface is observed in both the intact and damage cases which may cause large impact loads on the hull structure. Figure 8.9 displays the time histories of the pressure at different heights on the side wall for the Case G6 and G6i (the height is calculated as the vertical distance between the recorded point and the bottom of the cargo tank). The pressure is normalized by $\rho_o g H_{oil(t=0)}$ for comparison. Considering the constant liquid volume in the Case G6i, the obvious impulse pressure due to the impact of the free surface takes place mainly at H=0.8m and 0.7m reaching a high pressure value up to $0.29\rho_o g H_{oil(t=0)}$. As for the grounded tank (Case G6), the dropping mean level of the oil surface due to the spilling process leads to that the free-surface induced impulse pressure on the side wall moves downward. The maxima of all short windows of impulse during the first ten periods increases with the decrease of H, but still lower

than the corresponding maxima in the intact case as shown in Figure 8.9. After $10T$, the impulse envelope only emerges at the lower locations of H=0.6m and 0.5m with relatively smaller maxima in every short window of impulse (less than $0.2\rho_o gH_{oil(t=0)}$) than the one in Case G6i shown in Figures 8.9 (a) and (b).
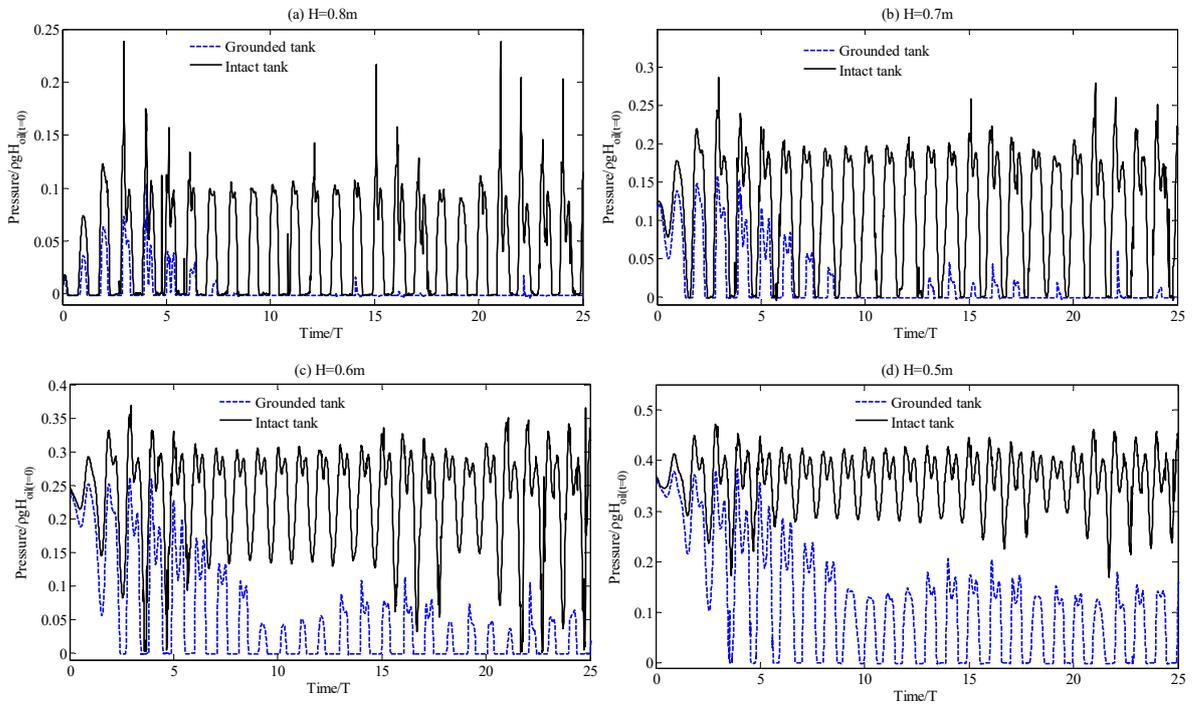
Figure 8.9 Time histories of the pressure on the left side wall at the height of (a) H=80cm, (b) H=70cm, (c) H=60cm and (d) H=50cm from the tank bottom in Case G6 and G6i. (Sway motion: ω_1=5.5 rad/s and A=0.02m)

Considering the fact that the natural frequency may change with time as the average liquid height inside the cargo tank decreases resulting from the oil spilling out of the tank, the frequency analysis of these impact pressure signals is of interest to the researchers. Using FFT analysis, the spectrum distribution of the pressure at H=0.6m and 0.5m over the first 25 periods in Case G6 and G6i is displayed in Figure 8.10. It is clearly shown that the distributions between the Case G6 and G6i are different. There are two dominant components located at approximately ω_1 and $2\omega_1$ respectively in Case G6i, while in Case G6 the harmonic corresponding to ω_1 dominates the frequency domain, but the spilling influences the higher order harmonics by flatting and enhancing the harmonics around second and third orders, respectively.
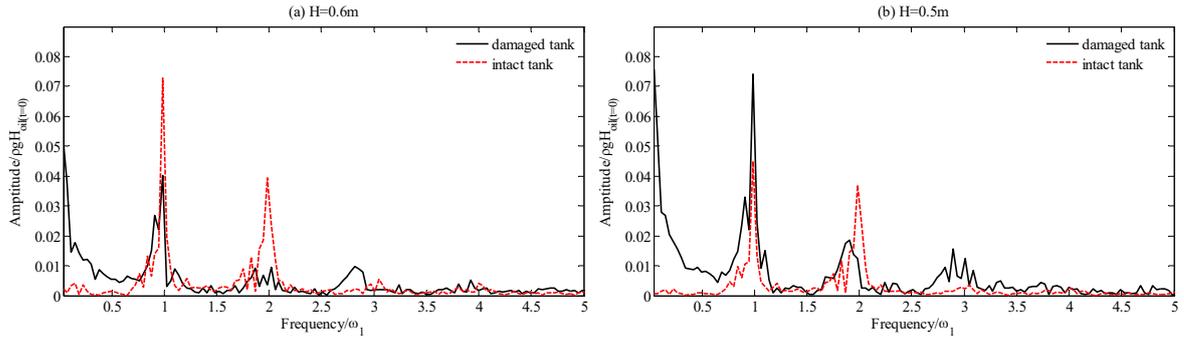
Figure 8.10 Spectrum distribution of the pressure on the left side wall at height of (a) H=0.6m and (b) H=0.5m from the tank bottom over the first 25 periods in Case G6 and G6i. (Sway with ω_1=5.5rad/s and A=0.02m)

It should be noticed that the conventional FFT analyses the signal as a whole by hiding the non-stationary behaviours where the frequency changes with time. However, the time-frequency representation of the signal is more important in the current damaged SHT case where the falling liquid height due to the spilling process, particularly in the early stage, greatly affects the natural frequency (highlighted in Figure 8.4). As a result, the continuous wavelet transform is employed as an alternative approach and the power spectra of the pressure signals are shown in Figure 8.11. In the intact case, both two pressure signals yield similar power spectra. There is a uniform power spectrum at ω_1 over the first 18 periods (stronger at H=0.6m in Figure 8.11(a)), except for the short duration at both ends of the period due to the boundary effect. Moreover, it is clearly indicated that the $2\omega_1$ frequency appears intermittently, which is invisible from the conventional FFT analysis (Figure 8.10). On the other hand, the power distribution around the first order is also significant, but oscillates with time in the damage case as shown in Figure 8.11(b) and (d). Also, the time-dependent natural frequency during the spilling process influences the non-linear effect by redistributing the higher order frequencies, where the power spectra spread over $2\omega_1$ and $3\omega_1$ at a certain period and are different between H=0.6m and H=0.5m. Although more analysis is required to build the temporal relationship between the nature frequency change and the nonlinear effect, this study introduces an alternative approach for the frequency analysis and demonstrates its feasibility for analysing the sloshing in conjunction with spilling.
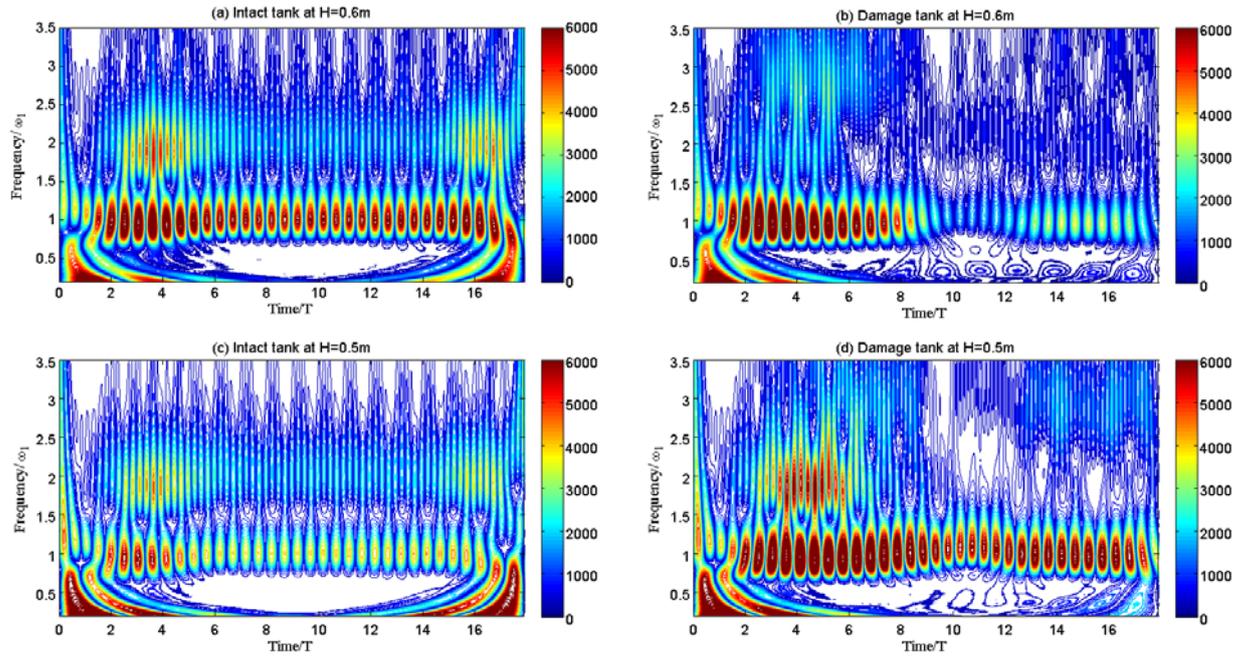
Figure 8.11 The local wavelet power spectrum of the pressure signals at height of (a, b) H=0.6m and (c, d) H=0.5m from the tank bottom in Case G6 and G6i (Sway with ω_1=5.5 rad/s and A=0.02m).

8.3.2 The sloshing effect on the spilling processes

Grounding scenarios

With respect to the grounded spilling process under ship motions, Figure 8.12 indicates the time histories of some relevant volumetric variables, such as the oil spilled into the water basin (V_s), the water flowing into the cargo tank (V_f) and the oil/water mixture in the cargo tank (V_m), in the sway cases with different motion amplitude. The case with fixed SHT is also included for the comparison. Figure 8.12 shows that in the fixed tank case the water flowing into the cargo tank (V_f) is negligible and the spilling process terminates at approximately t=17.5T as hydrostatic equilibrium is built. Moreover, as demonstrated by the above correlation analysis, the discharge from the hole from a fixed tank is dominated by the gravity over the period. It is interesting to notice that the motions of the tanks insignificantly affect the oil spilling into the water basin (V_s) during the same period. However, the motion results in continuously spilling of oil after t=17.5T (Figure 8.12(a)) along with an increasing volume of the water flowing into the cargo tank (V_f) (Figure 8.12(b)). As a result, the whole spilling process under tank motions lasts much longer than the fixed case causing more oil spilled out. These influences on V_s and V_f become more significant with the increase of the amplitude of the tank motion. It is also found that the volume of the oil/mixture volume in the cargo tank of all the sway cases keeps steady after t=17.5T being at a level similar to the case with fixed SHT. Based on the aforementioned discussion, one may

149

agree that the whole process can be divided into two phases by using the time instant that the hydrostatic equilibrium is built in the fixed grounded SHT case.
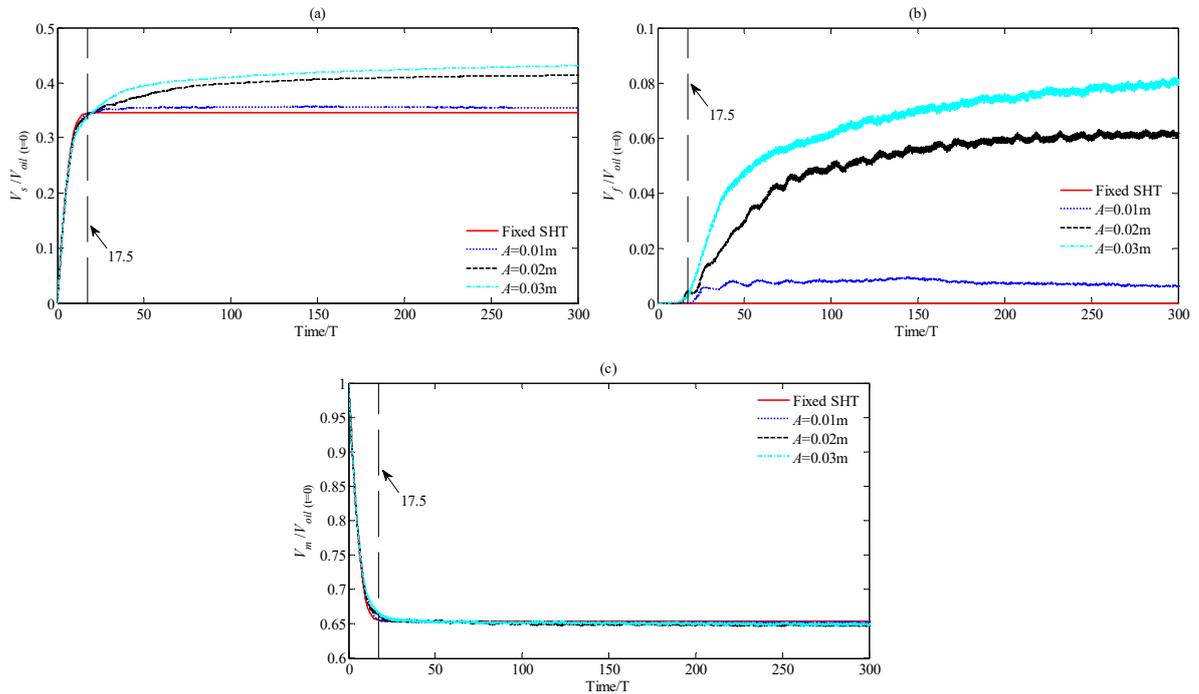
Figure 8.12 Time histories of volumes of (a) the oil spilled into the water basin (V_s), (b) the water flowing into the cargo tank (V_f) and (c) the oil/water mixture in the cargo tank (V_m) in the cases with different motion amplitude (forced sway with ω_1=5.5 rad/s)

In the first phase, the discharge through hole is featured by the continuous oil outflow and driven by the gravity. Figure 8.13 presents the corresponding time histories of discharge of the oil outflow (Q_o) and water inflow (Q_w) through the grounded hole during the first phase. As expected, Q_o suffers from a significant oscillation when the tank is subjected to sway motions shown in Figure 8.13(a). The oscillation grows with time in the early stage (t<5T) and behaves similar to a wave envelop suggesting the involvement of long-term effects. It is interesting to find that the Q_o oscillates with respect to the smooth Q_o curve of the fixed SHT and the mean value of that is close to zero in the late stage of this phase. Instead, the water inflow starts a convective oscillation due to the tank motion (Figure 8.13(b)), although the amplitude is very low. Using the spectrum analysis, Figure 8.14 duplicates the spectra of Q_o in the first phase of the spilling, from which it is worthy of noting that the oscillation of Q_o is dominated by the harmonics corresponding to approximately $2\omega_1$. Also, one may observe that in the case with A=0.01m, the most significant harmonic occurs at $1.9\omega_1$, approximately the doubled first-mode natural frequency corresponding to the fixed tank at hydrostatic equilibrium ($2\omega_0$); whereas in the case with A=0.03m, the most significant harmonic occurs at $2\omega_1$. As for the case with A=0.02m, both the harmonics of $2\omega_1$ and $1.9\omega_1$ happen simultaneously. A possible explanation of the occurrences of the dominated

150

harmonics at approximated two times of the motion frequency may be that the oil spilling is significantly affected by the nonlinear interaction of the liquid sloshing in the cargo tank and the convective motion between the fluids and the hole caused by the tank motion of ω_1. This leads to typical 2nd order harmonics with frequencies of $\omega_0+\omega_1$, $2\omega_1$, $2\omega_0$ and other higher order harmonics. Also, the increasing amplitude of sway motion affects the nonlinear effect on the oil discharge and thus the significant harmonic in Figure 8.14 switches from $2\omega_0$ to $2\omega_1$.
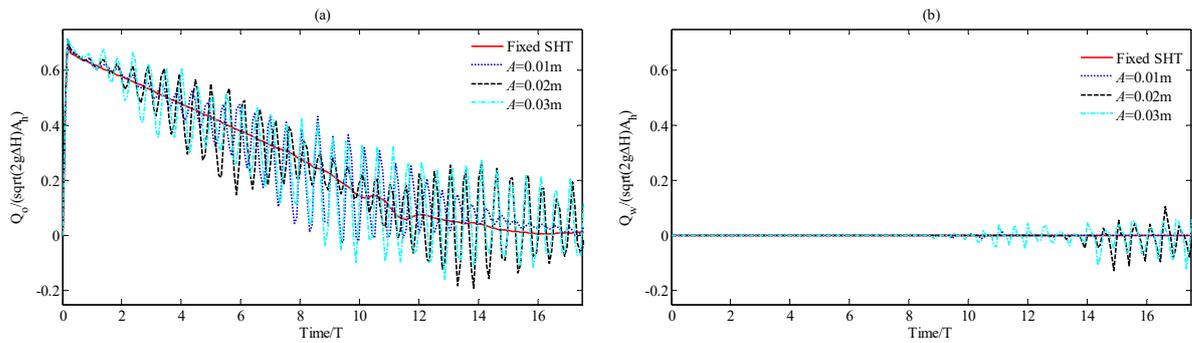
Figure 8.13 Time histories of the discharges of (a) the oil outflow (Q_o) and (b) the water inflow (Q_w) through the broken hole in the first phase. (forced sway with ω_1=5.5 rad/s)
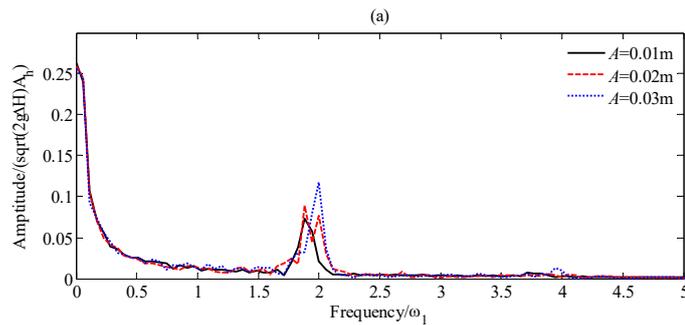
Figure 8.14 Spectrum distribution of the oil discharge (Q_o) in the first phase of spilling. (forced sway with ω_1=5.5 rad/s)

The second phase is featured by the significant oil/water convective flow through the broken hole and a resultant volume of oil/water mixture in cargo tank. Figure 8.15 indicates the time histories of the discharge of the oil outflow (Q_o) in this phase under sway motion with different amplitude. It shall be noted that in the cases with larger motion amplitude, i.e. A=0.02m and 0.03m (Figure 8.15(b) and (c)), Q_o becomes insignificant in the late stage, e.g. >87.5T, due to an entrapped water layer sealing the tank as demonstrated in Figure 8.16. Instead, the water flow oscillates through the broken hole as observed in Figure 8.17 over the same stage. The spectrum analysis is carried out individually for these two stages and shown in Figure 8.18. Similar oscillations with the dominated frequency of approximately $2\omega_1$ are observed in both Q_o in the early stage and Q_w in the later stage. For the former, the significant component at around $2\omega_0$ is also found in the case with 0.01m amplitude case and it clearly shown that considerable harmonics at approximate $4\omega_1$ exists and the magnitude increases with higher amplitude. It is noted that the natural frequencies

of the tank vary during the spilling process, particularly in the cases with larger motion amplitude where the significant water layer on the bottom of the tank leads to a stratified liquid sloshing in the cargo tank as demonstrated in Figure 8.16(b). The variation of the natural frequency results in a wider spectra of Q_o and Q_w in a range of $1.8\omega_1$ to $2.2\omega_1$. Especially for Q_w in Figure 8.18(b), the spectra become more confined as the motion amplitude reduces.
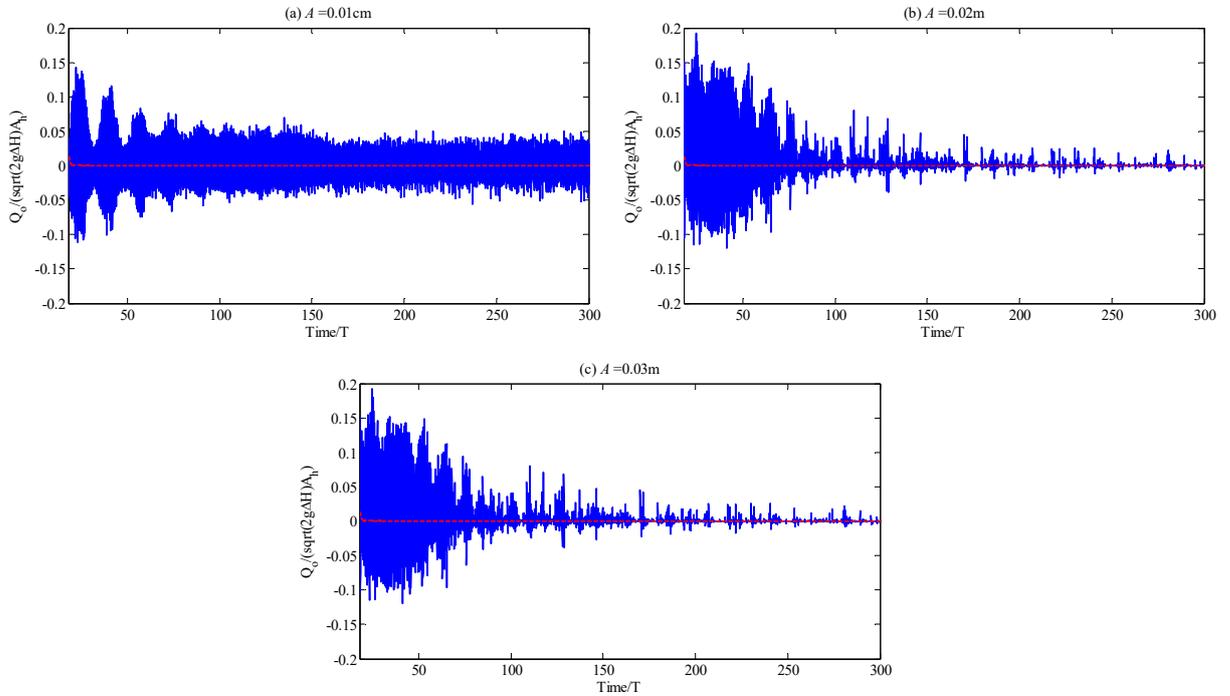
Figure 8.15 Time histories of the discharge of the oil inflow (Q_o) in the 2nd phase of spilling with different amplitude. (forced sway with ω_1=5.5 rad/s, red dashed line: Q_o in the fixed tank case)
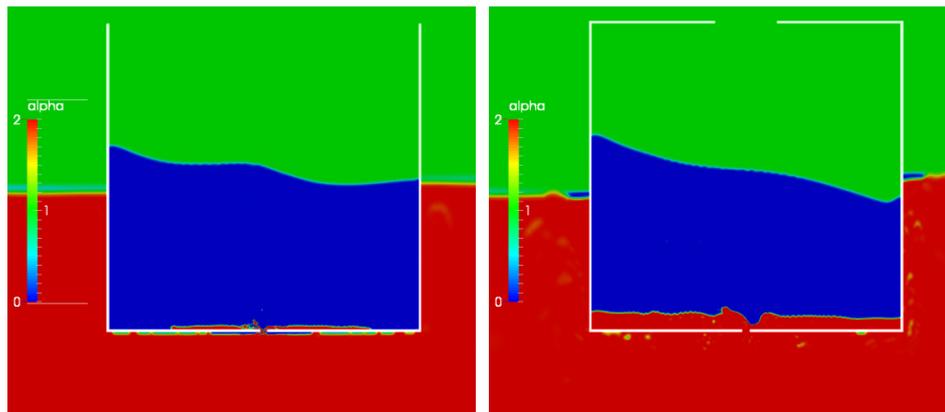
(a) A=0.01m   (b) A=0.02m

Figure 8.16 Snapshots of the spatial distributions of oil, water and air (volume of fraction α) at 175T (water: red (α=2); air: green (α=1); oil: blue (α=0); ω_1=5.5 rad/s)
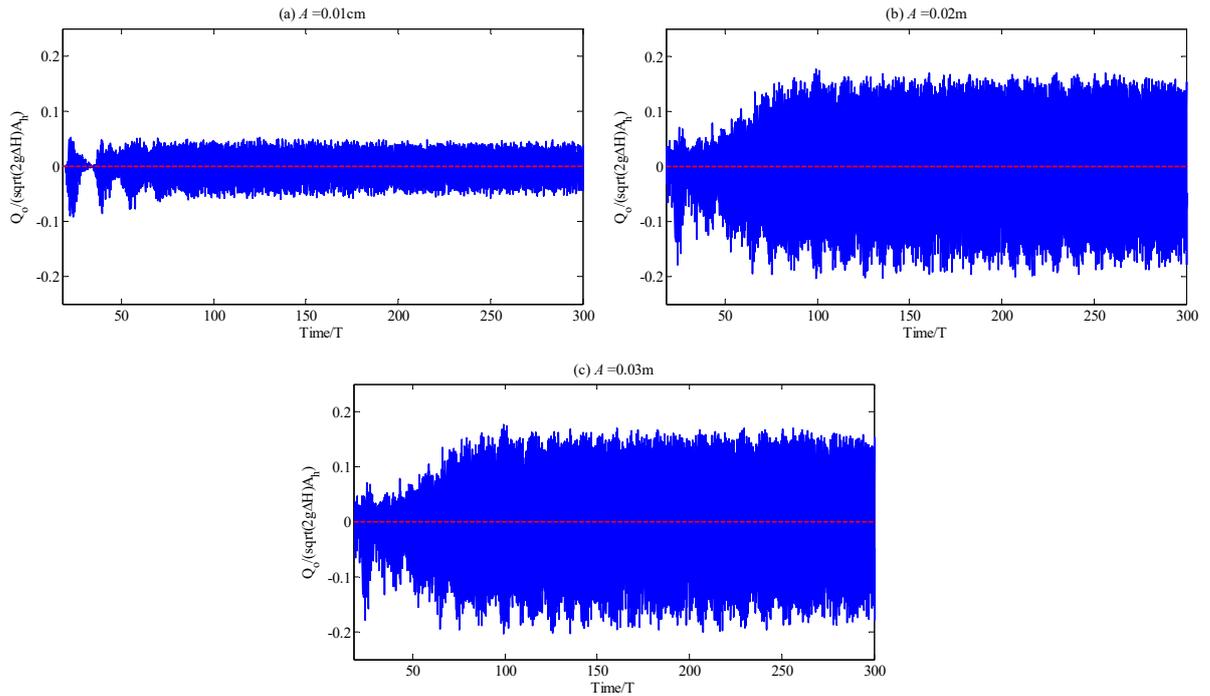
Figure 8.17 Time histories of the discharge of water outflow (Q_w) in the 2nd phase of spilling. (forced sway with ω_1=5.5 rad/s; red dashed line: Q_o in the fixed tank case)
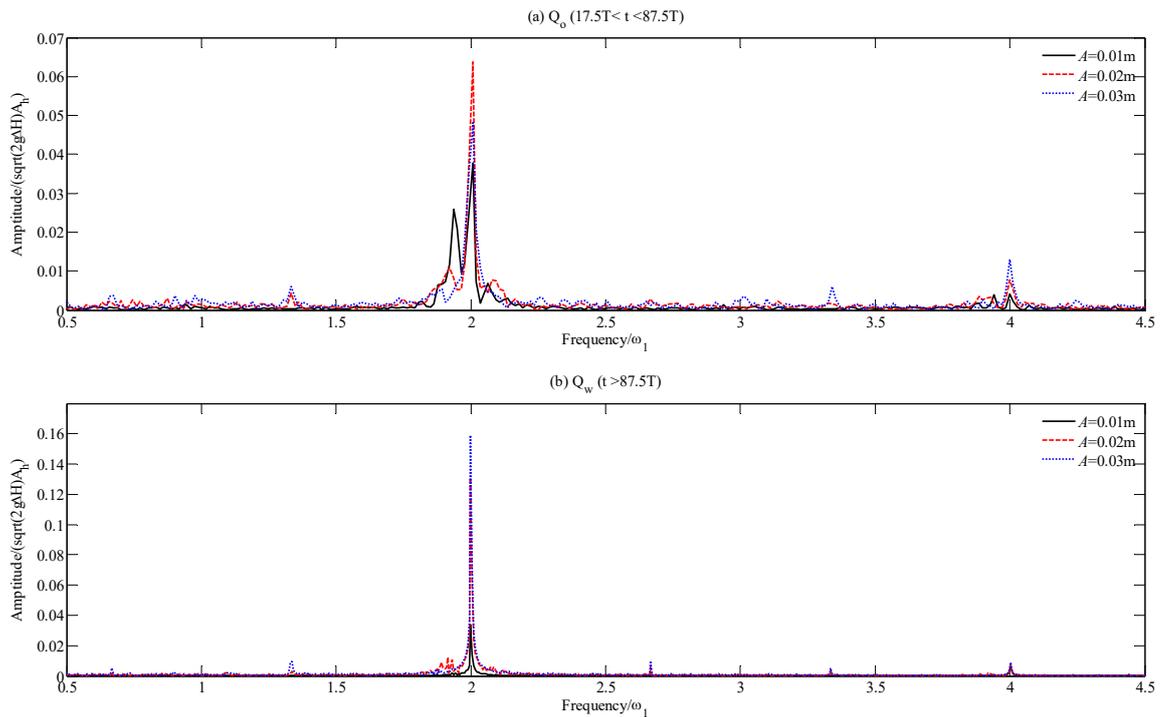
Figure 8.18 Spectrum distribution of (a) the oil discharge (Q_o) and (b) water discharge (Q_w) in the 2nd phase of spilling. (forced sway with ω_1=5.5 rad/s)

Apart from the motion amplitude, the motion frequency of the tank plays an important role in the volume of the oil spilled into the water basin as demonstrated in Figure 8.19, although the trends

153

of which are similar. More oil spilled into the water basin in the case with ω_2=5.35rad/s than that with ω_1=5.5rad/s.
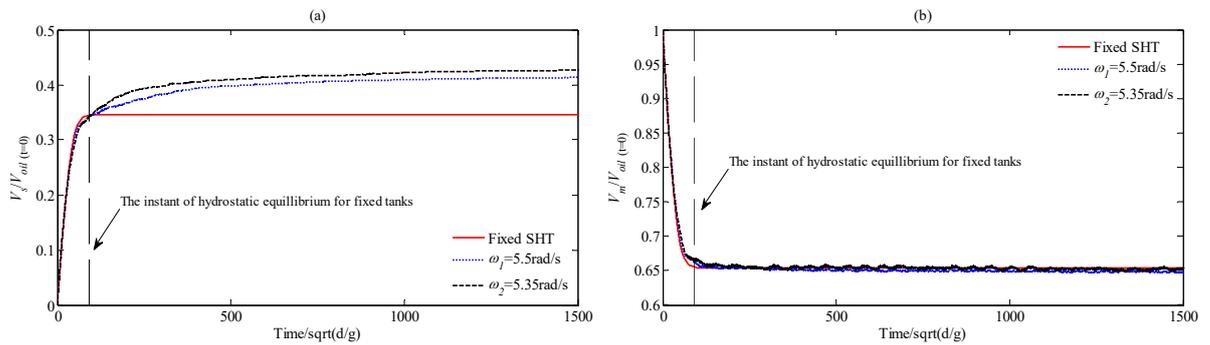
Figure 8.19 Time histories of volumes of (a) the oil spilled into the water basin (V_s) and (b) oil/water mixture in the cargo tank (V_m) in the cases with different motion frequencies. (forced sway with A =0.02m)

The case with rolling motions is similar to the one with sway motions, where the spilling is associated with violent liquid sloshing inside the tank; more oil spills out over a longer duration after the instant of the hydrostatic equilibrium of the fixed tank; water is entrapped by the tank due to the convective oil/water flow through the hole; The discharges of oil spilling into the water basin and the water flowing into the tank show oscillations relative to the motion frequency and the natural frequency of the tank. Figure 8.20 duplicates the spectrum distribution of the oil spilling into the water basin in the first and second phases of the spilling in the cases with heaving and rolling tank respectively. It is clearly indicated that the dominant harmonic for the rolling case falls in the frequency approximately to $2\omega_1$, similar to the sway motion. The different amplitude of motions also affects the most significant frequency of the nonlinear interaction as shown in Figure 8.20(c) and (d). However, due to no obvious liquid sloshing initiated by the heave motion as evidenced by Figure 8.6, the spectrum distribution of Q_o for the heaving cases are quite different. From Figure 8.20(a) and (b), it is indicated that the dominant harmonics locate at a frequency close to ω_1 over the whole spilling process under heave motions, and the 2nd order harmonic with frequency of $2\omega_1$ is observed with the magnitude at around 20% of the one at ω_1 in the second phase (Figure 8.20(b)).

154
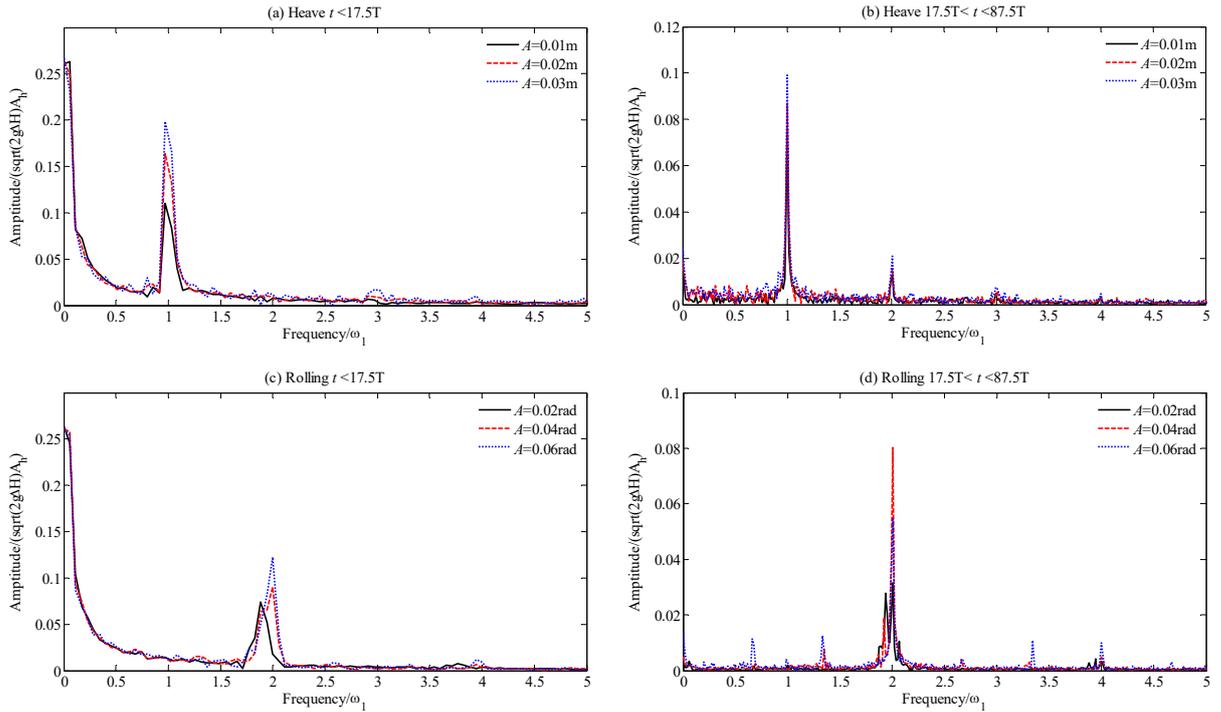
Figure 8.20 Spectrum distribution of the oil discharge (Q_o) in the first (a, c) and 2nd (b, d) phases of the spilling under heaving and rolling motions (ω_1=5.5 rad/s).

One of the most significant concerns regarding to the spilling issue is how the different motion modes i.e., heave, sway and rolling with different amplitude and frequencies affect the ultimate state. Figure 8.21 summarises the ultimate volume of spilled oil when the oil spilling stops based on the systematic investigations for the grounded cases. It is noticed that the ultimate volume of the oil/water mixture in the cargo tank is independent of the motion of the tank. With the increase of the motion amplitude the oil spilling into the water basin and the water entrapped by the tank enhance. The motion frequency posts more significant effect on the ultimate V_s and V_f in the sway and roll motion cases than the heave motion cases.
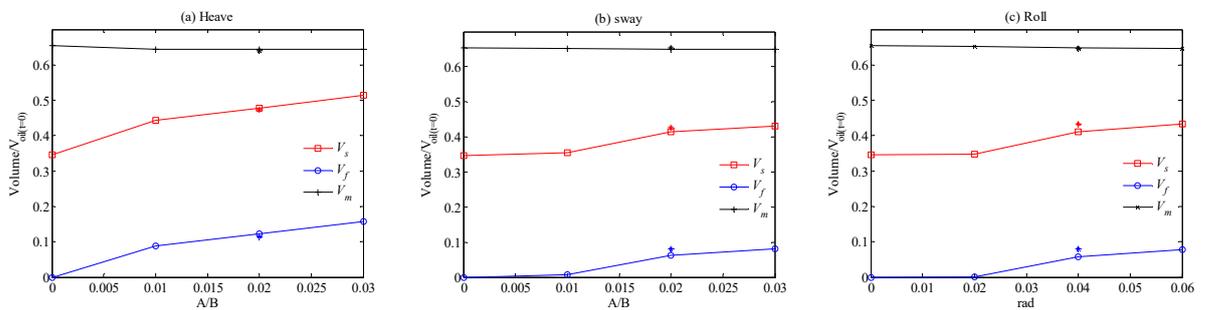
Figure 8.21 Ultimate volumes of the oil spilling into the water basin (V_s), the water entrapped by the tank (V_f) and the oil/water mixture in the cargo tank (V_m) in the grounding cases listed in Table 8.1 (the asterisk represents the corresponding result of the motion with ω_2=5.35 rad/s, the others are from ω_1=5.5 rad/s).

Collision scenarios

Comparing with the grounding case, the dynamic process of the oil spilling from the fixed SHT in collision scenario is more complicated due to the involvement of the water/oil convective flow through the hole in the late stage of the spilling due to the local density imbalance across the hole. The oil spilling from a collided fixed tank usually lasts much long duration and is divided into two phases, i.e., the gravity-dominant spilling phase and two-way flow spilling phase (Tavakoli *et al*., 2011; Tavakoli *et al*., 2012; Sergejeva *et al*., 2013). This is consistent with the way we adopted in the previous section for grounding cases subjected to tank motions.
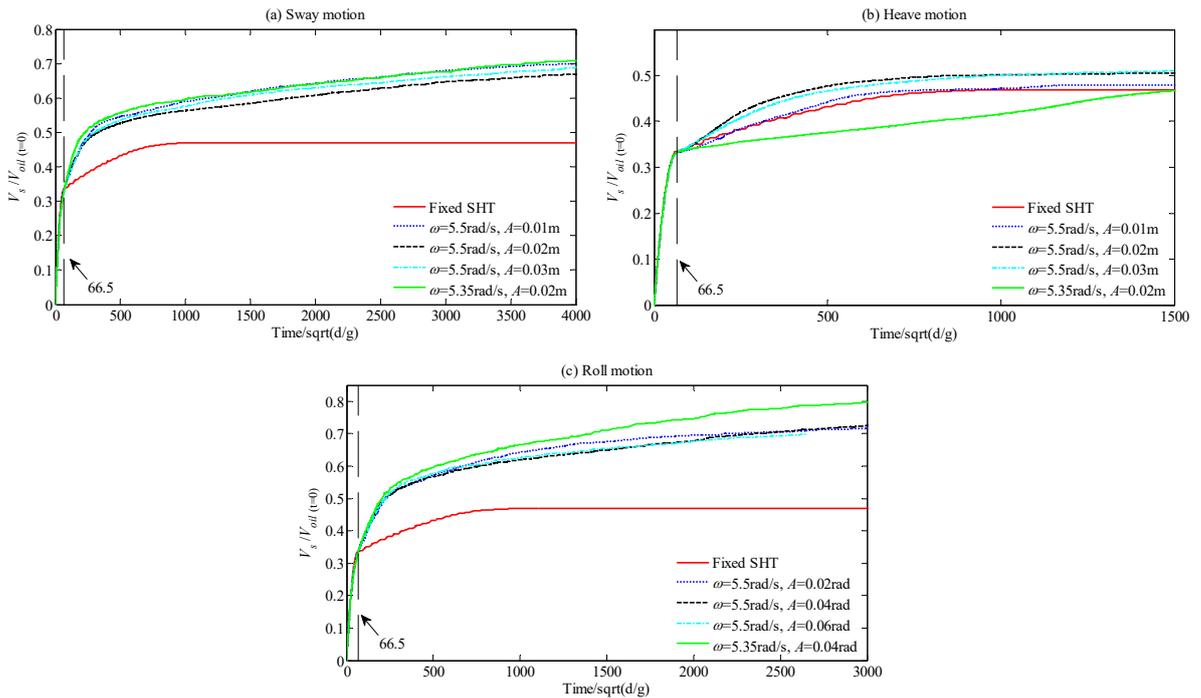
Figure 8.22 Time histories of volumes of the oil spilled into the water basin (V_s) in the cases with different motions in collision scenarios.

The time histories of the volume of the oil spilled into the water basin (V_s) in the cases with different motions listed in Table 8.1 are plotted in Figure 8.22. With the purpose of comparison, the corresponding curve for the fixed SHT tank case is also included. According to the hydrostatic analysis based on Bernoulli's equation, the gravity-dominant phase stops at approximately $t=66.5\sqrt{d/g}$ for the fixed SHT, which is used to divide the spilling process. Similar to the grounding cases, the motion of the tank plays the less important role in the volume of the spilled oil in the first phase of the spilling. However, this effect is enhanced during the following spilling phase, which in some cases (shown in Figure 8.22(a) and (c)) results in much larger amount of spilled oil reaching the level of almost twice of that in the fixed SHT case. The whole process is prolonged much, particularly for the sway and rolling cases. It is also important to remark that the oil spilling from the tank subjected to sway and roll motions may not be able to reach a steady

state as seen in the grounding cases, even in a much longer duration (nearly 3 times of the duration of corresponding grounding cases). This is mainly due to the significant sloshing of the oil/water interface and the convective flow of oil/water mixture in the swaying and rolling tank as demonstrated in Figure 8.23 leading to that the oil block may reach the side hole and spill out of the tank. It can be supposed that under sway or roll motions with large amplitude almost all the oil contained in the cargo tank shall release out after a long spilling period. On the other hand, in the case with heaving motions, no significant liquid sloshing is observed in the tank (similar to Figure 8.6) and the spilling hole will be eventually covered by the water layer.

(a) Case C6: $t \approx 1518.4\sqrt{d/g}$ (b) Case C10: $t \approx 1509.5\sqrt{d/g}$
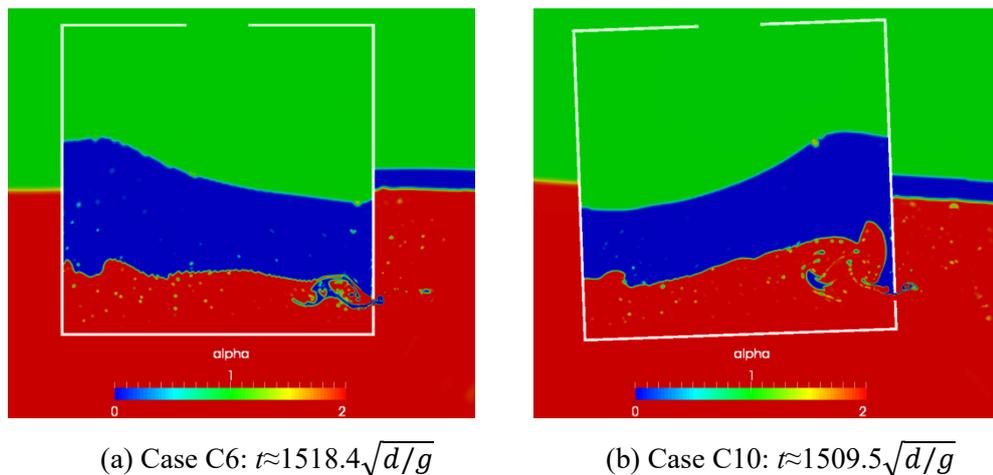
Figure 8.23 Snapshots of the spatial distributions of oil, water and air (volume of fraction α) in collision cases (water: red ($\alpha=2$); air: green ($\alpha=1$); oil: blue ($\alpha=0$)).

Similar to the grounding scenario, both the sloshing of the mixture in the cargo tank and the convective fluid motion relative to the broken hole significantly affect the oil spilling process. The nonlinear interaction of these two factors may be revealed from the spectrum distribution shown in Figure 8.24. It is clearly indicated that the typical difference in the spectrum of the discharges (Q_o) between the collision and grounding scenarios is that the harmonics corresponding to ω_1 are significant for all motion modes, although these with higher frequencies (e.g., $2\omega_1$, $3\omega_1$ and $4\omega_1$) are also at relatively high levels in the cases with sway and roll motions. This may be attributed to the fact that the local sloshing near the side of the broken hole plays a more significant role in the discharge than these on the other side, which yields the harmonics corresponding to ω_1 as evidenced by the spectrum distribution of the pressure on the left side wall (Figure 8.10). Moreover, the interaction between the free surface and oil/water interface sloshing is supposed to create higher order harmonics.
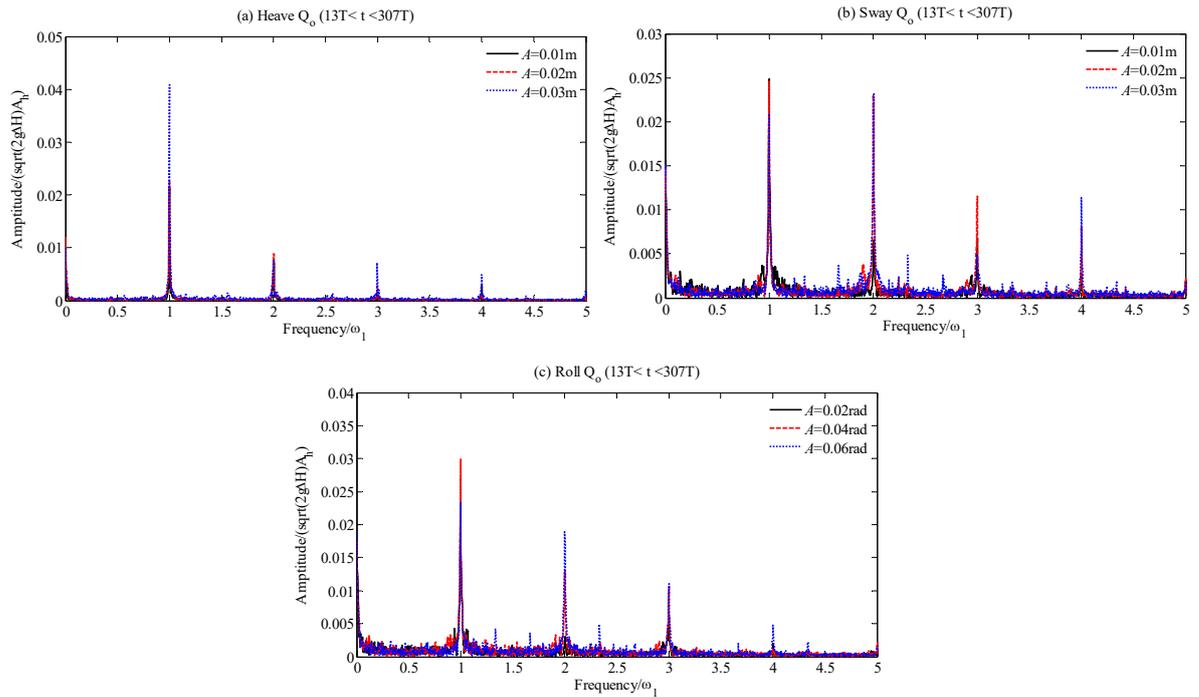
Figure 8.24 Spectrum distribution of the oil discharge (Q_o) in the second 2nd phases of the spilling under different tank motions (ω_1=5.5 rad/s).

8.4 Oil Spilling from Grounded DHTs under Tank Motions

The oil spilling from a grounded DHT subjected to tank motions is investigated in this section. According to the previous discussion, the incompressible LES model is supposed to be satisfactory for the current case by considering two aspects: firstly, it is confirmed that the LES incompressible model yields perfect performance on simulating the spilling from a fixed DHT; secondly, the LES model can also deliver accurate results for the intact tank sloshing case as demonstrated in Figures 8.1 and 8.2.

In order to take the sloshing inside the ballast tank into account, a U-shape ballast tank is employed. The model details are sketched in Figure 8.25. The internal tank of DHT is same as the SHT as sketched in Figure 8.3, but surrounding a U-shape ballast tank. The thickness of the ballast tank is 10cm based on the study of Tavakoli *et al*. (2011). The holes drilled on the internal and external hulls are coaxial with 0.022m length. According to the ship design patent (Thomas, 2005), it is mentioned that a need exists for a rebuilt tanker having a double hull with substantially the same cargo carrying capability at substantially the same or a reduced draft. Thus, the comparative water draft (*d*) for DHT cases is set as 0.47m. All the other variables are similar to the SHT case.
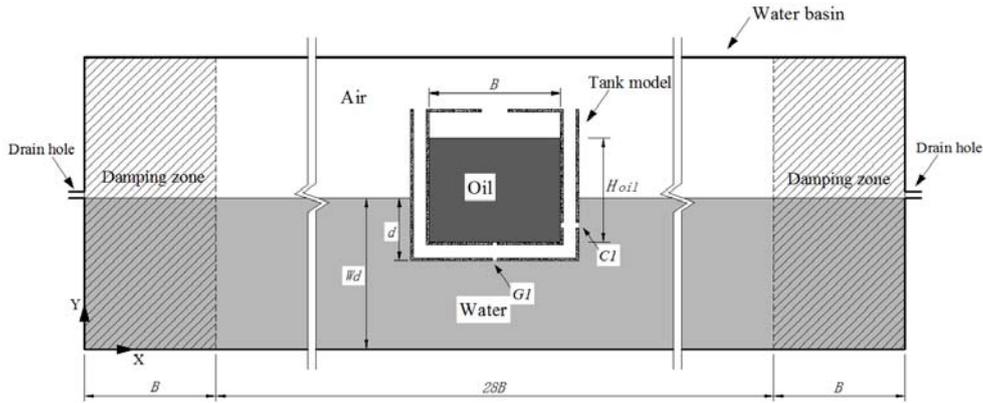
Figure 8.25 Sketch of the numerical configuration of DHT cases.

The convergence test which is similar to the previous one is carried out in prior. In this section, the tank under sway motions is considered. Different from the SHT case, the sloshing in the U-shape ballast tank of DHTs has to be considered and, thus the ballast tank is modelled as a U-tube model, of which the first mode natural frequency of sloshing can be calculated as $1/\sqrt{L_a/2g}$, L_a is the average length between the two free surfaces of the U-tube in the flow oscillation direction (Faltinsen and Timokha, 2009). In order to cover all the possible resonance for sloshing inside the internal tank or the ballast tank, a wider range of motion frequencies from 3.1 rad/s (the first-mode natural frequency of the ballast tank sloshing with the liquid depth under the final hydrostatic equilibrium) to 5.5 rad/s (the first-mode natural frequency of the internal tank sloshing with the initial oil height $H_{oil(t=0)}$) is assigned, among which the first-mode natural frequency of the internal tank sloshing with the liquid depth under the final hydrostatic equilibrium locates around 5.2 rad/s (Faltinsen, 1978). The motion amplitude is fixed at 0.02m in all the cases. Table 8.2 summarises the DHT cases employed in this investigation, where 'D' in the Case No represents the DHT design.

Table 8.2 The case list of DHT spilling problems.

Case No	Motion types	Frequency (ω, rad/s)	Amplitude (A)
D0	None	-	-
D1	Sway	5.5	2 cm
D2	Sway	5.2	2 cm
D3	Sway	4.5	2 cm
D4	Sway	3.8	2 cm
D5	Sway	3.1	2 cm

Figure 8.26 compares CaseD0 and CaseD1 in terms of some snapshots of the spatial distributions of oil, water and air (volume of fraction α) at some typical instants. At the very beginning, the oil spills from the internal hole, travels down through the ballast tank and then spills out from the external hole along with part of oil captured by the ballast tank as shown in Figure 8.26(a). Similar to the SHT case, the sway motion could excite violent liquid sloshing inside the internal tank, but

159

it does not affect the spilling volumetric profile during the early stage ($t/\sqrt{d/g}$<6.8) as shown in Figure 8.27, where the time histories of volumes of the oil spilled into the water basin (V_s), the water flowing into the DHT (V_f) and the oil volume in the internal tank (V_{oil}) are plotted. As shown in Figure 8.26(c) and (d), the sway motion in CaseD1 obviously enhances the fluid motion inside the ballast tank which disturbs the oil jet pattern inside the ballast tank. As a result, the oil spilling out of the water basin suspends earlier (Figure 8.27(a)) while more water flows into the ballast tank, by which V_f in CaseD1 peaks at the value more than twice as much as the one in CaseD0 (Figure 8.27(b)). After $t/\sqrt{d/g}$≈18, the oil releasing through the external hole resumes (Figure 8.26(e) and (f)). From Figure 8.27(b), it is clearly indicated that V_f drops gradually, especially in CaseD1, as some water mixed in the oil outflow escapes from the DHT.

Since the ballast tank has small free surface area and the motion frequency is far from the natural frequency of the U-shape ballast tank with the liquid depth under the hydrostatic equilibrium, the free surface keeps flat and there is no significant vertical oscillation inside the ballast tank. Different from the SHT case, the sway motion doesn't prolong the spilling duration in CaseD1 (Figure 8.27(a)). This is attributed to the fact that the water inside the ballast tank accumulates above the bottom of the ballast tank forming a layer (as shown in Figure 8.26(h)) which seals the external hole preventing the oil spilling out further. Finally, the sway motion causes approximately 11% more oil volume spilled out of the DHT (Figure 8.27(a)), but the residual oil volumes inside the internal tank between the CaseD0 and CaseD1 are similar (Figure 8.27(c)).

(a) CaseD0 ($t/\sqrt{d/g}$≈3.2)   (b) CaseD1 ($t/\sqrt{d/g}$≈3.2)
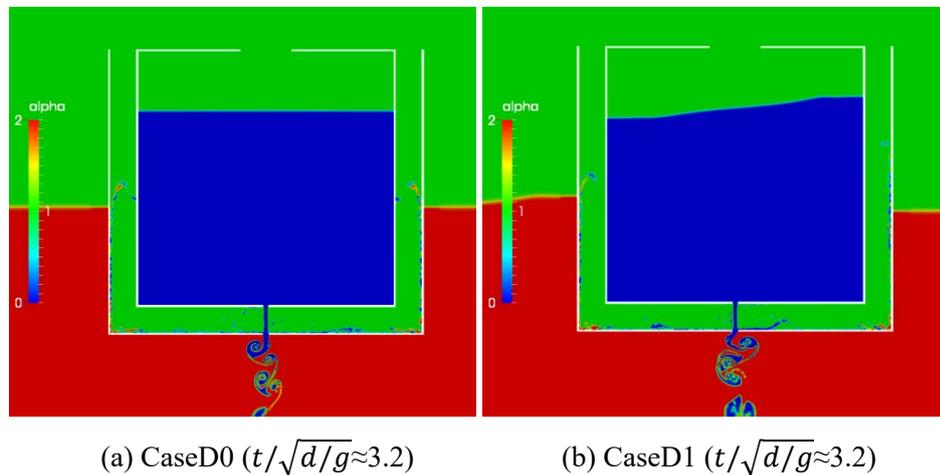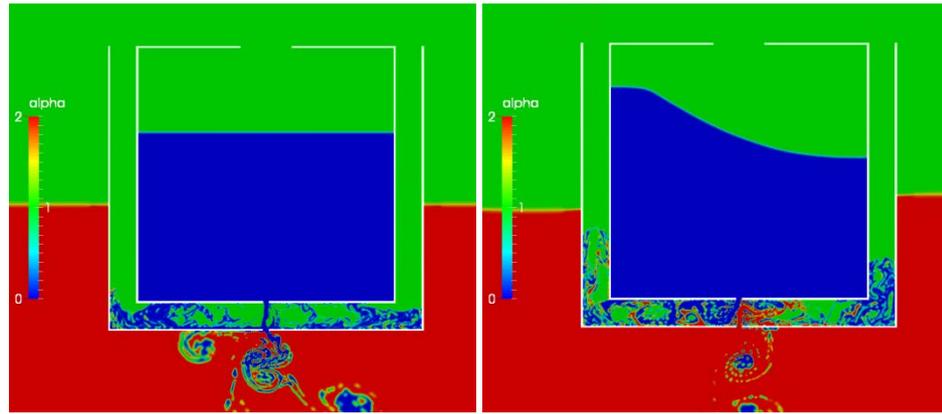
(c) CaseD0 ($t/\sqrt{d/g}\approx10.8$) (d) CaseD1 ($t/\sqrt{d/g}\approx10.8$)
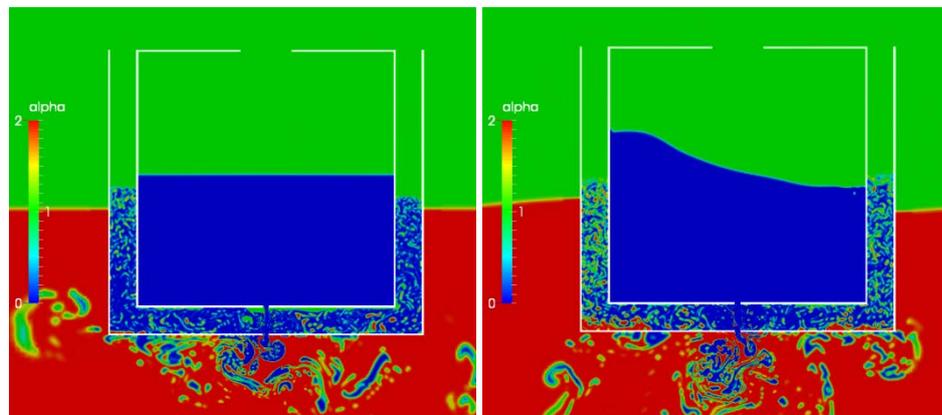
(e) CaseD0 ($t/\sqrt{d/g}\approx28.3$) (f) CaseD1 ($t/\sqrt{d/g}\approx28.3$)
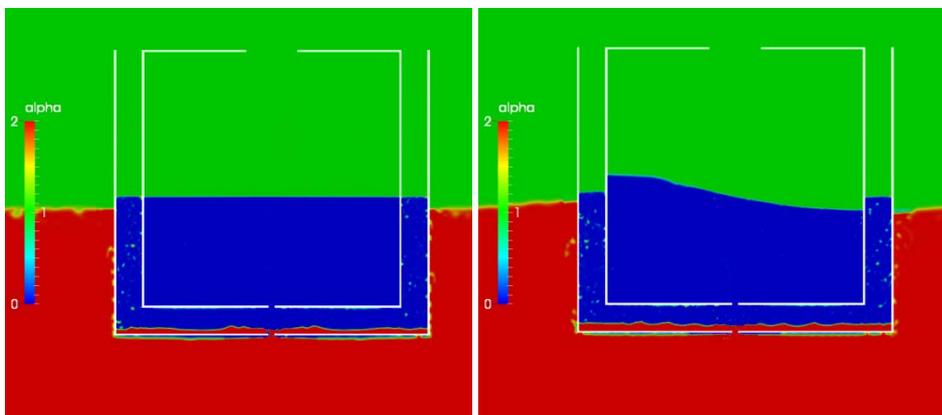
(g) CaseD0 ($t/\sqrt{d/g}\approx205.6$) (h) CaseD1 ($t/\sqrt{d/g}\approx205.6$)

Figure 8.26 The comparison between CaseD0 and CaseD1 in terms of some snapshots of the spatial distributions of oil, water and air (volume of fraction α) at different instants.
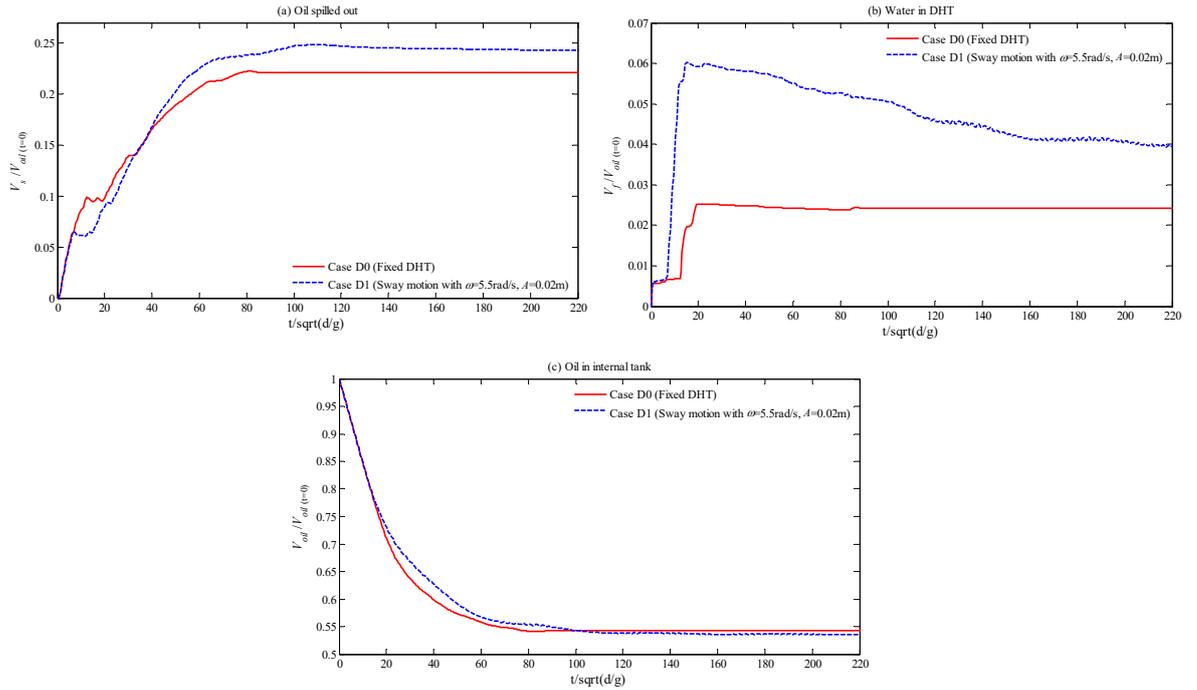
Figure 8.27 Time histories of volumes of (a) the oil spilled into the water basin (V_s), (b) the water flowing into the DHT (V_f) and (c) the oil in the internal tank (V_{oil}) in the Case D0 and D1.

8.4.1 Effect of motion frequencies on spilling from grounded DHTs

As for the DHT cases, it is more interesting to investigate the oil spilling under different motion frequencies, since there are different sloshing phenomena to be considered, namely, the sloshing in the internal tank and the sloshing in the ballast tank. Although the nature frequencies of these sloshing vary with time during the spilling process as demonstrated in Figure 8.4, only the nature frequencies of the simplified sloshing in the internal tank under the initial condition and the final hydrostatic equilibrium and the simplified sloshing in the U-shape ballast tank under the final hydrostatic equilibrium are chosen to define the motion frequency range. Totally, five cases with different motion frequencies ranging from 3.1rad/s to 5.5rad/s are carried out.

The time histories of elevation at the two different locations are presented in Figure 8.28. x_{ref} =0.56B represents the mixture surface elevation at the middle point of the width of the right side ballast tank and x_{ref} =0.375B represents the oil surface elevation inside the internal tank. Similar to the SHT case, the spilling also changes the average elevation, particularly when $t/\sqrt{d/g}$<50. After that, it is clearly indicated from Figure 8.28(a) that the mixture surface elevation oscillates significantly around a certain level in Case D5, since the motion frequency is closest to the nature frequency of the U-shape sloshing with the liquid depth under the final hydrostatic equilibrium. However, regarding the sloshing inside the internal tank, the resonance takes place in Case D2 and the oscillation becomes weaker as the frequency of the tank motion is farther away from the nature frequency of the sloshing with the liquid depth under the final hydrostatic equilibrium.
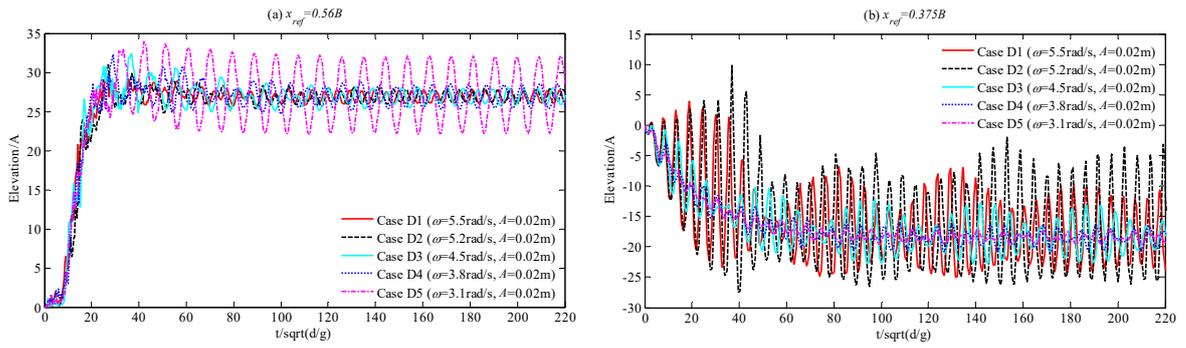
Figure 8.28 Time histories of the surface elevations recorded at two different locations under sway motion. (x_{ref}: horizontal coordinate relative to the vertical central axis of the tank)
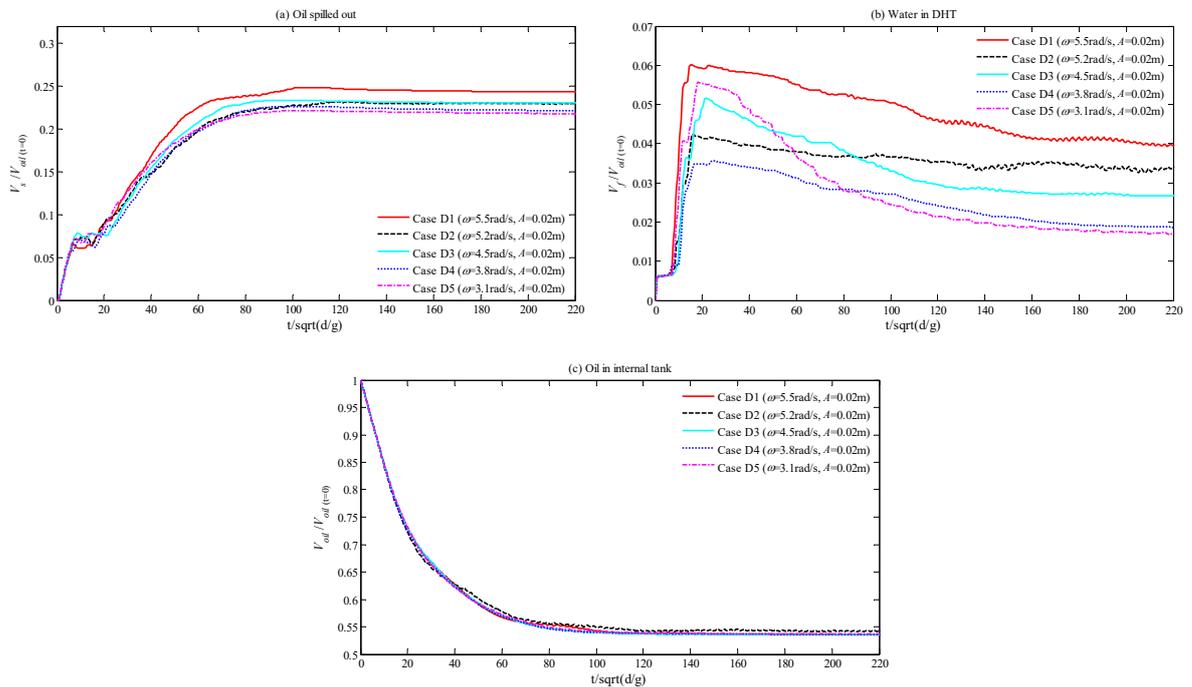
Figure 8.29 Time histories of volumes of (a) the oil spilled into the water basin (V_s), (b) the water flowing into the DHT (V_f) and (c) the oil in the internal tank (V_{oil}) in the cases with different tank motion frequencies.

Figure 8.29 compares these cases in terms of the oil spilled into the water basin (V_s), the water flowing into the DHT (V_f) and the oil in the internal tank (V_{oil}). Although different tank motion frequencies could lead to different sloshing behaviour inside the internal tank as shown in Figure 8.28(b), the V_{oil} profiles indicated in Figure 8.29(c) are similar among different cases. The V_s and V_f curves in Figure 8.29(a) and (b) differ from each other from $t/\sqrt{d/g} \approx 10$ and follows different trends. Different motion frequencies don't significantly affect the spilling duration. One may notice that with the increasing tank motion frequency, more oil shall spill out of the DHT ultimately (Figure 8.29(a)), meanwhile, more water pours into the DHT (Figure 8.29(b)) forming a thicker water layer above the ballast tank bottom at the end of the spilling process (shown in

163

Figure 8.30). Figure 8.30 also clearly indicates that the mixture level is up and down in the vertical columns of the ballast tank in Case D5 but with little sloshing inside the internal tank. Conversely, violent sloshing is excited in the internal tank but the mixture levels in the two ballast side tanks keep at the same level in Case D1 (Figure 8.30(a)).
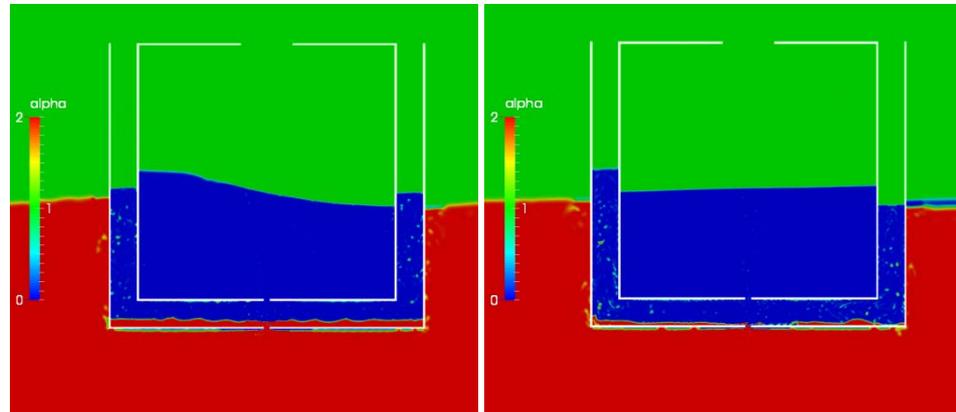
(a) CaseD1 ($t/\sqrt{d/g}{\approx}205.6$)　　　(b) CaseD5 ($t/\sqrt{d/g}{\approx}205.6$)

Figure 8.30 The comparison between CaseD1 and CaseD5 in terms of some snapshots of the spatial distributions of oil, water and air (volume of fraction α) at one instant.

8.5 Summary

The two-dimensional numerical investigation on the oil spilling from a damaged tank subjected to periodic motions is carried out. A customized solver coupling the multiphase VOF method and the dynamic mesh technology is developed. Two groups of lab tests including one-layer and two-layer sloshing in an intact tank are employed in the model validation. Also, the compressibility effect and turbulence model performance during the sloshing are examined. A satisfactory agreement has been observed.

A systematic case study is designed covering different types of motions, motion frequencies, motion amplitude, tank configurations and accidental scenarios. The analysis is divided in to two sections:

The first section is the oil spilling from SHTs under tank motions. In this section, the spilling effect on the liquid sloshing in the cargo tank is first considered. Some typical features on the wave elevation and the impulse pressure on the side wall are concluded. More importantly, considering the time-dependent natural frequency of the cargo liquid due to the spilling process, the continuous wavelet transform is used instead of the conventional FFT in the frequency analysis of pressure signals, by which different unsteady nonlinear effect on the frequency domain between the damage and intact cases is captured. The sloshing effect on the spilling process is then investigated for the SHT cases. It is found that the tank motion does not only cause a periodic

oscillation of the oil/water flow through the broken hole, but also results in a second long-duration stage of spilling after a quasi-hydrostatic-equilibrium condition occurs leading to more significant amount of spilled oil. The effect of motion frequency and amplitude on the ultimate spilling volume is dependent on the motion mode. Moreover, the FFT frequency analysis indicates that the second order harmonics of the discharges of the oil outflow for sway or roll motion dominates the spectra in grounding cases. Higher order harmonics up to 5th order are found in collision cases.

The second section is for the oil spilling from grounded DHTs subjected to the sway motion. The model is built following the similar model configuration of SHT cases. Different from the SHT case, the sloshing in the U-shape ballast tank of DHT shall be considered and, thus the case study is designed with a wider range of motion frequencies covering all the possible resonance for sloshing inside the internal tank or the ballast tank. The result indicates sloshing resonances in different tanks also follow the theory of the first mode natural frequency of sloshing for the individual tank. Moreover, regardless of the resonance phenomena, the increasing tank motion frequency results in more oil spilling out of the DHT ultimately, but does not affect the spilling duration.

Chapter 9 Conclusions and Recommendations

9.1 Experimental Works on Oil Spilling from Damaged Tanks

In this study, two new sets of laboratory tests are carried out to examine the effect of important accidental factors on the dynamic spilling procedures from a grounded or collided DHT. The different axial offsets of the bottom openings under groundings and the initial water thicknesses inside the ballast tank under collisions are considered to widen the damage conditions and approach the real spilling accident. The damaged tank is fixed in still water. The similarity principle considers both the Froude number and Reynolds number scale laws.

In each case, the whole spilling process was observed and measured in terms of the mean level of the oil surface in the cargo tank and that of the oil/water mixture in the ballast tank. Considering the different spilling characteristics, the oil spilling process is divided into several stages and the related dynamic features are discussed. The experimental observation records the complex multiphase flow inside the ballast tank of DHTs, which indicates that in some cases the oil could spill out of DHTs from the beginning of the spilling process due to the higher velocity and momentum carried by the oil flow under either collision or grounding scenarios. This phenomenon clarifies the inappropriate assumptions used in the previous analytical models, i.e., no oil spilling out of the DHT during the early spilling period. The experimental data is also used to validate the numerical model developed in this study.

The parametric study reveals that the accidental factors considered in this study could significantly affect the dynamic spilling process yielding different spilling durations and flow states, although all the cases from the perspective of the hydrostatic status are the same either at initial or at final equilibrium. It also emphasizes the importance of dynamic characteristics when estimating the effectiveness of DHT design on reducing the oil spilling into the sea.

9.2 Numerical Works on Oil Spilling from Damaged Tanks

In order to fill the gap of turbulence modelling and dimensional limitation of previous numerical works, a comprehensive three-dimensional numerical study on the oil spilling from fixed damaged tanks is carried out using the open source software OpenFOAM. The VOF is applied to deal with the air-oil-water multiphase flow. Different tank configurations (SHTs and DHTs) and accidental scenarios (grounding and collision) are considered. According to the turbulence

modelling tests, both the DNS and RANS standard k-ε models can yield accurate results comparing with the published experimental data for the SHT case, which further completes the model validation on this topic.

The spilling process of DHTs is different to that of SHTs due to the unique features of the turbulence, particularly in the ballast tank of DHTs where both violent jet flows and free shear layer appear. Considering the fact that there is a lack of related discussion regarding the turbulence modelling of DHT spilling problems in literature, in this study, the first attempt is from the common-used RANS standard k-ε model. Using the measured data from the current DHT physical tests, the comparison indicates that the applicability of the standard k-ε model is case-dependent and the significant gaps between the numerical result and experimental data are observed in some cases. In order to find a proper turbulence model, different common-used turbulence models, including k-ε, k-ω, LES and DNS models, are employed and their performance is examined in different cases. Overall, the LES model constantly leads to the most accurate results, which agree well with the experimental data in all the cases included in this study.

The different turbulence behaviours and their effects on the DHT spilling process obtained by different models are also discussed. The result indicates that the LES can deliver the most accurate result because it can properly capture the turbulence distribution associated with the flow through the rupture behaving similarly to jet flows through an orifice and the transition turbulence attached around the oil/water/air interface inside the ballast tank triggered by the free-shear layers as the oil jet travels through the ballast space with mixing and separation. However, the higher mesh resolution required by the LES model leads to higher computational consumptions. Due to the fact that different accidental conditions cause different dynamic spilling processes associated with different fluid motions inside the ballast tank, the applicability of other turbulence models is case-dependent.

To achieve the precise selection of turbulence models for DHTs, a new criterion is proposed by taking both the model accuracy and the computational robustness into account. An effective Reynolds number corresponding to both the oil outflow and the water inflow is introduced to classify the significance of turbulence in each case, by which all the cases are organized and the performance of different models is evaluated again. The criterion concludes that at the low effective Reynolds number (<17000), LES modelling should be adopted as the RANS models do not yield sufficiently accurate results. When the effective Reynolds number is large enough (>40000), RANS models can be used as they can give similar results to LES but cost much less CPU time. As for the middle range, it is inferred that the LES model is suggested if the high accuracy is required.

Investigating the compressibility effect on the dynamic spilling process seems to be regarded as an important aspect considering the sudden fluid-fluid or fluid-structure impacts associated with the jets of oil outflow and water inflow and the interaction between entrapped air bubbles in the oil/water mixture and fluid states (such as velocity, vorticity and turbulent kinetic energy) in the ballast tank of DHTs. A self-developed three-phase compressible solver is presented combining the compressible medium package and the VOF method. After the model validation, the compressible solver is applied to simulate the different DHT cases. The comparison between the compressible and incompressible results is presented in short and long term simulations. It concludes that the compressibility of the fluids may play an important role in a short duration of the impact yielding different jet-jet impact forces and jet-structure pressure fluctuations, but does not significantly influence the macroscopic process of the oil spilling in terms of discharge and height. It also suggests that in the view of predicting the dynamic spilling process from damaged tankers, the corresponding spilling duration and discharge are more important and, thus applying the incompressible solver is acceptable.

In order to extend the simulation from static case to a more realistic situation, the oil spilling from a damaged tank subjected to motions has been investigated. A customized solver coupling the multiphase VOF method and the dynamic mesh technology is developed and the numerical results are validated against the existing sloshing lab tests. To simplify the problem, the two-dimensional tank model under pre-specified periodic motions (covering heaving, sway and rolling) with various frequencies and amplitude is considered in this study. The tank motion effect on the oil spilling is analysed for both SHTs and DHTs.

In the SHT section, the corresponding spilling effect on the sloshing behaviour inside the cargo tank is also studied conversely. In order to capture the time-dependent natural frequency of the cargo liquid due to the spilling process, the continuous wavelet transform is employed instead of the conventional FFT and the temporal nonlinear effect on the frequency domain during the early spilling stage is found. The sloshing effect on the SHT spilling process is then investigated. The result indicates that it leads to a second long-duration stage of spilling after the quasi-hydrostatic-equilibrium condition resulting in the more significant amount of spilled oil. The FFT frequency analysis highlights the second order harmonic of the discharge of the oil outflow in the grounding cases under sway or roll motions and higher order harmonics in the collision cases.

As for the DHT cases, the grounded tank subjected to the sway motion with a range of frequencies covering all the possible resonances during the spilling process (e.g., sloshing inside the internal tank or the ballast tank) is considered. It is found that the first-mode natural frequency theory for the individual tank (i.e., rectangular or U-tube tanks) is also valid for the resonances in DHT cases.

Moreover, the ultimate spilling volume becomes more significant with increasing exciting frequencies.

9.3 Improved Analytical Model Development

Considering the inappropriate assumptions used in the previous analytical models, it is necessary to develop a new analytical model based on the experimental data and numerical results produced in this research. Using the experimental measurement, the correlation analysis is conduced to the flow through the internal hole. The satisfactory linear relationship suggests that the oil outflow through the internal hole can be characterized as the free orifice flow or the submerged orifice flow depending on the mixture height inside the ballast tank. In each orifice flow, a quasi-steady empirical model with a constant custom discharge coefficient is proposed to predict the oil discharge. Based on the comparison, the empirical solution accurately coincides with the measured data in all the studied cases. However, in some cases, the complex oil-water interaction around the external hole leads to the oil-water mixture inside the ballast tank and remains the proportion of the oil unknown. Therefore, it is difficult to further develop the current empirical model to predict the oil discharge through the external hole or estimating the final state condition. Further analysis needs the assistance of numerical modelling from which more detailed data can be obtained.

With the assistance of the numerical results, the correlation analysis has been extended to the discharge through the external hole in the DHT cases. Comparing with the discharge through the internal hole, the discharge through the external hole behaves much stronger nonlinear effect and its significance is affected by different accidental conditions. The capability of the previous analytical solutions is examined using the numerical result. It is found that the assumption that no oil spills out of the DHT at the early stage used in the previous prediction models is inappropriate, since it does not reflect the different hydrodynamic interactions between the oil and water jet flows inside the ballast tank at the early spilling stage in some cases indicated by experimental and numerical observations.

In order to deal with this issue, an improved analytical model is proposed. Two conditions with respect to the momentum balance and rupture situation are considered initially to identify whether the oil spills out of the DHT at the early stage of the spilling process. For the grounding cases, the ratio of the vertical overlapping area to the hole area is introduced to estimate the oil outflow through the external hole. An approach to assigning the proportion of the hole area occupied by oil and water flows is also adopted to simplify the convective oil-water flow through the external hole under the collision condition. The comparison between the numerical and analytical solutions indicates that the improved model is capable of handling the different spilling trends affected by

the case-dependent interaction between oil and water flows inside the ballast tank yielding more accurate predictions than the previous model.

9.4 Recommendations for Future Works

Although the current study advances the understanding of the oil spilling process from a damaged tank, further experimental and numerical investigations are recommended in the following aspects:

- Based on the experimental data and its corresponding numerical test against different turbulence models, current work proposed the criterion of selecting a proper turbulence model according to the effective Reynolds number. In order to extend this criterion to the oil spilling in real fields, the scale effect of the experimental model mentioned by Karafiath and Bell (1992) needs to be considered. In the current experiments, apart from the Froude scaling law, the Reynolds scaling law is introduced to scale the viscous force (Simecek-Beatty *et al*., 2001). Thus, the test oil (canola oil) is selected by a matched viscosity. However, considering the fact that it is hard to find any liquid with a matched viscosity to replace water, the water is remained in use in the experiments (similar to the study of Tavakoli *et al.*, 2011). Therefore, considering the over underestimated Reynolds number corresponding to the water flow in the lab test, the ability of the numerical criterion validated by the current lab test data needs further calibration by the full-scale field data.

- In the numerical simulation, the VOF method is adopted to deal with the multiphase flow including air, oil and water. Considering the violent oil-water mixing inside the ballast tank during the spilling process in some cases, the oil contained in the mixture may be emulsified as observed in the experiments, which affects the physical property greatly (especially for the viscosity of mixture) as mentioned in McNaught (2011). However, due to the inherent limitation that the viscosity of the mixture varies linearly following the volumes of the fraction of the fluids, the VOF model may not reflect the nonlinear behaviour of the viscosity associated with the emulsified oil. Further model improvement is recommended.

- In order to investigate the effect of the ship motion on the oil spilling from the damaged tank, a customized solver coupling the multiphase VOF method and the dynamic mesh technology is developed. The new solver is first validated against the published experimental data of sloshing in an intact tank and subsequently applied to oil spilling cases in a moving tank. Considering the lack of the experimental investigation on the oil spilling from a damaged tank subjected to a periodic motion, the corresponding physical model is recommended as a future work for further model validation.

- This study improved the previous quasi-steady prediction model for DHT spilling problems by considering different spilling features of oil and water jet flows inside the ballast tank at the early spilling stage resulting from different rupture offsets and the convective oil-water flow through the external side hole. Based on the cases included in this study, the improved model has been demonstrated accurate predictions for different spilling procedures. In the future, with more experimental and numerical tests involving different initial loading conditions, rupture shapes, tank designs, external dynamic environment (e.g., wave, tide and current), etc., this prediction model can be further validated and extended to be applicable to more spilling scenarios.

References

Afshar, M.A., 2010. *Numerical wave generation in OpenFOAM*. MSc. Chalmers University of Technology.

Arun, N., Malavarayan, S. and Kaushik, M., 2010. CFD analysis on discharge coefficient during non-Newtonian flows through orifice meter. *International Journal of Engineering Science and Technology*, 2, pp.3151-3164.

Aydogan, B. and Kobayashi, N., 2014. Breaking of positive and negative solitary waves. In: *Proceedings of Conference on Coastal Engineering*, 1, pp.2156-1028.

Brocchini, M. and Peregrine, D.H., 2001. The dynamics of strong turbulence at free surfaces. Part 1. Description. *Journal of Fluid Mechanics*, 449, pp.225-254.

Brown, A., 2001. *Alternative tanker designs, collision analysis*. Washington: NRC Marine Board Committee on Evaluating Double-Hull Tanker Design Alternatives.

Burgherr, P., 2007. In-depth analysis of accidental oil spills from tankers in the context of global spill trends from all sources. *Journal of Hazardous Materials*, 140, pp.245-256.

Calderón-Sánchez, J., Duque, D. and Gómez-Goñi, J., 2015. Modelling the impact pressure of a free falling liquid block with OpenFOAM. *Ocean Engineering*, 103, pp.144-152.

Card, J.C., 1975. Effectiveness of double bottoms in preventing oil outflow from tanker bottom damage incidents. *Marine Technology*, 12, pp.60-64.

Cheng, L.Y., Gomes, D.V. and Nishimoto, K., 2010. A numerical study on oil leakage and damaged stability of oil carrier. In: *Proceedings of the ASME 2010 29th International Conference on Ocean, Offshore and Arctic Engineering*, pp.829-836.

Cho, H.H. and Goldstein, R.J., 1994. An improved low-Reynolds-number k-ε turbulence model for recirculating flows. *International Journal of Heat and Mass Transfer*, 37, pp.1495-1508.

Dabiri, S., Sirignano, W.A. and Joseph, D.D., 2007. Cavitation in an orifice flow. *Physics of Fluids,* 19, pp.072112.

Daidola, J.C., Reyling, C.J. and Ameer, P.G., 1997. Oil outflow estimates for tankers and barges. *Spill Science & Technology Bulletin*, 4, pp. 89-98.

Dean, J.A., 1999. *Lange's handbook of chemistry*. London: McGraw-Hill.

Deshpande, S.S., Anumolu, L. and Trujillo, M.F., 2012. Evaluating the performance of the two-phase flow solver interFoam. *Computational Science and Discovery*, 5, pp.1-36.

Devanney, J., Beach, S. and Florida, T., 2006. *The tankship tromedy – the impending disasters in tankers*. Tavernier: The CTX Press.

Devolder, B., Schmitt, P., Rauwoens, P., Elsaesser, B. and Troch, P., 2015. A review of the implicit motion solver algorithm in OpenFOAM to simulate a heaving buoy. In: *Proceedings of the 18th Numerical Towing Tank Symposium*, pp.1-6.

Dodge, F.T., Bowlles, E.B., White, R.E. and Flessner, M.F., 1980. Release rate of hazardous chemicals from damaged cargo vessels. In: *Proceedings of the 1980 National Conference on Control of Hazardous Material Spills*, pp.381-385.

Eggers, J. and Villermaux, E., 2008. Physics of liquid jets. *Report on Progress in Physics*, 71, pp.1-79.

Eide, M.S., Endresen, Ø., Breivik, Ø., Brude, O.W., Ellingsen, I.H., Røang, K., Hauge, J. and Brett, P.O., 2007. Prevention of oil spill from shipping by modelling of dynamic risk. *Marine Pollution Bulletin*, 54, pp.1619-1633.

El-Behery, S.M. and Hamed, M.H., 2011. A comparative study of turbulence models performance for separating flow in a planar asymmetric diffuser. *Computers & Fluids*, 44, pp.248-257.

Faltinsen, O.M.,1978. A numerical nonlinear method of sloshing in tanks with two-dimensional flow. *Journal of Ship Research*, 18, pp.224-241.

Faltinsen, O.M. and Timokha. A.N., 2009. *Sloshing*. New York: Cambridge University Press.

Fannelop, T.K., 1994. *Fluid mechanics for industrial safety and environmental protection*. London: Elsevier Science.

Fay, J.A., 2003. Model of spills and fires from LNG and oil tankers. *Journal of Hazardous Materials*, B96, pp.171-188.

Ferziger, J.H. and Perić., 2002. *Computational Methods for Fluid Dynamics*. 3rd ed. London: Springer.

Fingas, M., 2013. *The basics of oil spill cleanup*. 3rd ed. London: CRC Press.

Flingoh, C.H.O.H. and Chong, C.L., 1992. Surface tensions of palm oil, palm olein and palm stearin. *ELAEIS*, 4, pp. 27-31.

French, J.A., 1969. *Wave uplift pressure on horizontal platforms*. Report No. KH_R_19, W.M. Keck Laboratory of Hydraulics and Water Resources, California Institution of Technology, Pasadena, California.

Fthenakis, V.M. and Rohatgi, U.S., 1999. A model of liquid releases from a submerged vessel. *Journal of Loss Prevention in the Process Industries*, 12, pp.437-449.

Fulgosi, M., Lakehal, D., Banergee, S. and Angelis, V.D., 2003. Direct numerical simulation of turbulence in a sheared air-water flow with a deformable interface. *Journal of Fluid Mechanics*, 482, pp. 319-345.

Gaeta, M.G. and Lamberti, A., 2015. The role of air modelling on the numerical investigation of coastal dynamics and wave-structure interactions. *Computers and Fluids*, 11, pp.114-126.

Gao, F., Ma, Z.H., Zang, J., Causon, D.M., MingHam, C.G. and Qian, L., 2015. Simulation of breaking wave impact on a vertical wall with a compressible two-phase flow model. In: *Proceedings of the 25th International Offshore and Polar Engineering Conference*, Hawaii (USA).

Gao, Q.X. and Vassalos, D., 2012. Numerical study of damage ship hydrodynamics. *Ocean Engineering*, 55, pp.199-205.

Gao, Z.L., Gao, Q.X. and Vassalos, D., 2013. Numerical study of damaged ship flooding in beam seas, *Ocean Engineering*, 61, pp.77-87.

Gaspar, B., Teixeira, A.P. and Soares, C.G., 2016. Sensitivity analysis of the IACS-CSR buckling strength requirements for stiffened panels. In: Soares, C.G. and Santos T.A., eds. 2016. *Maritime Technology and Engineering III-Proceedings of the 3rd International Conference on Maritime Technology and Engineering*. London: Taylor & Francis Group. pp.459-470.

Gebreslassie, M.G., Tabor, G.R. and Belmont, M.R., 2013. Numerical simulation of a new type of cross flow tidal turbine using OpenFOAM – Part I: calibration of energy extraction. *Renewable Energy*, 50, pp.994-1004.

Hedlund, A., 2014. *Evaluation of RANS turbulence models for the simulation of channel flow.* MSc. Uppsala University.

Gilbert, T. and Nawadra, S., 2003. Response to an oil spill from a sunken WWII oil tanker in Yap state, Micronesia. In: *Proceedings of the 2003 International Oil Spill Conference.* Washington, D.C., pp. 1-8.

Glen, D., 2010. Modelling the impact of double hull technology on oil spill numbers, Maritime Policy & Management. *The Flagship Journal of International Shipping and Port Research*, 37, pp.475-487.

Goerlandt, F. and Montewka, J., 2014. A probabilistic model for accidental cargo oil outflow from product tankers in a ship-ship collision. *Marine Pollution Bulletin*, 79, pp.130-144.

Gourdain, N., 2015. Prediction of the unsteady turbulent flow in an axial compressor stage. Part 1: Comparison of unsteady RANS and LES with experiments. *Computers & Fluids*, 106, pp.119-129.

Higuera, P., Lara, J.L. and Losada, I.J., 2013. Realistic wave generation and active wave absorption for Navier-Stokes models Application to OpenFOAM. *Costal Engineering*, 71, pp.102-118.

Hollingshead, C.L., Johnson, M.C., Barfuss, S.L. and Spall, R.E., 2011. Discharge coefficient performance of Venturi, standard concentric orifice plate, V-cone and wedge flow meters at low Reynolds numbers. *Journal of Petroleum Science and Engineering,* 78, pp.559-566.

Homan, A.C. and Steiner, T., 2008. OPA 90's impact at reducing oil spills. *Marine Policy*, 32, pp.711-718.

Höhne, T. and Mehlhoop, J.P., 2014. Validation of closure models for interfacial drag and turbulence in numerical simulations of horizontal stratified gas-liquid flows. *International Journal of Multiphase Flow*, 62, pp.1-16.

Hu, C.H. and Kashiwagi, M., 2004. A CIP-based method for numerical simulations of violent free-surface flows. *Journal of Marine Science and Technology*, 9, pp.143-157.

Hunt, C.R., Eames, I. and Westerweel, J., 2006. Mechanics of inhomogeneous turbulence and interfacial layers. *Journal of Fluid Mechanics*, 554, pp.499-519.

Igci, A.A. and Arici, M.E., 2016. A comparative study of four low-Reynolds-number k-ε turbulence models for periodic fully developed duct flow and heat transfer. *Numerical Heat Transfer, Part B: Fundamentals*, 69, pp.234-248.

IMO, 1994a. *Interim guidelines for the approval of alternative methods of design and construction of oil tankers under Regulation 13F(5) of Annex I of MARPOL 73/78*. London: IMO.

IMO, 1994b. *Guidelines for approval of alternative structural or operational arrangements as called for in MARPOL 73/78 of Annex I, Regulation 13G(7)*. London: IMO.

IMO, 2001. *Amendments to Regulation 13G of Annex I to MARPOL 73/78 and to the Supplement to the IOPP Certificate.* London: IMO.

IMO, 2003. *Revised interim guidelines for the approval of alternative methods of design and construction of oil tankers under Regulation 13F(5) of Annex I of MARPOL 73/78*. London: IMO.

IMO, 2004a. *Amendments to the Annex of the protocol of 1978 relating to the international convention for the prevention of pollution from ships, 1973 (revised Annex I of MARPOL 73/78)*. London: IMO.

IMO, 2004b. *Explanatory notes on matters related to the accidental oil outflow performance under Regulation 23 of the revised MARPOL Annex I*. London: IMO.

ITOPF, 2016. *Oil tanker spill statistics 2015*. London: The International Tanker Owners Pollution Federation Limited.

Jasak, H. and Tuković, Ž., 2010. Dynamic mesh handling in OpenFOAM applied to fluid-structure interaction simulations. In: *Proceedings of V European Conference on Computational Fluid Dynamics ECCOMAS CFD*, Lisbon (Portugal), pp.14-17.

Jeong, S.M., Nam, J.W., Hwang, S.C. and Kim, M.H., 2012. Numerical prediction for oil amount leaked from damaged tank using two-dimensional moving particle simulation method. In: *OCEANS*, pp.1-8.

John, M.P., 2014. *Tanker accidents: double hull is not the only viable alternative*. MSc. World Maritime University.

Kaminski, M.L., Amdahl, J., Fasano, E., Frieze, P.A., Gordo, J.M., Grundy, P., Hess, P.E., Kawamoto, Y., Kujala, P., Paik, J.K., Rohr, U. and Simonsen, B.C., 2000. Technical

Committee III.1 ultimate strength. In: *The 14th International Ship and Offshore Structures Congress*. Nagasaki, Japan.

Karafiath, G., 1992. *Accidental oil spill due to grounding: summary of model test results*. Bethesda: NSWC.

Karafiath, G. and Bell, R.M., 1992. Model tests of accidental oil spill due to grounding. In: *Proceedings of the International Conference on Hydroscience and Engineering*.

Karim, M.M., Rahman, M.M. and Alim, M.A. Computation of axisymmetric turbulent viscous flow around sphere. *Journal of Scientific Research*, 1, pp.209-219.

Kim, I., 2002. Ten years after the enactment of the Oil Pollution Act of 1990: a success or a failure. *Marine Policy*, 26, pp.197-207.

Kishev, Z.R., Hu, C.H. and Kashiwagi, M., 2006. Numerical simulation of violent sloshing by a CIP-based method. *Journal of Marine Science and Technology*, 11, pp.111-122.

Konno, A. and Izumiyama, K., 2002. On the Relationship of the Oil/water Interfacial Tension and the Spread of Oil Slick under Ice Cover. In: *Proceedings of the 17th International Symposium on Okhotsk Sea and Sea Ice*, pp. 275-282.

Koshizuka, S. and Oka, Y., 1996. Moving-particle semi-implicit method for fragmentation of incompressible fluid. *Nuclear Science and Engineering*, 123, pp.421-434.

Krata, P., Jachowski, J. and Montewka, J., 2012. Modelling of accidental bunker oil spills as a result of ship's bunker tanks rupture – a case study. In: *Proceedings of the International Journal on Marine Navigation and Safety of Sea Transportation*, pp.495-500.

Laanearu, J. and Davies, P.A., 2007. Hydraulic control of two-layer flow in quadratic type channels. *Journal of Hydraulic Research*, 45, pp.3-12.

Lakehal, D., Meier, M. and Fulgosi, M., 2002. Interface tracking towards the direct simulation of heat and mass transfer in multiphase flows. *International Journal of Heat and Fluid Flow*, 23, pp.242-257.

Lee, B.H., Park, J.C., Kim, M.H. and Hwang, S.C., 2011. Step-by-step improvement of MPS method in simulating violent free-surface motions and impact loads. *Computer Methods in Applied Mechanics and Engineering*, 200, pp.1113-1125.

Li, A., Sobey, A.J. and Tan, M., 2013. Investigation into the effects of petalling on coefficient of discharge during compartment flooding. *Journal of Fluids and Structures*, 45, pp.66-78.

Liu, F.Q., 2016. A thorough description of how wall functions are implemented in OpenFOAM. In: *Proceedings of CFD with OpenSource Software*, pp.1-33.

Liu, X., Meng, R., Xing, Q., Lou, M., Chao, H. and Bing, L., 2015. Assessing oil spill risk in the Chinese Bohai Sea: A case study for both ship and platform related oil spills. *Ocean & Coastal Management*, 108, pp.140-146.

Lombardi, P., Angelis, V.D. and Banerjee, S., 1996. Direct numerical simulation of near-interface turbulence in coupled gas-liquid flow. *Physics of Fluids*, 8, pp. 1643-1665.

Lu, J.S., Gong, X.W., Yan, S.Q., Wen, X.F. and Wu, W.Q., 2010. Experimental and numerical study on leakage of underwater hole on an oil tanker. In: *Proceedings of the 20th International Offshore and Polar Engineering Conference*, Beijing (China), pp.1047-1053.

Lu, J.S., Liu, F.C. and Zhu, Z.Y., 2014. Effects of initial water layer thickness on oil leakage from damaged DHTs. In: *Proceedings of the 24th International Offshore and Polar Engineering Conference*, Busan (South Korea), pp.618-623.

Ma, Q.W. and Yan, S.Q., 2006. Quasi ALE finite element method for nonlinear water waves. *Journal of Computational Physics*, 212, pp.52-72.

Ma. Z.H., Causon, D.M., Qian, L., Mingham, C.G. and Ferrer, P.M., 2016. Numerical investigation of air enclosed wave impacts in a depressurised tank. *Ocean Engineering*, 123, pp.15-27.

Ma, Z.H., Causon, D.M., Qian, L., Mingham, C.G., Gu, H.B. and Ferrer, P.M., 2014. A compressible multiphase flow model for violent aerated wave impact problem. *Proceedings of the Royal Society A*, 470, pp.20140542.

Ma, Z.H., Qian, L., Causon, D.M., Mingham, C.G., Mar, T., Greaves, D. and Raby, A., 2015. The role of fluid compressibility in predicting slamming loads during water entry of flat plates. In: *Proceedings of the 25th International Offshore and Polar Engineering Conference*, Hawaii (USA).

Manderbacka, T., Kulovesi, J., Celis, M.A.C., Matusiak, J.E. and Neves, M.A.S., 2014. Model tests on the impact of the opening location on the water motion in a flooded tank with two compartments. *Ocean Engineering*, 84, pp.67-80.

Manderbacka, T., Ruponen, P., Kulovesi, J. and Matusiak, J., 2015. Model experiments of the transient response to flooding of the box shaped barge. *Journal of Fluid and Structures*, 57, pp.127-143.

Massey, B.S., 1968. *Mechanics of fluids*. London: Taylor & Francis.

McNaught, J.M., 2011. *Methods for effective viscosity of two immiscible liquid phases*. AspenTech: Houston (USA).

Menon, S., Yeung, P.K. and Kim, W.W., 1996. Effect of subgrid models on the computed interscale energy transfer in isotropic turbulence. *Computers & Fluids*, 2, pp.165-180.

Michel, K. and Moore, C., 1995. Application of IMO's probabilistic oil outflow methodology. In: *SNAME Joint California Sections Meeting*, California, April 1995.

Michel, K., Moore, C. and Tagg, R., 1996. A simplified methodology for evaluating alternative tanker configurations. *Marine Science and Technology*, 1, pp.209-219.

Michel, K. and Winslow, T.S., 1999. Cargo ship bunker tanks: designing to mitigate oil spillage. In: *SNAME Joint California Sections Meeting*. California, May 1999.

Miloshevsky, G. and Hassanein, A., 2013. Splashing and boiling mechanisms of melt layer losses of PFCs during plasma instabilities. *Journal of Nuclear Materials*, 438, pp.S155-S159.

Montewka, J., Goerlandt, F. and Zheng, X., 2014. Probabilistic Meta-models evaluating accidental oil spill size from tankers. In: Weintrit, A. and Neumann, T., eds. 2015. *Information, Communication and Environment: Marine Navigation and Safety of Sea Transportation*. London: CRC Press. Ch.6.

Morris, B.F. and Loughlin, T.R., 2013. Overview of the Exxon Valdez oil spill 1989-1992. In: Loughlin, T.R., ed. 2013. *Marine Mammals and the Exxon Valdez*. London: Academic Press Limited. Ch.1.

Paik, J.K., 2003. Innovative structure designs of tankers against ship collisions and grounding: a recent state-of-art review. *Marine Technology*, 40, pp.25-33.

Pan, Y. and Suga, K., 2006. A numerical study on the breakup process of laminar liquid jets. *Physics of Fluids*, 18, pp.052101-1.

Papanikolaou, A., Zaraphonitis, G., Boulougouris, E., Langbecker, U., Matho, S. and Sames, P., 2010. Multi-objective optimization of oil tanker design. *Journal of Marine Science and Technology*, 15, pp.359-373.

Patrick, B., 2010. *Oil spills: Legacy of the Torrey Canyon*. [online] Available at:< https://www.theguardian.com/environment/2010/jun/24/torrey-canyon-oil-spill-deepwater-bp> [Accessed 04 October 2016].

Peregrine, D.H., Bredmose, H., McCabe, A., Bullock, G., Obhrai, C., Muller, and Wolters, G., 2005. Violent water wave impact on walls and the role of air. In: *Processing of the 29th International Conference of Coastal Engineering*, Lisbon, 4, pp.4005-4017.

Peter, A.C.III and Lin, C.W., 1994. Hydrodynamic analysis of oil outflow from double hull tankers. In: *Proceedings of the Advanced Double-Hull Technical Symposium*.

Rawson, C., Crake, K. and Brown, A., 1998. Assessing the environmental performance of tankers in accidental grounding and collision. *SNAME Transactions*, 106, pp.41-58.

Reboux, S., Sagaut, P. and Lakehal, D., 2006. Large-eddy simulation of sheared interfacial flow. *Physics of Fluids*, 18, pp.105-105.

Rodd, J.L. and McCampbell, S., 1994. Double hull tanker grounding experiments. In: *Proceedings of the Advanced Double-Hull Technical Symposium*.

Samuelides, M., 1999. Prediction of oil outflow in the case of a ship-ship collision based on energy considerations. *Journal of Ship Research*, 43, pp.194-200.

Schneekluth, H. and Bertram, V., 1998. *Ship design for efficiency and economy*. Oxford: Butterworth-Heinemann.

Sciortino, G., Adduce, C. and Rocca, M.L., 2009. Sloshing of a layered fluid with a free surface as a hamiltonian system. *Physics of Fluids*, 21, pp .052102.

Seiffert, B. and Ertekin, R.C., 2012. Numerical modelling of solitary and cnoidal waves propagating over a submerged bridge deck. In: *Proceeding of OCEANS Conference*, Yeosu (S. Korea).

Seiffert, B., Ertekin, R.C. and Robertson, I.N., 2015. Wave loads on a coastal bridge deck and the role of entrapped air. *Applied Ocean Research*, 53, pp.91-106.

Sergejeva, M., Laanearu, J. and Tabri, K., 2013. Hydraulic modelling of submerged oil spill including tanker hydrostatic overpressure. *Analysis and Design of Marine Structures*, Taylor and Francis Group, London.

Seyedein, S.H., Hasan, M. and Mujumdar, A.S., 1994. Modelling of a single confined turbulent slot jet impingement using various k-ε turbulence models. *Applied Mathematical Modelling*, 10, pp.526-537.

Simecek-Beatty, D., Lehr, W.J. and Lankford, J.E., 2001. Leaking tank experiments with Orimulsion™ and Canola oil. *National Oceanic and Atmospheric Administration (NOAA) Technical Memorandum, NOS OR&R*, 6, pp.1-30.

Sirkar, J., Ameer, P., Brown, A., Goss, P., Michel, K. and Willis, W., 1997. A framework for assessing the environmental performance of tankers in accidental groundings and collisions. *SNAME Transactions*, 105, pp.253-295.

Smailys, V. and Česnauskis, M., 2006. Estimation of expected cargo oil outflow from tanker involved in casualty. *Transport*, 21, pp.293-300.

Stringer, R., Zang. J. and Hillis A.J., 2014. Unsteady RANS computations of flow around a circular cylinder for a wide range of Reynolds numbers. *Ocean Engineering*, 87, pp.1-9.

Suponitsky, V., Froese, A. and Barsky, S., 2014. Richtmyer-Meshkov instability of a liquid-gas interface driven by a cylindrical imploding pressure wave. *Computers and Fluids*, 89, pp.1-19.

Taghinia, J., Rahamn, M.M., Siikonen, T. and Agarwal, R.K., 2015. One-equation sub-grid scale model with variable eddy-viscosity coefficient. *Computers & Fluid*, 107, pp.155-164.

Tavakoli, M.T., Amdahl, J., Ashrafian, A. and Leira, B.J., 2008. Analytical predictions of oil spill from grounded cargo tankers. In: *Proceedings of the ASME 27th International Conference on Offshore Mechanics and Arctic Engineering*, Estoril (Portugal), pp.911-920.

Tavakoli, M.T., Amdahl, J. and Leira, B.J., 2009. Investigation of interaction between oil spills and hydrostatic changes. In: *Proceedings of the ASME 28th International Conference on Offshore Mechanics and Arctic Engineering*, pp.1.

Tavakoli, M.T., Amdahl, J. and Leira, B.J., 2011. Experimental investigation of oil leakage from damaged ships due to collision and grounding. *Ocean Engineering*, 38, pp.1894-1907.

Tavakoli, M.T., Amdahl, J. and Leira, B.J., 2012. Analytical and numerical modelling of oil spill from a side tank with collision damage. *Ship and Offshore Structures*, 7, pp.73-86.

Terhune, K., 2011. *Tanker technology: limitations of double hulls. A report by living Oceans Society*. Sointula, BC: Living Oceans Society.

Thomae, R., 1995. Design of a retrofittable alternative to the double hull oil tanker. *Massachusetts Institute of Technology*.

Thomas, R.H., 2005. *Rebuilt double hull tanker and method of rebuilding an existing single hull tanker into a rebuilt double hull tanker*. U.S. Pat. 6,907,836 B2.

Tikka, K., 2001. *Alternative tanker designs, grounding analysis*. Washington: NRC Marine Board Committee on Evaluating Double-Hull Tanker Design Alternatives.

Ubbink, O., 1997. *Numerical prediction of two fluid systems with sharp interfaces*. PhD. Imperial College London.

Udeagbara, S.G., 2009. *Effect of Temperature and Impurities on Surface Tension of Crude Oil*. Dissertation.com.

Vakhrushev, A., Ludwig, A., Wu, M., Tang, Y., Nitzl, G. and Hackl, G., 2010. Modelling of turbulent melt flow and solidification processes in steel continuous caster with the open source software package OpenFOAM. In: *The 4th Open Source CFD International Conference*, Munich (Germany).

Van de Wiel, G., 2008. *A probabilistic model for oil spill volume in tanker collisions and groundings*. MSc. The George Washington University.

Van de Wiel, G. and Dorp, J.R.V., 2009. An oil outflow model for tanker collisions and groundings. *Annals of Operations Research*, 187, pp.279-304.

Wang, X., Li, A., Sobey, A.J. and Tan, M., 2016. Investigation into the effects of two immiscible fluids on coefficient of discharge during compartment flooding. *Ocean Engineering*, 111, pp.254-266.

Wardle, K.E., 2011. Open-source CFD simulations of liquid-liquid flow in the annular centrifugal contactor. *Separation Science and Technology,* 46, pp.2409-2417.

Wardle, K.E. and Weller, H.G., 2013. Hybrid multiphase CFD solver for coupled dispersed/segregated flows in liquid-liquid Extraction. *International Journal of Chemical Engineering*, 2013, pp. 1-13.

Weller, H.G., 2008. *A new approach to VOF-based interface capturing methods for incompressible and compressible flow*. Technical Report, OpenCFD.

White, F.M., 1998. *Fluid mechanics*. 4th ed. Boston: McGraw-Hill Higher Education.

Xiao, M., Li, W., Lin, J.G. and Liang, X., 2010. Numerical simulation of oil spill trajectory and velocity for wrecked ship. *Journal of Dalian Maritime University*, 36, pp.121-124.

Xu, G. and Duan, W.Y., 2013. Time-domain simulation of wave structure interaction based on multi-transmitted formula coupled with damping zone method for radiation boundary condition. *Applied Ocean Research*, 42, pp.136-143.

Yamaguchi, K. and Yamanouchi, H., 1992. Oil spills from the double hull model tanks. *The Report of Ship Technology Research Station*, 29, pp.1-38.

Yan, S.Q. and Ma, Q.W., 2010. Numerical simulation of interaction between wind and 2D freak waves. *European Journal of Mechanics B/Fluids,* 29, pp.18-31.

Yang, L., Yang, H., Yan, S.Q., Ma, Q.W. and Bihnam, M., 2016. Comparative study on water impact problem. In: *Proceedings of the 26th International Ocean and Polar Engineering Conference*, Rhodes (Greece).

Yebra, F., Troncoso, J. and Romani, L., 2017. Fully automatized apparatus for determining speed of sound for liquids in the temperature and pressure interval (283.15-343.15) K and (0.1-95) Mpa. *The Journal of Chemical Thermodynamics*, 104, pp.102-109.

Yip, T.L., Talley, W.K. and Jin, D., 2011. The effectiveness of double hulls in reducing vessel-accident oil spillage. *Marine Pollution Bulletin*, 62, pp.2427-2432.

Zha, J.J., 2011. *Numerical model of wave generation and absorption based on OpenFOAM and its applications*. MSc. Shanghai Jiao Tang University.

Zhang, A. and Suzuki, K., 2006. Numerical simulation of fluid-structure interaction of liquid cargo filled tank during ship collision using the ALE finite element method. *International Journal of Crashworthiness*, 11, pp.291-298.

Zou, C.F., Wang, D.Y. and Cai, Z.H., 2015. Effects of boundary layer and liquid viscosity and compressible air on sloshing characteristics. *International Journal of Naval Architecture and Ocean Engineering*, 7, pp.670-690.

Appendix A

The author's publications by the date of submitting this thesis are listed below:

[1] Yang, H., Lu, J.S. and Yan, S.Q., 2014. Preliminary numerical study on oil spilling from a DHT. In: *Proceedings of the 24th International Offshore and Polar Engineering Conference*, Busan (South Korea), pp.610-617.

[2] Yang, H., Yan, S.Q., Ma, Q.W., Lu, J.S. and Zhou, Y., 2016. Turbulence modelling and role of compressibility on oil spilling from a damaged double hull tank. *International Journal for Numerical Methods in Fluids*, 83, pp.841-865.

[3] Yang, H., Yan, S.Q. and Ma, Q.W., 2016. Effects of tank motion on oil spilling from damaged oil tanks. In: *Proceedings of the 26th International Ocean and Polar Engineering Conference*, Rhodes (Greece), pp.1013-1020.

[4] Lu, J.S., Yang, Z.B., Wu, H.X., Wu, W.F., Liu, F.C., Xu, S., Yang, H. and Yan, S.Q., 2016. Model experiment on the dynamic process of oil leakage from the double hull tanker. *Journal of Loss Prevention in the Process Industries*, 43, pp.174-180.